An *in vitro* study into the effects of erastin in the SH-SY5Y cell line, as a model of Parkinson's disease

Hayley Earle

MPhil

June 2022

Contents

Abstract

Ferroptosis is a non-apoptotic, iron-dependent cell death pathway first identified in an engineered tumorigenic cell line in 2012. Hallmark characteristics include direct or indirect loss of functional GPX4 enzymes, resulting in depletion of glutathione and upregulated lipid peroxidation. The alignment of these (and other) characteristics with those reportedly resulting from dopaminergic degeneration in Parkinson's disease provides an interesting avenue for research – does ferroptosis play a role in Parkinson's disease pathology? SH-SY5Y cells, utilised as an *in vitro* model of Parkinson's disease, were treated with erastin (the first identified ferroptosis inducer), either alone or in combination with DHA (an ω-3 polyunsaturated fatty acid), $AACOCF_3$ (an inhibitor of $cPLA_2$), BEL (an inhibitor of $iPLA_2\beta$) or Fer-1 (an ROS-scavenging inhibitor of ferroptosis). MTT cell viability assay determined these cells to be undergoing significant cell death induced by erastin, though the lack of significant difference when cells were co-treated with the additional compounds suggests the cell death pathway induced may not be ferroptosis. Repeating the experiment using trypan blue to measure cell viability failed to uncover any significant cell death over the same concentration range of erastin. TEM investigation was also conducted with these erastin concentrations, and determined a lack of cell death, in addition to a lack of shrunken mitochondria (considered the gold standard morphological observation in ferroptotic identification). Possible explanations for these discrepancies and potential further work are also discussed.

Introduction

Parkinson's Disease

Parkinson's disease (PD) has two main characterisations of disease manifestation. Firstly, the presence of Lewy bodies - intracytoplasmic protein inclusions of aggregated wild-type or mutated α-synuclein (aSyn) present in various states (e.g. fibrils, oligomers, etc.), depending on Lewy body maturity (Covell et al., 2017; Conway et al., 2000). The second is degeneration of dopaminergic (DAergic) neurones of the nigrostriatal pathway, which projects from the substantia nigra (SN), a nucleus of the basal ganglia in the midbrain, to regions within the dorsal striatum (Alexander, 2004; Rice & Cragg, 2008). Despite symptoms of this condition presenting as both motor and non-motor in nature, current UK diagnostic criteria relies heavily on motor dysfunction (National Health Service, 2016a). Antiparkinsonian medication allows for symptomatic relief, but offers no overall mitigation of disease progression and bring with them substantial complications that further decrease the patient's quality of life, including L-dopa-induced dyskinesia (Martinez-Ramirez et al., 2015). PD affects around 1 to 2% of the global population aged over 65, and slow disease progression means this condition is of significant socioeconomic burden (Olivares et al., 2009; Fineberg et al., 2013).

PD was first classified as a neurological condition by English surgeon James Parkinson in 1817. In his pioneering paper, Parkinson proposed PD - which he termed the shaking palsy, or *paralysis agitans* - as a disease contained within the spinal cord, beginning in the superior cervical vertebrae and extending to the medulla oblongata of the brain stem in later stages (Goetz, 2011; Parkinson, 2002). Since PD's classification 200 years ago, improvement in medical understanding following technological advances has enhanced our knowledge of this disease. For instance, PD as a condition of the spinal cord has since been disproven; first proposed by Hoehn and Yahr (1967), a staging system is now well-documented. Braak et al. (2003) suggested that PD-associated α-synucleinopathy progresses in six stages, beginning in the dorsal motor nucleus of the vagus nerve or the olfactory bulb at stage 1 and extending to medulla oblongata of the brainstem amongst other areas by stage 2. By stage 3, the SN pars compacta (SNpc) exhibits aSyn inclusions (Lewy bodies) and by stage 4, marked degeneration of DAergic populations in this region of the brain is observed, in addition to inclusions in the temporal cortex. Stages 5 and 6 involve pathological observations in the neocortex and premotor cortex. More importantly, Lewy body inclusions and DAergic degeneration of the nigrostriatal pathway, as in stages 3 and 4, are now considered the two main characteristic manifestations of PD (Xicoy et al., 2017).

Lewy bodies

PD can be sporadic or familial, displaying an autosomal-recessive pattern of inheritance (Klein & Westenberger, 2012). Mutations of several genes have been linked to PD, including *SNCA*. This gene – located on chromosome 17 – encodes aSyn, a protein found abundantly in both the brain and erythrocytes that is believed to play a role in SNARE-mediated vesicle docking, although the exact function remains elusive (Marques & Outeiro, 2012; Spinelli et al., 2014; Siddiqui et al., 2016). In PD pathology, aggregated insoluble aSyn is the major component of neuronal Lewy bodies and can also be observed as glial cell cytoplasmic inclusions (Bruck et al., 2016). Covell et al. (2017) determined, using immunostaining of conformational-selective aSyn monoclonal antibodies, that different conformations of aSyn are present in a PD-affected brain that correspond to Lewy body maturity. Additionally, Kingsbury et al. (2010) determined that severity of Lewy body pathology in the medulla (including the dorsal motor nucleus of the vagus nerve) of 25 confirmed PD cases was not correlated with the severity of cortical pathology, supporting Braak's hypothesis of a caudo-rostral pattern of disease progression but suggesting that disease severity in the medulla and cortex are independent of one another. It should be noted that these protein inclusions are not exclusive to PD and are also characteristic of other diseases, including dementia with Lewy bodies (Cantuti-Castelvetri et al., 2005; Kim et al., 2014).

Multiplications of, or mutations within, the *SNCA* gene have been determined as increasing the risk of aSyn aggregation. Multiplications of *SNCA* cause upregulated translation of aSyn, which increases the chance of the protein molecules binding together to form aggregates (Ferese et al., 2015). Despite the rarity of this form of *SNCA* mutation as reported by Johnson et al. (2004), there are seven kindred worldwide who are known to harbour multiplications within their gene, mostly identified by semiquantitative PCR analysis and confirmed by FISH (fluorescent in-situ hybridisation). The Iowan kindred harbours *SNCA* triplication, five kindreds harbour duplications (two French, two Japanese and one Italian) and one kindred, known as the Lister family complex with members in Sweden and the USA, harbour either duplication or triplication of the gene (Ross et al., 2008). Studies of these families suggests that intrinsic instability in this chromosomal region results in a dosage effect of *SNCA* relating to PD onset, progression and severity; average age of onset and average duration before death was much lower in the Iowan triplication kindred compared to one French duplication kindred (34 years vs 48 years and 8.4 years vs 16.8 years respectively). Moreover, whist clinical phenotype of the French kindred was reported as closely resembling that of idiopathic PD, with depression as the main non-motor symptom, that of the Iowan kindred was instead reported as more rapid and progressive, with

pronounced depression, memory loss and cognitive and visuospatial dysfunction (Chartier-Harlin et al., 2004; Muenter et al., 1998).

Alternatively, point mutations within the *SNCA* gene have been determined to modify the primary structure in a way that enhances the propensity of aSyn to misfold and bind to other molecules (Conway et al., 2000). The A53T point mutation, whereby alanine at point 53 is replaced by threonine, was the first point mutation of *SNCA* identified as causing PD, described in a large family of Italian descent – the Contursi kindred – in which of the over 400 globally identified family members, over 60 suffered from clinically confirmed parkinsonism. Genetic penetrance in this family was estimated at 85% (Deusser et al., 2015; Polymeropoulos et al., 1997). Since then, at least 5 other point mutations have been identified – A30P, E46K, H50Q, G51D and A53E (Petrucci et al., 2015). It has been reported that the majority of A53T carriers develop PD between the ages of 35 and 55 (approximately 10 years earlier on average than other *SNCA* mutations) with rapid disease progression – mean time from onset to death is approximately 8 years. Variable occurrence of cognitive and psychiatric disorders is also reported (Kasten & Klein, 2013). Evidence suggests, however, that these phenotypic characteristics are affected by genetic penetrance, whereby higher penetrance causes more severe and earlier-onset disease; Yamaguchi et al. (2005) report of an A53T carrier diagnosed with PD at 41. The proband, who had a family history of PD, developed cognitive dysfunction and moderate dementia before dying at the age of 50. In contrast, Michell et al. (2005) reports of a carrier diagnosed at the age of 74, presenting with bradykinesia (amongst other motor symptoms), resembling idiopathic PD. He had been treated for hypertension and hypercholesterolaemia, but no family history of PD was noted.

Nigrostriatal degeneration

The nigrostriatal pathway is one of four major DAergic pathways in the brain and projects from the SNpc to the caudate and putamen of the dorsal striatum. This pathway is critical in fine motor control and thus the degeneration of contributing DAergic neurones causes decreased innervation and underlies the motor dysfunction symptomatic of PD (Rice & Cragg, 2008; Deumens et al., 2002; Kim et al., 2003). Stereotaxic transplantation of HB1.F3 cells, human neural stem cells (hNSCs) cloned by v-myc- gene transfer, into the 6-OHDA (6-hydroxydopamine) lesioned striatum of rats significantly reduced parkinsonian behavioural symptoms in comparison to the control groups. The hNSC grafts allowed for maintained tyrosine hydroxylase (TH) immunoreactivity along the nigrostriatal pathway indicative of DA synthesis, and endogenous neurogenesis in the subventricular zone was activated (Yasuhara et al., 2006). 6-OHDA is a synthetic neurotoxic compound used to induce animal models of PD by selectively destroying catecholaminergic neurones (Kostrzewa & Jacobowitz, 1974). Similar

findings resulted using undifferentiated human mesenchymal stem cells (Blandini et al., 2010). Symptomatic improvements have also been reported in non-human primate models of PD. Bjugstad and colleagues (2008) implanted hNSCs into the caudate nucleus and SN of 7 adult African green monkeys who had previously been delivered MPTP (1-methyl-4-phenyl-1,2,3,6-tetrahydropyridine – a prodrug which produces a neurotoxin that destroys DAergic nigrostriatal neurones when metabolised within the brain). Quantitative analysis of hNSC migration suggests that over 80% of cells migrated from the implantation site to and along the impaired nigrostriatal pathway. Similar findings are reported by Redmond et al. (2007). Aside from transplantation of stem cells, pharmacological methods – including delivery of the DA D_3 receptor agonist 7-OH-DPAT (7-hydroxy-N,N-di-n-propyl-2-aminotetralin) to a 6-OHDA rat model – have also shown some success in nigrostriatal neurogenesis and symptomatic relief (Van Kampen & Eckman, 2006).

It is believed that aSyn inclusions are the cause of this nigrostriatal cell death (Mazzulli et al., 2006). Overexpression of wild-type human aSyn in rats results in asymmetrical spontaneous motor activity due to loss of DAergic neurones and decreased DAergic striatal innervation, resulting from a 40% loss of presynaptic DA vesicles in aSyn expressing terminals. This suggests dysfunction of presynaptic vesicle genesis and/or recycling and axonal degeneration cause reduced DAergic innervation and underpins the abnormal motor behaviours symptomatic of PD (Gaugler et al., 2012). This is supported by Paumier et al. (2015) who observed Lewy body-like inclusions in several brain areas including the SNpc following unilateral injection of pre-formed aSyn fibrils into the striatum of rats, resulting in reduced ipsilateral striatal DAergic innervation. There are many theories as to how aSyn causes nigrostriatal degeneration. Danzer et al. (2007), for example, determined that some oligomers form a heterogenous population in cell culture and induced cell death via the disruption of ion homeostasis. A Ca^{2+} influx resulted, which the authors presume occurred via a pore-forming mechanism. Another study found that prolonged exposure of rat hippocampal (CA3-CA1) slices to aSyn oligomers upregulated glutamate-induced NMDA (*N*-methyl-D-aspartate) receptor activation and increased basal synaptic transmission. This triggered enhanced contribution of calcium-permeable AMPA (α-amino-3-hydroxy-5-methyl-4-isoxazolepropionic acid) receptors by upregulating AMPA receptor trafficking and insertion into the postsynaptic membrane. Application of theta-burst stimulation was unable to produce further potentiation and lead to impaired long-term potentiation (LTP). This suggests that the role of aSyn in SNARE complex formation may be perturbed by the protein under pathological conditions, resulting in synaptotoxicity (Diogenes et al., 2012). This is supported by Choi et al., 2013, who found aSyn oligomers to inhibit SNARE-mediated vesicle docking in neurones.

How detrimental is Parkinson's disease?

Symptoms of PD can be motor and non-motor in nature. The more obvious motor symptoms include tremor at rest (often beginning in a hand), rigidity, postural instability and bradykinesia, the slowing down of spontaneous and automatic movement. Symptoms typically display on one side of the patient's body although both sides eventually become affected (National Institute of Health, USA, 2018). A review by Poewe (2008) notes that prior to the development of clinical motor symptoms, non-motor symptoms consistent with Braak's staging system are often overlooked, including constipation, rapid eye movement sleep behaviour disorder and hyposmia. Other non-motor symptoms consist of depression, anhedonia and cognitive dysfunction. Furthermore, one study determined nocturia, fatigue and dribbling to be the most frequently reported complaints in a multicentre cross-sectional analysis of 411 PD patients. The group determined patients with non-motor symptoms to have significantly worse health-related quality of life scores compared to patients reporting a lack of non-motor symptoms (Martinez-Martin et al., 2011). A more recent study found frequent voiding/incontinence to be the non-motor symptom reported by 100 PD patients as most disruptive to quality of life, but found tremor and bradykinesia to be overall most disruptive (Gökçal et al., 2017). In addition to these non-motor symptoms, approximately 80% of PD patients eventually develop dementia (Hely et al., 2008).

According to the National Health Service website (2016a), diagnosis is based on symptoms, medical history and a physical examination, wherein a neurologist or geriatrician examines the patient for tremor at rest, bradykinesia and rigidity. A minimum of two of these symptoms will likely lead to a diagnosis, confirmed by symptomatic improvement following levodopa treatment. This is suggestive of a heavy reliance on motor symptoms for positive diagnosis, detailed by Braak's staging system as occurring in the mid to late stages of disease progression. Research by various groups state a loss of between 50 to 80% of DAergic neurones within the SNpc occurs prior to the onset of motor symptoms (Pakkenberg et al., 1991; Ma et al., 1997) Studies suggest that intervention in the earlier stages of disease significantly improves the patient's prognosis (Murman, 2012).

At present, there are three different forms of treatment for PD: pharmacological, neurosurgical (deep brain stimulation, DBS) and supportive therapies (Oertel & Schulz, 2016). Orally administered pharmacological interventions include levodopa with a decarboxylase inhibitor (typically carbidopa) to prevent peripheral levodopa metabolism, DA agonists, MAO-B inhibitors and COMT (catechol-O-methyltransferase) inhibitors. L-dopa can also be infused directly to the jejunum of the small intestine via duodopa pump or, in the case of apomorphine therapy, injected subcutaneously (National Health

Service, 2016b). Prescribed pharmacological avenue depends on disease severity and which symptoms each patient displays (Oertel & Schulz, 2016). DA replacement therapy or inhibition of DA metabolism aims to mitigate symptoms by increasing DAergic innervation (Melamed et al., 1980). DBS involves implanting electrodes into the brain, generally the thalamus, globus pallidus or subthalamic nuclei, and can be unilateral or bilateral. These electrodes are then connected to a pulse generator implanted subcutaneously into the chest wall. 1 to 10% of PD patients are believed to be suitable for this procedure, which aims to correct the movement difficulties caused by DAergic degeneration in the SN (National Institute for Health and Care Excellence, 2003). Supportive therapies, meanwhile, include physiotherapy, occupational therapy, speech therapy and dietary intervention. These aim to improve the patient's symptoms by, for example, relieving muscle stiffness, providing exercises to somewhat alleviate speech and swallowing difficulties and by increasing fibre consumption to reduce constipation, but also to ensure the patient can safely remain within their home (National Health Service, 2016b).

Therapeutic avenues for the treatment of PD are currently limited and allow only symptomatic relief, with no overall effect on disease progression (Martinez-Ramirez et al., 2015). Moreover, treatment often leads to unwanted complications. Levodopa is the most commonly prescribed antiparkinsonian medication, owing to its reported efficacy at all disease stages (Aquino & Fox, 2015). The main complication reported following long-term treatment is motor fluctuations which, after 10 years of therapy, almost 100% of patients are affected by (Metman, 2002). The most debilitating of which is L-dopa-induce dyskinesia (LID) which can occur at peak plasma concentrations (peak-dose dyskinesia) or before and after treatment (diphasic dyskinesia), and is most commonly associated with chorea and dystonia. Chorea is characterised by irregular, involuntary and purposeless non-rhythmic movements mostly affecting the neck and limbs whereas dystonia is the sustained contraction of focal agonistic and antagonistic muscles (Bastide et al., 2015). It is important to recognise that LID can result from long-term treatment of not only L-dopa but also DA a~~nta~~gonists; Maratos et al. (2002) determined LID induced by DA agonists pergolide and ampomorphine to increase steadily in severity but remained significantly less severe than that induced following L-dopa treatment in MPTP-lesioned primate models of PD. Theories as to why LID develops are extensive; physiologically, DAergic neurones of the nigrostriatal pathway fire tonically and release DA in a continuous manner. L-dopa treatment in PD causes pulsatile stimulation of the postsynaptic neurones and leads to motor fluctuations, presumably by producing changes in the postsynaptic receptors (Thanvi & Lo, 2004). In support of this theory, continuous intestinal infusion has been linked to significantly lower incidence of dyskinesia compared to oral sustained-release L-dopa (Nyholm et al., 2003; Băjenaru et al., 2015).

Moreover, Lin and Laureno (2019) determined less pulsatile L-dopa therapy, achieved through 6 daily doses, produced a cumulative dyskinesia incidence of 4.9% in patients between 2002 and 2018, significantly lower than the incidence of 50% reported in patients treated with traditional dosage therapy. Dyskinesia has additionally been correlated with 5-HT_{1B} receptor levels in the striatum and global pallidus of MPTP-treated monkeys and in the basal ganglia of PD patients who reported motor complications (Morin et al., 2015).

Treatments for LID are also limited at present; therapeutic strategies often involve management of current treatments, i.e. beginning PD treatment with DA agonists or COMT inhibitors, taking levodopa before meals (to achieve better absorption) or on a low-protein diet (to prevent dietary amino acid competition in L-dopa absorption) (Thanvi & Lo, 2004). To date, only one distinct pharmacological approach has been approved by the FDA for treating LID: amantadine extended-release capsules, marketed as Gocovri™. Amantadine acts presynaptically to increase DA release and inhibit DA reuptake, in addition to acting as an antagonist of NMDA receptors. Gocovri™ has been shown to significantly reduce incidence of dyskinesia in the majority of experimental conditions but adverse events including hallucinations, constipation and peripheral oedema have also been reported (Pahwa et al., 2015; Pahwa et al., 2017; Oertel et al., 2017).

Succeeded only by Alzheimer's disease (AD), PD is the second most prevalent neurodegenerative condition, and has been predicted as affecting between 8.7 and 9.3 million people globally by 2030 (Bertram & Tanzi, 2005; Dorsey et al., 2006). These statistics mean that this disease is of great socioeconomic burden, reportedly costing the United Kingdom alone £260 million per annum (Fineberg et al., 2013). A sex difference in incidence rate is clear: PD is more frequently diagnosed in men than women. Evidence of this is provided by Savica et al. (2016) who analysed cases of PD in Olmsted County, Minnesota, from 1976 to 2005, that were confirmed as PD by a movement disorder specialist using defined criteria. As can be seen in Fig. 1, a significant increase in incidence rates was found for men ($P = 0.003$) but not for women ($P = 0.45$). The reasons for this difference remain unclear, though the authors suggest changes in smoking behaviour that occurred around the 1950s or other lifestyle/environmental changes as explanations. Taken together, the limitations of current therapeutic avenues and the facts stated here highlight how detrimental further research into this insidious disease is, to one day develop a curative or preventative measure. Treatments aimed at improving neuronal integrity may allow restoration of the nigrostriatal pathway to a more physiological capacity, but for this to be attainable, we must first understand indisputably the complexity of PD aetiology and pathology.

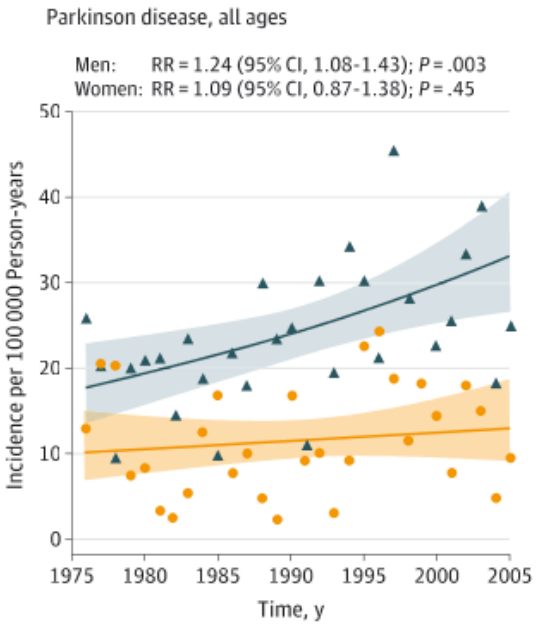

Figure 1 – Graph depicting rates of PD diagnosis in Olmsted County, Minnesota, USA, from 1975 to 2005 in men (blue) and women (orange). RR represents relative risk. Graph taken from Savica et al., 2016.

Modelling Parkinson's disease

Modelling of PD for experimentation can be achieved *in vitro* (by addition of stress agents to immortal cell lines, primary neurones derived from animals, typically rodents, or engineered human stem cells) or *in vivo*, whereby mimetic PD is pharmacologically or genetically induced in live animals, including rodents, *Drosophila melanogaster*, or non-human primates (Xicoy et al., 2017). Immortal cell lines (SH-SY5Y cells, LUHMES (Lund human mesencephalic) cells and PC12 cells, for example) are often utilised due to the similar biochemistry of these lines to the neuronal population found in the SN. SH-SY5Y cells are a human-derived neuroblastoma cell line containing catecholaminergic machinery and intact genes related to major PD pathways (Biedler et al., 1973; Biedler et al., 1978, Krishna et al., 2014). LUHMES cells are also of human origin, derived from embryonic neuronal precursor cells and display biochemical, morphological and functional features of DAergic neurones upon differentiation (Lotharius et al., 2002; Zhang et al., 2014; Edwards & Bloom, 2019). PC12 cells on the other hand are derived from a rat adrenal pheochromocytoma (tumour of chromaffin cells in the adrenal gland) and are catecholaminergic in nature (Greene & Tischler, 1976). Primary neurones (primary mesencephalic cultures, for example), allow for increased physiological relevancy compared to immortal cell lines in that these cultures contain glial cells in addition to the neuronal populations from the area of the brain

the cultures are harvested from. The use of induced pluripotent stem cells derived from PD patients is emerging as a new category of cellular model, referring to pluripotent stem cells that have been generated from terminally differentiated somatic adult cells by manipulation of various transcription factors (Takahashi & Tamanaka, 2006). The use of immortal cell lines, primary neurones and stem cells in PD research will be discussed in greater detail further on.

Whether *in vitro* or *in vivo*, the agents typically utilised to induce DAergic cell death are 6-OHDA and MPTP. Direct *in vivo* delivery of 6-OHDA to target brain regions via injection (since 6-OHDA cannot cross the blood brain barrier) results in mitochondrial dysfunction and increased oxidative stress. This then causes the death of DA- and NA- (noradrenalin-)containing neurones due to the compound's structural similarity to both catecholaminergic neurotransmitters (Kostrzewa & Jacobowitz, 1974). However, 6-OHDA cannot mimic all motor symptoms of PD and typically results in rotational behaviour when injected unilaterally. The use of this neurotoxin has been demonstrated by van Kampen & Eckman (2006) whose study was outlined previously. MPTP on the other hand is noted as the gold standard for researchers due to the compound's ability to mimic additional aspects of PD than 6-OHDA, including the development of Lewy body inclusions. Moreover, MPTP can cross the blood brain barrier where it is immediately metabolised to MPP^+, the active form. Via DA transporter (DAT), MPP^+ is transported into and stored in neurones, where the compound interacts with the mitochondrial electron transport chain (ETC) and results in cell death via energy depletion. Studies utilising MPTP to induce PD have been demonstrated by groups including the previously outlined Bjugstad et al. (2008) and Redmond et al. (2007).

Transgenic animal models of PD can also be developed to study the familial form of the disease. Cronin et al. (2009), for example, determined expansion of SNCA-Rep1, a polymorphic microsatellite upstream of the *SNCA* gene, to result in a 1.7- and 1.25-fold increase in human SNCA-mRNA and protein levels respectively in the brains of 72 mice transgenic for the entire *SNCA* locus. Moreover, Siddique et al. (2012) determined transgenic *Drosophila* expressing neuronal wild-type human aSyn to display significantly lower climbing response compared to control flies.

Differentiation of SH-SY5Y cells

This immortal cell line, can be differentiated into phenotypically different neuronal classes - depending on the differentiation agonist - to include mature NAergic, cholinergic and DAergic. Whilst not the most common use of this cell line, undifferentiated SH-SY5Y cells have also been utilised in studies. Morphologically, these cells display neuroblast-like cell bodies with truncated, neurite-like

processes. When grown in culture, undifferentiated cells have a tendency to cluster and grow in clumps, with both adherent and floating cells. Reminiscent of immature catecholaminergic neurones, undifferentiated SH-SY5Y cells express immature neuronal markers (including DAergic, NAergic, cholinergic and glutamatergic), lacking any mature neuronal markers (Kovalevich & Langford, 2013; Pahlman et al., 1984; Filograna et al., 2015).

During differentiation, proliferation ceases, neurites are extended and mature neuronal markers expressed, more similar to primary neurones. RA-induced differentiation of SH-SY5Y cells (typically 10 μM for 3 to 5 days) has been associated with a DAergic phenotype (see Fig. 2), inferred by the significant increase of TH expression but a lack of NA increase (Kume et al., 2008). A more in-depth study utilising genome-wide transcriptional profiling combined with gene ontology, transcription factor and molecular pathway analysis determined RA to induce a more general differentiation program in this cell line, with cells developing into a predominantly mature DAergic-like phenotype, with NAergic, cholinergic and glutamatergic phenotypes substantially reduced in comparison to undifferentiated cells (Korecka et al., 2013). Sequential treatment of SH-SY5Y cells with RA and TPA (12-o-tetradecanoylphorbol-13, a phorbol ester, at a concentration of 80 nM, again for 3 to 5 days) has instead been reported to induce a more efficient DAergic phenotype in terms of higher proliferation rates, exhibiting higher levels of TH and the DA transporter (DAT) compared to cells differentiation by RA alone, as well as 3-fold and 6-fold higher levels of DA D_2 and D_3 receptors respectively (Presgraves et al., 2004a; Magalingam et al., 2020).

Differentiation of SH-SY5Y cells utilising TPA alone (80 nM for 3 to 5 days) has instead been shown to increase noradrenaline content 200-fold, suggestive of a NAergic phenotype (see Fig. 2) (Pahlman et al., 1984; Akerman et al., 1984). Differentiation induced by dibutyryl cyclic AMP (db-cAMP) at a concentration of 1 mM for 5 days results in a cell population that expresses TH at a much higher percentage than cells induced by RA alone, as determined by immunocytochemical analysis. Moreover, intracellular NA content was also significantly increased in db-cAMP-treated cells, suggestive of a NAergic phenotype in these cells (Kume et al., 2008).

Interestingly, there is much debate as to the primary phenotype of neurones resulting from the sequential differentiation using RA and BDNF (brain-derived neurotrophic factor, typically 10 – 100 ng/mL for up to 7 days). Evidence from target-directed qPCR and microarray studies is indicative of the RA and BDNF differentiation protocol inducing a homogenous neuronal population that is phenotypically cholinergic (Goldie et al., 2014; Edsjo et al., 2003). Though most lines of evidence

suggest RA+BDNF to result in a cholinergic line of neurones, evidence provided by Encinas and colleagues (2000) instead suggests RA+BDNF treatment of SH-SY5Y cells to induce a primarily NAergic phenotype, and Neuhaus et al. (2014) suggest a DAergic phenotype instead results in the mature cells (see Fig. 2).

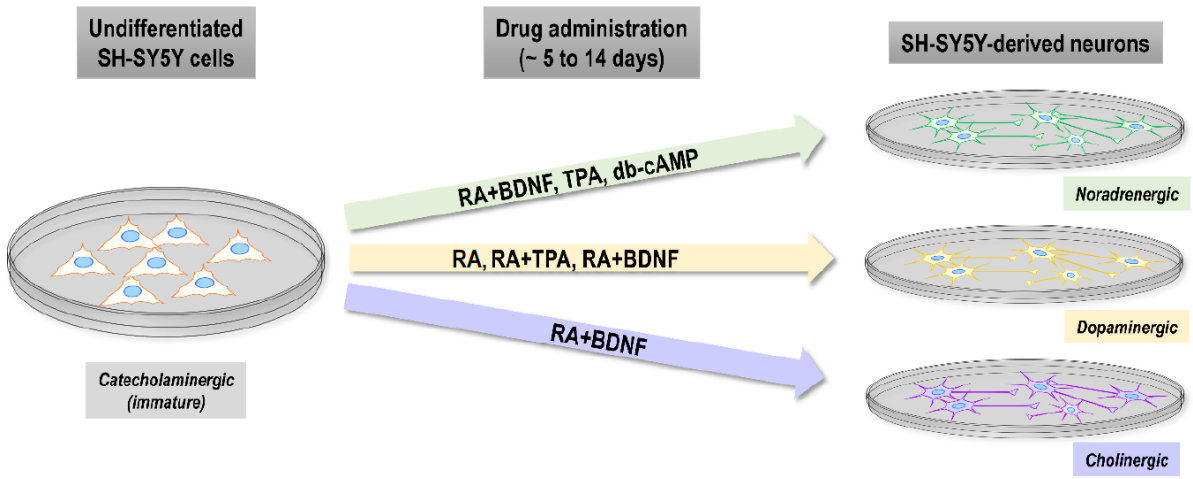

Figure 2 *– The differentiation pathways of SH-SY5Y cells by various inducers and the resulting primary phenotypes. Treatment of SH-SY5Y cells with TPA or db-cAMP induces an NAergic phenotype (green arrow), whereas treatment of cells with RA alone or co-treatment with TPA induces a DAergic phenotype (yellow arrow). Co-treatment of cells with RA and BDNF has been reported to induce NAergic, DAergic or cholinergic phenotypes (green, yellow and purple arrows respectively). Provided by Bell and Zempel, 2020.*

Ferroptosis

Ferroptosis is a cell death pathway that was termed and defined by Stockwell's group in 2012 (Dixon et al., 2012) (see Fig. 3 for an overview of core molecular mechanisms regulating ferroptosis). Induced by erastin, a small molecule identified in 2003 (amongst other since discovered molecules), ferroptosis differs from other well-characterised cell death pathways in terms of morphological, bioenergetic and genetic criteria. For example, apoptotic characteristics of DNA fragmentation and chromatin margination do not occur (Dolma et al., 2003). Moreover, a depletion of intracellular ATP is not observed following erastin treatment, and no overlap has been identified between the six mitochondrial genes determined as controlling ferroptosis and those underlying other forms of cell death (Dixon et al., 2012). Ferrostatin-1 (Fer-1), the first known ferroptosis inhibitor, was also discovered by Stockwell's group and is thought to act as a scavenger of lipidic reactive oxygen species (L-ROS) (Dixon et al., 2012). Other inhibitors have since been identified. Dixon and colleagues (2012) determined that Fer-1 inhibited glutamate-mediated excitotoxic cell death in a rat organotypic hippocampal slice culture (OHSC) model following treatment with L-glutamate. This cell death can be prevented by co-treatment with Ca^{2+} chelators (including BAPTA-AM) but these chelators were unable

to prevent erastin-induced ferroptosis in cancer cells. This led to the suggestion that inhibition of system x_c^- may play a role in ferroptosis. This system imports extracellular cystine for conversion to cysteine, an amino acid that is used intracellularly to synthesise reduced glutathione (GSH) (Toroser & Sohal, 2007; Bridges et al., 2012). GSH acts as an essential cofactor in the reduction of both esterified oxidised fatty acids and cholesterol hyperoxides by GPX4 (glutathione peroxidase 4), an enzyme that comprises part of a cell's intrinsic antioxidant machinery (Conrad & Friedmann, 2015).

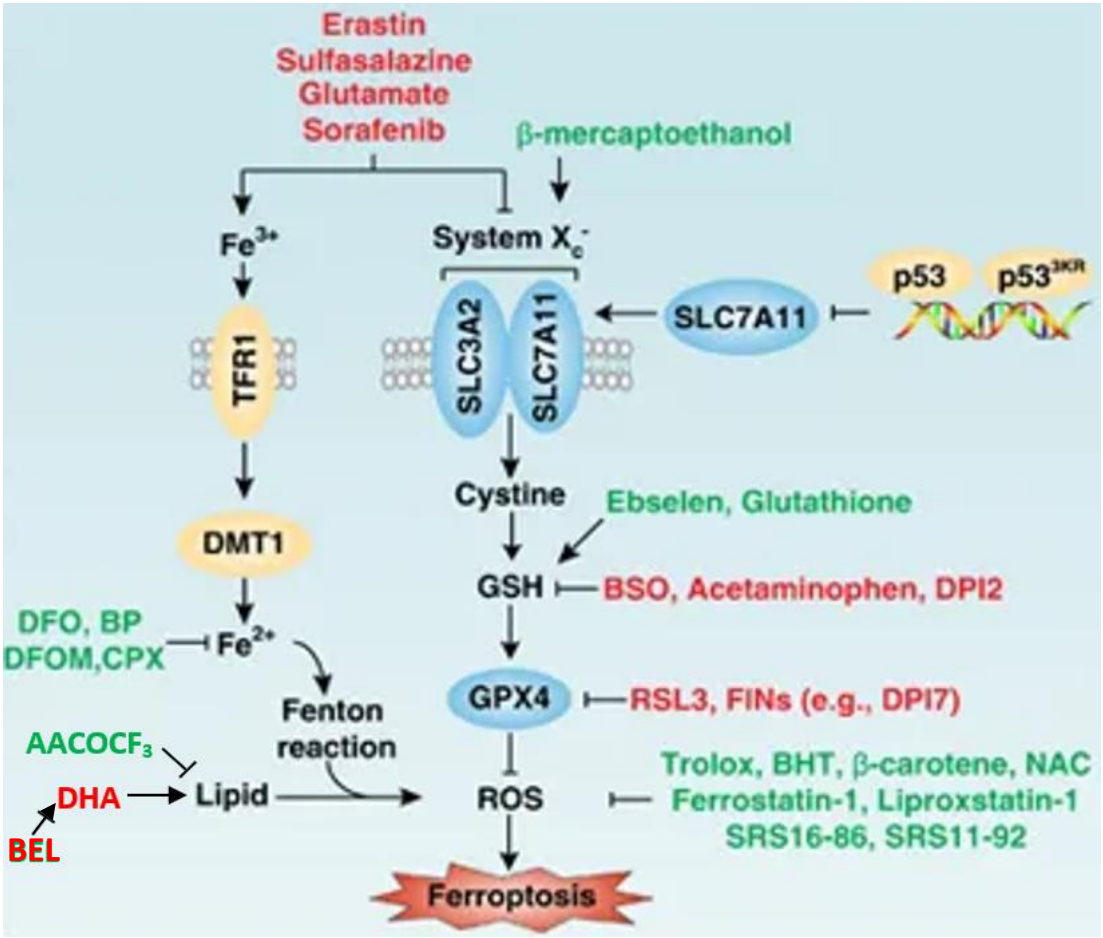

Figure 3 *– Core molecular mechanisms regulating ferroptosis. Those in green are protective against ferroptosis whilst those in red promote ferroptosis. Modified from Xie et al. (2016a) to include $AACOCF_3$, DHA and BEL.*

In addition to ferroptosis-inhibitor Fer-1, this project utilised DHA, $AACOCF_3$ and BEL, which interact with lipids (see Fig. 3). DHA (docosahexaenoic acid) is an ω-3 polyunsaturated fatty acid (PUFA) and is a major constituent of neuronal cell membrane phospholipids. This compound has been found to be beneficial in PD and evidence suggests DHA may play a role in ferroptotic cell death. $AACOCF_3$, also known as arachidonyl trifluoromethyl ketone, inhibits calcium-dependent cytosolic phospholipases A ($cPLA_2$). Uninhibited $cPLA_2$ enzymes catalyse the hydrolysis of arachidonoyl-containing phospholipids and causes the release of fatty acids, particularly arachidonic acid (AA). Whilst there is no evidence of

$AACOCF_3$ playing a direct role in PD or ferroptosis, there is limited evidence of $cPLA_2$ involvement in PD, and of PLA_2 and AA in ferroptosis. BEL (bromoenol lactone), on the other hand, inhibits $PLA_2\beta$ ($iPLA_2\beta$). This class of enzymes, amongst other functions, preferentially releases DHA and AA from neuronal phospholipids. Limited evidence is indicative of a potential role of $iPLA_2\beta$ in PD and ferroptosis. These compounds will be discussed in greater detail further on.

Inducers

Erastin

Working in Stockwell's laboratory, Dolma et al. (2003) utilised a large-scale screen of over 23 thousand small molecules collated from three separate compound libraries to identify those displaying selective synthetic lethality to a series of tumorigenic cell lines that had been experimentally transformed by the group to express defined genetic elements, but not to their isogenic counterparts. Synthetic lethality is defined as a genetic interaction wherein mutation 'B' is synthetically lethal to the cell or organism in the presence of mutation 'A' because lethality requires the presence of both (Yang & Stockwell, 2008; Nijman, 2011). Dolma and colleagues engineered multiple cell series derived from the primary human foreskin fibroblast BJ cell line by sequentially delivering vectors expressing telomerase reverse transcriptase (hTERT), then a genomic construct encoding the Simian Virus 40 large tumour antigen (LT) and small tumour antigen (ST) oncoproteins followed by an oncogenic allele of HRAS, herein referred to as RAS^{V12}, resulting in the BJ-TERT/LT/ST/RAS^{V12} cell series. This method of engineering tumorigenic BJ cells is a modified version of that first developed by Hahn et al. (1999), who based their work on observations reported by other groups that telomerase activity can confer immortality in some human cell lines and, in particular, Shay and Bacchetti's 1997 finding that almost all human tumours have detectable telomerase activity. Known characteristics of the BJ-TERT/LT/ST/RAS^{V12} cell series include their ability to form tumours in immunodeficient mice and their ability to overcome both replicative senescence and crisis, the importance of which will be outlined further on (Hahn et al., 1999).

First, Dolma and colleagues treated BJ-TERT/LT/ST/RAS^{V12} cells with each of the 23,550 compounds for a period of 48 hours, using a concentration of 4 µg/ml which the authors note equates to 10 µM for a compound with a molecular weight of 400, the approximate median molecular weight of all compounds in the screen. Cell viability was measured with the calcein acetoxymethyl ester (calcein AM), a nonfluorescent, freely-diffusing dye that in live cells is cleaved by esterases to produce the fluorescent derivative calcein and thus live cells, but not dead ones, display a green fluorescence. This led to the identification of nine compounds that were at least 4-fold more potent in BJ-

TERT/LT/ST/RAS^{V12} cells than in primary BJ cells in terms of 50% or greater inhibition of cell viability (IC_{50}). These nine small molecules included the discovery of a novel compound the authors termed erastin, for eradicator of RAS and ST-expressing cells (Fig. 4). As the name suggests, erastin was found to inhibit cell viability by 50% in BJ-TERT/LT/ST/RAS^{V12} cells at approximately 4 µM, whereas concentrations up to 10 µM were unable to inhibit cell viability in the isogenic BJ-TERT cell line by more than 20% (see Fig. 5). This suggests erastin concentrations of 1 - 10 µM will inhibit cell viability.

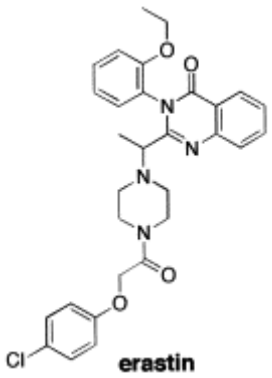

Figure 4 – Chemical structure of erastin, taken from Dolma et al., 2003.

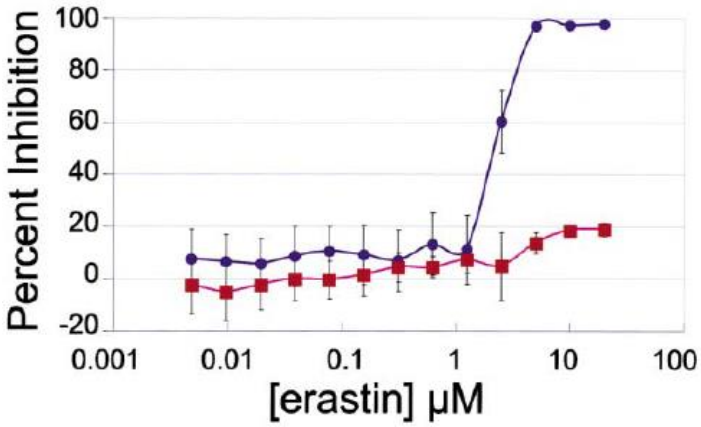

Figure 5 – Graphs depicting percentage inhibition of cell viability following 24-hour erastin treatment measured via the Alamar Blue viability assay in isogenic BT-TERT cells (red) and tumorigenic BJ-TERT/LT/ST/RASV^{12} cells (blue). Taken from Dolma et al., 2003.

To become immortalised, human cells must overcome two barriers – replicative senescence and crisis. Replicative senescence is characterised by the arrest of cellular growth but maintained metabolic activity (Hahn et al., 2002). Crisis, on the other hand, is characterised by widespread chromosomal instability, cytogenic abnormalities and cell death. In non-tumorigenic human somatic cells, each round of cell division causes telomeres – a region at the end of each chromosome that protects from

deterioration – to shorten, allowing cells to reach "Hayflick's limit". This is a phenomenon in which cells can divide a limited number of times before division is no longer possible. When the telomere has reached a critical length, DNA damage response (DDR) is activated. This is a signalling cascade involving the phosphorylation and activation of several downstream proteins and kinases, including tumour suppressors p53 and pRB (retinoblastoma protein). Functions of p53 include prevention and repair of DNA mutations to promote normal cell growth and cell survival, but also apoptosis initiation to eliminate mutation-carrying cells. pRB instead acts as a major G1 checkpoint by blocking entry of the cell into the S-phase of the cell cycle, suppressing gene transcription. DDR signalling aims to halt cell proliferation to allow for DNA repair, or if damaged past threshold, to signal for cell senescence. The action of LT allows BJ-TERT/LT/ST/RAS^{V12} cells to bypass senescence by binding to and inactivating p53 and pRB. This protection and restored proliferative ability is short-lived, however, in that telomeres remain vulnerable to erosion and thus crisis (Manfredi & Prives, 1994; Poulin et al., 2004; Bensaad & Vousden, 2007; Giacinti & Giordano, 2006; Greenberg, 2005). Telomerase is not expressed in human somatic cells and therefore telomere length is not maintained at a sufficient length to permanently supress eventual crisis. Stabilisation of telomere length through ectopic expression of hTERT (the catalytic subunit of the telomerase complex, the other being the telomerase RNA component) therefore confers immortality by lengthening telomeres beyond senescence threshold and rendering cells protected from crisis, further enabling proliferative activity (Masutomi et al., 2003; Kuilman et al., 2010). This is supported by Shay and Bacchetti's 1997 study previously mentioned.

ST on the other hand acts on the pp2A phosphatase to disrupt pathways involved in cell proliferation, signal transduction and cell survival. The exact reasoning as to why ST is required for sensitivity to erastin-induced cell death is unclear as ST was not part of Hahn et al's 1999 immortality protocol. However, the BJ-TERT/LT/RAS^{V12} cell line produced by Dolma and colleagues was not deemed sensitive to erastin in that the IC_{50} concentration was greater than 5 μg/ml (Ahuja et al., 2005; White et al., 2014; Seshacharyulu et al., 2013; Hahn et al., 1999; Dolma et al., 2003). All three subtypes of the RAS GTPase family are present in humans (HRAS, KRAS and NRAS) and mutations within these protein's genes are found in approximately 30% of all cancers. Over 70% of these are *KRAS* mutations, whilst 25% are *NRAS* and less than 5% are *HRAS* mutations, displaying a clear mutation bias (Vigil et al., 2010; Rodenhuis, 1992). Under normal physiological conditions, the HRAS protein is involved primarily in regulating cell division through signal transduction (via activation of the RAF-MEK-ERK pathway) and is activated by bound GTP. The exchange of GTP for GDP inactivates the protein. When mutated, HRAS cannot hydrolyse bound GTP and so is continuously activated, consequently upregulating activation

of downstream effectors and allowing for uncontrolled cell division. RAS is proposed to interact with over 360 proteins with various functions (Colicelli, 2004; Bernards, 2006).

RSL3 and RSL5

A second screening cascade performed by Yang and Stockwell (2008) tested over 47 thousand compounds collated from six different sources, again in BJ-TERT/LT/ST/RAS^{V12} cells, at a concentration of 5 µg/ml corresponding to 13 µM for a compound with a molecular weight of 400. Cell viability was measured via alamar blue analysis and compounds inhibiting the metabolism of alamar blue (and thus cellular growth) in these cells by 50% or greater were tested again in BJ-TERT/LT/ST/RAS^{V12} but also in isogenic counterparts BJ-TERT and BJ-TERT/LT/ST that lack oncogenic HRAS. Alamar blue is a non-fluorescent cell viability reagent that becomes fluorescent red upon entering live cells. This allowed Yang and Stockwell to identify two additional compounds capable of inducing selective cell death in the engineered tumorigenic cell line of interest. These compounds were termed RSL3 and RSL5, for oncogenic-*RAS*-selective lethal compounds (Fig. 6). No quantitative value is given in the paper for IC_{50} concentration, but from the graphs included, the IC_{50} for RSL3 is approximately 0.025 µg/ml and 3.75 µg/ml for RSL5.

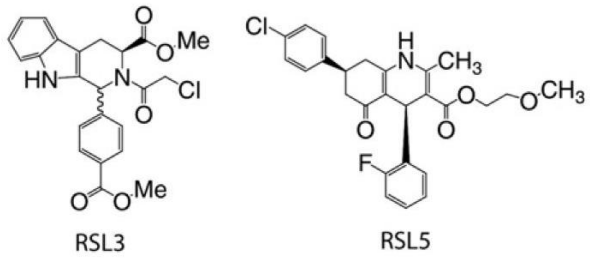

Figure 6 – Chemical structure of RSL3 and RSL5, taken from Yang and Stockwell (2008).

In order to assess possible underlying mechanisms of action in RSL3 and RSL5 induced cell death, these two compounds were tested with biologically active compounds for 24 hours. The first compounds tested were chosen based on their ability to inhibit various aspects of cell death signalling. Pan-caspase inhibitors z-VAD-fmk and Boc-D-fmk were unable to prevent cell death, suggesting RSL3 and RSL5, like erastin, induced cell death that is caspase-independent and not characteristic of apoptosis at the molecular level. This is supported by a lack of poly (ADP-ribose) polymerase-1 (PARP-1) cleavage by activated caspase 3/7 observed following treatment of cells with both RSL3 and RSL5, determined by western blot analysis using an anti-PARP-1 antibody, as a more sensitive method of measuring caspase activation. Instead, the iron chelator DFOM (deferoxamine mesylate) and a lipophilic antioxidant vitamin E (α-tocopherol) were able to suppress cell death induced by RSL3 and RSL5. This

suggests an involvement of iron (possibly through Fenton chemistry) and ROS generation – Fenton chemistry allows for the generation of hydroxide molecules, a form of ROS, from the oxidation of iron in the presence of H_2O_2 (Thomas et al., 2009). Antioxidants, of which α-tocopherol is an example, bind to ROS and essentially inactivate them (Traber & Atkinson, 2007). Without functional antioxidant systems, ROS accumulate and cause damage to lipids, proteins and DNA, a process that results in cell death (Birben et al., 2012).

The second collection of compounds tested against RSL3 and RSL5 were chosen due to their ability to inhibit RAS-related kinase signalling. SU6656 (an inhibitor of SRC kinase which acts as an upstream regulator of RAS signalling) and MEK1/2 inhibitor U0126 suppressed RSL3-induced cell death and completely blocked RSL-5 induced cell death. No explanation is given as to why these compounds suppressed cell death with RSL3 treatment but blocked RSL5-induced cell death. Wortmannin (a PI3K inhibitor), rapamycin (an mTOR inhibitor) or the SAPK inhibitor SB203580 failed to protect BJ-TERT/LT/ST/RASV^{12} cells from cell death induced by either compound.

To study erastin, RSL3 and RSL5 in non-engineered tumorigenic cells, HT-1080 cells were utilised. Whilst z-VAD-fmk and Boc-D-fmk were not tested, cell death induced by all three compounds was suppressed by DFOM, α-tocopherol, SU665 and U0126, as was found in BJ-TERT/LT/ST/RAS^{V12} cells for RSL3 and RSL5. Taken together, this provides evidence of these three compounds inducing a RAS-RAF-MEK-dependent, iron-dependent oxidative cell death phenotype. Interestingly, however, cyclohexamide (CHX), a translation inhibitor that blocks protein synthesis, prevented cell death in BJ-TERT/LT/ST/RAS^{V12} cells upon treatment of RSL5 but not RSL3 and, when tested in HT-1080 cells, prevented erastin- and RSL5-induced cell death but again, not cell death induced by RSL3. This suggests that RSL5 and erastin require protein synthesis to confer lethality whereas RSL3 does not. Moreover, this provides evidence that despite a number of shared phenotypic cell death properties, RSL3 may act via a different underlying mechanism compared to the other two inducers.

This apparent difference and RSL3's high potency (see Fig. 7) garnered interest in the compounds' mechanism of action, and so more detailed studies were performed. First, RSL3 was tested in four cell lines harbouring KRAS mutations, of which human non-small cell lung carcinoma Calu-1 cells were determined as most sensitive to cell death with an IC_{50} value of 20 ng/ml, although all cell lines had an IC_{50} below 5 µg/ml. Reduced efficacy of RSL3 was found in Calu-1 cells delivered shRNAs (short hairpin RNAs) targeting *HRAS, KRAS* or *NRAS*, indicative of a lack of RAS isoform-selectivity. When submitted to the NCI (National Cancer Institute, USA) and tested in 60 cancer cell lines of human origin, it was

determined that the sensitivity profile of RSL3 across all cell lines was distinct compared to those in the NCI database - i.e. no other compound in the database had a similar pattern of cell death. This suggests a truly unique mechanism of action for RSL3.

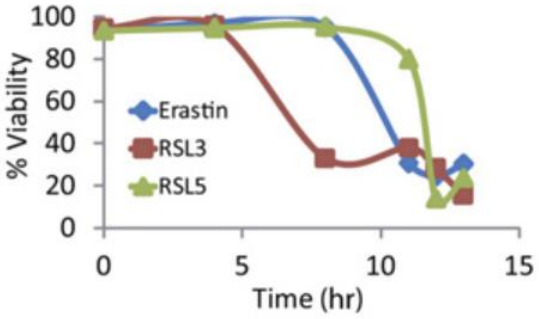

Figure 7 – Kinetic analysis of cell death induced by erastin, RSL3 and RSL5 in BJ-TERT/LT/ST/RAS^{V12} cells. Growth inhibition was induced by RSL3 as early as 8 hours following treatment. Cells were treated with 5 µg/ml of erastin, 0.5 µg/ml of RSL3 or 20 µg/ml of RSL5. Cell viability was determined by trypan blue exclusion following 4, 8, 11, 12 and 13 hours of treatment. Graph taken from Yang and Stockwell (2008).

Also studied more in-depth was the observation that iron chelator DFOM could prevent cell death induced by all three selectively lethal compounds. Depletion of the cellular iron pool by both DFOM and a second iron chelator (compound 311) in BJ-TERT/LT/ST/RAS^{V12} cells was confirmed using Phen Green SK (PGSK), a cell-permeable fluorescent iron sensor exhibiting a green fluorescence, detected by flow cytometry, that diminishes when bound to cellular iron. Increased fluorescence was seen in these cells following iron chelator treatment, indicative of a depletion of the cellular iron pool. Further investigation determined that untreated BJ-TERT/LT/ST/RAS^{V12} cells have a higher basal iron content compared to untreated BJ-TERT and BJ-TERT/LT/ST cells, which displayed a similar fluorescence profile. Investigation as to why this difference occurs found that BJ-TERT/LT/ST/RAS^{V12} cells express higher levels of *TfR1* than the two isogenic BJ cell lines, as determined by western blot analysis. The *TfR1* gene codes for transferrin receptor 1 (TRF1), a membrane protein that internalises and releases iron into the cytoplasm of the cell upon binding to the transferrin-iron complex, and therefore increases iron uptake into cells. This was confirmed in that lentiviral delivery of shRNA clones knocked down the *TfR1* gene and decreased the sensitivity of BJ-TERT/LT/ST/RAS^{V12} cells to erastin, although to a smaller degree than iron chelators. This partial rescuing activity is noted by Yang and Stockwell to possibly reflect insufficient gene knockdown or the involvement of other iron-enriching mechanisms. Interestingly, real-time PCR (polymerase chain reaction) analysis showed a gradual decrease in expression of *FTH1* (ferritin heavy chain 1) and *FTL* (ferritin light chain) – both of which code for iron storing molecules – in terms of mRNA levels in BJ-TERT/LT/ST/RAS^{V12} cells. mRNA levels of *TfR1*

increased. The authors suggest that this is indicative of oncogenic RAS signalling both to increase iron uptake and decrease iron storage, enhancing the cellular iron pool within sensitive cells.

Other known inducers

This RAS-RAF-MEK-dependent, iron-dependent cell death pathway was termed 'ferroptosis' by Stockwell's group (Dixon et al., 2012). Much of what we know of ferroptosis stems from the discovery of erastin, RSL3 and RSL5. Other compounds have since been identified as ferroptosis-inducing agents (FINs) and are classified by their mechanism of action – class I compounds inhibit system x_c^- and block enzymatic activity of GPX4 indirectly by preventing synthesis of GSH (Yang et al., 2014). These include erastin, RSL5, sulfasalazine (SAS) and sorafenib. Sorafenib is a RAF kinase inhibitor acting downstream of RAS that has received FDA approval for treatment of renal cell carcinoma. Three different lines of hepatocellular carcinoma (HCC) cells treated with DFOM were protected from sorafenib-induced cell death. When further examined, ferroptosis inhibitor ferrostatin-1 (Fer-1) and genetic procedures interfering with ferroptosis-associated genes blocked the cytotoxic effects. Sorafenib was reported to induce ferroptosis in two further HCC lines, as well as eight cancerous cell lines of non-liver origin (Wilhelm et al., 2006; Louandre et al., 2013; Lachaier et al., 2014). Class II FINs instead induce ferroptosis through the direct inhibition of GPX4 activity without depleting levels of GSH. Examples include RSL3, BSO (buthioninesulfoximine), acetaminophen, FDA-approved anticancer drug altretamine and various forms of DPI (diphenylene iodonium) (Friedmann et al., 2014; Lorincz et al., 2015; Woo et al., 2015; Yang et al., 2014). Altretamine was identified as a FIN in 2015, as determined by computational DeMAND (detecting mechanism of action by network dysregulation) approach. DeMAND interrogates tissue-specific regulatory networks and identified altretamine as a GPX4 inhibitor. Further studies by the group confirmed the drugs' ability to induce ferroptosis in U-2932 cells. This cell line was established from a patient with diffuse large B-cell lymphoma previously treated for relapsing Hodgkin lymphoma (Woo et al.,2015; Amini et al., 2002).

Inhibitors

Ferrostatin-1

Fer-1 was the first confirmed inhibitor of ferroptosis, reported by Dixon et al. (2012). Identified via high-throughput screening of 9,517 small molecules, Fer-1 was found to be the most potent inhibitor of 5 μM erastin-induced ferroptosis in HT-1080 cells, with an EC_{50} of 60 nM. Moreover, Fer-1 was found to inhibit cell death induced by erastin, RSL3 and SAS, but not H_2O_2-induced necrosis, STS-induced apoptosis or rotenone-induced inhibition of complex I of the mitochondrial ETC. This inhibitor was suggested to act as an ROS scavenger in that the molecule prevented the accumulation of both

C-ROS (cytosolic-ROS) and L-ROS following erastin treatment, assayed by H_2CDF and BODIPY-C11 flow cytometry. The ROS-scavenging ability of Fer-1 was determined to be dependent on both aromatic amines of the molecule – the antioxidant capacity of Fer-1 was abolished following the substitution of the primary aromatic amine for a nitro group in the SRS8-24 analog or elimination of the N-cyclohexyl moiety as in the CA-1 analog (see Fig. 8). Both amines were additionally found necessary for the ability of this molecule to prevent erastin-induced cell death in HT-1080 cells. The researchers suggested that the N-cyclohexyl region of Fer-1 promotes the harnessing of Fer-1 within lipid membranes; a significant correlation was found between the ability of ten Fer-1 analogs (synthesised with varying numbers of carbons in the N-substituted cyclic moiety) to prevent ferroptotic cell death induced by erastin and predicted lipophilicity. Fer-1 is, however, considerably more potent an inhibitor of ferroptosis than phenolic antioxidants trolox and BHT (butylated hydroxyltoluene), despite Fer-1's similar predicted lipophilicity. This difference may suggest that the presence of an aromatic amine in Fer-1 confers a profile of radical reactivity that is uniquely tuned to mechanisms underlying ferroptosis.

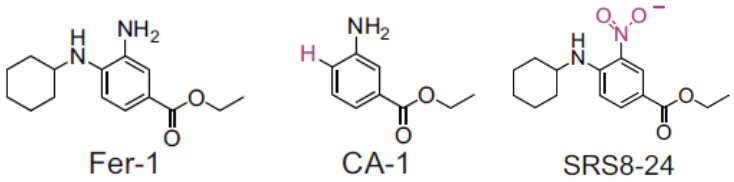

Figure 8 – Chemical structure of Fer-1 and analogs CA-1 and SRS8-24. Taken from Dixon et al., 2012.

Noting that excitotoxic cell death as occurs in epilepsy, stroke and other neurologically traumatic situations is an oxidative, iron-dependent process, Dixon and colleagues (2012) speculated a possible link to ferroptosis. To investigate this, a rat organotypic hippocampal slice culture (OHSC) model was used, reported to preserve the integrity of both inhibitory and excitatory connections as well as that of supporting astrocytes and microglia, thereby closely resembling the hippocampus *in vivo*. Fer-1, CPX (ciclopirox olamine) and MK-801 were determined to significantly attenuate cell death induced by L-glutamate in the dentate gyrus (DG), CA1 and CA3 of the hippocampus. CPX is an iron chelator whereas MK-801 is an NMDA receptor inhibitor. Evidence of Fer-1's rescuing abilities is also reported by Li et al. (2017) in models of intracerebral haemorrhage (ICH), a condition whereby haemoglobin released from lysed erythrocytes following the rupture of a cerebral blood vessel causes tissue damage and cell death in the surrounding brain areas (metabolism releases the central iron which can cause ROS generation). Fer-1 was found to significantly attenuate Hb-induced cell death in OHSCs, including reduced neuronal degeneration observed in the DG, CA1 and CA3, even when delivered 30 minutes before, during or after Hb treatment. Furthermore, BODIPY-C11 determined Fer-1 inhibited

accumulation of L-ROS, confirmed by malondialdehyde (MDA; an end product of lipid peroxidation) assay. GPX activity assay found decreased functional activity of this family of enzymes following Hb treatment, which again was significantly attenuated by Fer-1. Fer-1 also rescued these cells from Fe^{2+}-induced cell death. When ICH was induced in mice by injection of collagenase into the left striatum, Fer-1 treatment significantly increased the number of surviving neurones compared to the vehicle control group, and injury volume was significantly lower. Significantly less iron deposition was also reported in the experimental group. More importantly, Fer-1-treated mice displayed significantly reduced neurological deficit and less limb muscle weakness.

Since the molecule's discovery, second and third generation ferrostatins have been synthesised from Fer-1, necessitated by the low functionality of Fer-1 reported *in vivo* due to potential metabolic and plasma instability (Linkermann et al., 2014). SRS11-92 (Fig. 9) is a second-generation ferrostatin synthesised by researchers at Stockwell's laboratory. Both Fer-1 and SRS11-92 were found to significantly increase the number of healthy medium spiny neurones in huntingtin (htt)-transfected rat corticostriatal brain slices in comparison to those treated with vehicle control. The authors note that Huntington's disease involves perturbation of glutamate, GSH and iron levels, in addition to accumulation of breakdown products of lipid peroxidation. The group next exposed cultured oligodendrocytes to cystine-free conditions, allowing for GSH depletion and cell death. Fer-1 and SRS11-92 protected these glial cells at concentrations of 100 nM, suggesting that ferrostatins could protect cells from periventricular leukomalacia (PVL), a syndrome that affects premature infants and is caused primarily by the death of developing oligodendrocytes in an iron-dependent manner, with biomarkers of L-ROS observed at elevated levels. Lastly, Fer-1 and SRS11-92 were found to prevent cell death in a mouse model resembling rhabdomyolysis-induced acute kidney injury, induced by hydroxyquinoline and ammonium iron(II) sulphate. Overall, the group reports SRS11-92 to be 15-fold more potent than Fer-1, with an EC_{50} (concentration to rescue 50% of cells from erastin-induced cell death) of 6 nM compared to 95 nM respectively (Skouta et al., 2014). According to Bosch et al. (2009), rhabdomyolysis is the rapid breakdown of skeletal muscle, causing the release of myoglobin and lactate dehydrogenase, amongst other muscle-cell contents, into circulation. Acute kidney injury results as a complication of severe forms of rhabdomyolysis. Furthermore, Cotticelli and colleagues (2019) found Fer-1 and SRS11-92 inferred protection in cellular human and mouse models of Friedreich ataxia treated with ammonium iron(III) citrate and BSO, an inhibitor of GSH synthesis. The authors note that key biochemical defects of Friedreich ataxia cells include two hallmarks of ferroptosis – mitochondrial iron accumulation and generation of L-ROS.

In 2014, Stockwell's group published an additional paper highlighting the synthesis of a third-generation ferrostatin, SRS16-86 (Fig. 9). This analog was found to have high metabolic and plasma stability, as tested in mouse liver microsomes and plasma respectively. The ability of SRS16-86 to inhibit ferroptosis was confirmed in erastin-treated HT-1080 and NIH 3T3 cells (a cell line of mouse embryonic fibroblast origin). Fer-1 and, to a greater extent, SRS16-86, were found to protect mice from functional acute renal failure (determined by serum urea concentration) and structural organ damage in a model of severe ischemia-reperfusion injury. Furthermore, no side effects were reported from SRS16-86 treatment 4 weeks after application (Linkermann et al., 2014). Recently, SRS16-86 was shown by Zhang et al. (2019) to allow functional recovery in a rat model of contusion spinal cord injury (SCI). To induce injury, rats were anaesthetised and a 10 g bar was allowed to free fall onto the exposed spinal cord from a height of 2.5 cm. Using transmission electron microscopy (TEM), the ultrastructure of cells was analysed following insult and cell death determined as ferroptotic by observation of shrunken mitochondria. Following treatment with SRS16-86, locomotor activity significantly improved and mitochondrial morphology returned to a more physiologically normal size. Moreover, SRS16-86 treatment increased the number of surviving neurones in the ventral horn of the spinal cord (representative of motor neurone location) at 4 weeks post SCI. SCI is reported to be characterised by elevated iron and glutamate, and generation of L-ROS. Taken together, these studies are indicative of a clinically beneficial role of ferroptosis inhibition by Fer-1 and its daughter molecules.

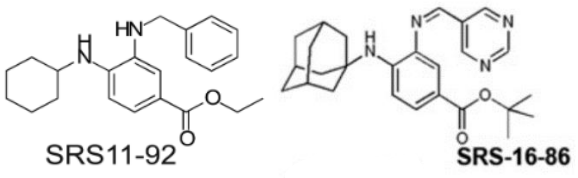

Figure 9 – Chemical structure of Fer-1 analogs SRS11-92 (second generation) and SRS-16-86 (third generation). Taken from Skouta et al., 2014 and Linkermann et al., 2014, respectively.

Liproxstatin-1

Liproxstatin-1 (Lip-1, Fig. 10) was discovered by Friedmann and colleagues in 2014 in a high throughput screening of over 40 thousand small molecules displaying drug-like characteristics in inducible $Gpx4^{-/-}$ mouse embryonic fibroblast (MEF) Pfa1 cells. This resulted in the identification of an uncharacterised class of spiroquinoxalinamine derivatives which included Lip-1. This molecule was determined to prevent L-ROS generation in Pfa1 cells at 50 nM, assayed 48 hours after GPX4 knockout by BODIPY-C11 flow cytometry. Confirming ferroptosis-specific activity, Lip-1 prevented Pfa1 cell death induced by BSO, erastin and RSL3 but not TNFα-induced apoptosis or H_2O_2-induced necrosis. Similar results were observed following treatment with RLS3 in both HRPTEpiC and HK-2 cells, human

renal proximal tubule epithelial cell lines. Additionally, Lip-1 was determined to extend survival in a mouse model of acute renal failure and reduce both DNA fragmentation (assayed by TUNEL staining) and tissue injury compared to the vehicle-only control group. Moreover, Lip-1 was used in the previously mentioned ICH study by Li and colleagues (2017) to confirm the occurrence of ferroptosis; at 5 μM, Lip-1 was determined to inhibit Hb-induced OHSC death when delivered with a 30-minute delay, and observed to decrease neurological deficits and lesion volume in the mouse model when delivered 4 hours after collagenase injection, in addition to rescuing neurones. Further evidence is provided by Hambright et al. (2017) who generated a mouse model with conditional deletion of GPX4 in forebrain neurones (GPX4BIKO mice). 12 weeks following GPX4 deletion, these mice exhibited significant AD-like symptoms compared to the control group, including deficient spatial learning and memory. Further examination revealed hippocampal degeneration, confirming AD modelling, in addition to elevated markers of ferroptosis to include lipid peroxidation, ERK activation and neuroinflammation. Hippocampal degeneration and behavioural dysfunction occurred at an increased rate in mice fed a vitamin E-deficient diet (GPX4BIKO-VED). Although no significant difference was found between GPX4BIKO mice delivered Lip-1 and those delivered control in terms of rotarod performance score, hippocampal slices from the Lip-1 treated mice showed significantly higher levels of synaptophysin, a marker of synaptic transmission, amongst other neuronal proteins. This allowed the researchers to conclude a somewhat beneficial role for Lip-1 in this animal model of AD.

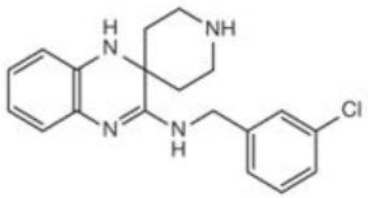

Figure 10 – Chemical structure of Lip-1, taken from Friedmann et al., 2014.

An interesting study by Kim et al. (2016) highlights Lip-1 protection in nanoparticle-induced ferroptosis. Treatment of human melanoma M21 cells expressing the melanocortin-1 receptor (herein referred to as MM21 cells) with 15 μM of αMSH-PEG-C' dots (α-melanocyte stimulating hormone surface-functionalised (ethylene glycol)-coated fluorescent silica C' dot nanoparticles) in amino acid-deprived conditions caused unexpected cell death – no nanoparticle-induced cell death was observed in amino acid replete media. Characterisation led the authors to determine ferroptosis as the cell death pathway; Fer-1 and Lip-1 significantly rescued cell viability and nanoparticle-induced cell death was inhibited by DFOM, Trolox and GSH repletion. When imaged with BODIPY-C11, increased fluorescence indicative of L-ROS generation was observed prior to cell death, inhibitable by Lip-1. Intriguingly, Kim

reports this context resulted in propagation of ferroptosis from cell to cell, in a wave-like manner (Fig. 11). High rates of cell death were also observed in non-tumourous MCF10A human mammary epithelial cells and MEFs, as well BxPC3 pancreatic, H1650 lung and 786-O renal carcinoma cells, and HT-1080 fibrosarcoma cells, following amino acid starvation and nanoparticle exposure. Of these, HT-1080 cells were deemed most sensitive, requiring nanoparticle concentrations tenfold lower than the other four cell lines, and even underwent ferroptosis following nanoparticle exposure in non-amino acid starved conditions. Lastly, the group generated 786-O and HT-1080 cell xenograft models whereby immunosuppressed mice were injected with both particle-exposed and particle-unexposed cells into the flank and then delivered three intravenous injections of targeted nanoparticle-containing probe or saline solution over ten days. Nanoparticle delivery was found to significantly reduce tumour volumes in both the HT-1080 and 786-O groups. At study termination, tumour-bearing mice were treated daily with intraperitoneal delivery of Lip-1 for a further 10 days, resulting in significantly reduced inhibition of tumour growth. This study suggests that hybrid organo-silica-based nanoparticles, as have been approved by the FDA as an Investigational New Drug, induces ferroptosis across cell lines of various origins under amino acid starved conditions and shows *in vivo* potential.

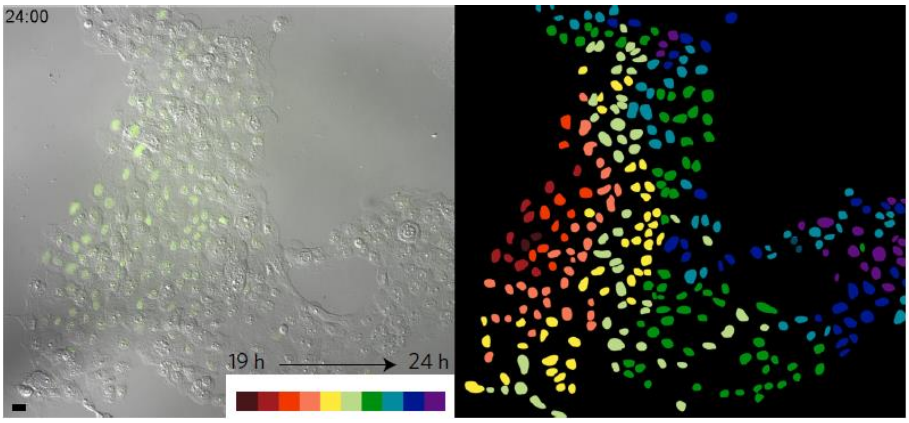

Figure 11 *– Images from time-lapse analysis of MCF10A undergoing ferroptosis in amino-acid-starved conditions with 15 μM αMSH-PEG-C' dots. Note that death (Sytox Green positivity) spreads cell-to-cell from the left side of the image to the right. Right image: position of each dead cell nucleus pseudocoloured to represent the relative timing of cell death. Scale bar, 10 μm. Taken from Kim et al. (2016)*

The mechanism of Fer-1 and Lip-1 in preventing ferroptosis has been investigated by Zilka et al. (2017). One way in which L-ROS are generated is through iron-catalysed autoxidation of peroxyl radicals, in a process known as lipid peroxidation, and so the group began by assessing the radical-trapping antioxidant (RTA) abilities of Fer-1 and Lip-1. Noting that α-tocopherol (the most biologically active form of vitamin E) is a relatively poor inhibitor of ferroptosis in comparison to Fer-1 and Lip-1, the group utilised a small library of substituted tetrahydronaphthyridinols (THNs) with varying lipid-solubility which, despite being approximately 30-fold more reactive than α-tocopherol in organic

solutions and lipid bilayer models of cell membranes, had not yet been studied in cell culture. RTA activities of Fer-1, Lip-1, α-tocopherol and a representative THN (C_{15}-THN) to peroxyl radicals were analysed, determining Fer-1 and Lip-1 to be an order of magnitude less reactive than α-tocopherol. C_{15}-THN, on the other hand, was found to be too reactive for that particular approach. Further investigation using styryl-associated BODIPY found Fer-1 and Lip-1 to be significantly more reactive than α-tocopherol in phosphatidylcholine lipid bilayers (believed due to the poor H-donating abilities of the two arylamine molecules) but again, less so than C_{15}-THN. Together, the authors suggest these studies provide evidence that the oxidative reaction of Fer-1 and Lip-1 with peroxyl radicals generates compounds that remain reactive to these radicals, further mitigating autoxidation by their additional radical trapping abilities. Furthermore, the authors suggest similarity in mechanism of action by Fer-1 and Lip-1 with already-established catechol and hydroquinone RTAs. L-ROS can also be generated by the iron-dependent activity of lipoxygenase enzymes. Testing of Fer-1 and Lip-1 in Hek-293 cells transfected to overexpress the 15-LOX-1 isoenzyme found these molecules unable to significantly inhibit production of 15-hydroperoxyeicosatetraenoic acid (15-HPETE; the product of 15-LOX-1-catalysed oxygenation of the enzyme's natural substrate – AA). GPX4 inhibition in Pfa1 cells by RSL3 determined lipophilic THNs to display similar potency to Fer-1 and Lip-1. Hydrophilic THNs, however, were ineffective in inhibiting ferroptosis. Similar findings resulted from genetic GPX4 disruption studies in MEFs and glutamatergic-induced excitotoxicity in HT22 mouse hippocampal cells. Overall, this study provides evidence that L-ROS generation in ferroptosis is driven by non-enzymatic lipid peroxidation and that the mechanism of action of Fer-1 and Lip-1 is as RTAs whose oxidative products are further capable of trapping radicals. Building on this, Sheng et al. (2018) determined that the radical-trapping mechanism of Fer-1 and Lip-1 was dependent on the ortho-amine moiety, which interacts with L-ROS and then forms a planar seven-membered ring in the transition state before realigning to a state that allows for greater reactivity. The authors note that despite the numerous parallels of Fer-1 and Lip-1 to other diphenylamine antioxidants, this radical-trapping mechanism is novel.

Other known inhibitors

In addition to iron chelators (e.g. DFOM) and the vitamin E α-tocopherol, for example, other ferroptosis inhibitors have been suggested. Necroptosis inhibitor necrostatin-1 (Nec-1) has been shown to exhibit off-target activity that inhibits ferroptosis at high concentrations but in a manner unrelated to necroptosis (Friedmann et al., 2014). Liu et al. (2015) report that zileuton, a 5-lipoxygenase inhibitor, can prevent erastin-induced cell death in HT22 mouse hippocampal cells by inhibiting the production of C-ROS. Krainz and colleagues (2016) suggest that ferroptosis can also be

inhibited by XJB-5-131 and JP4-039 in HT-1080, BJ-TERT/LT/ST/RAS^{V12} and panc-1 cell lines. XJB-5-131 is a synthetic antioxidant that targets mitochondria and has been reported to improve mitochondrial response to acute and chronic cellular stress, whereas JP4-039 is said to be a more broadly distributed antioxidant. Both compounds suppress ROS generation (Xun et al., 2012; Kraniz et al., 2016). Alternatively, the naturally occurring flavonoid baicalein (also known as 5,6,7-trihydroxyflavone), found in the roots of *S. baicalensis* and *S. lateriflora*, was determined by Xie et al. (2016 b) to enhance a cell's defence against ferroptosis via multiple mechanisms, including (but not limited to) the prevention of Fe^{2+} production, GSH depletion, lipid peroxidation and, at protein level, GPX4 degradation. Interestingly, Wang et al. (2016) determined non-oxidative DA to be a strong inhibitor of ferroptotic cell death in both cancerous (panc-1 and HEY cell lines) and non-cancerous MEFs and HEK293 (human embryonic kidney) cells following treatment with erastin by reducing Fe^{2+} accumulation and GSH depletion. The researchers also report that DA increased mechanical stability of GPX4, suppressed DA D_4 receptor degradation and promoted DA D_5 receptor gene expression. In support of this, Hauser et al. (2013) found DA *o*-quinones to decrease GPX4 abundance, thus reducing the antioxidant capacity of the rat and immortal cell lines studied.

System x_c^-

The ability of Fer-1 and CPX to inhibit ferroptosis in the previously mentioned rat OHSC model suggested to Dixon et al. (2012) a shared mechanism of action between glutamate-induced excitotoxic cell death and erastin-induced ferroptosis. Glutamatergic cell death as a result of upregulated Ca^{2+} influx via ionotropic glutamate receptors (primarily NMDA) was disproven in that calcium chelators BAPTA-AM, Fura-2 and EGTA were unable to prevent ferroptosis in cancer cells (Zhou et al., 2013; Dixon et al., 2012). Alternatively, glutamatergic cell death can be initiated by inhibition of cystine uptake via system x_c^- (Albrecht et al., 2010; Lewerenz et al., 2013). This is a highly specific Na^+-independent cystine/glutamate antiporter embedded in the plasma membrane of cells that imports extracellular L-cystine and exports intracellular L-glutamate at a 1:1 molar ratio (Bridges et al., 2012). A heterodimer protein, system x_c^- is made up of a 12-pass transmembrane transporter protein encoded by *SLC7A11* (chloride-dependent light chain subunit, xCT, responsible for transport activity) and a heavy chain single-pass transmembrane regulatory subunit, 4F2hc which is encoded by the *SLC3A2* gene and is responsible for heterodimer membrane location. These subunits are linked by a disulphide bridge (Dixon et al., 2014; Albrecht et al., 2010; Bassi et al., 2001; Conrad & Sato, 2012). Once in the cytoplasm of the cell, cystine is reduced to cysteine by thioredoxin reductase 1 (TRR1). Under physiological conditions, cysteine, glutamate and glycine are utilised in the biosynthesis of GSH through the actions of glutathione-cysteine ligase (GCL) and glutamine synthetase. GSH plays a vital

antioxidant role by preventing the accumulation of lipid peroxides (Toroser & Sohal, 2007; Lewerenz et al., 2013). Of note, emerging evidence suggests system x_c^- to have a two-pronged role by also acting as a redox cycle independent of GSH, whereby surplus cysteine is released into the extracellular space. This provides a reducing microenvironment necessary for cell signalling (Conrad & Sato, 2012).

Erastin has been shown to prevent cystine uptake through the inhibition of system x_c^-; co-treatment of HT-1080 cells with erastin, SAS or glutamate and β-ME (β-Mercaptoethanol; a hydroxyl radical scavenger) impeded ferroptotic cell death. Moreover, erastin, glutamate and SAS blocked the uptake of radiolabelled [^{14}C]-cystine into HT-1080 and Calu-1 cells via system x_c^- but not the uptake of [^{14}C]-phenylalanine through system L (composed of SLC7A5 and SLC3A2) (Dixon et al., 2012 Dixon et al., 2014). Inhibition of system x_c^- has been shown to cause compensatory transcriptional upregulation of *SLC7A11*, as was found following treatment of HT-1080 cells with erastin or SAS. This effect was suppressed by β-ME but not DFOM or Fer-1, suggesting the roles of iron and ROS accumulation in ferroptosis to be downstream of system x_c^- inhibition by erastin and SAS. Furthermore, HT-1080 cells became more sensitive to erastin-induced cell death following the siRNA-mediated silencing of *SLC7A11* using two independent siRNAs, whereas transfection of a plasmid encoding *SLC7A11* conferred protection from erastin and SAS (Dixon et al., 2012). Taken together, these findings suggest a selective mechanism of action of erastin and SAS for system x_c^- over similarly composed amino acid transporter systems. Consistently, erastin has been shown to interact specifically with the xCT component of system x_c^- (Sato et al., 2018).

Promoter analysis determined that two AAREs (amino acid response elements), found in the 5'-flanking region of *SLC7A11* in murine NIH3T3 cells, were necessary for the maximal induction of xCT mRNA as a response to deprivation of not only cystine but other amino acids. Electrophoretic mobility shift assay found ATF4 to be involved in this amino acid control of *SLC7A11* transcription (Sato et al., 2004). Transcriptome analysis has identified 33 mRNAs upregulated and four mRNAs downregulated following erastin treatment in HT-1080 cells, changes that were reversed by co-treatment with β-ME. Several of the upregulated genes are associated with activation of the eIF2α-ATF4 pathway of the endoplasmic reticulum (ER) stress response (ERSR), whereby ER stress or amino acid deprivation causes the phosphorylation of the α subunit of translation initiation factor 2 (eIF2α). This decreases activity of the eIF2 complex and so inhibits synthesis of general proteins, but upregulates translation and expression of transcription factor ATF4. ATF4 upregulates the transcription of genes that enable adaptation of the cell to the ERSR. ATF4$^{-/-}$ MEFs were severely impaired in activating genes involved in amino acid import and metabolism and in protecting cells from oxidative stress (e.g. the glycine

transporter gene *Glyt1* necessary for GSH synthesis), including SLC3A2 at 63% that of wild-type MEFs. The researchers determined activation of the eIF2α-ATF4 pathway to be specific to the adaptation of cells to amino acid starvation. Erastin treatment was found to cause eIF2α subunit phosphorylation and ATF4 upregulation in HT-1080 cells which was reversed by co-treatment with actinomycin D, a transcriptional inhibitor. This delayed but did not ultimately prevent erastin-induced ferroptosis. This may suggest that intracellular cysteine deprivation due to inhibition of system x_c^- by the actions of erastin results in adaptation mechanisms due to the ERSR that include the upregulation of SLC7A11 and SLC3A2 translation, but that this adaptation is not substantial to overcome cell death. Alternatively, it could be that actinomycin D is not a potent transcription inhibitor under erastin-treated cellular conditions. This evidence may explain Kim et al.'s 2016 observation of nanoparticle-induced cell death under amino acid deprived conditions (Dixon et al., 2014; Harding et al., 2003).

Exploration of potential pharmacodynamic markers through RNA-Seq profiles found *CHAC1* (encoding cation transport regulator homolog 1) to be the gene most highly upregulated in erastin-treated HT-1080 cells, confirmed by quantitative-reverse transcriptase PCR (RT-qPCR). Upregulation of *CHAC1*, an ERSR gene downstream of ATF4, was found to be fully reversible by co-treatment with β-ME. Similar findings were determined when tested in 13 other cancer cell lines. Transcriptional upregulation was observed following treatment with SAS and erastin (system x_c^- inhibitors), but not RSL3, which acts downstream of system x_c^-. This suggests that induction of ERSR and *CHAC1* upregulation to be more sensitive to system x_c^- inhibition than cell viability. Actinomycin D and CHX both prevented increased *CHAC1* gene expression in erastin-treated HT-1080 cells, suggesting upregulated mRNA downstream of erastin treatment necessitates transcription and translation (Dixon et al., 2014). This may explain why CHX failed to inhibit RSL3-induced cell death in BJ-TERT/LT/RAS^{V12} and HT-1080 cell lines as observed by Yang and Stockwell (2008). Exactly why *CHAC1* mRNA increases following eIF2α-ATF4-driven adaptation signalling is elusive – upregulated translation of the CHAC1 protein has been found to degrade GSH by functioning as a γ-glutamyl cyclotransferase, thereby increasing availability of amino acids for further GSH synthesis and increased antioxidant capacity of the cell (Crawford et al., 2015; Tattoli et al., 2012). In contrast to a protective role, studies have found *CHAC1* upregulation to enhance apoptosis (Kumar et al., 2012; Mungrue et al., 2009).

Cysteine is a non-essential amino acid, meaning it can be synthesised within mammalian cells via the transsulfuration pathway, synthesising cysteine from methionine. Cells that utilise this pathway and bypass the need of cystine imported by system x_c^- are resistant to class I FINs. Genome-wide siRNA screening determined knockdown of *CARS* (the cysteine-tRNA synthetase) in HT-1080 cells increased

transsulfuration activity and allowed resistance to ferroptosis. Sensitivity was reinstated following *CARS* knockdown by transsulfuration inhibition. *CARS* is an enzyme that aminoacylates tRNA with cysteine for protein translation (Hayano et al., 2016).

GPX4 and Lipid Peroxidation

Subjection of polar and lipid metabolites extracted from erastin-treated HT-1080 cells to liquid chromatography-tandem mass spectrometry analysis determined levels of GSH and GSSG to be significantly depleted, whereas those of lysophosphatidylcholines (lysoPCs) (deacetylated phosphatidylcholines that act as an indicator of L-ROS generation via lipid peroxidation) were increased. Supplementation of culture medium with GSH prevented erastin-induced cell death. Furthermore, treatment of BJ-TERT/LT/ST/RAS^{V12} cells with three antioxidant inhibitors with varying mechanisms of action caused cell death that was independent of GSH depletion, C-ROS and L-ROS generation and selective lethality, suggesting ferroptosis cannot be initiated simply by targeting a cell's intrinsic antioxidant network. Moreover, BJ-TERT, BJ-TERT/LT/ST and BJ-TERT/LT/ST/RAS^{V12} cells were found to have differing basal GSH levels, but were depleted to a similar level following erastin treatment which caused cell death in only the latter cell line. Taken together, this evidence supports unique metabolic and biochemical changes occurring downstream of GSH depletion as underlying the selective induction of ferroptosis. One consequence considered by the researchers was the inactivation of GPXs by GSH depletion (Yang et al., 2014).

Activity of GPXs was examined by Yang et al. (2014) by monitoring the rate of NADPH (nicotinamide adenine dinucleotide phosphate) oxidation, using *tert*-butylhydroperoxide (tBuOOH) as a substrate. Decreased NADPH was observed in vehicle-treated BJ-TERT/LT/ST/RAS^{V12} cell lysates, indicating the reduction of tBuOOH. NADPH oxidation was prevented in lysates treated with erastin or BSO, suggesting these compounds to inactivate cellular GPXs and allow for the generation of C-ROS and L-ROS. Questioning the possible mechanism of action for RSL3, BJ-TERT/LT/ST/RAS^{V12} cells were treated with the compound and L-ROS generation was observed in a manner independent of GSH depletion. The researchers determined that the activity of RSL3 necessitated the chloroacetamide moiety of the compound; replacement with other electrophiles resulted in reduced potency, suggesting that RSL3 targets a protein containing a nucleophilic active site, e.g. serine, threonine, cysteine or selenocysteine.

GPX4 is an isoenzyme of the GPX family that contains selenocysteine (an amino acid differing from cysteine by a single atom) that is thought to enhance efficacy in redox reactions and provide higher reactivity. GPX enzymes catalyse the reduction of H_2O_2 and organic hydroperoxides to water or the

corresponding alcohols, making GPX4 a phospholipid hydroperoxidase. This reaction requires GSH as an essential cofactor, which is converted to oxidised glutathione disulphide (GSSG) in the process. GSSG can then be converted back to GSH by glutathione reductase at the expense of NADPH. GPX4 additionally reduces esterified oxidised fatty acids and cholesterol hyperoxides. Together, these GPX functions protect cells against oxidative damage (Conrad & Friedmann, 2015; Yang et al., 2014).

Affinity-based chemoproteomics identified GPX4 as the top candidate protein target for RSL3, confirmed by western blot analysis of GPX4 abundance. As mentioned, the ability to reduce cholesterol hyperoxides is unique to GPX4. No reduction of 7α-cholesterol hyperoxide (7α-cholesterol-OOH) to the corresponding alcohol (7α-cholesterol-OH) was observed following the treatment of L7G4 cells (a GPX4 overexpressing COH-BR1 breast cancer cell line clone) with RSL3, indicating the inhibition of GPX4. Furthermore, siRNA-mediated silencing of GPX4 strongly sensitised HT-1080 cells to RSL3, whereas GPX4 overexpression conveyed resistance. When tested in other cell lines, siRNA-mediated GPX4 silencing caused cell death selective to oncogenic HRAS-containing cell lines (Yang et al., 2014). Further evidence as to the importance of GPX4 in ferroptotic cell death was highlighted by the Friedmann et al. (2014) and Hambright et al. (2017) studies covered in the liproxstatin-1 section and by Chen et al.'s 2015 finding that neuron-specific ablation of *GPX4* resulted in rapid onset of paralysis and death in adult mice, which could be delayed by vitamin E supplementation.

As mentioned, lipid peroxides (of which there are two classes: lipid endoperoxides and lipid hydroperoxides, with the latter being of importance in ferroptosis) can be synthesised by iron-catalysed autoxidation of peroxyl radicals or iron-dependent activity of lipoxygenases, the products of which can act as signalling mediators at physiological levels (Zilka et al., 2017). Non-enzymatic autoxidation of lipids occurs in three distinct phases, like all radical reactions. During initiation, whereby radicals are produced from non-radical molecules, loosely ligated cellular ferrous iron and endogenously produced H_2O_2 undergo Fenton chemistry, generating ~~a hydroxide anion,~~ a hydroxyl radical and a peroxyl radical. During propagation, radicals further generate new radicals; the hydroxyl and peroxyl radicals abstract a hydrogen atom from the bisallylic methylene of membrane PUFAs and create a carbon-centred radical. This can then react with oxygen to generate a lipid peroxyl radical which continues to remove hydrogen from another bisallylic methylene, resulting in a lipid hydroperoxide and another carbon-centred, oxygen reactive radical. This reaction continues, generating more radicals. Termination of radicals can occur when the concentration is high enough for two radical molecules to react together and form new bonds to eliminate the radical or by

antioxidants – molecules able to donate electrons and stabilise the radical without becoming radicals themselves, of which GPX4 is an example (Gaschler & Stockwell, 2017).

Lipid peroxide degradation products can be grouped into hydroxy acids that arise from the direct reduction of lipid peroxide products, and reactive aldehydes. Lipoxygenase (LOX) enzymes are the main synthesisers of lipid hydroperoxides and can be viewed as akin to lipid peroxides in that these enzymes degrade PUFAs, generating lipid signalling mediators. The 5-LOX gene, encoded by *ALOX5*, oxidises the ω-6 PUFA AA at carbon 5 to form 5-HPETE (5-hydroperoxyeicosatetraenoic acid, also known as arachidonic acid 5-hydroperoxide), stimulated by increased Ca^{2+} levels within specific tissues. 12-LOX (1 and 2) and 15-LOX (1 and 2) similarly degrade AA to synthesise 12-HPETE and 15-HPETE, exhibiting incomplete regioselectivity in that 15-LOX 1 can convert AA to 12-HPETE in some cases. Degradation of linoleic acid by 12-LOX and 15-LOX similarly produces 9-HPODE (9-hydroperoxyoctadecadienoic acid) and 13-HPODE respectively. All -HPETE and -HPODE products are hydroxy acids (Gaschler & Stockwell, 2017). The major reactive aldehyde end-products are 4-HNE (4-hydroxynonenal) and MDA. As a secondary product of lipid peroxidation, studies suggest that the main precursors of 4-HNE synthesis in humans are 13-HPODE and 15-HPETE, arising from the enzymatic transformation of ω-6 PUFAs, although 4-HNE can be synthesised by various non-enzymatic pathways of PUFA degradation (Ayala et al., 2014; Schneider et al., 2001; Riahi et al., 2010). Production of MDA is less well characterised.

PUFAs are particularly vulnerable to oxidation due to the highly reactive hydrogen atoms in the bisallylic methylene carbon bridge, with those containing a pentadiene moiety reported as most susceptible (Gaschler & Stockwell, 2017). PUFAs are key structural components in the lipid membranes surrounding cells and organelles (including both the inner and outer mitochondrial membranes and rough and smooth ER), comprising the tail(s) of phospholipids (Agmon & Stockwell, 2017). Accordingly, lipid peroxides impose two general cytotoxic effects; extensive peroxidation of lipids alters the physical properties of lipid membranes by reorientating lipids, thus affecting lipid-lipid interactions, increasing membrane permeability and membrane fluidity, and altering ion gradients (Catala & Diaz, 2016). 4-HNE and MDA instead carry out covalent modifications that alter the furture and functions of proteins and nucleic acids. When generated at high levels, 4-HNE can induce programmed cell death (apoptosis or necroptosis) (Gaschler & Stockwell, 2017; Dalleau et al., 2013). Evidence suggests MDA to be the most mutagenic lipid peroxidation product and 4-HNE to be the most toxic (Esterbauer & Cheeseman, 1990). Taken together, this evidence highlights the necessity of functioning GPX4 enzymes to reduce lipid peroxides to the corresponding alcohol and prevent cell

death induced by products of lipid peroxidation, as is noted to underlie ferroptotic cell death (Gaschler & Stockwell, 2017).

How does ferroptosis differ from other known cell death pathways?

Morphology

Dolma et al. (2003) studied the nuclear morphology of BJ-TERT/LT/ST/RAS^{V12} cells treated with erastin using fluorescence microscopy. Karyorrhexis and margination of chromatin, as occurs in apoptosis, were not observed in these cells. Moreover, DNA fragmentation and the appearance of cleaved, active caspase 3 were also absent, and the rounded-up cells failed to exclude trypan blue, a dye used to assay cell viability. A lack of mitochondrial membrane potential observed using the potentiometric dye JC-1, provided confirmation that erastin induces cell death rather than cell detachment. Taken together, evidence is indicative of erastin inducing irreversible, nonapoptotic cell death. Further evidence is provided by Dixon et al. (2012), in which researchers used transmission electron microscopy (TEM) to determine that erastin-induced cell death in BJ-TERT/LT/ST/RAS^{V12} cells displayed no overlapping morphological features with STS-induced apoptosis, including chromatin condensation and margination, H_2O_2-induced necrosis (e.g. cytoplasmic and organelle swelling and plasma membrane rupture) or rapamycin-induced autophagy, which is characterised by the formation of double-membrane enclosed vesicles. The authors report that following erastin treatment, mitochondria appear smaller than normal and display condensed membrane densities with a vanishing or reduction of mitochondrial crista.

Bioenergetics

Dixon et al. (2012) note that following H_2O_2 treatment, BJ-TERT/LT/ST/RAS^{V12} and HT-1080 cells displayed a substantial intracellular ATP depletion - bioenergetic failure is characteristic of various forms of necrosis. This was not observed following treatment with erastin, STS or rapamycin.

Genetics

Using a customised library of 5,817 shRNAs targeting 1,087 mitochondrial genes, Dixon et al. (2012) found no significant correlation between shRNAs that rescue oncogenic *KRAS* Calu-1 cells from erastin-induced ferroptosis and those that rescue cells from STS-induced apoptotic cell death. This confirms that distinct genetic networks control each cell death pathway without overlap. Using HT-1080, Calu-1, BJ-TERT/LT/ST/RAS^{V12} and cells from 5 other cell lines, Stockwell and colleagues next identified six high-confidence mitochondrial genes required for erastin-induced ferroptosis –*RPL8*, *IREB2*, *ATP5G3*, *CS*, *TTC35* and *ACSF2*. When silenced using the most effective shRNA of each gene, all six genes

protected cells against erastin-induced ferroptosis by at least 40%, but offered no protection against STS-induced apoptosis, rapamycin-induced autophagy or cell death induced by MG132 (a proteasome inhibitor), camptothecin (a DNA-damaging agent), thapsigargin, the Ca^{2+}-dependent ATPase inhibitor, or rotenone, an inhibitor of complex I of the mitochondrial ETC.

But what do these genes do? *RPL8* codes for the L8 component of the large 60S ribosomal subunit in eukaryotic cells, a protein belonging to the L2P family of ribosomal proteins. Studies indicate that this gene is involved in osteosarcoma and HCC, although research is limited (Sun et al., 2015; Zhou et al., 2017). The involvement of *RPL8* in ribosomal structure could indicate an effect on protein translation when perturbed, consistent with Yang and Stockwell's 2008 report detailing the inhibition of erastin-induced ferroptosis by CHX, a translation inhibitor that prevents protein synthesis.

The *IREB2* gene codes for iron-responsive element-binding protein 2, also referred to as iron regulatory protein 2 (IRP2). This protein plays a critical role in controlling the expression of iron metabolism-related proteins via posttranscriptional regulation. The binding of IRP2 to iron-responsive elements (RNA motifs) in the 5' UTR of ferritin (H and L chain) or ferroportin, for example, inhibits translation of these proteins and thus prevents iron sequestration and export respectively. In contrast, the binding of IRP2 to IREs in the 3' UTR of transferrin receptor 1 (TRF1) or divalent metal transporter 1 (DMT1) mRNA prevents the degradation of these essential proteins and instead aids in the transportation and importation of iron (Galy et al., 2007). When further explored by Dixon et al. (2012), it was determined that shRNA-mediated silencing of *IREB2* and *FBXL5*, the negative regulator of IREB2, resulted in reciprocal changes in the expression of *TRFC* (transferrin receptor gene), *ISCU* (gene encoding the iron-sulfur cluster assembly enzyme), *FTH1* and *FTL* (encoding both subunits of ferritin), and an increase in erastin sensitivity.

ACSF2 codes for acyl-CoA synthetase family member 2, an enzyme that preferentially activates (by thioesterification to coenzyme A) 6 to 10 carbon medium-chain saturated fatty acids. The *CS* gene encodes citrate synthase, an enzyme localised within the mitochondrial matrix but encoded by nuclear DNA (Watkins et al., 2007; Suissa et al., 1984). Dixon et al. (2012) suggest that involvement of these genes in ferroptosis is due to their implication in the regulation of mitochondrial fatty acid synthesis described by Mullen et al. (2011), and the observation reported by Wise et al. (2008) that fatty acid synthesis in tumorigenic cells is in part dependent on the metabolism of glutamine to α-ketoglutarate. This process was determined by Wise et al. to be inhibited by the small molecule pan transaminase inhibitor aminooxyacetic acid (AOA). Dixon et al. (2012) reported the ability of AOA to rescue both HT-

1080 and BJ-TERT/LT/ST/RAS^{V12} cells from erastin-induced ferroptosis when the cells were cultured in media containing both glucose and glutamine, to levels mimicking the effect of silencing *CS* and *ACSF2*. Lethality was restored by cotreatment with dimethyl α-ketoglutarate (DMK), providing the metabolite whose production is blocked by AOA.

TTC35 encodes tetratricopeptide repeat protein 35, otherwise known as the *EMC2* gene encoding ER membrane protein complex subunit 2 (Shurtleff et al., 2018). The function of the resulting protein is currently unknown, although Shurtleff et al. (2018) determined the ER membrane complex (EMC) to bind and promote the synthesis of a range of multipass transmembrane proteins particularly transporters. No further details on the gene's involvement in ferroptosis is offered by Dixon et al. (2012) or any later papers published by Stockwell's group. ATP5G3 is now known as ATP5MC3 (ATP synthase membrane subunit c locus 3) and encodes the membrane-spanning F_0 complex subunit C3 (subunit 9), comprising the proton channel of mitochondrial ATP synthase (Carroll et al., 2019). An electrochemical gradient of protons across the inner mitochondrial membrane, established during oxidative phosphorylation, enables ATP synthase to catalyse the synthesis of ATP (Junge & Nelson, 2015). No reasoning is given by Dixon et al. (2012) for the involvement of this ATP generation-related gene in ferroptosis, despite reporting that bioenergetic failure determined by ATP depletion is not characteristic of erastin-induced ferroptosis as it is for H_2O_2-induced necrosis. Interestingly, percentage rescue conferred by silencing each gene is reported for HT-1080 cells treated with various death-inducing or cytostatic compounds, but not H_2O_2.

Ferroptosis *in vivo* and *in vitro*

To date, evidence of ferroptosis can be found *in vivo* and *in vitro* across multiple tissue/organ types. The studies detailed below in Table 1 offer a brief insight, categories by internal systems.

Table 1 - an overview, categorised by internal systems, of evidence of ferroptosis in vivo and in vitro

Tissue	Function	References
Cardiac	Induction of cardiac injury in mice results in molecular and transcriptional ferroptotic observations. Inhibition by Fer-1 or iron chelation therapy reduces cardiac injury *in vivo* and *in vitro*, whereas erastin treatment further exacerbates ferroptosis and resulting cardiac injury.	Fang et al. (2019); Fang et al. (2020); Tadokoro et al. (2020); Li et al. (2020a); Park et al. (2019); Menon et al. (2020); Li et al. (2020b); Baba et al. (2018).
	Ferroptotic cell death has been identified as initiating inflammatory responses following cardiac transplantation	Li et al., 2019.
Hepatic	Ferroptotic death of HCC cells induced by FINs including erastin, sorafenib or erastin and BSO cotreatment has been shown to occur via the canonical GPX4 downregulation pathway, preventable by DFOM or Fer-1 treatment and RNAi knockdown of ferroptosis-related genes. Evidence suggests downregulation of pRB promotes ferroptotic cell death *in vivo* following sorafenib treatment, compared to tumour stabilisation observed in control animals. Ferroptosis-related gene signature has been suggested to provide prognostic prediction in HCC.	Sun et al. (2015); Shang et al. (2020); Liang et al. (2020); Lippmann et al. (2020); Louandre et al. (2015); Louandre et al. (2013); Lachaier et al. (2014); Li et al. (2020c); Tang et al. (2019).
	Liver damage, lipid peroxidation and upregulation of *PTGS2*, a ferroptosis marker, were observed in a mouse model of hepatic I/R and were prevented by Fer-1, DFOM or α-tocopherol. Fer-1 also inhibited inflammatory responses, whilst a high iron diet exacerbated I/R injury. Indicators of I/R were also found in a study of 202 human liver transplant donors, including high serum ferritin level.	Yamada et al. (2020); Chen et al. (2020).
	Magnesium isoglycyrrhizinate (MgIG), artemether and artesunate have independently been determined to attenuate hepatic injury and reduce fibrotic scar formation in rodent models of liver fibrosis. *In vitro*, both induced ferroptosis in hepatic stellate cells via iron accumulation, GSH depletion, lipid peroxidation and *PTG S2* upregulation. Fer-1 and DFOM prevented these ferroptotic changes and abolished the anti-fibrosis effect.	Sui et al. (2018); Kong et al. (2019); Wang et al. (2018).
Gastrointestinal	The drug apatinib has been found to induce ferroptosis via lipid peroxidation in gastric cancer (GC) *in vitro* and *in vivo*. Regulation of intracellular AA and adrenic acid (AdA) levels has been suggested to act as a critical checkpoint in the ferroptotic pathway, evidenced in GC cells, whereas silencing cysteine dioxygenase 1 inhibited erastin-induced ferroptosis *in vitro* and *in vivo*, restoring cellular GSH and reducing ROS and MLA production. Chemotherapy drug resistance in GC has been linked to the inhibition of ferroptosis via ALOX15 targeting by cancer-associated fibroblasts.	Zhao et al. (2021); Lee et al. (2020); Hao et al. (2017); Zhang et al. (2020a); Gao et al. (2020).
	Various FINs have been determined to induce ferroptosis in colorectal cancer (CRC) cells via SLC7A11-mediated GPX4 inactivation and ROS production and the AMPK/mTOR signalling pathway, *in vitro* and *in vivo*.	Sui et al. (2018); Zhang et al. (2020b); Xia et al. (2020); Park et al. (2018); Sharma et al. (2020); Xu et al. (2020).

	Ischemia immediately following intestinal reperfusion promotes ferroptotic cell death, associated with protein and lipid peroxidation. Inhibition by Lip-1 ameliorated I/R-induced intestinal injury and distant organ damage, and ACSL4 inhibition prior to reperfusion was found to be protective against ferroptotic cell death.	Li et al. (2019); Wu et al. (2021).
Lung	Sorafenib has been found to significantly inhibit growth of small cell lung cancer (SCLC) cells and result in cell death. Fer-1 ad DFOM prevented cell death, and accumulation of iron and L-ROS was observed. mRNA expression levels of SLC7A11 were significantly downregulated with sorafenib treatment. Evidence also suggests a potential role in the treatment of non-small cell lung cancer.	Iida et al. (2020); Bebber et al. (2020); Li et al. (2020d); Gai et al. (2019).
Kidney	Induction of acute kidney injury (AKI) is followed by iron accumulation, elevated lipid peroxidation and upregulation of ferroptosis-associated genes and proteins. AKI can be alleviated by ferroptosis inhibitors including Fer-1 and Lip-1. Vice versa, GPX4-deficient mice have been shown to die of acute renal failure within 2 weeks of depletion.	Ma et al. (2020); Wang et al. (2021); Guo et al. (2020); Hu et al. (2020); Friedmann et al., 2014.
	Renal I/R resulted in upregulated MDA levels *in vivo* and tubular cell death characteristic of ferroptosis, via the MAPK/ERK pathway. Tubular cell death can be inhibited by XJB-5-131	Su et al. (2019); Linkermann et al. (2014); Huang et al. (2019); Zhao et al. (2020).
	Prior to the identification of ferroptosis, sorafenib was approved by the FDA to treat renal cell carcinoma. These cells have been determined as highly sensitive to the depletion of glutamine and cystine, and silencing of enzymes required for GSH biosynthesis or GPX4 reduce viability of cells. GSH and GPX4 inactivation has been determined to result in ferroptosis and block tumour growth in a murine model of renal cancer. Ferroptosis-related genes have been identified as a model of prognostic prediction.	Wilhelm et al. (2006); Miess et al. (2018); Yang et al. (2019); Wu et al. (2020).
	Adrenocortical carcinomas (ACCs) have similarly been determined as highly sensitive to ferroptosis and display elevated levels of GPX4 expression. One explanation provided is the active synthesis of steroid hormones; steroidogenic cells were significantly more sensitive to RSL-3-mediated GPX4 inhibition and resulting cell death, whereas inhibition of steroidogenesis reversed these observations.	Belavgeni et al. (2019); Weigand et al. (2020).
Pancreas	A wide range of known and novel FINs have been found to induce ferroptosis in pancreatic cancer cells via the KRAS/ERK signalling pathway and mediated by cysteine depletion, which can be inhibited by Fer-1 and DFOM. Pancreatic ductal adenocarcinoma patient mRNA expression studies indicate a dependency on antioxidant homeostasis and increased LIP.	Eling et al. (2015); Song et al. (2019); Yamaguchi et al. (2018); Ye et al. (2020); Wang et al. (2019); Badgley et al. (2020).
Nervous system	In terms of AD, hydroxylated chalcones 14a-c have been determined to inhibit ferroptosis induced by RSL-3 and erastin, whilst loss of ferroportin has been linked to memory impairment by ferroptotic promotion. Post mortem brain tissue studies have provided evidence of iron	Cong et al. (2019); Bao et al. (2021); Ashraf et al. (2020); Cheng et al. (2020).

	dyshomeostasis, upregulated xCT (implying impaired GSH metabolism) and lipid peroxidation. Evidence of ferroptosis has been found underlying a number of other neurodegenerative diseases.	
	A rodent study determined unilateral, transient middle cerebral artery occlusion (MCAO) to suppress haemorrhagic tau and increase iron levels, suggesting tau-mediated iron export to prevent ferroptotic damage after ischemic stroke. ICH induction in mice is significantly attenuated by Fer-1, increasing the number of surviving neurones and decreasing injury volume compared to control animals, translating to significantly reduced neurological deficit and decreased limb muscle weakness.	Tuo et al. (2017); Li et al. (2017); Zille et al. (2017)
	In a controlled cortical impact injury (representative of traumatic brain injury), mice receiving baicalein (12/15-LOX inhibitor) showed decreased ferroptotic markers and improved outcome compared to control animals. Similar results were observed using SRS16-86.	Kenny et al. (2019); Zhang et al. (2019); Xie et al. (2018);

Is there a role for ferroptosis in Parkinson's?

A potential underlying cause of ferroptosis in PD pathology is encouraged by evidence demonstrating individual interactions of ferroptotic characteristics in the disease, including upregulated iron levels, system x_c^- inhibition, GSH depletion and GPX4 inactivity. The first study demonstrating ferroptotic cell death in a DAergic immortal cell line model of PD was published by Do Van et al. (2016), and will be outlined below.

Dysregulated iron has long been reported in PD. As mentioned previously, inhibition of erastin-induced ferroptosis by iron chelators (e.g. DFOM) and the involvement of GPX4 in this cell death pathway led to the consensus that iron is required for catalysing ROS generation via Fenton chemistry and the iron-dependent activity of lipoxygenases in the production of lipid hydroperoxides. Upregulated iron levels in PD has been reported by many, including He and colleagues (2015). The group utilised quantitative susceptibility mapping MRI and observed elevated iron levels in the bilateral SN and in the red nucleus contralateral to the limb most affected by clinical features in 44 early-stage PD patients compared to controls. It has been reported by Yang and Stockwell (2008) that levels of iron importer TfR1 are upregulated in cancer cells that display sensitivity to ferroptosis, although little evidence points to a role for TfR1 in PD. An alternative iron importer, DMT1 has instead been implicated in the disease by many groups. One example is Salazar et al. (2008), who found DMT1 expression to be upregulated in the ventral mesencephalon of an MPTP-treated mouse model, concomitant with the accumulation of iron and oxidative stress ultimately resulting in DAergic

neurone loss. With the discovery of ferroptosis being a relatively new development and with little experimental evidence currently available, the release of excess iron from endosomes into the cytoplasm via DMT1 under ferroptotic conditions cannot be ruled out as underlying the degeneration of DAergic nigrostriatal neurones in PD. Interestingly, Shi et al. (2010) report *IREB2*$^{-/-}$ mice to develop iron accumulation in white matter tracts and nuclei of different brain areas, as well as severe neurodegeneration in cerebral Purkinje cells.

Studies into the role of system x_c^- in PD are limited. Massie et al. (2010), however, report of mice lacking xCT (the subunit specific to system x_c^-) as less susceptible to 6-OHDA-induced SNpc degeneration in comparison to age matched controls, despite observing no decrease in striatal GSH levels or signs of increased oxidative stress. The authors attribute this protective effect to the 70% decrease in striatal extracellular glutamate levels.

The high oxygen demands of the brain results in high ROS generation resulting from ATP synthesis. CNS membrane phospholipids are highly enriched in PUFAs, making neurones particularly vulnerable to lipid peroxidation (Chen et al., 2008). BSO is an inhibitor of glutamylcysteine ligase, the first enzyme incorporated in the synthesis of GSH. Depletion of GSH utilising BSO has been found to decrease accumulation of exogenous DA (Drukarch et al., 1996), and increase the death of TH-positive neurones following MPTP treatment by 18.5% (Wullner et al., 1996). Whilst depletion of GSH alone was unable to cause nigrostriatal degeneration in rats (Toffa et al., 1997), depletion under oxidative stress conditions has been demonstrated to cause neuronal loss via altered mitochondrial complex I activity (Chinta et al., 2007). Activity of this complex is reduced in PD and has been demonstrated as vital to survival of DAergic neurones (Greenamyre et al., 2001). Evidence from humans suggests PD patients in the early stages of disease have significantly lower levels of GSH in the SN compared to controls (Jha et al., 2000).

Consistently, post-mortem studies indicate levels of GPX4, which was found to be colocalised with neuromelanin in the SN, to be significantly reduced in the SN of PD patients compared to controls but increased relative to the cell density of surviving neurones in the region, indicating a possible compensatory protective role (Bellinger et al., 2011). Interestingly, electrophilic DA quinones, produced from the autooxidation of DA by monoamine enzymes, were found to react with the selenocysteine residue of GPX4 and decrease the enzyme's activity in a dose-dependent manner. This was confirmed following the observation of GPX4 degradation in PC12 cells treated with DA (Hauser et al., 2013). DA quinones are considered one explanation underlying the vulnerability of DAergic

neurones to cell death (Giguere et al., 2018). Consistently, post-mortem evidence suggests basal rates of lipid peroxidation, determined by MDA levels, are increased in the SN of PD patients (Dexter et al., 1989). This is supported by Agil et al. (2006) who additionally suggest L-dopa to play an antioxidant role. Interestingly, Shamoto-Nagai et al. (2007) reports the presence of acrolein-modified aSyn in the DAergic SN neurones of PD patients. Acrolein is an aldehyde product of lipid peroxidation, which the authors suggest modified aSyn and proteolysis-associated proteins in a manner increasing aSyn aggregation and impairing the proteolysis system, ultimately resulting in the death of these neurones.

In the first study relating ferroptosis to PD, Do Van and colleagues (2016) report the increased generation of L-ROS (and to a lesser extent C-ROS) in Lund human mesencephalic (LUHMES) cells in response to increasing concentrations of erastin, whereas total glutathione (GHS/GSSG) concentration decreased. SH-SY5Y cells (a human neuroblastoma cell line) were reported as resistant to ferroptosis. In terms of solute carriers, the researchers reported an overexpression of SLC7A11 mRNA following erastin treatment and an upregulation of SLC7A5 mRNA, which the group suggested to be compensatory. Post-mortem studies revealed the SN to overexpress genes of all solute carrier isoforms in PD brains compared to those of controls. The same was found to be true of the striatum, though with fewer differences. In contrast to Dixon et al. (2012), Do Van et al. (2016) found the Ca^{2+} chelator, BAPTA, to inhibit erastin-induced cell death in LUHMES cells, as did BisII, an inhibitor of PKC (protein kinase c) activation. Interestingly, manumycin A, which abolishes basal RAS activity, was unable to inhibit cell death. Confirming this, a western blot performed using anti-PKCα and anti-phospho-PKCα antibodies determined erastin treatment to cause PKCα phosphorylation in these cells. Using PKC isoform-specific siRNAs, the researchers found that only siRNAs against PKCα were able to protect cells from ferroptotic cell death. In comparison, inhibition of PKCε was ascertained as harmful to cells at higher concentrations of erastin. Since activation of PKCα can activate MEK downstream, these findings suggest LUHMES cells to be sensitive to ferroptotic cell death in a manner independent of RAS activation but requiring the activation of PKCα, seemingly consistent with the consensus that the activation of the RAF-MEK-ERK pathway allows for ferroptosis signalling. This is supported by the finding that U0126, a MEK1/2 inhibitor, blocked ferroptosis following erastin treatment, and Fer-1 and DFOM inhibited PKCα phosphorylation, preventing cell death. No other studies to date have been published linking ferroptosis to PD.

Summary

To summarise, PD is an insidious disease characterised by the presence of intracytoplasmic inclusions of aggregated aSyn known as Lewy bodies and the degeneration of DAergic neurones of the

nigrostriatal pathway (Xicoy et al., 2017). Symptoms display as both motor and non-motor, although diagnosis relies substantially on the former (National Health Service, 2016a). Current therapies allow for symptomatic relief but have no effect on disease progression and are themselves associated with substantial complications (Martinez-Ramirez et al., 2015). PD is predicted to affect 9 million individuals by 2030 (Dorsey et al., 2006).

The identification of ferroptosis arose from the discovery of erastin, a small molecule selectively lethal to tumorigenic cells possessing oncogenic RAS (Dolma et al., 2003). RSL3 and RSL5 were identified 5 years later and whilst erastin and RSL5 were determined to have a similar mechanism of action, that of RSL3 was determined as unique (Yang & Stockwell, 2008). The first inhibitor of ferroptosis, Fer-1, was identified in 2012 and determined to be an ROS scavenger. Fer-1's antioxidant capacity was proven to prevent ferroptosis in various cell types and experimental conditions (Dixon et al., 2012; Li et al., 2017). Since then, second- and third-generations ferrostatins with improved properties for *in vivo* experimentation have been developed (Skouta et al., 2014; Linkermann et al., 2014).

Recent evidence suggests erastin's ferroptosis-inducing ability is primarily determined by binding to the xCT component of system x_c^- and inhibiting cystine uptake (Dixon et al., 2012). This prevents the cysteine-dependent biosynthesis of GSH, an observation supported by the study of radiolabelled cystine (Dixon et al., 2014). Compounds inhibiting this system are categorised as class I FINs. Cells with machinery to utilise the transsulfuration pathway are resistant to class I FINs (Yang et al., 2014; Hayano et al., 2016). Class II FINs including RSL3 instead inhibit GPX4, a phospholipid hydroperoxidase enzyme found downstream of system x_c^- which utilises GSH to protect cells against oxidative damage (Yang et al., 2014; Conrad & Friedmann, 2015). Inhibition of GPX4 causes a build-up of lipid peroxides synthesised by iron-catalysed autoxidation of peroxyl radicals or iron-dependent lipoxygenase activities. These radicals propagate, creating lipid hydroperoxides, and cause damage to the cell's lipids, proteins and DNA (Gaschler & Stockwell, 2017).

But how does ferroptosis differ from other cell death pathways? Studies by Stockwell's group report distinct morphology of ferroptotic cells, most notably shrunken mitochondria (Dixon et al., 2012). Moreover, six mitochondrial genes have been identified as associated with the genetic network underlying ferroptosis which display no overlap to those underlying the genetic control of other cell death pathways (Dixon et al., 2012). A potential role for ferroptosis in PD is to date based on overlapping characteristics, including dysregulated iron levels, an involvement of system x_c^- and GPX4, GSH depletion and increased levels of lipid peroxidation (Haacke et al., 2015; Massie et al., 2011;

Hauser et al., 2013; Jha et al., 2000; Shamoto-Nagai et al., 2007). Do Van and colleagues (2016) determined ferroptosis to occur in erastin-treated LUHMES cells in a manner dependent on PKCα phosphorylation.

The aim of this Master of Philosophy project is to determine whether there is a potential role for ferroptosis as a cell death pathway in an *in vitro* SH-SY5Y model of PD, and hypothesise that there will be a significant difference between erastin concentration, the concentration of compound B and time conditions in terms of cell viability percentage relative to the control.

Materials and Methods

Chemicals and materials

Maintenance media is composed of DMEM/F12 (Dulbecco's Modified Eagle Medium with nutrient mixture F12 at a 1:1 ratio) with L-glutamine, supplemented with 10% (50 ml) heat-inactivated foetal calf serum (FCS; 60^{o}C for 30 minutes to inhibit serum haemolytic activity), 1% (5 ml) non-essential amino acids (NEAA) and 1% (5 ml) penicillin/streptomycin. Differentiation media is used to differentiate immature SH-SY5Y cells into a mature neuronal phenotype and genotype, and is comprised of the above in addition to 500 µl of 10 µM retinoic acid (RA) in 500 ml of media. For a period during experimentation, use of a different medium base was utilised (RPMI-1640) and was composed of FCS, NEAA and penicillin/streptomycin as outlined above. All materials were purchased from Corning (United Kingdom) and Thermo Fisher (United Kingdom). The experimental compounds (erastin, AACOCF$_3$, DHA, BEL and Fer-1) were purchased from Cayman (United Kingdom), and those utilised in cell viability assays (trypsin, trypan blue, PBS), MTT and DMSO (dimethyl sulfoxide)) purchased from Lonzo (United Kingdom) and Sigma Aldrich (United Kingdom). PBS, or phosphate-buffered saline, is a water-based salt solution comprised of disodium hydrogen phosphate and sodium chloride (Thermo Fisher, undated).

Type 1 collagen solution derived from rat tail, sodium cacodylate buffer, glutaraldehyde, osmium tetroxide, ethanol solutions at 70%, 80%, 90% 100% and 100% dry, NSA (nonenyl succinic anhydride), ERL, DER (diglycidyl ether of polypropylene glycol), DMAE (dimethylaminoethanol), chloroform, uranyl acetate and lead citrate were purchased from Sigma Aldrich (United Kingdom) and Thermo Fisher (United Kingdom).

Cell line

Cryotubes containing cells from the SH-SY5Y human neuroblastoma cell line (American Type Culture Collection (ATCC), USA) at passage 8 were removed from storage in liquid nitrogen vapour, where the cells had been maintained at -80^{o}C, and placed in a water bath at 37^{o}C to rapidly thaw. Once thawed, the cells were transferred to a 15 ml centrifuge tube and 9 ml of maintenance media, as described above, added. The cells were then centrifuged at 1000 RPM (revolutions per minute) for 5 minutes before the supernatant cryopreservation media was removed and 10 ml of fresh maintenance media added. A pipette was used to gently agitate the cell pellet from the bottom of the tube and resuspend the cells. 100 µl of cell suspension was transferred to a micro tube and 100 µl of trypan blue added to count the cells using a haemocytometer under a light microscope in a process that will be described below. The remaining cell suspension was seeded into T25 cell culture flasks (5 ml per flask) at a concentration of 2x10^{5} and stored in a humidified tissue culture incubator at 37^{o}C with 5% CO_2. Maintenance media was changed the following day and then every other day. Once having reached approximately 70-80% confluency, the cells were diluted 1:3 and split into T75 flasks (Starstedt, UK), requiring 20 ml of maintenance media per flask. Splitting of confluent flasks continued until the cells reached passage 25, after which cryotubes of low-passage cells were again removed from storage.

Cell counting and cell seeding

To count cells for seeding or for trypan blue cell viability analysis, cells were dissociated from the electrostatic forces of the flask surface by incubation with 10 ml of trypsin per T75 for approximately 60 seconds. Dissociation was checked using light microscopy to ensure cells were not over-incubated. 10 ml of maintenance media was then added to allow the FCS to neutralise the dissociative effects of the trypsin. The suspension was transferred to a centrifuge tube and 100 µl of suspension again transferred to a 500 µl micro tube. The centrifuge tube was centrifuged, whilst 100 µl of trypan blue was added to the micro tube.

The haemocytometer was cleaned using methylated spirits and a glass coverslip moistened with water applied so that it adhered to the haemocytometer. 20 µl of cell suspension/trypan blue mixture was carefully pipetted between the coverslip and the haemocytometer and placed under the light microscope. After adjusting the resolution and focus, a gridded structure can be seen, and the white cells in all four highlighted quadrants (see Fig. 12) were counted, excluding blue cells and those touching the thicker boarder lines.

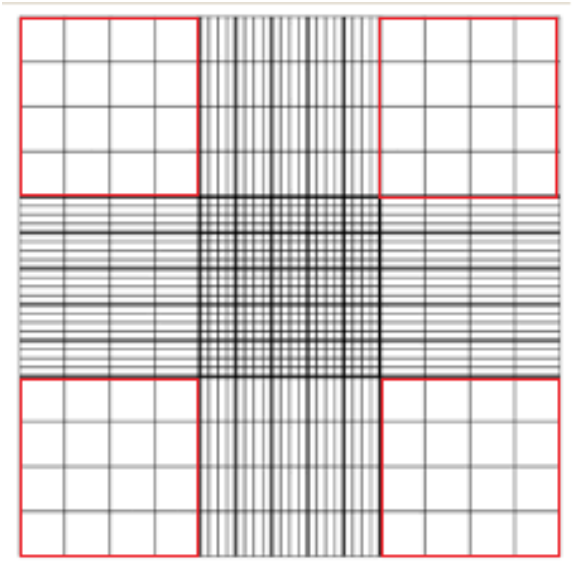

Figure 12 *– an image of the haemocytometer gride whereby the number of cells in the highlighted red quadrants is used to determine cell concentration in a volume of cell suspension.*

The number of cells was then halved to account for the 1:1 ratio of trypan blue and cell suspension and then multiplied by 10^4. This volume was divided by the desired concentration (for example, $1x10^5$ for MTT plating) and multiplied by the volume of cell suspension in the centrifuge tube, resulting in the volume of media required to resuspend cells at the desired concentration. The equation can be simplified to $C_1V_1 = C_2V_2$, whereby C_1 and V_1 are the starting concentration and volume, and C_2 (known) and V_2 are the final concentration and volume (V_2 is the volume of media the cells are required to be resuspended in to give the desired concentration). As an example, whereby 344 cells have been counted in the quadrants:

a. $$344 \div 2 = 172.$$

b. $$172 \times 10^4 = 1.72 \times 10^6 \leftarrow C_1$$

c. $$\left(\frac{1.72\times10^6}{1\times10^5}\right) \times 10.5\ ml = 206.4\ ml \leftarrow V_2$$

(V_1 points to $10.5\ ml$; C_2 points to 1×10^5)

The supernatant was removed from the tube and cells resuspended in differentiation media, again gently agitating the cell pellet (see Fig. 13 for undifferentiated cells and differentiated cells).

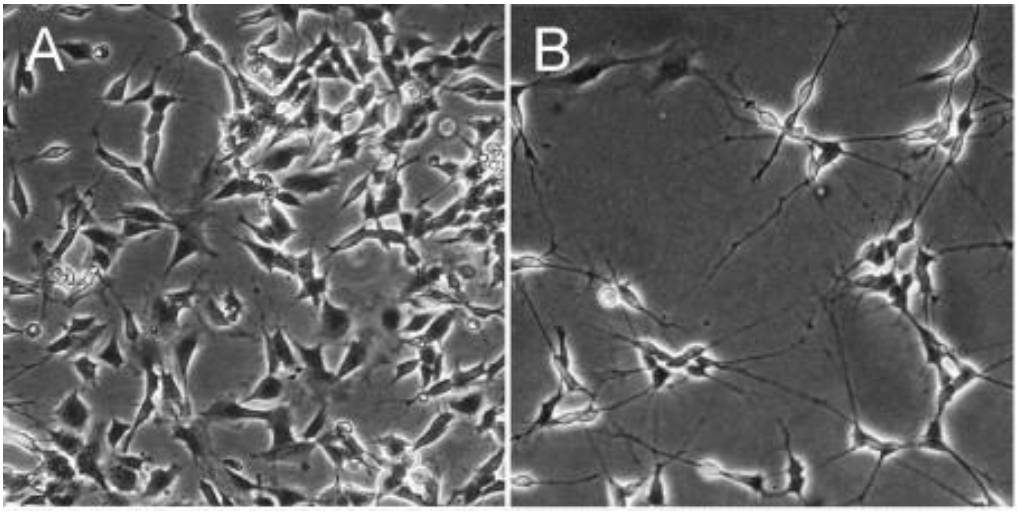

Figure 13 *– image of A. undifferentiated SH-SY5Y cell and B. SH-SY5Y cells differentiated with 10 µM RA for 3 days. Image taken from Xun et al. (2012).*

MTT

Cells suspended in differentiation media were seeded in 96-well plates (Starstedt, UK), utilising the inner 54 wells (six rows of nine wells; 100 µl cell suspension per well), at a density of $1x10^5$ as determined using the calculation previously described. The cells were incubated for 5 days (maintenance media being replaced every other day) before the cells were treated with the compound(s) of interest at the appropriate concentration, and returned to the incubator. Four of the plates were incubated for 24 hours and the other four for 48 hours. For the experiments utilising only erastin (n = 18), 96-well plates were set up to allow for triplicate replication, whereby the average output for every 3 wells is averaged and treated as a single value so that plates designed as in Fig. 14 provides 3 values for 0 µM, 3 values for 2 µM and so on, where the green number if the number of values provided per plate and the pink value denotes the concentration of erastin in each well. Given this design, 6 plates in total were utilised to provide the data for the 24-hour condition and an additional 6 plates for the 48-hour condition.

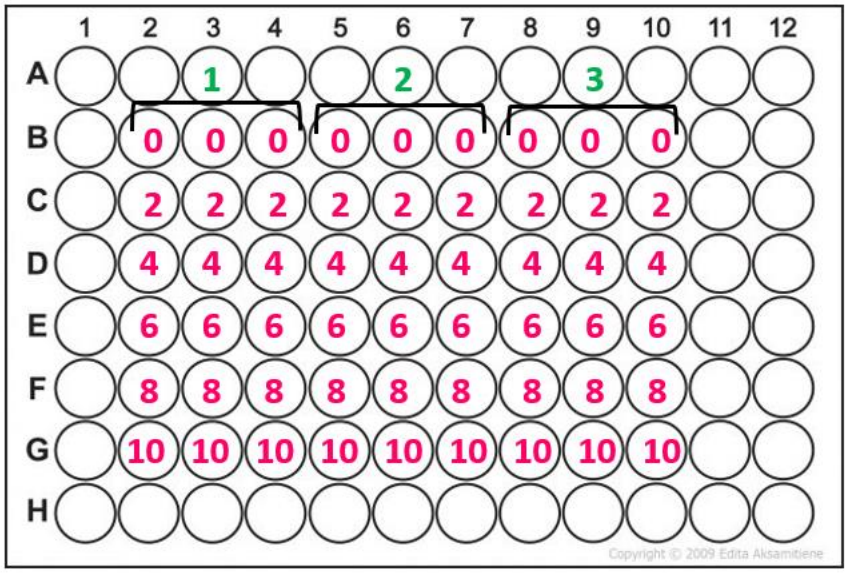

Figure 14 *– a diagram depicting the layout of cell treatments in the erastin-only experiments in a 96-well plate. The green number denotes n, so n = 3 (requiring 2 plates for n = 6) and the pink number denotes the concentration in μM of erastin.*

In the experiments utilising the IC_{50} concentration of erastin for each time condition (6 μM for the 24-hour condition and 4 μM for the 48-hour condition) in combination with an additional experimental compound (n = 6), plates were instead set up as seen in Fig. 15, again allowing for triplicate replication. In Fig. 15a, the green number again denotes the number of experimental values derived from the plate (6 total) and the pink the concentration of erastin in each well – this is the erastin control plate where no other compound (DHA, for example) is present. One plate was designed in this manner per time condition per additional compound, therefore 2 plates for the DHA condition. In Fig. 15b is the plate representing the control plate of the additional compound, whereby 0 μM of erastin is present and concentrations of 0.1 μM, 1.0 μM and 10 μM DHA has been added to each well, for example, again with triplicate replication offering n = 6 so 2 plates designed in this manner per additional compound (1 plate for each time condition). Similar in design to Fig. 15b, Fig. 15c and Fig. 15d are the experimental plates whereby 6 μM has been used for the 24-hour condition (see Fig. 15c) and 4 μM for the 48-hour condition (see Fig. 15d), in combination with 0.1 μM, 1.0 μM and 10 μM of the additional compound in each plate.

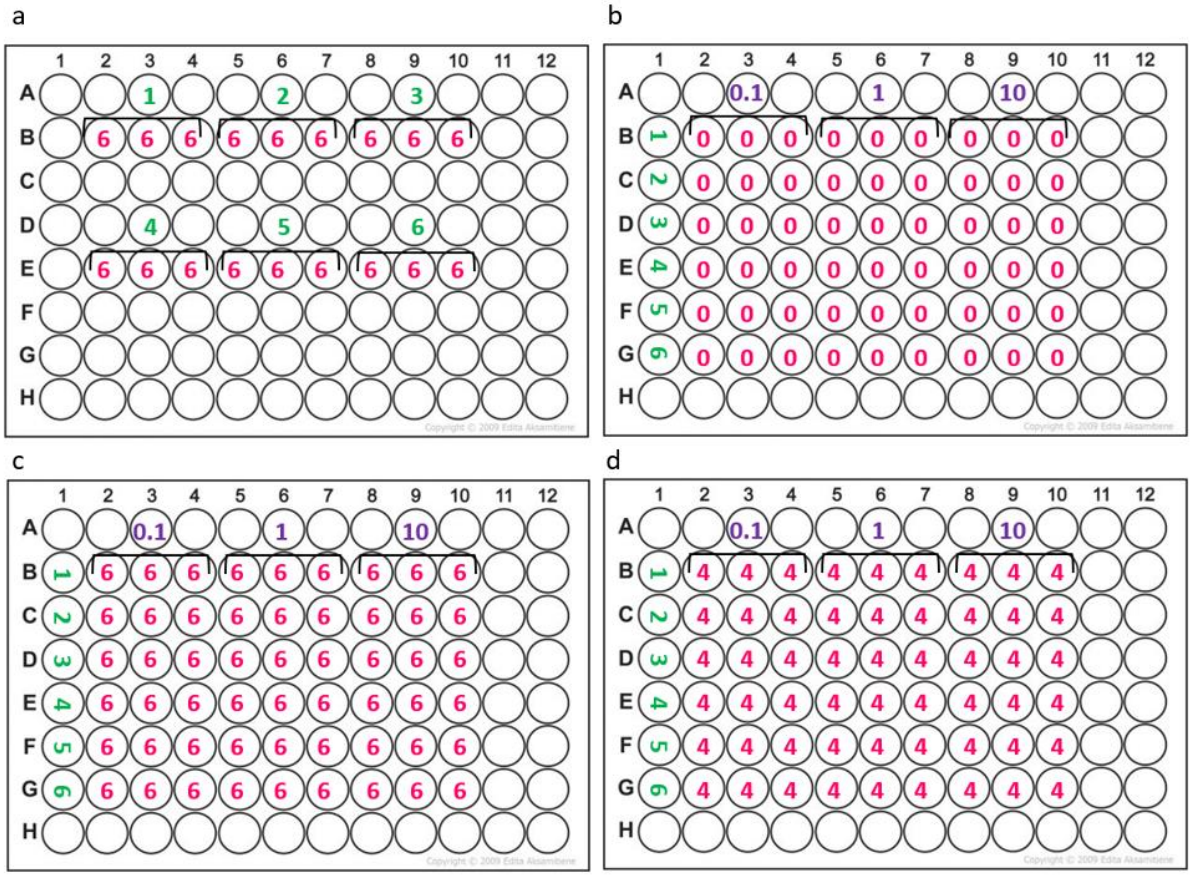

Figure 15 *– a diagram depicting the layout of cell treatment layouts in the experiments utilising erastin in combination with a second compound. a: triplicate replication (green number denotes n, so n = 6) of erastin alone (pink number denotes concentration erastin) in the 24-hour condition. b: triplicate replication of 0 µM erastin with 0.1 µM, 1 µM and 10 µM (purple number denotes concentration of second compound) of the second compound. This layout of the 96-well plate was utilised in both the 24-hour and 48-hour time conditions. c: triplicate replication of 6 µM erastin with 0.1 µM, 1 µM and 10 µM of the second compound. This layout was used in the 24-hour time condition. d: triplicate replication of 4 µM erastin with 0.1 µM, 1 µM and 10 µM of the second compound. This layout was used in the 48-hour time condition.*

When the treated plates had been incubated for the designated time, 20 µl of MTT was added to each well and the plates replaced in the incubator for 2 hours. The required volume of MTT, stored at -20°C, was made up in PBS at a concentration of 5 mg/ml, vortexed for 2 minutes to ensure maximal dissolution of MTT powder in the PBS, and then sterilised by syringe filtration into a second 15 ml centrifuge tube. Throughout this procedure, MTT-containing tubes remained wrapped in aluminium foil so as to avoid light exposure. After the 2-hour incubation period, the solution was removed from each well and replaced with 100 µl of cell culture grade DMSO before the plates were transferred to an orbital shaker for 15 minutes to allow the dye to dissolve in the solution. The plates were then individually placed in a Tecan Infinite M200 pro plate reader and the absorbance of each cell-containing well determined spectrophotometrically at 565 nm. Following the advice of others, excess MTT made up in PBS was kept in a centrifuge tube wrapped in aluminium foil, labelled with the date

it was made up, and stored in the fridge at 4°C for no longer than a month so as to ensure avoidance of unwanted MTT oxidation whilst also preventing the unnecessary waste of MTT solution.

Developed by Mosmann in 1983 and later modified by van Rensburg and colleagues in 1997, the 3-(4, 5-dimethylthiazon-2-yl]-2,5-diphenyltetrazolium bromide (MTT) assay is a colorimetric enumeration assay that, in dividing cells including the SH-SY5Y cell line used, quantifies cell growth inhibition, and is often employed to measure the *in vitro* cytotoxic effects of drugs on immortal cell lines or primary cells. MTT is a water soluble yellow tetrazolium salt that is reduced to purple water insoluble formazan (E,Z)-5-(4,5-dimethylthiazol-2-yl)-1,3-diphenylformazan) crystals within the mitochondria of living cells by NADPH-dependent oxidoreductase enzymes. Reducing agents and enzymes located in organelles including the ER are also involved to a lesser degree. Given that the intensity of purple colour is directly proportional to the number of cells with maintained reductive capacity, formazan concentration reflected in optical density can be utilised to determine cellular growth inhibition (as a measure of cell viability) when compared to the optical density of wells containing untreated control cells, as a percentage. Using logarithmic concentrations of the compound of interest (e.g. 0.1 µM, 1.0 µM and 10 µM as was used in this project), a dose-response curve can be plotted (Mosmann, 1983; van Rosenburg at el., 1997; van Meerloo et al., 2011; Kuete et al., 2017; Lu et al., 2012; Stockert et al., 2012).

Trypan blue

When counting cells for data collection, cells were seeded at a concentration of $1x10^5$ in 12-well plates (Starstedt, UK), following the procedure outlined above. The cells were then allowed to differentiate for 5 days before treatment and, having been incubated with the treatment for the desired time, the media (containing dead and mitotic cells) from each well was removed and transferred to the allocated 5 ml micro tube. The wells were washed 5 times each with 100 µl PBS and the PBS transferred to the appropriate micro tube before incubation with trypsin. Upon cell dissociation, the trypsin was removed and again transferred to the appropriate micro tube. Micro tubes were centrifuged, supernatant removed and resuspended in 100 µl of media. 100 µl of trypan blue was added and all cells (white and blue) counted. The white cells were then counted again and this number removed from the total cells, to give the number of dead cells (blue) and those alive (white). From this data, the percentage of dead cells for each treatment condition was calculated relative to the total number of cells.

IC_{50} concentrations were calculated using AAT Bioquest IC_{50} online calculator. Statistical analysis was performed using a two-way ANOVA without replication, performed in Microsoft Office Excel 2016. This statistical test was chosen due to this data set having two independent variables – erastin concentration or concentration of the second compound (with six levels or four respectively) and time (two levels). Degree of freedom is calculated as 'a – 1' (a = number of groups) and the degree of freedom for the denominator is 'N – a' (N = total number of subjects).

TEM

Cell preparation

Circular aclar film placed in 8 wells of a 24-well plate were coated in 0.01% collagen in distilled water for 5 hours before 500 µl of SH-SY5Y cell suspension at a concentration of $1x10^6$ in differentiation media was plated into each aclar-containing well. Differentiation media was changed daily due to the high cell concentration to ensure maximal cell survival. On day 5 following plating, cells in half of the wells were treated with 500 µl of maintenance media, as the control condition, and the remaining 4 wells were treated with 500 µl of 6 µM erastin prepared in maintenance media. The choice to use only 6 µM erastin in the experimental condition instead of the multiple concentrations as were utilised in the MTT assays was based on this being the approximate IC_{50} concentration as determined by MTT (and should thus provide an adequate number of live and dead cells).

Fixation

After 24 hours of treatment, the wells were washed 3 times for 5 minutes each with EM grade 0.1 M sodium cacodylate buffer before 500 µl of 2.5% glutaraldehyde in sodium cacodylate was added to each well for 1 hour. The cells were again washed 3 times for 5 minutes each with sodium cacodylate buffer and stored overnight (approximately 16 hours) at 4^oC in 0.1% glutaraldehyde. The following day, the cells were washed 3 times for 5 minutes with sodium cacodylate buffer before 1% osmium tetroxide (OsO_4) in 1 ml of sodium cacodylate was added to each well for one hour. After another 3 washes of 5 minutes each with sodium cacodylate buffer, the cells were covered with 70%, 80%, 90%, 100% and then 100% dry ethanol for 15 minutes each.

Resin development

The cells were coated with 100% dry ethanol with Spurr resin at a ratio of 3:1 for 2 hours, before replacement with a 1:1 ratio overnight. The following day, the well contents were replaced with 1:3 100% dry ethanol to Spurr resin overnight and then coated in pure Spurr resin, changed every 2 hours. One cell-coated aclar circle from each concentration was then selected for transfer to planchettes

(based on the fewest disruptions to the cell layer, for example having not folded over) and cured in an oven for approximately 40 hours at 70°C.

Spurr resin is composed of 13 g of NSA (nonenyl succinic anhydride; a hardener specifically purified from EM usage), 5 g of ERL (a low viscosity cycloaliphatic epoxy embedding medium), 3 g of DER (diglycidyl ether of polypropylene glycol; an epoxy resin flexibiliser) and 0.2 g of S-1 (dimethylaminoethanol, or DMAE, an accelerator that allows for higher transparency in the resulting blocks and induces rapid cure at 70°C) for half quantity (doubled for full quantity), stirred for 30 minutes with a metal electric stirrer at a moderate rate, to avoid air mixing into the resin (Wallis & Griffin, 1973; Electron Microscopy Sciences, undated).

Hardened resin blocks were removed from the metal planchettes and divided into smaller sections (allowing for the selectivity of section with highest cell coverage) using a razor blade and hammer, before being mounted in a chuck of the Reichert Ultracut E ultramicrotome. The chuck was then mounted into a flat stage and orientation adjusted.

Knife making

To make the knife, specialised knife glass was first cleaned with Decan 90 and washed with hot water. With the coarse edge down, the glass was cut to approximately an inch and a half long, rotated 90 degrees, scored with a razor and broken in half to produce two triangular shapes. Careful not to touch or otherwise mar any edges, the pieces were removed from the machine using a metal fork and inspected under microscope. The most appropriate glass piece was chosen for use, determined by sharpness and evenness of the edge. The knife was modified utilising metal tape placed at an angle and wax to create a boat. This boat was then filled with water so that the water just touched the edge of the knife.

Sectioning

Ultrathin sections were taken longitudinally utilising a glass boat in the ultramicrotome, with the knife being replaced when sections no longer appeared iridescent on the water or approximately every 15 minutes, to ensure the edge of the knife remained sharp and resulted in high quality sections. Sections were expanded using chloroform vapor before being transferred to a grid that had been cleaned with chloroform and stored in a grid box. Having collected roughly 6 grids of sections from both erastin conditions, the grids were left to dry overnight before staining.

Staining

Wax was placed in a petri dish and 6 dots of 30 µl of uranyl acetate pipetted onto the wax. All grids from the 0 µM erastin condition were fully submerged into the dots and left for 20 minutes. The grids were then individually dipped in 30% ethanol (rinse 1) 20 times and rinses 2 and 3 (both distilled water) 20 times each, before distilled water in a wash bottle was directed onto the forceps to gently wash the grids with the stream. Excess water was removed by carefully blotting the grid around the section with filter paper and then grids immersed into spots of lead citrate, formed on wax atop potassium hydroxide pellets in a second petri dish and left for 5 minutes each. Each grid was then dipped 30 times in distilled water, washed with water directed down the forceps and excess water removed using filter paper. The grids were placed back into the grid box until ready to image.

Imaging

The grid was then inserted into the specimen stage and returned to the vacuum. When visible on the monitor, the TEM stage was adjusted to allow for increased resolution of the sample. Having found a cell, a scale bar was inserted. The images obtained using an SYS Systems® megaview III camera using analysis® software and processed using Adobe Photoshop® Whilst searching for mitochondria, few dead cells were noticed. 50 cells were chosen at random in both the treated and untreated conditions and determined as dead or alive, so as to determine cell death percentage.

Sample analysis

With shrunken mitochondria being the present gold standard morphological characteristic of cells having undergone ferroptosis, those TEM images offering captured mitochondria were analysed by determining the length (diameter) of the transversely orientated mitochondria. Using IC Measure software, images of mitochondria (taken at magnifications ranging from 10k to 40k) were uploaded and the line tool used to measure each mitochondria (8 in the untreated condition identified across 4 cells and 11 mitochondria in the treated condition identified across 6 cells, chosen at random following the assumption of transverse orientation) by drawing a line from one side to the other. Another line was then drawn for the scale bar in the bottom right corner of the TEM image and the two lines compared to determine the length of the organelle based on the length of the scale bar. To account for the simplicity of this measuring technique and limitations of the software (mainly difficulty in viewing the perimeter of the image when zoomed in), the calculated lengths were rounded to the nearest 0.05 µm. The length of the mitochondria was then averaged for those in treated and untreated cells. It was assumed that those mitochondria selected were of correct orientation and that this measurement was related to actual mitochondrial length.

Results with MTT

MTT analysis of cell viability

MTT data was compiled and analysed so that a mean value was determined per three MTT output values, allowing for triplicate replication. Compilation of these means was then utilised to calculate mean variance from that of the control in each data set. From this data, dose-response curves for the erastin treatment at 24- and 48-hours were plotted, and IC_{50} values (the concentrations at which 50% of cell growth is inhibited) calculated as 5.64 µM and 3.40 µM respectively (see Fig. 16). For ease of concentration calculations, these IC_{50} concentrations were rounded to 6 µM and 4 µM respectively, and it is these concentrations that were used in subsequent experiments utilising erastin in combination with additional compounds (see Fig. 17 for erastin and DHA, Fig. 18 for erastin and $AACOCF_3$ (left) and BEL (right) and Fig. 19 for erastin and Fer-1). It should be noted that these co-treatment graphs are plotted as cell viability relative to the absolute control of 0 µM erastin and 0 µM of the second compound.

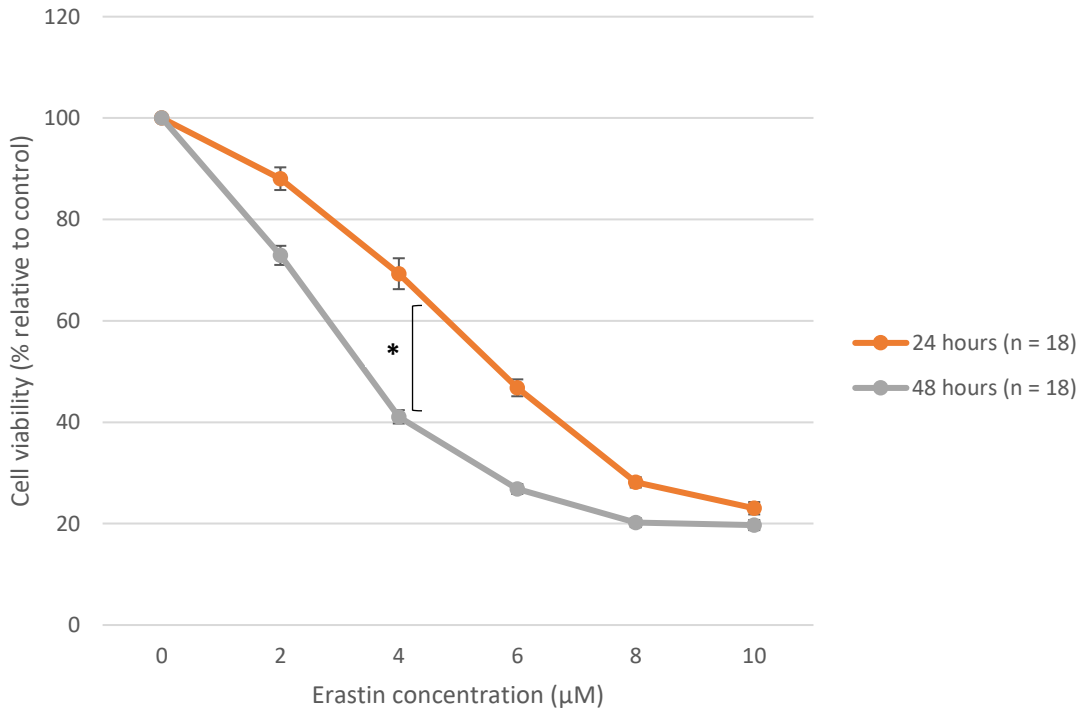

Figure 16 *– Dose-response curve of erastin concentration (0 µM to 10 µM) for the 24-hour time condition (orange line) and 48-hour condition (grey line), determined by cell viability as a percentage relative to the control calculated from MTT data (6 plates, 3 replicates per value, n = 18). Error bars denote standard error from the mean. * denotes a significant difference between time conditions of* $p < 0.05$.

Comparison of erastin's effect on cell growth inhibition in the 24-hour condition to the 48-hour condition determined there to be a significant difference between erastin concentrations (F (5, 102) = 35.47, $p < 0.001$) and time conditions (F (1, 106) = 8.12, $p < 0.05$).

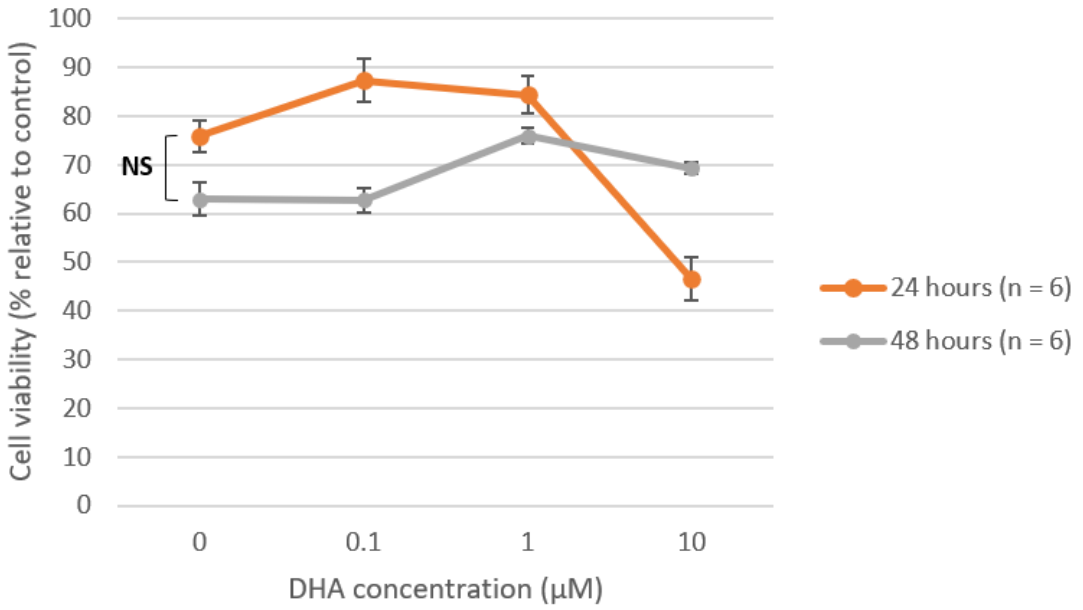

Figure 17 *– Dose-response curve of erastin for the 24-hour time condition (orange line, 6 µM) and 48-hour condition (grey line, 4 µM) with logarithmic concentrations of DHA (0 µM, 0.1 µM, 1 µM and 10 µM), determined by cell viability as a percentage relative to the control (0 µM erastin and 0 µM DHA) calculated from MTT data. Error bars denote standard error from the mean. NS denotes there being no significant difference between time conditions.*

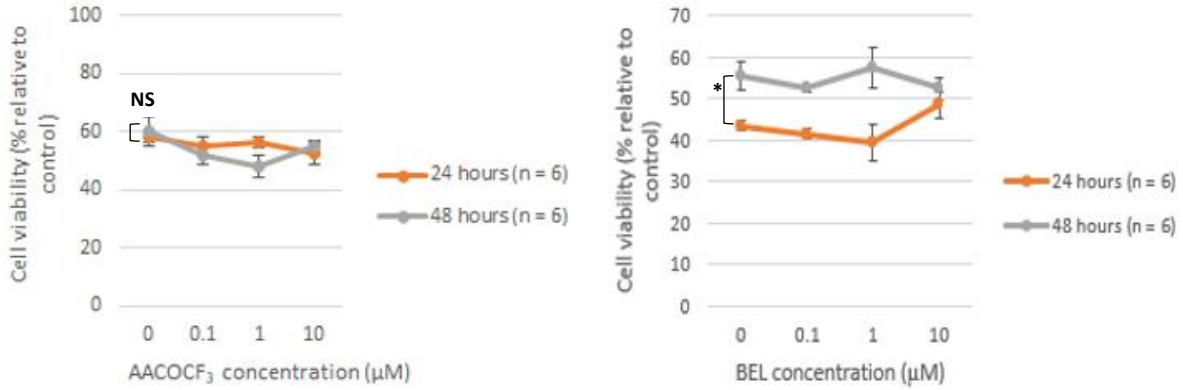

Figure 18 *– **Left**: Dose-response curve of erastin for the 24-hour time condition (orange line, 6 µM) and 48-hour condition (grey line, 4 µM) with logarithmic concentrations of $AACOCF_3$ (0 µM, 0.1 µM, 1 µM and 10 µM), determined by cell viability as a percentage relative to the control (0 µM erastin and 0 µM $AACOCF_3$) calculated from MTT data. **Right**: Dose-response curve of erastin for the 24-hour time condition (orange line, 6 µM) and 48-hour condition (grey line, 4 µM) with logarithmic concentrations of BEL (0 µM, 0.1 µM, 1 µM and 10 µM), determined by cell viability as a percentage relative to the control (0 µM erastin and 0 µM BEL) calculated from MTT data. Error bars denote standard error from the mean. NS denotes no significant difference and * denotes a significant difference of $p < 0.05$ between time conditions.*

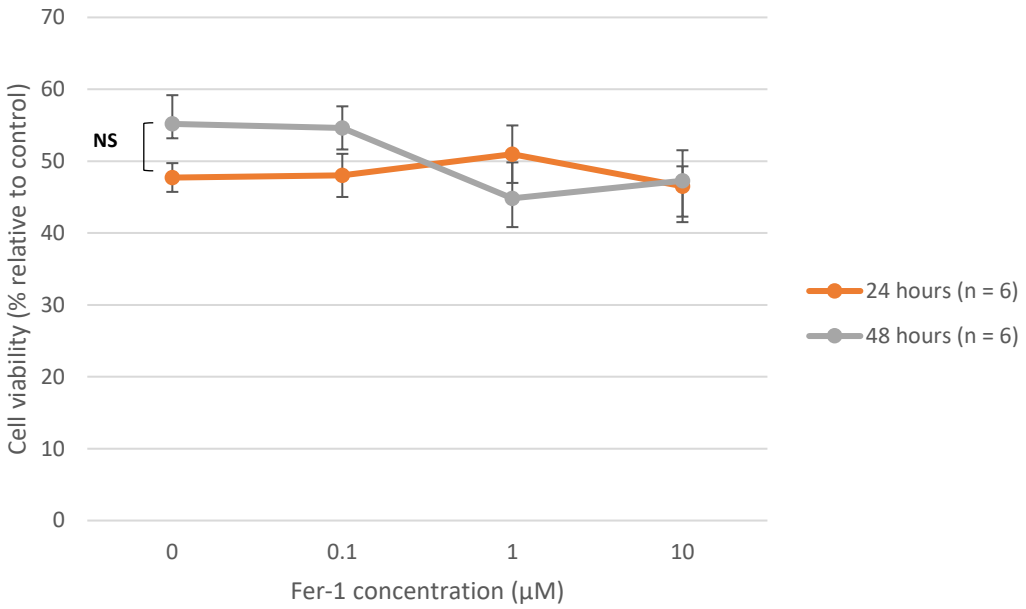

Figure 19 *– Dose-response curve of erastin for the 24-hour time condition (orange line, 6 µM) and 48-hour condition (grey line, 4 µM) with logarithmic concentrations of Fer-1 (0 µM, 0.1 µM, 1 µM and 10 µM), determined by cell viability as a percentage relative to the control (0 µM erastin and 0 µM Fer-1) calculated from MTT data. Error bars denote standard error from the mean. NS denotes a lack of significant difference between time conditions.*

Comparison of MTT data sets derived from cells treated with 6 µM erastin for the 24-hour condition and 4 µM erastin for the 48-hour condition, in combination with a second compound, also utilised a two-way ANOVA. From the DHA data set, analysis determined there to be no significant difference in terms of time condition (F (1, 10) = 0.12, $p > 0.05$) or DHA concentration (F (3, 20) = 0.48, $p > 0.05$). Data from the $AACOCF_3$ data set was determined as not significantly different both in terms of time condition (F (1, 10) = 0.72, $p > 0.05$) and $AACOCF_3$ concentration (F (3, 20) = 1.88, $p > 0.05$). In the BEL data set, there was determined to be a significant difference in term of time conditions (F (1, 10) = 15.08, $p < 0.05$) but not for BEL concentration (F (3, 20) = 0.27, $p > 0.05$). Lastly, the Fer-1 data set resulted in no significant difference in terms of time conditions (F (1, 10) = 3.62, $p > 0.05$) and Fer-1 concentration (F (3, 20) = 2.13, $p > 0.05$).

Discussion

The data depicted in Figure 16 suggests erastin induces cell death in the SH-SY5Y cell line that is statistically significant both in terms of concentration and time. When cells were co-treated with erastin and DHA, $AACOCF_3$ or BEL, moderate cell death was observed (Figs. 17 – 19) although the lack of significance in terms of concentration and time ($p > 0.05$) for all additional compounds suggests this is due to the effect of erastin. Moreover, the lack of significant difference ($p > 0.05$) when cells were co-treated with Fer-1 suggests cells were dying via a pathway other than ferroptosis.

Whilst this is a possible explanation, various other factors, including the reliability of MTT as a cell viability assay, must be brought into question. Evidence provided by Fotakis and Timbrell (2006) determined MTT to be the most sensitive test compared to the lactate dehydrogenase (LDH) assay, a protein assay and the neutral red assay, revealing cytotoxicity of cadmium chloride in HepG2 cells 3 hours following treatment. In the second hepatoma cell line, HTC, only the neutral red assay was capable of detecting early cytotoxicity of $CdCl_2$ following a 3-hour incubation period. However, Lobner (2000) instead reports that despite both LDH and MTT assays accurately determining apoptotic cell death in neurones, the MTT assay was of limited value in quantifying the neuroprotective effects of anti-apoptotic agents. This evidence suggests that the suitability of the MTT assay as a method of quantifying cell viability is determined by multiple factors.

Sylvester (2011) warns of parameters affecting cellular metabolism and other factors that can significantly modify MTT-specific activity, resulting in the calculation of false high or false low cell counts. Control of these parameters is thus paramount for the optimal utilisation of MTT. Firstly, an MTT standard curve needs to be characterised for the cell line(s) being used – metabolic activity varies greatly between cell lines and thus effects the reduction rate of the tetrazolium salt to formazan by mitochondrial oxidoreductase enzymes. Standard curves are created by seeding various concentrations of cells (typically 5×10^4 to 1×10^6) in triplicate and performing MTT on the plates after the cells have been allowed to adhere. Measuring the optical density of the plates at 570 nm, zeroed against blank wells (containing 0 cells/well), allows for a linear graph to be plotted showing the relationship of formazan concentration to that of the cells. Moreover, Sylvester notes the importance of establishing the optimal MTT concentration and exposure time for each cell line, explaining that different cell types display a wide variability in dose- and time-response in maximal formazan production. Studies by Mosmann (1983) and Denizot and Lang (1986) using various cell lines suggest an optimal concentration of 0.83 mg/mL MTT, but reported standardised concentration of 1mg/mL to be an acceptable compromise in that this concentration provided excellent results whilst remaining cost-effective; a steep increase in formazan production was reported between 0 and 1 mg/mL but concentrations between 2 mg/mL and 4 mg/mL resulted in a plateau. Sylvester next cautions that glucose depletion in culture medium can significantly reduce MTT-specific activity, advising MTT to be performed in the presence of fresh media to obtain optimal formazan production. Moreover, the red-coloured pH indicator commonly added to cell culture media, phenol red, is noted as having an absorbance overlapping with formazan that may affect optical density readings, resulting in a high background in blank samples and false highs in wells containing treated cells. The use of phenol red-

free media would allow avoidance of this problem. Lastly, drugs or other chemical agents affecting mitochondrial respiration, or that cause metabolic uncoupling, would result in a false low or large false high in MTT-specific activity compared to control wells, respectively.

Others, however, suggest that MTT is not the best assay for cell enumeration and must be complemented by a second assay. Li et al. (2012) report of a zebrafish embryo screen identifying 59 toxic compounds from a library of 502 natural compounds and MTT assay identifying 21, indicating zebrafish to be a reliable and highly efficient screening tool that could complement MTT. The zebrafish screen involved placing 5 embryos per well in a 96-well plate at 24 hours post-fertilisation and incubating the embryos with the compound of interest in Hank's salts. Utilisation of this assay to complement MTT may raise moral and ethical concerns, however, and thus other assays should instead be used. The use of complementary haemocytometer counts of cells stained with trypan blue using light microscopy, as was performed in this study, has been supported by groups including Kwizera et al. (2017).

Alternatively, some suggest MTT to be an outdated tool and that more accurate cell enumeration assays that have since been developed should be utilised in place of MTT. Van Tonder and colleagues (2015) compared MTT to three other cell enumeration assays – neutral red assay, resazurin reduction (RES) and sulforhodamine B (SRB). Of the four assays, MTT was determined to observe the largest variation, implying MTT would be unable to detect small changes in cell number. SRB not only produced the lowest variance in terms of IC_{50} but was also found to give the most reproducible results. Interference was noted in the MTT assay for three glycolysis inhibitors, limiting the use of MTT, but none of the three other enumeration assays evaluated. This evidence suggests that rather than MTT, which has long been regarded as the gold standard of cytotoxicity assays, SRB should instead be considered the superior assay. This is supported by Sliwka et al. (2016) who determined MTT to be less reliable than CVA (crystal violet staining), resulting in a false negative for one anticancer compound and a false positive for another. Interestingly, Lu et al. (2012) studied the effect of MTT itself in SH-SY5Y cells, and determined that MTT reduction could induce cell death, the severity of which was closely related to incubation time in that the exocytosis of intracellular granules and the formation of higher concentrations of needle-like formazan crystals caused the loss of plasma membrane integrity in a larger percentage of cells – 120 minutes of incubation with MTT resulted in 70% of cells having lost membrane integrity. The authors determine cell death to have occurred at incubation periods as low as 30 minutes with 0.5 mg/mL MTT, suggesting these conditions to be the maximum utilised for experimentation *in vitro*, at least when using the SH-SY5Y cell line. However, the

use of 5 mg/mL with an incubation period of 120 minutes did not result in total cell death in this experimental project, as Lu and colleagues suggest should have occurred, and control cells provided an output within the expected range. This suggests that whilst a lower concentration of MTT and a shorter incubation period may have been more cost effective, time efficient and have resulted in more desirable read outs, Lu et al.'s study should be taken as advice rather than a direct warning.

The use of MTT assay to quantify the viability of cells following treatment with erastin has been demonstrated by many groups. Dahlmanns and colleagues (2017) determined 5 μM and 10 μM erastin to significantly reduce cell viability ($p < 0.01$ and $p < 0.001$ respectively) in rodent hippocampal cells comprised mainly of neurones and astrocytes. Similarly, Huo et al. (2016) report 10 μM erastin to significantly reduce cell viability of HT-29 colorectal cancer cells. Evidence provided by Wang et al. (2019) suggests concentrations of erastin up to 1 μM as sufficient to reduce cell viability of ATF3-expressing HT-1080 cells and empty vector control cells by 50%. Regarding the investigation of erastin in SH-SY5Y cells utilising MTT, only two studies could be found. Treatment of wild-type, empty vector transfectants and mitochondrial ferritin transfectant SH-SY5Y cells with 10 μM erastin for 24 hours resulted in significant cell death in all three conditions compared to untreated control cells (Wang et al. 2016). The studies by Dahlmanns et al. (2017), Huo et al. (2016) and Wang et al. (2016) support the evidence provided by this experimental project of erastin concentrations of 6 μM (24-hour condition) and 4 μM (48-hour condition) resulting in significant cell death, although no IC_{50} concentrations were reported in any of the above studies for direct comparison.

Although none of the steps outlined by Sylvester (2011) or Lu et al. (2012) as required to perform an optimal MTT assay were undertaken in this project, it is important to note that MTT analysis of cell viability was performed the same way each time, resulting in consistently collected data. The maintenance of consistency ensured the data provided by each plate and the data sets could be compared with each other whilst avoiding significant variability in terms of methodology. It is, however, important to note the effect of factors beyond my control. One factor may have been the concentration of MTT; the scales used to measure MTT prior to dissolving in PBS measured in grams, and thus 40 mg required to make 8 ml of MTT solution would be 0.04 g. This would inevitably lead to some inaccuracy in concentration. For example, it would not be easily apparent if 45 mg of MTT, for example, was used instead of 40 mg, as both would give readings of 0.04 g. Moreover, the use of MTT avoids the obvious ethical issues of utilising animal embryos in experimentation associated with the zebrafish embryo assay, for example, as utilised by Li and colleagues in their 2012 paper. Taken together, the evidence provided demonstrates the varied conclusions research groups have come to

in their evaluation of the use of the MTT assay, highlighting the difficulty in coming to one overall opinion of this technique. It is therefore important to acknowledge the reassurance that could be gained from performing other assays alongside MTT and drawing conclusions from multiple cell enumeration techniques, as was done in this study – MTT data determined erastin to have an IC_{50} of 5.64 μM for the 24-hour condition and 3.40 μM for the 48-hour condition in SH-SY5Y cells, whereas trypan blue assay determined these concentrations to inhibit cell growth by a reduced rate of 99% and 96% respectively, relative to the control.

Results with Trypan Blue

Trypan blue exclusion viability assay

As with MTT, erastin 24-hour and 48-hour trypan blue data was analysed with triplicate replication as mean variance from that of the control, as seen in Fig. 20. IC_{50} concentrations determined by trypan blue experiments were 25.0 μM and 117.9 μM respectively (see Fig. 21). The data outlined in Fig. 20 demonstrated minimal cell death, resulting in IC_{50} concentrations significantly higher compared to those determined from MTT cell viability data. As with MTT, trypan blue assay was also performed utilising erastin (although with the MTT-determined IC_{50} concentrations) with DHA (see Fig. 22), $AACOCF_3$ and BEL (see Fig. 23), and Fer-1 (see Fig. 24).

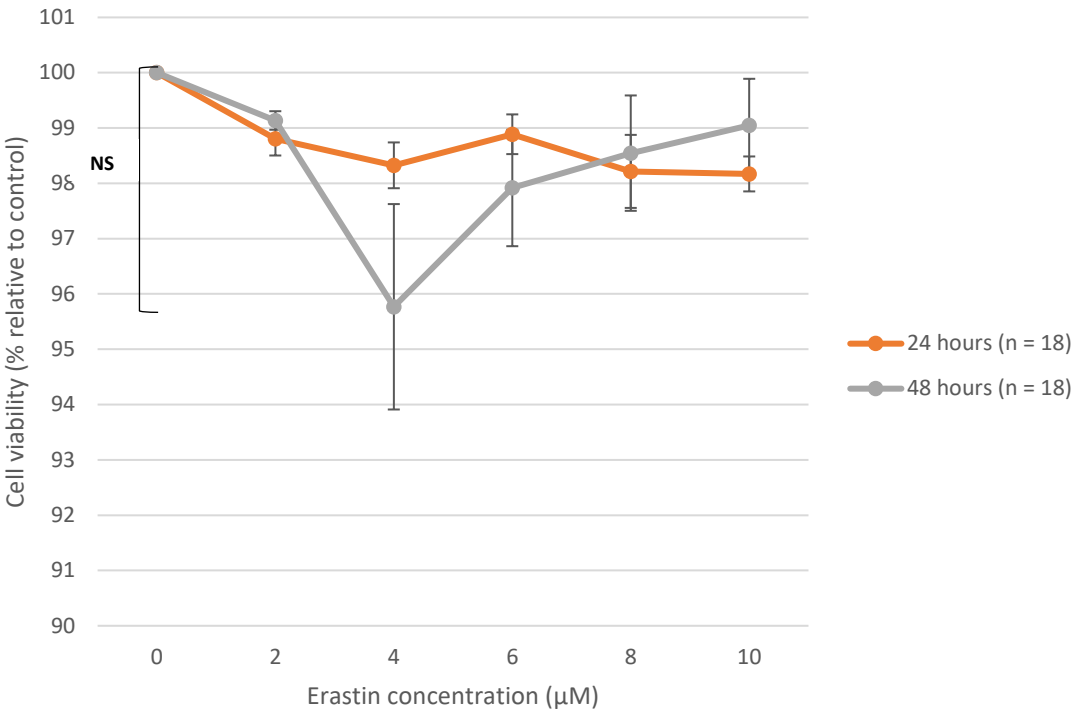

Figure 20 *- Dose-response curve of erastin for the 24-hour time condition (orange line, 6 µM) and 48-hour condition (grey line, 4 µM), determined by cell viability as a percentage relative to the control, calculated from trypan blue data. Error bars denote standard error from the mean. NS denotes a lack of significant difference between time conditions.*

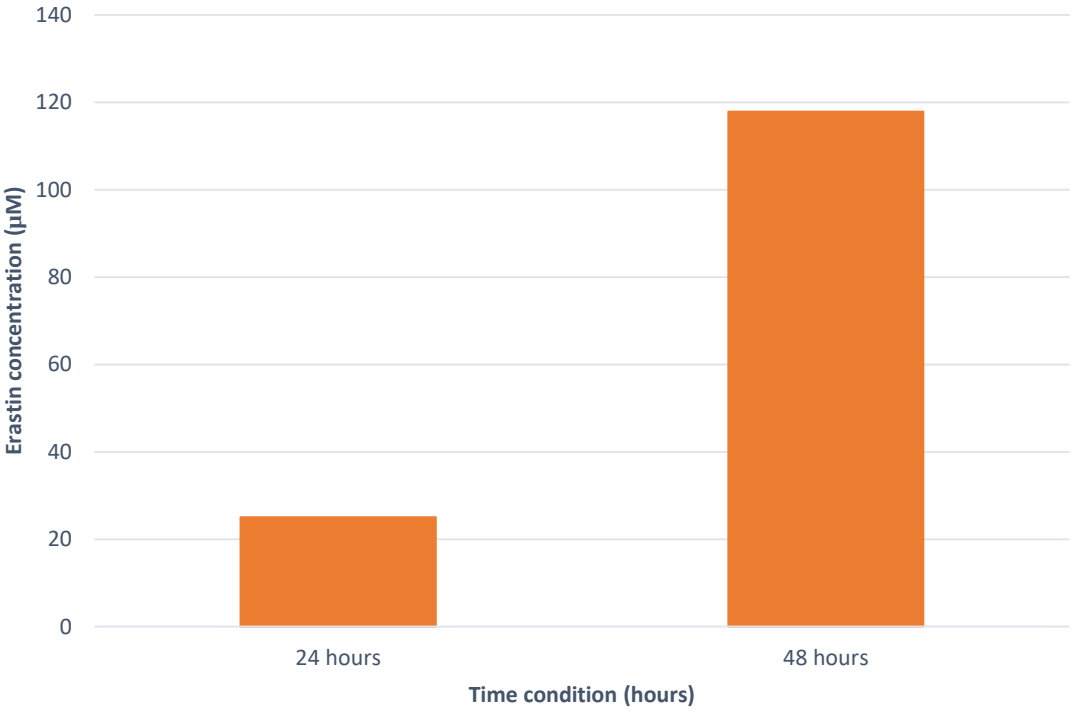

Figure 21 *– IC_{50} concentrations of erastin at 24 hours and 48 hours, calculated from trypan blue cell viability analysis data.*

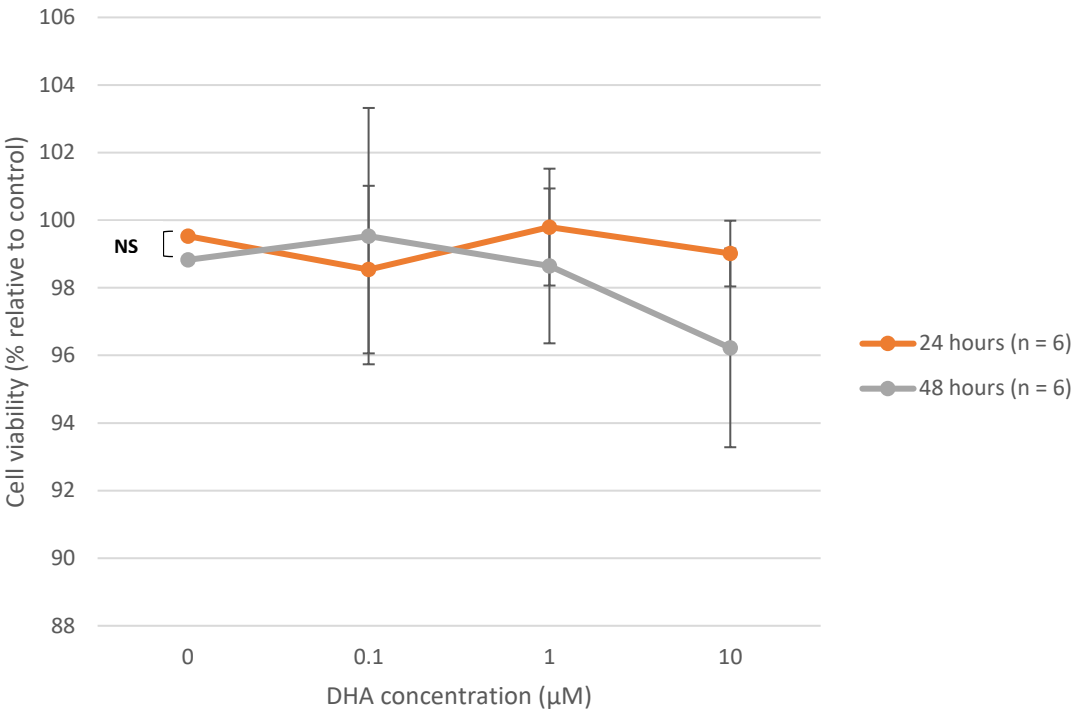

Figure 22 *- Dose-response curve of erastin for the 24-hour time condition (orange line, 6 µM) and 48-hour condition (grey line, 4 µM) with logarithmic concentrations of DHA (0 µM, 0.1 µM, 1 µM and 10 µM), determined by cell viability as a percentage relative to the control (0 µM erastin and 0 µM DHA) calculated from trypan blue data. Error bars denote standard error from the mean. NS denotes a lack of significant difference between time conditions.*

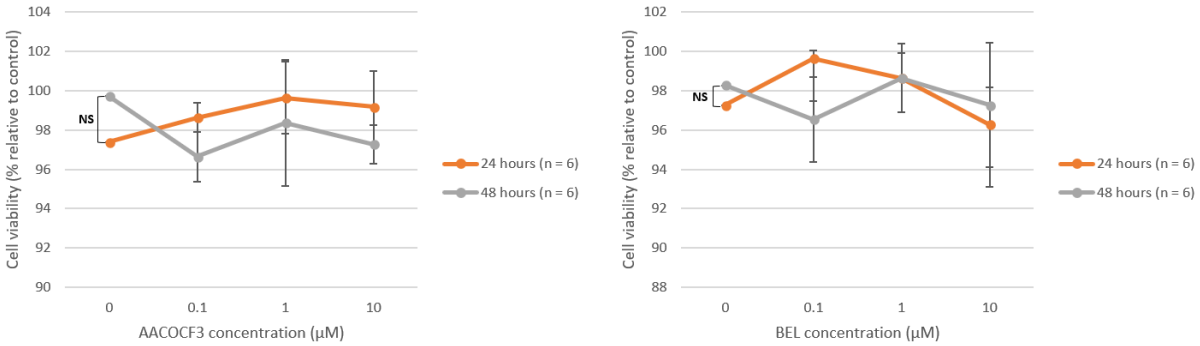

Figure 23 *- **Left**: Dose-response curve of erastin for the 24-hour time condition (orange line, 6 µM) and 48-hour condition (grey line, 4 µM) with logarithmic concentrations of $AACOCF_3$ (0 µM, 0.1 µM, 1 µM and 10 µM), determined by cell viability as a percentage relative to the control (0 µM erastin and 0 µM $AACOCF_3$) calculated from trypan blue data. **Right**: Dose-response curve of erastin for the 24-hour time condition (orange line, 6 µM) and 48-hour condition (grey line, 4 µM) with logarithmic concentrations of BEL (0 µM, 0.1 µM, 1 µM and 10 µM), determined by cell viability as a percentage relative to the control (0 µM erastin and 0 µM BEL) calculated from trypan blue data. Error bars denote standard error from the mean. NS denotes a lack of significant difference between time conditions.*

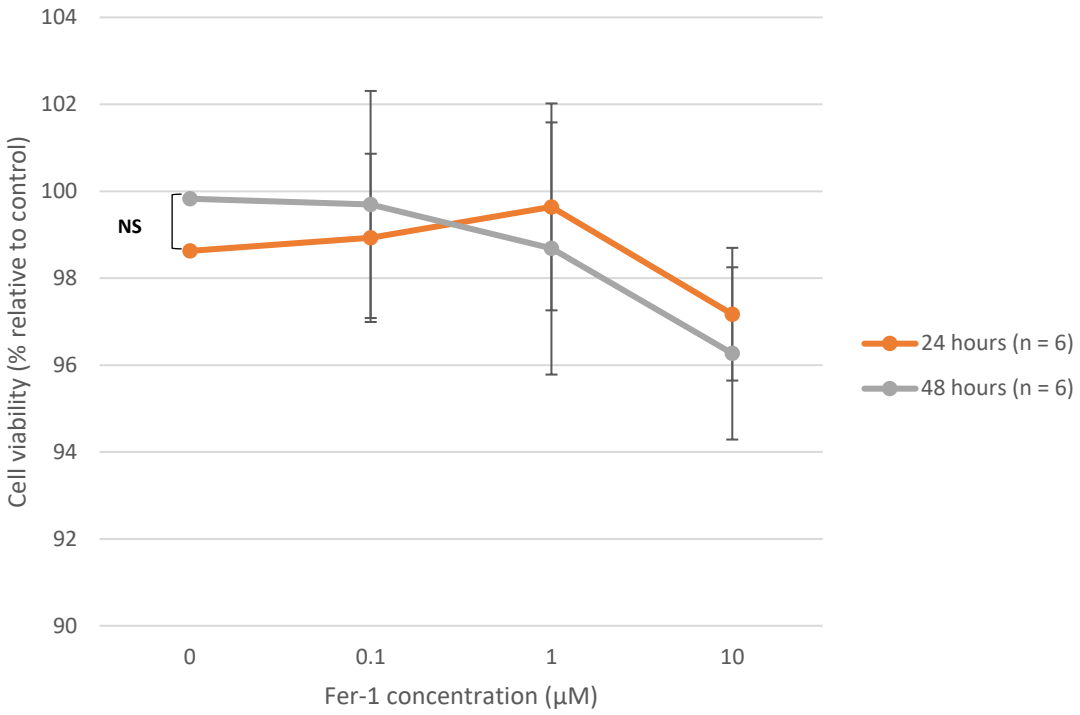

Figure 24 *- Dose-response curve of erastin for the 24-hour time condition (orange line, 6 µM) and 48-hour condition (grey line, 4 µM) with logarithmic concentrations of Fer-1 (0 µM, 0.1 µM, 1 µM and 10 µM), determined by cell viability as a percentage relative to the control (0 µM erastin and 0 µM Fer-1) calculated from trypan blue data. Error bars denote standard error from the mean. NS denotes a lack of significant difference between time conditions.*

A two-way ANOVA was performed on these data sets, collected utilising the MTT-derived IC_{50} concentrations (6 µM for the 24-hour condition and 4 µM for the 48-hour condition), with the exception of the erastin-only condition. In the erastin-only data set, there was no significant difference between erastin concentrations and time conditions (F (5, 102) = 2.35, $p > 0.05$) and (F (1, 106) = 0.33, $p > 0.05$) respectively. For the erastin and DHA data set, there was no significant difference between time condition (F (1, 10) = 1.13, $p > 0.05$) or DHA concentration (F (3, 20) = 0.53, $p > 0.05$). This lack of significant difference between time condition and concentration of the additional compound continued in the $AACOCF_3$ data set ((F (1, 10) = 2.51, $p > 0.05$) and (F (3, 20) = 0.28, $p > 0.05$) respectively), the BEL data set ((F (1, 10) = 0.22, $p > 0.05$) and (F (3, 20) = 3.46, $p > 0.05$) respectively) and the Fer-1 data set ((F (1, 10) = 2.64, $p > 0.05$) and (F (3, 20) = 0.66, $p > 0.05$) respectively).

Discussion

The use of trypan blue as a complementary assay to MTT showed that there were discrepancies between the two when utilising 4 µM and 6 µM as the IC_{50} concentrations for the 24- and 48-hour time conditions respectively. All data sets were collected within a short space of time, and so a dose-response curve was not generated. Instead, IC_{50} concentrations determined by MTT analysis data was

utilised. When a dose-response curve was attempted, only modest changes in cell viability were detected. Consequently, IC_{50} concentrations could only be determined by extrapolation of Fig. 20, and were much higher than those determined by MTT (25.0 μM for the 24-hour condition and 117.9 μM for the 48-hour condition). Additionally, there was an unexpected increase in IC_{50} for the longer incubation which was not observed in MTT-derived data. Once the error had been realised, it was too late to repeat these experiments or conduct experiments utilising the IC_{50} concentrations as determined by trypan blue experimentation due to the limited erastin stock remaining. Unless the IC_{50} concentrations of 25.0 μM and 118 μM (rounded) could be confirmed or challenged, these experimental conditions would have been unsuitable for further testing of the additional compounds. Although differences between tests are to be expected, 10 μM erastin has been determined as sufficient to cause significant cell death assayed by trypan blue staining in HT-22 cells over a 24-hour period. Co-treatment with Fer-1 allowed for significant cell rescue (Tang & Tang, 2019). Moreover, Pan et al. (2019) determined 4 μM erastin over a 12-hour period to result in significant cell death of NSCLC cells, again determined by trypan blue. Additionally, Dixon et al. (2012) report some experiments to have been completed using trypan blue assay, employing an automated cell counter. No IC_{50} concentrations were determined for any of these studies.

Only one study employing both MTT and trypan blue could be identified. Huo and colleagues (2016) determined the IC_{50} concentration of erastin for a 24-hour incubation period in HT-29 colorectal cancer cells to be greater than 30 μM from MTT-derived data. The IC_{50} concentration for a 48-hour incubation period in this cell line was approximately 30 μM, whilst the 96-hour incubation condition determined a concentration of approximately 1 μM. Similar to the results of this project, Huo and colleagues demonstrate a decreased IC_{50} concentration of erastin required for longer incubation periods, though it is unclear whether the large difference in IC_{50} concentrations in this project compared to those determined by Huo et al. is due to the different cell lines utilised or additional factors. Comparison of MTT- and trypan blue-derived data is possible only with the 72-hour incubation period. Similar to those results in this experimental project, Huo et al. determined MTT to result in lower IC_{50} concentrations compared to trypan blue (approximately 10 μM and greater than 30 μM respectively), although again these concentrations are much higher than those resulting from this project.

1 μM erastin to significantly reduce cell viability of HT-29 colorectal cancer cells via both MTT and trypan blue assays, although no IC_{50} concentration was determined for erastin in this cell line by either

assay. No studies could be found reporting the use of both MTT and trypan blue in SH-SY5Y cells to determine a cell-specific explanation.

When assessing studies employing both MTT and trypan blue in broader research, few studies were found. Interestingly, Chung and colleagues (2015) determined trypan blue to be a more sensitive assay when determining cell viability of HepG2 cells exposed to radiation than MTT, suggesting the plating density ($1x10^4$) to be inefficient. Subsequent investigation by the group suggests $1x10^3$ to be the most effective density under these conditions. In comparison, Ghorbani-Anarkooli et al. (2019) report of MTT and trypan blue as determining similar IC_{50} concentrations in a study of melatonin treatment in a human anaplastic thyroid cancer cell line – 4.8 mM and 4.4 mM respectively. In support of the variation of IC_{50} calculations determined by MTT and trypan blue assays in this project, Shokrgozar et al. (2007) report significantly lower LC_{50} concentrations resulting from MTT than trypan blue despite the significant correlation between the two methods. This is further supported by Wang et al. (2011), who report MTT to have inaccurately reported cell toxicity compared to trypan blue. Intriguingly, the researchers suggest these inaccurate results are due to the increased formation of superoxide radicals in the cultured cell line.

The minimal cell death observed in this set of experiments may alternatively have arisen from issues with the erastin, causing the compound to become ineffective (for example incorrect storage causing degradation), and thus the accuracy of the IC_{50} concentration cannot be taken for granted. Repeating the experiments with fresh erastin, for example, may provide results more in line with those determined from MTT analysis.

Results with TEM

Transmission electron microscopy

Imaging of SH-SY5Y cells utilising TEM resulted in the visualisation of mitochondria from numerous cells, from which a mean length of 1.00 μm was calculated for the 8 mitochondria measured from 4 untreated cells. In comparison, the mean length of 11 mitochondria found across 6 cells treated with 6 μM erastin was calculated as 1.00 μm (see Table 2). The mitochondria measured for the mitochondrial length data for the untreated condition can be found in Fig. 25 and those from the treated condition in Fig. 26. See Fig. 27 for examples of imaged mitochondria.

Table 2 *-Table of recorded length (μm) of mitochondria observed in untreated (0 μM erastin, n = 8) and treated (6 μM erastin, n = 11) cells visualised by transmission electron microscopy, with average dimensions calculated.*

MITOCHONDRIA NUMBER	UNTREATED (0 μM ERASTIN)	TREATED (6 μM ERASTIN)
	Length (μm)	Length (μm)
1	1.10	0.90
2	1.00	0.95
3	0.95	1.10
4	1.00	1.00
5	1.00	1.00
6	0.95	0.90
7	1.05	1.05
8	1.10	1.00
9		1.10
10		0.95
11		1.05
MEAN (μM)	1.01	1.00

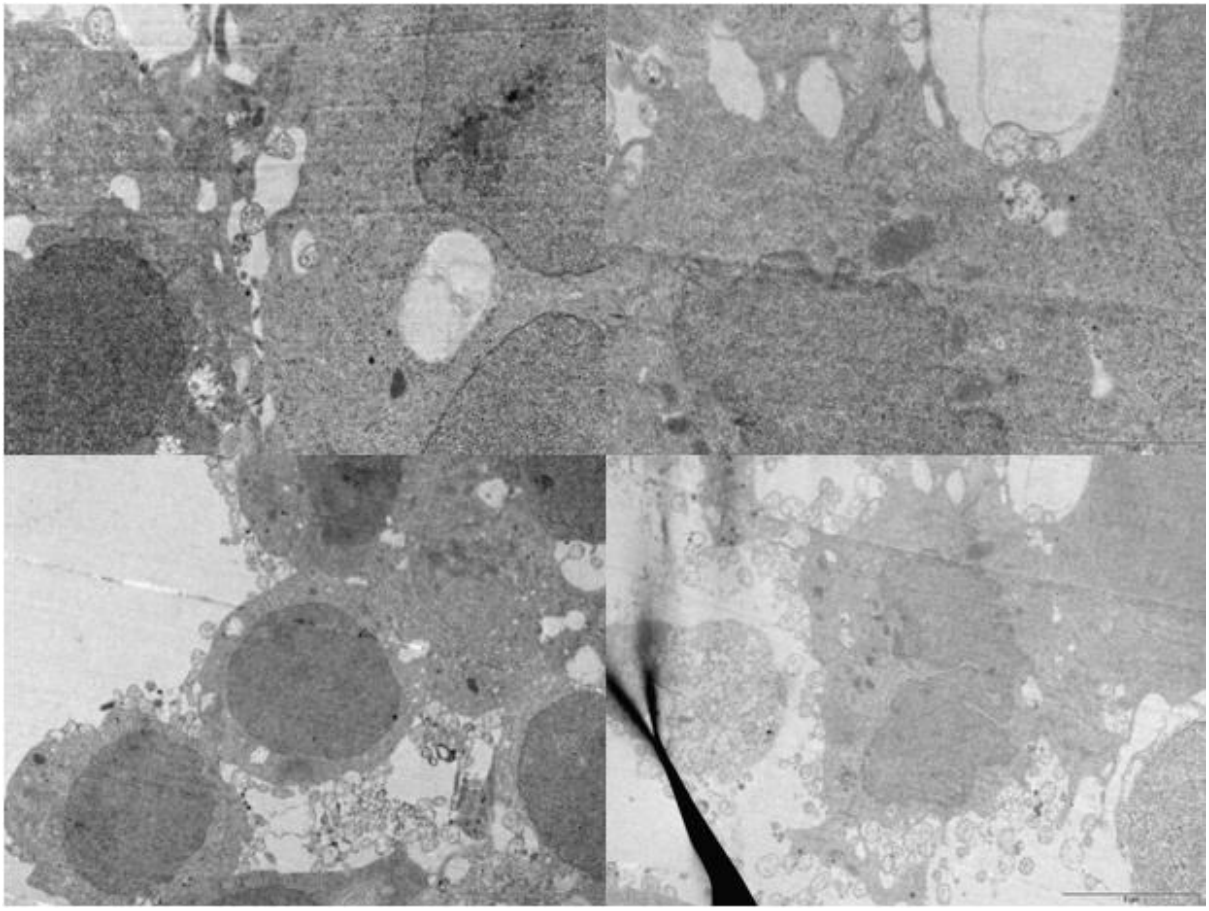

Figure 25 *– TEM images of untreated cells, the mitochondria of which were used to calculate average length of mitochondria in this condition*

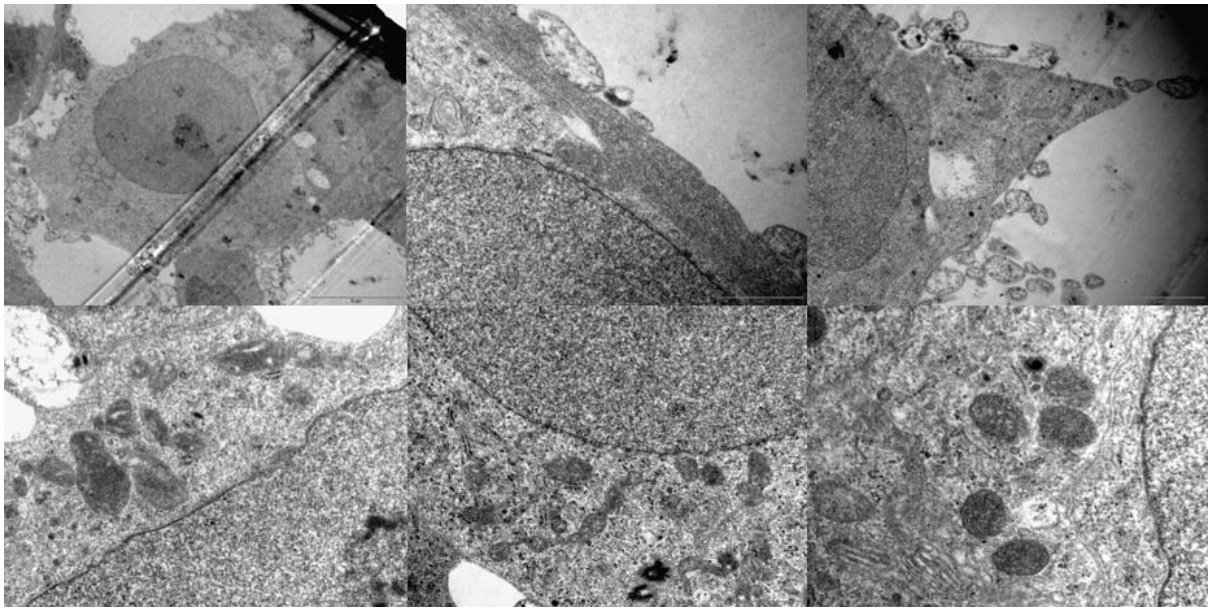

Figure 26 *- TEM images of treated cells, the mitochondria of which were used to calculate average length of mitochondria in this condition*

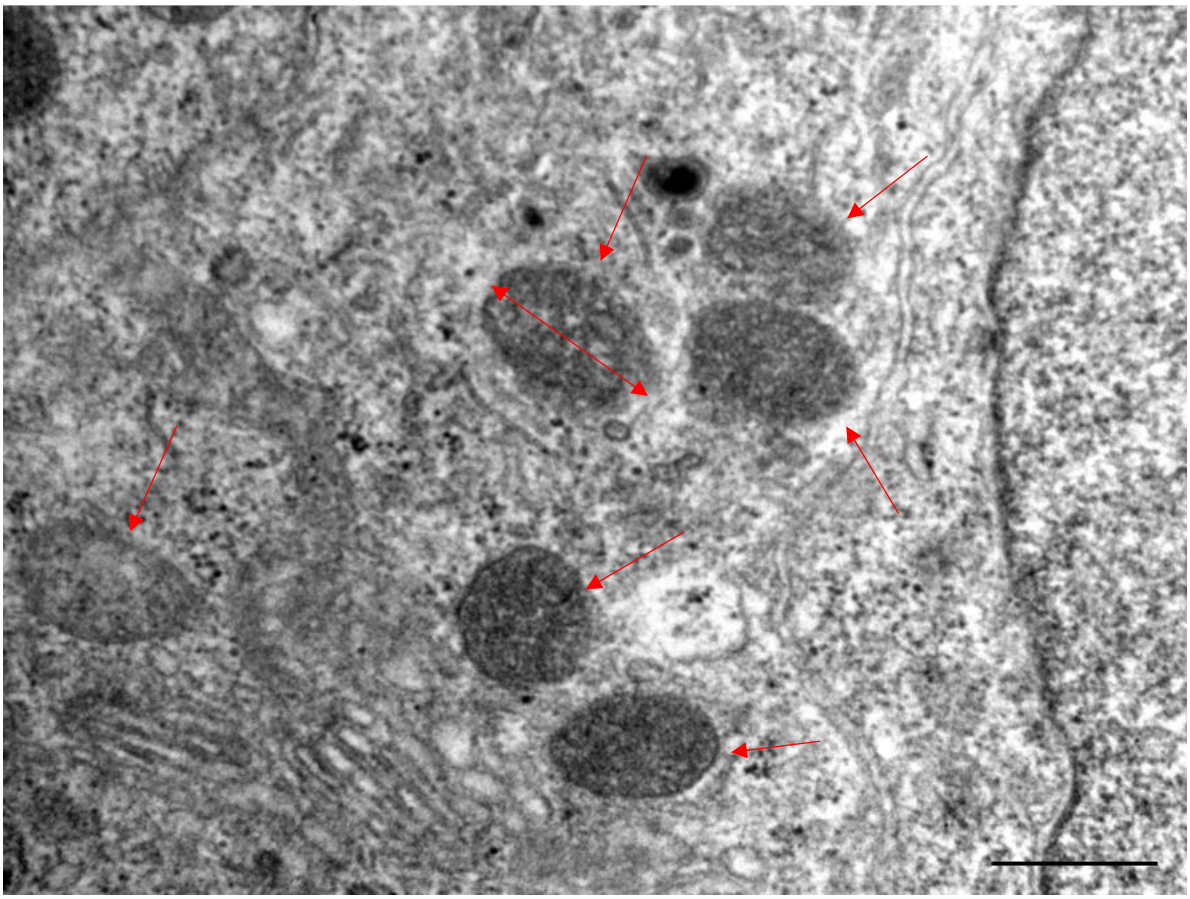

Figure 27 *– Cluster of mitochondria in a treated SH-SY5Y cell (single-headed red arrows) and an example of how mitochondrial length was analysed (double-headed red arrows), as imaged vie transmission electron microscopy. It was assumed that those mitochondria orientated as those above were transversely orientated and that mitochondrial length as measured in this experiment was relative to actual mitochondrial length. Scale bar is 1 µm.*

Whilst searching for visible mitochondria when utilising the TEM, few dead cells were present and so 50 cells in each treatment group were selected at random and determined as dead or alive - 98% of cells in the untreated group were determined as alive compared to 96% of cells in the treated group (see Fig. 28 for images of a live and a dead cell).

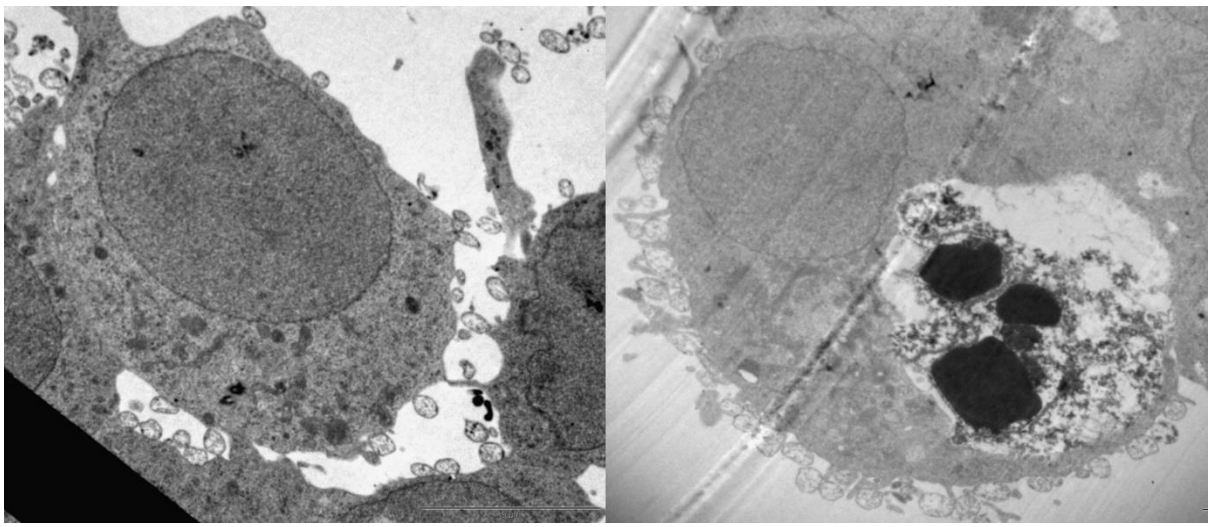

Figure 28 *– Comparison of live (left) and dead (right) cells imaged by TEM. Both cells imaged are from the treated (6 µM erastin) group. Scale bar is 5 µm on the left and 2 µm on the right.*

Discussion

As seen in the results, the average length of few mitochondria was reported due to the difficulties in visualising these organelles, particularly in terms of low resolution at the required magnification resulting in grainy images or a general lack of mitochondria visible in the plane. This may have been caused by a number of reasons, including poor quality of ultrathin sections, although is likely due to a lack of practise at adjusting the TEM stage and contrast of the image. Additionally, TEM images were taken following 24 hours of erastin treatment instead of both 24- and 48- hour time conditions as was done for the MTT and trypan blue assays. This is due to the high concentrations of cells; media required changing every day and thus doing so may have resulted in disruption of cells on the collagen matrix.

The method used to measure the length of the mitochondrial major axis in this study is a more basic version of that outlined by groups including Song et al. (2008), whereby the maximum projection images of the cells were 'skeletonized' so as to produce a version of the image where objects were instead a single pixel wide. The number of pixels comprising the perimeter of a single skeleton was halved and used to indicate the length of the mitochondrion. Along similar lines, Malla et al. (2020) utilised the shape factor method, whereby the circularity of the mitochondria on a scale of 0 (longer

mitochondrion) to 1 (perfect circle) to measure mitochondrial length. Although other methods can be used, this is a cost-effective and accessible method, requiring little software once images have been achieved.

The observation of shrunken mitochondria as the gold standard for the morphological identification of cells having undergone ferroptotic cell death began with Yagoda and colleagues in 2007. In this paper, the group briefly reported ferroptotic mitochondria as having lost structural integrity following treatment of BJ-TERT/LT/ST/RAS^{V12} cells with 37 μM erastin for 10 hours – a much greater concentration, albeit for less time, than was used in this project. Dixon et al. (2012) referred to the mitochondria as smaller than normal with increased membrane density. Despite this, shrunken mitochondria continues to be used as a morphological distinction of ferroptotic cell death; Zhang et al. (2019) used TEM to identify shrunken mitochondria, confirming ferroptotic cell death in a rat model of contusion SCI. Similar results are reported by Xie et al. (2018) in a controlled cortical impact injury mouse model of traumatic brain injury, and Cao et al. (2021) in an *in vivo* study of hemin-induced injury. Yu et al. (2019) report SAS (1.0 mM and 2.0 mM for 24 hours) inducing shrunken mitochondria with increased membrane density in T47D human breast cancer cells, while Ma et al. (2021) also reports shrunken mitochondria in a severe acute pancreatitis-induced AKI in rats. However, it should be noted that no paper reporting shrunken mitochondria as present includes quantitative data allowing for comparison of mitochondrial length or area of ferroptotic cells to control cells, as was done in this project.

Despite the number of studies reporting this distinctive morphological feature as confirmation of ferroptotic cell death, no studies provide an in-depth investigation as to why this occurs or how shrunken the mitochondria of ferroptotic cells are compared to untreated cells (either as percentages or definitive lengths), providing little justification as to why this feature is considered the gold standard of identification. Li et al. (2017 & 2018) report shrunken mitochondria as hindering in the distinction of cell death mechanisms, suggesting the need to quantify large numbers of cells *in vivo* leads to generalised assumptions of cell death mechanisms in specific brain regions.

General Discussion

Rejection of the hypothesis

The determination of erastin inducing significant cell death as determined by MTT offered a hopeful start to experimentation. The lack of significance when cells were co-treated with DHA, $AACOCF_3$ and BEL suggests a continuation of erastin's effect in this cell line, though the lack of effect by these compounds and a lack of significant rescue by Fer-1 (all $p > 0.05$) suggests this cell death to be the result of a cell death pathway other than ferroptosis. However, the conclusions drawn from trypan blue and TEM data means the experimental hypothesis (that there will be a significant difference between erastin concentration, the concentration of compound B and time conditions in terms of cell growth inhibition as a percentage relative to the control) cannot comfortably be accepted. We must therefore accept the null hypothesis. Possible explanations for different statistical analysis conclusions with regards to the reliability of MTT and trypan blue assays for the determination of cell viability, in addition to other errors likely to have occurred, will be outlined further on. Here, reasons as to why the compounds investigated in combination with erastin were chosen and possible explanations behind the discrepancies are given in terms of said compounds.

DHA

DHA is a 22-carbon ω-3 PUFA with 6 double bonds. DHA or the precursor, ω-3 PUFA α-linolenic acid, are found in many dietary components, most notably oily fish (Stillwell & Wassall, 2003). A major constituent of neuronal cell membrane phospholipids, DHA is a pleiotropic molecule involved in many areas of neurobiology and neuroprotection. This compound has been shown to upregulate GPX4 expression when murine hippocampal HT22 cells were supplemented with the ω-3 PUFA, suggesting DHA to increase the antioxidant capacity of cultured hippocampal cells (Casanas-Sanchez et al., 2014).

The evidence of ω-3 PUFAs (including DHA) as beneficial in PD is extensive. Bousquet et al. (2007), for example, determined a 10-month diet high in ω-3 prevented an MPTP-induced decrease in TH-positive nigral cells in mice compared to those given the control diet. Similar results are reported by Ozsoy et al. (2011) following 4 weeks of DHA treatment. Additionally, Samadi et al. (2006) found success in an MPTP primate model. In terms of human PD patients, Fabelo et al. (2011) identified a dramatic reduction of ω-3 PUFAs, especially DHA and AA, in a lipid composition analysis of frontal cortices from PD suffers. DHA has also been found to improve depressive symptoms in PD suffers, independent of antidepressant treatment (Moralez da Silva et al., 2008).

The involvement of DHA in cell death has been reported for various cell death pathways; DHA-induced cell death in non-small cell lung cancer (NSCLC) cells was determined to be apoptotic and autophagic

in nature (Kim et al., 2015). Similarly, DHA has been found to induce apoptosis in MCF-7 breast cancer cells (Xue et al., 2017) and in acute myeloid leukaemia cells (Yamagami et al., 2009), although Yano et al. (2000) report DHA to attenuate TNF-induced apoptosis by 40-70%, accompanied by enrichment of DHA into membrane phospholipids. Jing et al. (2011) report DHA to induce autophagy in SiHa cervical cancer cells. Interacting with a cell death-inducing compound like in this project, Jeong et al. (2019) determined DHA to enhance oxaliplatin-induced autophagy in colorectal cancer cells. Moreover, research by Pizato et al. (2018) suggests DHA to induce pyroptotic cell death in MDA-MB-231 triple-negative breast cancer cells. Pyroptosis is an inflammation-related cell death pathway.

Evidence of a role for DHA in regards to ferroptosis is limited at present, though the ω-3 PUFA has recently been reported to inhibit the proliferation of three acute myeloid leukaemia cell lines and instead promote ferroptotic cell death (Du et al., 2019). In 2017, Ou and colleagues observed low-density lipoprotein nanoparticles reconstituted with DHA (LDL-DHA) to cause an iron-dependent cell death in rat hepatoma and human HCC cell lines, exhibiting pronounced lipid peroxidation, GSH depletion and GPX4 inactivation, and was later confirmed to reflect ferroptosis. In murine human HCC tumour xenograft models, injection of LDL-DHA into the tumour severely inhibited tumour growth and again was confirmed as ferroptotic. The evidence highlighted here suggests that the neuroprotective role of DHA observed in PD studies extends to promoting the death of tumorigenic cells via multiple cell death pathways.

The causes underlying a lack of significant difference in cell viability relative to the control ($p > 0.05$) following erastin and DHA cotreatment are enigmatic. The evidence outlined above suggests that even in the absence of cell death induced by erastin, cell death should have been induced by DHA independently, provided there is no interaction between erastin and DHA. The catecholaminergic nature of SH-SY5Y cells may explain this – the beneficial effects of DHA in PD-related studies may reflect a neuroprotective effect induced by an interaction of DHA and DA. Interestingly, Kishida and colleagues (2006) found pre-treatment with DHA to enrich phospholipids in L929 mouse fibrosarcoma cells and attenuate necrotic cell death induced by tumour necrosis factor (TNF) with actinomycin D. DHA-associated inhibition of necrosis in tumorigenic cells brings about discussion as to whether erastin-induced ferroptosis is a unique cell death pathway or instead a form of necrosis. This topic will be discussed in more detail later.

$AACOCF_3$

$AACOCF_3$ is an analog of the ω-6 PUFA AA in which the carboxylic acid (COOH-) group has been replaced with $COCF_3$. This alteration allows $AACOCF_3$ to act as an inhibitor of $cPLA_2$ by binding directly to these enzymes (Street et al., 1993). $cPLA_2$-catalysed hydrolysis of arachidonoyl-containing glycerophospholipids (including phosphatidylcholine and phosphatidylethanolamine) causes the release of fatty acids, particularly AA, and lysophospholipids (Huang et al., 2009). Both these products and their downstream metabolites initiate signalling cascades influencing inflammation and cell viability (Linkous & Yazlovitskaya, 2010).

Although the use of $AACOCF_3$ in the study of PD is severely limited, a role for $cPLA_2$ enzymes in the disease has been demonstrated by Klivenyi et al. (1998) and Bonventre et al. (1999), who found $cPLA_2^{-/-}$ mice to be significantly more resistant to MPTP-induced neurotoxicity than their wild-type counterparts. Consistently, Yoshinaga et al. (2000) determined $AACOCF_3$ to inhibit MPP^+-induced cell death and AA release in rat pituitary tumour-derived GH3 cells. This is further supported by findings from Chalimoniuk et al. (2009) in PC12 cells – the group suggests $cPLA_2$ phosphorylation activates downstream pathways including the activation of PKC and ERK1/2 that, when upregulated in experimental PD models, results in DAergic degeneration. These studies indicate a protective role of inhibiting $cPLA_2$ phosphorylation against DAergic degeneration.

Huang et al. (2009) found $AACOCF_3$ to significantly increase the number of surviving neurones and oligodendrocytes in a compression-induced murine model of spinal cord injury. Moreover, locomotor recovery was also greater in the inhibitor-treated group than those delivered saline, though the authors make no attempt at defining the form of regulated cell death occurring. Yang and colleagues (2016) determined addition of exogenous AA to sensitise cells of the BJ-TERT/LT/ST/RAS^{V12}, HT-1080 and G-401 cell lines to RSL3-induced cell death. Based on Yang and Stockwell's 2016 report that oxygenated lipids act as proximal cell death signals in ferroptosis, Kagan et al. (2017) determined KO of ACSL4 to confer protection against RSL3 by inhibiting the acyl-CoA synthase-dependent esterification of PUFAs (preferentially AA) into phospholipids. Consistently, treatment of ACSL4-KO cells with RSL3 resulted in accumulation of free oxygenated PUFAs, whereas wild-type cells generated higher levels of esterified oxygenated AA. Supplementation of wild-type and ACSL4-KO cells with exogenous AA increased the rate of ferroptosis in both groups, albeit to a higher extent in wild-type cells (24% vs 13% increase), owing to increased levels of esterified oxygenated AA and AdA following RSL3 treatment. Redox phospholipidomic investigation determined four doubly- and triply-oxygenated molecular species of phosphatidylethanolamines (PEs) to act as ferroptotic signals;

C18:0/C20:4 and C18:0/C22:4 respectively. These species were confirmed as biomarkers by LC-MS/MS employing stable isotopic labelling following RSL3 treatment. Further investigation determined PE oxygenation and signalling cascade induction during ferroptosis to occur via the esterification of non-oxygenated AA/AdA into PEs, followed by PE oxygenation. 15-LOX was identified as the enzymatic generator of the ferroptotic signals, in that application of liproxstatin and vitamin E inhibited the production of pro-ferroptotic oxygenated PE *in vivo*. LOX activity in lipid hydroperoxide generation first requires the hydrolytic release of PUFAs from lipid membranes, a reaction controlled by PLA_2. Is it therefore possible that PLA_2 levels are elevated in ferroptosis-sensitive cells? Whether or not this is the case, inhibition of these enzymes by $AACOCF_3$ ($cPLA_2$) should have had some protective effect against erastin-induced cell death. Given there is no report of $AACOCF_3$ as causative of cell death independently, the lack of significant difference ($p > 0.05$) demonstrated in this project is likely due to the inability of erastin to induce ferroptosis under the experimental conditions.

No evidence is currently available into the direct effects of $AACOCF_3$ in ferroptotic cell death, though Huang et al.'s 2009 study shows clear similarities to that of Zhang et al. (2019) who, as mentioned previously, determined third-generation ferrostatin SRS16-86 to significantly improve locomotor scores and return mitochondrial morphology from shrunken ferroptotic-affected mitochondria to a more physiological state in a murine model of SCI, and therefore it may be ferroptotic cell death from which $AACOCF_3$ provided a neuroprotective effect in Huang et al.'s study.

BEL

BEL is an irreversible inhibitor of $iPLA_2\beta$ that preferentially releases DHA from neuronal glycerophospholipids, and mutations in the enzyme's gene have been identified as underlying PD (Yang et al., 1999; Gui et al., 2013). Blanchard et al. (2014) concluded $iPLA_2\beta^{-/-}$ mice to exhibit life-long distortions in DHA content and metabolism, resulting in motor disturbances, loss of neuroprotective BDNF and disturbed expression of AA metabolism-associated enzymes, which the authors suggest mimics aspects of many human motor diseases to include PD. In 2016, Zhou and colleagues determined inhibition of PARK14-dependent Ca^{2+} signalling using BEL caused autophagic dysfunction and resulted in the death of DAergic SNpc neurones and age-dependent L-dopa-sensitive motor dysfunction in a cellular model of PD. One study by Calderon and colleagues (2015) suggests BEL to significantly attenuate the basal and nicotine-induced $iPLA_2\beta$-mediated proliferation and migration of 4T1 breast cancer cells, as determined by MTT assay and scratch and transwell assays respectively. Furthermore, basal and nicotine-induced tumour growth were significantly reduced by BEL in a mouse breast cancer model.

As demonstrated by the evidence above, DHA, $AACOCF_3$ and BEL have reported or implied roles in PD pathology (whether beneficial or detrimental) and ferroptotic cell death, and so were selected for investigation due to these reasons. Moreover, all compounds were readily available within the pre-existing laboratory stock upon beginning the experimental year. DHA and BEL were hypothesised to increase ferroptotic-associated arrest of cellular growth whereas $AACOCF_3$ was hypothesised to offer some degree of protection against erastin.

Experimental and experimenter error

One explanation for the lack of significantly different main effects and interaction effects besides the erastin-only condition as determined by MTT is experimental and experimenter error. Some errors will be outlined here, before surmising possible effects of said errors and any improvements that could be implemented to increase the reliability and integrity of the research and resulting data, were this project to be repeated.

Erastin

The focal compound of this investigation was erastin, discovered by Dolma and colleagues in 2003. The purity of erastin used was reported as ≥98% by the supplying company, Sigma Aldrich (United States of America), determined by high performance liquid chromatography. Experimenting with the development of erastin analogs, Yang and colleagues (2014) developed aldehyde erastin, morpholine erastin II, and piperazine erastin. These analogs vary from the erastin parent compound by introducing an aldehyde moiety, a piperazine moiety or a morpholine moiety on the meta position of the aniline ring of erastin. Compared to the parent erastin compound, all require lower concentrations to produce GI_{50} (50% growth inhibition) in BJ-TERT/LT/ST/RAS^{V12} cells (1.8 µM compared to 8 nM, 0.13 µM and 0.9 µM respectively). Moreover, the three erastin analogs displayed improved selectivity, which the group define as a ratio of GI_{50} in HRAS wild-type cells divided by GI_{50} in HRAS mutant BJ-TERT/LT/ST/RAS^{V12} cells – erastin's selectivity was calculated as 7.2, whereas that of aldehyde erastin (AE), piperazine erastin (PE) and morpholine erastin (ME) was 10.7, 9.2 and 7.3 respectively. PE was shown by the group to have improved suitability for *in vitro* experimentation compared to erastin, with greater water solubility (1.4 mM vs 0.09 mM). Yang et al. found PE to display significant anti-tumour activity in a murine HT-1080 tumour prevention model when injected prior to tumour establishment but provided limited growth inhibition on already established tumours, which the group suggest is due to the modest potency of this analog.

A year later, Larraufie et al. (2015) developed multiple erastin analogs, including piperazine ketone erastin (PKE) and imidazole ketone erastin (IKE). The potency of PKE and IKE as inhibitors of system x_c^- was evaluated in a glutamate release assay utilising human astrocytoma cells (CCF-STTG1), a test which determined IKE to display improved potency over AE (30 nM compared to 60 nM). The IC_{50} determined for PKE was 100 nM. Moreover, when tested in isogenic and non-transformed tumorigenic cell lines, both analogs were preferentially lethal to the latter, displaying low nanomolar potencies. PKE and IKE were next evaluated on their ability to inhibit the growth of the highly tumorigenic HT-1080 cells. Following a 48-hour incubation period, IKE was determined as almost twice as potent as PKE (GI_{50} of 310 nM compared to 550 nM). Lastly, half-life evaluation as a measure of metabolic stability determined that of PKE to be >90 minutes and IKE $T^{1/2}$ = 79 minutes. The analogs were found to display high plasma stability, remaining stable for up to 120 minutes when 500 ng/ml was dissolved in mouse plasma and incubated at 37^{o}C. These findings suggest that IKE in particular displays optimised properties for use *in vivo* over erastin, PE and AE; substituting an ethoxy moiety with isopropoxy allowed for increased metabolic stability, and the imidazole moiety improved water solubility and stability of the ketone, resulting in enhanced solubility of IKE in acidic conditions.

Interestingly, only two studies to date could be found utilising the more suitable IKE analog. Yang and colleagues (2016) determined silencing the expression of the six ALOX genes found in humans to confer resistance to IKE-induced ferroptosis in G-401 cells. A more focused study of IKE is provided by Zhang et al. (2019) who confirmed the induction of ferroptosis by IKE treatment in terms of (1) Fer-1 rescuing diffuse large B cell lymphoma (DLBCL) cell lines from cell death; (2) dose-dependent GSH depletion, reversed by β-ME co-treatment; (3) dose-dependent increase in L-ROS in SUDHL6 cells (a DLBCL cell line), again inhibited by Fer-1, as determined by flow cytometry with C11-BODIPY; (4) lipid peroxidation of PUFAs, measured by the abundance of immunofluorescent staining with mAb 1f83, an anti-dihydropyridine-MDA-lysine adduct antibody, and (5) upregulated expression of SLC7A11, PTGS2 and CHAC1, inhibited by β-ME, as determined by qRT-PCR. Zhang and colleagues next tested the anti-tumour effects of IKE in mice. Having determined intraperitoneal delivery to be the most effective and practical, similar findings resulted in IKE-treated SUDHL6 xenografts in mice – CHAC1, SLC7A11 and PTGS2 mRNA were upregulated, and abundance of dihydropyridine-MDA-lysine adduct and 8-hydroxy-2'-deoxyguanosine increased. Noting the lower solubility of IKE in neutral aqueous conditions compared to acidic aqueous conditions, the use of a nanoparticle carrier formulation was evaluated. PEG-PLGA di-block copolymer-based nanoparticles were selected for the IKE carrier system, based on their biocompatibility and biodegradable properties. Compared to free IKE, PEG-PLGA nanoparticle-associated IKE displayed enhanced cellular activity in SUDHL6 cells, suggesting increased

internalisation into cells, and Fer-1 cotreatment conferred protection of cells from IKE nanoparticle-induced cell death. In SUDHL6 xenograft-bearing mice, tumour growth inhibition was not significantly different between free IKE and IKE nanoparticles, though the latter resulted in fewer signs of toxicity, which the authors speculate is caused by the nanoparticle's effects on hydrophobic drug distribution. Taken together, evidence from the Larraufie group and Zhang group suggest IKE to provide better suitability for *in vivo* experimentation.

Fer-1

As discussed in the introduction, second- and third-generation ferrostatins have been developed since the identification of Fer-1 by Linkermann and colleagues in 2014. SRS11-92, developed by Skouta et al. (2014), is a second generation ferrostatin that was determined by the group to confer protection of cultured oligodendrocytes from cystine-starvation in the nanomolar range, and was reported to be 15-fold more potent than Fer-1 overall. Third generation ferrostatin SRS16-86 was developed by Stockwell's group in 2014 and was found to protect mice from functional acute renal failure and structural organ damage in a model of severe ischemia-reperfusion injury to a greater extent than parent compound Fer-1 (Linkermann et al., 2014). Recently, Zhang et al. (2019) reported SRS16-86 to significantly improve locomotor activity and restore mitochondrial morphology, assessed by TEM, to a more physiologically normal size following the free fall of a 10 g bar onto the exposed spinal cord of mice in an animal model of contusion spinal cord injury.

Contamination and cell detachment

One issue faced during the course of this project was the contamination of cell culture flasks with white spore-like particles, visible without the need for microscopy. Said flasks were immediately discarded and sterility measures taken. More importantly, TEM imaging led to the discovery of bacterial contamination of the SH-SY5Y cell culture, likely to be a species of the mycoplasma bacterium (see Fig. 29). Of the 100+ species of mycoplasma identified, fifteen are reported to infect humans and can underlie respiratory tract infection, for example (Drezler & Uphoff, 2002; Miyashita et al., 2016). Unlike conventional bacteria, mycoplasma species employ a triple-layered membrane instead of a rigid cell wall and are approximately 300 nm in diameter (Taylor-Robinson & Bebear, 1997).

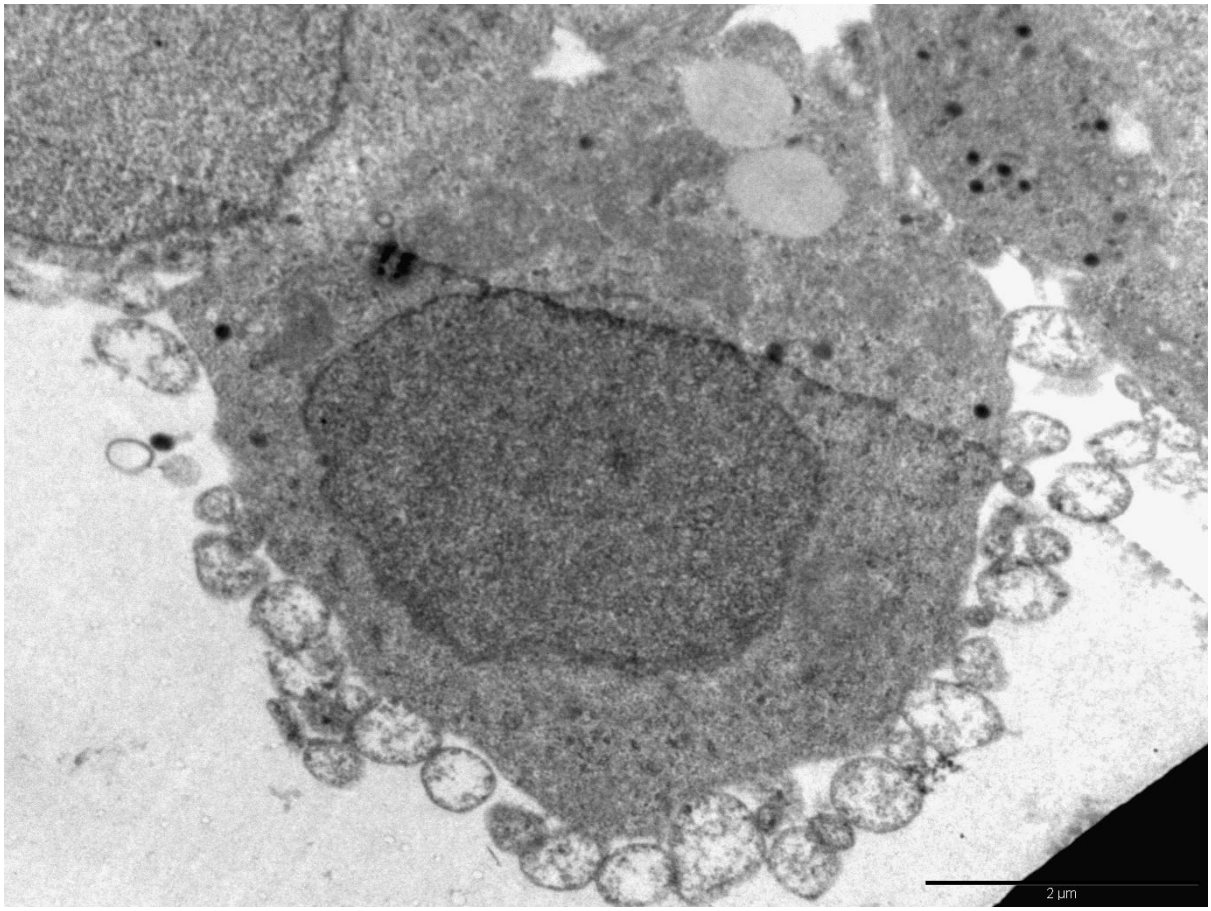

Figure 29 *– Mycoplasmal infection of SH-SY5Y cells visualised by transmission electron microscopy. Scale bar of 2 µm.*

Various cellular consequences occur upon mycoplasma contamination, which differ depending on the infecting species, culture conditions, intensity and duration of infection and presence of other contaminating species. Contamination therefore interferes with all measurable parameters, whether during routine cultivation or in experimental investigations. General effects on eukaryotic cells include (1) altered levels of protein, RNA and DNA synthesis; (2) altered cellular metabolism; (3) induction of chromosomal aberrations to include numerical and structural alterations; (4) alterations in cell membrane composition (in terms of surface antigen and receptor expression); and (5) altered cell morphology. It should be noted that this is by no means an exhaustive list (Drexler & Uphoff, 2002). One example is provided by Elkind et al. (2011) who determined contamination of SH-SY5Y cells by mycoplasma hyorhinis (Mh), derived from SH-SY5Y cell culture, lead to increased levels of calpastatin, the endogenous inhibitor of the Ca^{2+}-dependent protease, calpain. When studied in relation to amyloid-beta (Aβ) toxicity, central to the pathogenesis of Alzheimer's disease (AD), high calpastatin activity resulting from Mh infection was found to attenuate the Aβ toxicity observed in uncontaminated SH-SY5Y cells, in that calpain activation and activity was inhibited, and normal cell morphology and mitochondrial enzyme activity were maintained. This study demonstrates the ability

of mycoplasma contamination to affect cell culture-derived results. This is the only paper to date that was found to examine the effects of mycoplasma contamination in the SH-SY5Y cell line; most studies are regarding pneumonia caused by M. *pneumoniae*. Interestingly, a study by Kim et al. (1995) found M. *pneumoniae* to underlie parkinsonism in a 7-year-old boy. A T2-weighted MRI (magnetic resonance imaging) scan observed high signal intensities in both basal ganglia. In contrast, Tay et al. (2014) report M. *pneumoniae* to result in parkinsonism of two previously healthy children but with normal MRI scans. Despite other parkinsonism-causing reports, there is little discussion of mycoplasma species as underlying Parkinson's disease.

Mycoplasma contamination can be confirmed via the microbiological culture method, whereby a sample of cell culture supernatant is grown on agar plates in conditions that promote mycoplasma growth for approximately two weeks. Observation of small colonies is indicative of a positive sample. Other methods include DNA staining by fluorochromes including DAPI (4, 6-diamidino-2-phenylindole-dihydrochloride) and polymerase chain reaction (PCR), involving the detection of 16S rRNA (recombinant RNA) molecules of more commonly contaminating mycoplasma species. Fluorescence in situ hybridisation (FISH) and fluorescent assays based on ATP detection may also be used (Nikfarjam & Farzaneh, 2012). Most cell populations infected originate from commercial suppliers or other research laboratories, though the source differs by species; laboratory personnel have been determined as the main source of M. *orale*, M. *fermentans* and M. *hominis*, species physiologically found in the oropharyngeal tract of humans (spread by droplet dispersion) and which account for over half of all mycoplasma contaminations in cell cultures (Hay, 1991). Other sources include FBS (M. *arginini* and the acholeplasma A. *laidlawii*) and trypsin, a major source of M. *hyorhinis* (Barile et al., 1973). Improper sterilisation increases contamination risk and aids in the spread of infection. Moreover, mycoplasma can survive in liquid nitrogen, and so this method of cryopreservation does not prevent mycoplasma spread (Nikfarjam & Farzaneh, 2012). Interestingly, live mycoplasma have been found in a laminar hood up to six days after working with infected cells, and uncontaminated cells subcultured in the same hood tested positive for contamination six weeks later (McGarrity, 1976)

How can contamination be prevented or eradicated? Due to the triple-layered cell membrane, penicillin (an antibiotic that acts through the disruption of the invading bacteria's cell wall) is ineffective against mycoplasma (Taylor-Robinson & Bebear, 1997). Moreover, a study by Ryan and Mariano from Bionique Testing Laboratories (2011) determined 88% of mycoplasma isolated from infected cell cultures to be resistant to streptomycin, demonstrating antibiotic resistance of mycoplasma likely following the overuse of these drugs. As in this investigation, penicillin and

streptomycin are often utilised in combination in cell culturing to limit bacterial contamination (Nikfarjam & Farzaneh, 2012). Plasmocin™ and Plasmocure™ are mycoplasma elimination reagents that can be utilised to both prevent and eliminate contamination, with the latter recommended for the rare species resistant to Plasmocin™ (InvivoGen, undated a; InvivoGen, undated b). One study determined Plasmocin™ to cure 45 out of 58 (78%) mycoplasma-positive cell lines of contamination. In a second round of investigation using cryopreserved original cells, 49 of 58 cell lines were cured (84%), and no mycoplasma were detected at 14 days posttreatment and at later time points (Uphoff et al., 2012). Another group determined Plasmocin™ to eradicate mycoplasma in 65% of infected cell lines tested. After 4 months, 10% of cell lines were found to be re-infected, and cytotoxicity and cell death was observed in 25% of cell lines. The authors suggested another antibiotic tested, BM-cyclin, may overall provide more desirable anti-mycoplasma results, curing 66.25% of cell lines and displaying cytotoxicity and cell death in 17.5% of cell lines. Regrowth was however greater than that of Plasmocin™ at 16.25% (Kazemiha et al., 2011).

Cell culture media

For several weeks during experimentation, a national shortage of DMEM/F12 media resulted in the use of RPMI-1640 as the base media for cell maintenance. No experiments were conducted during this time so as to avoid the introduction of additional variables, though the RPMI media may have affected the physiology of the cells. A systematic review of the SH-SY5Y cell line in PD research, conducted by Xicoy and colleagues (2017), determined RPMI-1640 to be used as base media in 37 of the 962 publications the group reviewed, whereas the use of DMEM/F12 is reported by a substantially higher 230 publications. Studies comparing DMEM and RPMI-1640 have found media type to change the metabolome and the differentiation capacity of cells from various cell lines, suggesting these results may also be applicable to the SH-SY5Y cell line (Wu et al., 2009; Huang et al., 2015). Huang et al. (2015) noted gradual acclimatisation of cells from RPMI-1640 to DMEM resulted in the metabolic profiles and levels of most of the discrepant metabolites to eventually converge to levels similar to those of cells originally cultured in DMEM, with little difference in rates of cell proliferation. However, many metabolite levels did not converge. This suggests that whilst gradual acclimatisation of SH-SY5Y cells to a different media type may be possible in situations including the national DMEM/F12 shortage, the process was not done for this project – cells were maintained in DMEM/F12 and, when this ran out, were immediately maintained in RPMI-1640 media without acclimatisation. The detachment of cells in some flasks highlighted the inability of some cell populations to withstand the sudden media change, but those populations that survived proliferated and likely generated cells more suited to maintenance in RPMI-1640. Upon availability of DMEM/F12, RPMI-1640 was no longer used. Cells

were maintained in DMEM/F12 and allowed time to proliferate (indirectly allowing time for adjustment) before plating for experimentation to resume. Although these circumstances were unforeseen and thus uncontrollable, it is unknown what affects the RPMI-1640 media had on the surviving cell populations, whether any changes were long-lasting and whether these changes had any effect on data collection from that point forward.

Summary

As outlined above, improved analogues of erastin and Fer-1 have been developed. In terms of erastin, the IKE analog displays greater potency, higher metabolic stability and higher water and acidic solubility compared to erastin, making this molecule more suitable for *in vitro* experimentation than the parent molecule. The use of the parent erastin was necessitated by the lack of commercial availability of second- or third- generation analogues – IKE has only become available for purchase since 2018, after experimentation for this project began. Moreover, many ferroptotic studies utilise erastin and the compound's performance as a biologically active compound has not been evaluated and reported in a manner suggesting the molecule to be inadequate for *in vitro* study. Moreover, the second- and third-generation ferrostatins developed are not available for purchase at present.

With the differing conclusions resulting from MTT- and trypan blue-derived cell viability data, it would have been beneficial to utilise a third assay to improve the reliability of either conclusion – that erastin decreases viability of SH-SY5Y cells as determined by MTT or has no effect, as was found from trypan blue staining. Given the simple nature of the trypan blue staining assay and the ability to see the cells individually as dead or alive, it is tempting to rely more heavily on the conclusion derived from this data over that of the MTT assay. It is important to remember, however, that various factors may have resulted in said discrepancies – the unconfirmed effect of erastin activity in SH-SY5Y cells means it cannot be concluded from either cell viability analysis technique that erastin does or does not inhibit cellular growth, despite promising MTT results suggesting erastin to induce a non-ferroptotic cell death in SH-SY5Y cells. Moreover, as outlined above, Elkind and colleagues (2011) determined mycoplasma contamination of SH-SY5Y cells to interfere with investigation results. It is impossible to tell when the cell population became contaminated and it is unknown how intense said contamination was, so consistency cannot be guaranteed in terms of this potential data-influencing factor. More importantly, the contamination was never confirmed as that from a mycoplasma species; this suggestion is based purely on likelihood.

Immortal cell lines in the study of Parkinson's

The discrepancies between MTT and haemocytometer-derived cell count data additionally bring about questions regarding the suitability of the SH-SY5Y cell line in the study of PD, or at least ferroptosis – Do Van and colleagues (2016) determined SH-SY5Y cells to be totally resistant to cell death induced by erastin. Although most immortalised cell lines arise spontaneously, the SH-SY5Y cells are a subline of cells from the SK-N-SH line (Stacey, 2006). Developed by Biedler et al. in 1973, the original cell line was established in cell culture from a bone marrow biopsy of a metastatic neuroblastoma derived from a 4-year-old female of unknown ethnicity in 1970 and maintained *in vitro* for 1 to 2 years. Initial characterisation of SK-N-SH cells found that tumorigenic properties were maintained, including high saturation densities and plating efficiencies (despite slow attachment), indicative of high proliferation rates. In their 1978 paper, Biedler et al. report of several sublines cloned from the parental SK-N-SH line; first, the SH-SY line was generated and from this, the SH-SY5 line was cloned. The cell line of interest, SH-SY5Y, was subsequently subcloned from the SH-SY5 line. Reasons underlying the popularity of this cell line in PD research and possible drawbacks of using these cells in the study of ferroptosis will be outlined below.

The SH-SY5Y genotype

In order of the catecholaminergic synthesis pathway, Ross and Biedler (1985) report basal tyrosine hydroxylase (TH) activity in SH-SY5Y cells as 6.8 ± 0.1 pmol/h/mg, although offer no guidance as to whether this should be interpreted as low, moderate or high levels of TH activity. TH is a rate-limiting enzyme that converts tyrosine (an amino acid endogenously produced from a second amino acid, phenylalanine) to DA, confirming this cell line's ability to produce DA. In Biedler et al.'s 1978 paper, the group reports dopamine-β-hydroxylase (DβH) activity levels as moderate to high in SH-SY5Y cells, reporting the levels as comparable to those observed in the adrenergic cell bodies of the superior cervical ganglia of rats. DβH is an enzyme that catalyses the conversion of DA to NA. Interestingly, Biedler et al. (1978) reported the inability of SH-SY cells to convert DA to NA; levels of this neurotransmitter were not detectable despite the reportedly high levels of DβH. The authors suggested missing machinery of a normal noradrenergic cell, a lack of localisation of the enzyme to storage vesicles or the rapid deterioration of free noradrenaline by monoamine oxidases within the cell as possible explanations. However, the lack of reference to differentiation of these cells into a neurone-like phenotype in Biedler's paper may provide an alternative explanation – Pahlman et al. (1984) reported that RA-induced differentiation of SH-SY5Y cells resulted in a four-fold increase in NA concentration, suggesting the biochemical properties relating to a catecholaminergic phenotype are indeed present in this subcloned cell line. Interestingly, DHA has been reported to enhance basal NA

release by 25%, suggesting DHA in neuronal cell membranes to influence exocytosis and thus neurotransmission in terms of vesicle release (Mathieu et al., 2010).

More recently, the first whole genome analysis of SH-SY5Y cells was conducted by Krishna et al. (2014) who utilised systems genomic analysis to integrate genomic variation, copy number and structural variation with high-throughput gene expression, metabolomics and proteomics to conclude the genetic architecture of this cell line. It was determined that despite the presence of genetic aberrations due to the tumorigenic nature of the parental SK-N-SH cell line, most genes in the undifferentiated cells belonging to major PD pathways remain intact. Particularly, SH-SY5Y cells were found to have at least one intact copy of each PD-related gene that was analysed. Furthermore, a disease-specific network analysis approach determined the genetic integrity of SH-SY5Y cells as higher for PD compared to Alzheimer's disease but lower than Huntington's disease and amyotrophic lateral sclerosis (ASL) in terms of loss of function experiments. The same approach ranked ROS metabolism as the most intact PD-related subsystem, followed by the ubiquitin-proteasome system, DA metabolism, calcium signalling, mitochondria and glycolysis. The authors note that despite the systems genomics analysis being performed on undifferentiated cells, differentiated cell lines are considered as better *in vitro* models for PD.

Building on Krishna et al.'s study, Filograna et al. (2015) first compared expression levels of eight genes key to catecholamine synthesis and storage in undifferentiated SH-SY5Y cells to expression levels in differentiated cells. Undifferentiated SH-SY5Y cells were shown to express all DAergic/NAergic markers, and markers of both cholinergic and glutamatergic phenotypes were also expressed. Differentiation of cells with RA caused little change in expression levels of DAergic gene markers 7 days after differentiation, but those of cholinergic and glutamatergic phenotypes appeared somewhat upregulated. Gene expression profiles determined expression of *TH*, *AADC* and *DβH* to decrease between 4- and 7-days following RA-induced differentiation. Interestingly, quantification of catecholaminergic levels found those of DA to be below the detectable range determined using HPLC coupled with an electrochemical detector 7 days after differentiation of SH-SY5Y cells with RA. In further dispute of Biedler et al.'s 1978 claim, DA and NA levels in undifferentiated SH-SY5Y cells were also quantified via this method; levels of NA were determined as more than twice that of DA. Only VMAT2 expression was somewhat increased on day 7 compared to day 4. Taken together, these studies suggest undifferentiated SH-SY5Y cells maintain machinery to synthesise all compounds of the catecholamine synthesis pathway, although the synthesis of DA following RA-induced differentiation is still disputed. In terms of PD-related genes, these networks are undisturbed in undifferentiated cells.

SH-SY5Y cells in the study of ferroptosis

Despite the conclusion of SH-SY5Y cells as resistant to ferroptosis by Do Van and colleagues (2016) and the lack of consensus regarding erastin-induced cell death in this experimental project (MTT data suggesting cell death to have occurred in terms of reduced cell viability, and trypan blue and TEM data disagreeing with this), other groups have found success. These studies can be grouped in terms of iron-related investigations and cell death inducer experiments. Investigating the role of mitochondrial ferritin (an iron-storage protein that plays a crucial role in the modulation of cellular iron metabolism) in ferroptosis, Wang et al. (2016) report significant increases of the cellular liable iron pool and C-ROS in SH-SY5Y cells following erastin treatment, effects that were significantly inhibited by the overexpression of the sole iron exporter protein, ferroportin. Moreover, *drosophila melanogaster* fed an erastin-containing diet did not survive more than 3 weeks, whereas those overexpressing ferroportin survived. Similar results are reported by Geng et al. (2018) - confirming erastin to induce ferroptosis in SH-SY5Ys at 5 μg/ml at 6 hours following treatment, the group determined the expression of the ferroportin gene and protein to decrease in erastin-treated cells. Upon siRNA transfection of ferroportin, ferroptotic-associated phenotypical changes were accelerated, indicating ferroportin to act as a negative regulator of ferroptosis by reducing the concentration of intracellular iron. Taken together, these two studies suggest reduction of the liable iron pool by ferroportin can prevent erastin-induced ferroptotic cell death in SH-SY5Y cells.

Evidence from Ito and colleagues (2017) suggests that MPP^+, a commonly employed neurotoxin utilised to induce mimetic PD in animal models, induces a cell death pathway strongly inhibited by Fer-1 and characterised by lipid peroxidation. Despite this, the authors additionally report the inhibition of MPP^+-induced cell death by Nec-1 (albeit in a manner independent of necroptosis-associated protein kinases), the independence of p53 and the accompanying ATP depletion and mitochondrial swelling, suggesting this cell death to be distinct from ferroptosis. Conversely, Hou et al. (2019) report combined treatment of SH-SY5Y cells with paraquat and maneb to induce ferroptotic cell death associated with the activation of NADPH oxidase. Paraquat and maneb are pesticides, the exposure to which have been linked to PD (Chinta et al., 2018; Kumar et al., 2016; Colle et al. 2019). Inhibition of NADPH oxidase utilising two widely used inhibitors reduced the severity of paraquat and maneb-induced ferroptosis. Consistently, stimulating the activation of NADPH oxidase using phorbol myristate acetate (PMA) exacerbated ferroptosis when cells were treated with both cell death inducers. Intriguingly, evidence from Wang and colleagues (2016) suggests the non-oxidative form of DA to dose-dependently inhibit ferroptotic cell death in the tumorigenic PANC1 and HEY cell lines and

non-cancerous MEF and HEK293 cell lines following treatment with erastin. A reduction of erastin-induced ferrous iron accumulation, GSH depletion and MDA production was observed, believed to result from DA increasing the protein stability of GPX4. Furthermore, DA suppressed the degradation of DA receptor 4 (DAR4) and increased DA receptor 5 (DAR5) gene expression.

Taken together, these studies confirm that SH-SY5Y cells are comprised of the machinery necessary to undergo ferroptotic cell death, whether induced by ferroptosis-associated erastin or by compounds already widely used in research to induce mimetic PD. The latter category of studies suggests ferroptotic cell death may have been observed previously but misidentified, although this would require further investigation.

Other cell lines utilised

Despite the wide-spread use of the SH-SY5Y cell line in the study of PD, other immortal cell lines are also commonplace. Derived from a rat adrenal pheochromocytoma (tumour of chromaffin cells in the adrenal gland) cultured by Greene and Tischler in 1976, the PC12 cell line was reported to reversibly extend neurite varicosities upon treatment with nerve growth factor (NGF) as a morphological characteristic of neuronal differentiation, and cells treated with NGF were said to contain small vesicles accumulating in varicose endings. PC12 cells, like chromaffin cells, contain the appropriate enzymes to synthesise, store and, upon stimulation, release both DA and NA (but not adrenalin) at levels comparable to or higher than those observed in rat adrenal glands. For these reasons, PC12 cells have been utilised in the study of PD since their development due to the sensitivity of these cells to mimetic PD toxins including 6-OHDA, MPP^+, rotenone and paraquat (Lee et al., 2018; Zou et al., 2015; Jing et al., 2014; Zhou et al., 2017). Moreover, Wu et al. (2018) determined ferroptosis to occur in PC12 cells following tert-butylhydroperoxide-induced oxidative stress; cell death was inhibited by Fer-1 and DFO cotreatment, and mitochondrial dysfunction was accompanied by a decrease in membrane potential and ATP production and an increase in mitochondrial ROS production. JNK1/2 and ERK1/2 were determined as activated upstream of ferroptosis and mitochondrial dysfunction. Taken together, the evidence outlined here suggests the PC12 cell line to be amongst those sensitive to ferroptotic cell death.

Alternatively, Lund human mesencephalic (LUHMES) cells are embryonic neuronal precursor cells developed by Lotharius et al. (2002) at Lund University, Sweden. These cells exhibit biochemical, morphological and functional features of DAergic neurones upon differentiation utilising dbcAMP and GDNF (glial-derived neurotrophic factor) (Zhang et al., 2014; Edwards & Bloom, 2019). Scholz et al.

(2011) suggests the expression of DA uptake- and release-machinery to be intrinsically predetermined in that the development of this machinery proceeded following the removal of continuous dbcAMP and GDNF during differentiation of LUHMES. TH expression, however, was found to require continuous dbcAMP presence. These cells are amongst the most commonly used cell lines in PD research (Falkenburger et al., 2016), and the 3D culture of LUHMES (providing higher physiological and disease relevance), has shown promise (Harris et al., 2017). Furthermore, the use of LUHMES in the study of ferroptosis has been demonstrated by Do Van et al. (2016) and Bouchaoui et al. (2019). Briefly, Bouchaoui and colleagues determined inhibition or siRNA-mediated silencing of LOXs conferred protection of LUHMES against erastin- and RSL3-induced ferroptosis. Nebie et al. (2019) determined virally inactivated platelet lysates, known to be rich in neurotrophic factors, to exert no detectable signs of toxicity in LUHMES and primary neurones when studied in relation to neuroprotective activity in PD models. Doses of 0.5% and 5% increased TH expression in LUHMES and had no significant impact on synaptic protein expression in primary neurones. More importantly, the platelet lysates exerted a strong neuroprotective effect in both cell types when exposed to erastin.

The use of primary mesencephalic cultures allows the study of neuronal populations that are more DAergic in phenotype and provide increased physiological relevancy compared to immortalised cell lines. To collect these cultures, pregnant animals are euthanised and whole brains collected from the embryos. The removal of the ventral two-thirds of the mesencephalon ensures the dissected regions include the DAergic neuron population of the SN and ventral tegmental area (VTA) whilst avoiding the noradrenergic neurones of the locus coeruleus. Each embryo provides approximately 10^6 viable cells. By day 7, typical values of cell cultures are 45% astrocytes, 40% neurones, 1% DAergic neurones and the remainder are microglia (Xicoy et al., 2017; Skaper et al., 2012). Evidence provided by Lautenschlager and colleagues in 2018 suggests the collection of mesencephalic cultures postnatally greatly increases the percentage of TH-positive cells. In the group's protocol, 40.86 ± 6.24% and 34.10 ± 2.40% of neurones were TH-positive in the ~~ventral tegmental area (~~VTA~~)~~ and the SN respectively, compared to the 1 to 2% of TH-positive neurones reported in embryonic ventral midbrain neuronal cultures. In terms of use in PD research, Gille et al. (2002) determined lisuride, an agonist of DA D_1/D_2 receptors, to enhance survival of DAergic neurones in primary mouse mesencephalic cultures against toxicity induced by MPP^+ or L-dopa. Similarly, Chen and colleagues (2015) determined EGCG (epigallocatechin gallate) pretreatment to protect primary mesencephalic neurones against 6-OHDA-induced neurotoxicity by regulating iron metabolism. No data is as of yet available regarding the use of primary mesencephalic cells in the study of ferroptosis.

Induced pluripotent stem cells (iPSCs) derived from PD patients are emerging as a new category of cell models for this disease (Xicoy et al., 2017). iPSCs refer to pluripotent stem cells that have been generated from terminally differentiated adult somatic cells, and was first developed by Takahashi and Yamanaka upon discovery that manipulation of transcription factors OCT4, SOX2, KLF4 and c-Myc resulted in the reprogramming of skin fibroblasts to pluripotent cells capable of differentiating into various cell types (Xiao et al., 2016; Takahashi & Yamanaka, 2006). The first human trial of iPSC-derived cells for PD, conducted by Takahashi, began in August 2018 and is currently ongoing (Takahashi, 2019). Zhu et al. (2019) recently determined iPSC-derived neuronal stem cells (NSCs) obtained from early-onset PD patients to display increased susceptibility to stress. The authors identified stress-induced downregulation of SIRT1 to lead to autophagic dysfunction and result in these deficits. The utilisation of iPSCs in the study of ferroptosis can be demonstrated by Li et al. (2017) in a haemoglobin-induced model of ICH, determining Fer-1, a caspase 3 inhibitor and Nec-1 in combination, to improve Hb-exposed neuronal viability to a greater degree than any compound alone. A recent study by Cozzi et al. (2019) utilised lines of iPSCs derived from fibroblasts from two neuroferritinopathy (NF) patients and an isogenic control line. Human primary neuronal models of NF determined the free cytosolic iron resulting from alterations of ferritin structure/function to trigger a cascade of events leading to a clear senescence phenotype and spontaneous cell death by ferroptosis.

Summary

The immortalised SH-SY5Y cell line, genetically engineered by Biedler and colleagues in 1973, has long been utilised in the study of Parkinson's disease due to the cost-effective, easy to maintain nature of this human cell line. Addition of 10 μM RA to cell culture medium induces a DAergic phenotype of differentiated SH-SY5Y cells, as was done in this project. A more efficient DAergic phenotype could instead have been induced by the sequential addition of 10 μM of RA and 80 nM of TPA, although one study suggests optimal differentiation of SH-SY5Y cells for use as a cell-based model of PD to contain RA only (Presgraves et al., 2004b; Bellucci et al., 2008; Knaryan et al., 2014; Magalingam et al., 2020). Ross et al. (1981) reports enzyme activity to be dependent on growth phase, culture medium and concentration of FBS in medium. A systematic review of 962 experimental papers utilising SH-SY5Y cells determined there to be no standard protocol of media composition for this cell line; DMEM was the most popular base medium, followed by DMEM/F12 at a 1:1 ratio and high glucose DMEM. FBS concentrations also differed, ranging from 5% to 15% (Xicoy et al., 2017). The composition used in this project more closely matches that recommended by the American Type Culture Collection of DMEM/F12 at a 1:1 ratio with 10% FBS rather than the European Collection of Authenticated Cell Cultures which instead recommends 15% FBS (ATCC, 2016; ECACC, undated).

Alternatively, specifically DAergic immortal cell lines including LUHMES could have been utilised. As mentioned, LUHMES were utilised by Do Van et al. (2016) in the first experimental project studying the potential role of ferroptosis in PD and have recently been utilised by the same group (Bouchaoui et al., 2019). Although cells of this line are noted as difficult to culture over long periods of time, work by Smirnova and colleagues (2016) suggests 3D culturing of LUHMES with slight modifications to differentiation media was able to overcome this problem. The 3D neuronal aggregates were determined by the group to allow penetration of small molecules, and the innermost cells were reported to receive sufficient supply of oxygen and nutrients required for survival. Moreover, the use of a 3D cultured structure more closely resembles *in vivo* conditions. However, DAergic neurones represent less than 1% of the total number of neurones within the brain (Gaven et al., 2014). Although the regions affected in PD are comprised of higher percentages of DAergic neurones, immortalised cell lines of purely DAergic phenotype are less relevant to the physiology of PD-associated brain areas, not accounting for glial cells or neurones possessing the machinery to synthesise and secrete other neurotransmitters. In this instance, it may be that the SH-SY5Y cell line more closely represents the SN compared to LUHMES because of the broader phenotype of these cells. Evidence supporting this notion is provided by Tong and colleagues (2018) who determined LUHMES to display not only higher expression levels of neuronal marker genes in comparison to SH-SY5Y cells but also higher expression levels of genes characteristic of DAergic neurones. Whether LUHMES or SH-SY5Y cells are ultimately the elite immortal cell line for PD research would require further investigation.

The use of primary mesencephalic cell cultures would have provided improved physiological relevancy in that the mesencephalon, or midbrain, is where the SN is located and is thus enriched with DAergic neurones. Moreover, isolation of VTA neurones from SN neurones following Lautenschlager et al.'s 2018 protocol would be beneficial for studies comparing the vulnerability of these neuronal populations in PD. However, the use of these cultures would have been inappropriate for this project in that the collection of primary cultures requires a skill set unlikely to be mastered within the year allowed for experimentation, primary cultures are reportedly difficult to maintain, and use of primary cells can increase experimental variability, depending on the age of the source animals and the accuracy of dissection. More obviously, the use of primary cultures also introduces ethical concerns that are avoided by the use of immortalised cell lines and iPSCs. The use of animals for research purposes is highly regulated in the United Kingdom by the Home Office, requiring a project licence, an establishment licence and a personal licence, and additionally requires first that the research necessitate the use of animals and that there is substantial evidence gained prior to animal

experimentation that the desired outcome would be achieved (GOV.uk, 2019). The inability to prove erastin treatment results in ferroptotic cell death in SH-SY5Y cells means these requirements would not have been met. iPSCs avoid ethical issues that arise from the destruction of an embryo, as required for the collection of primary mesencephalic cell cultures, and moreover allow for patient matching, thus avoiding the risk of immune rejection. However, generation of iPSC PD cellular models is an expensive and time-consuming process, requiring high levels of skill. Immortal cell lines instead allow the luxury of conducting experiments requiring large numbers of clonal cells with identical genetics in a cost-effective manner. Additionally, cells are generally easier to maintain, experiment on and collect data from than primary neurones and iPSCs (Kaur & Dufour, 2012; Maqsood et al., 2013; Stacey, 2006).

Is ferroptosis truly novel?

Ferroptosis was declared a unique cell death pathway by Stockwell's group and has been supported by a number of others. Caution is required, however, in that the most notable (and most commonly referenced) ferroptosis-related research papers currently available, including those offering support of the novel cell death pathway notion, are authored by Stockwell's group and associated researchers/research groups. This therefore brings into question whether ferroptosis truly is novel. Cell death has been observed since the 1800s. Cellular and molecular understanding of cell death began in the 1960s where several laboratories demonstrated cell death is mostly biologically controlled and displays common and distinct morphological patterns. By 1990, the genetic network underlying programmed cell death (apoptosis) had been established, and basic components of cell death machinery identified, sequenced and recognised as highly evolutionarily conserved. This work has allowed us to acknowledge that cell death can occur via a multitude of pathways and, having passed the commitment stage, a cell blocked from undergoing cell death via one pathway will do so by another (Zakeri & Lockshin, 2008). The Nomenclature Committee on Cell Death proposed cell death should be defined as 1) the cell has lost plasma membrane integrity, as identified by incorporation of dyes; 2) the cell, including the nucleus, has undergone complete fragmentation into apoptotic bodies; and/or 3) the corpse or fragments have been engulfed by an adjacent cell. The committee rejects arrest of cell cycle as sufficient evidence of cell death (Kroemer et al., 2009). Here, ferroptosis will be discussed in relation to apoptosis, autophagy and necrosis/necroptosis – the best understood and most widely recognised cell death pathways to date.

Apoptosis

Apoptosis is the most well-known programmed cell death pathway, and occurs in all multicellular organisms. Apoptotic cell death confers many advantages during an organism's life cycle, from

separation of toes and fingers during embryonic development to the clearance of aged or superfluous cells as a homeostatic mechanism to maintain cell populations, and in response to pathological instances of cellular damage. During the early stage of apoptosis, the cell shrinks and chromatin condenses in a process called pyknosis. Membrane blebbing then occurs, followed by fragmentation of the cell and cytoskeletal collapse. The nucleus fragments in the karyorrhexis process, and budding allows the fragments to be separated into apoptotic bodies consisting of tightly packed organelles and cytoplasm. Apoptotic bodies are then phagocytosed by tangible body macrophages, parenchymal cells or neoplastic cells, and degraded by phagolysosomes (Elmore, 2007). Apoptotic cell death avoids occurrence of an inflammatory reaction by four key methods: (1) cells undergoing apoptosis do not typically release their cellular contents into the extracellular space; (2) the apoptotic cells release anti-inflammatory molecules and trigger anti-inflammatory signalling pathways via receptors on the phagolysosome; (3) the cells are quickly phagocytosed; and (4) the engulfing cell releases anti-inflammatory molecules, and the release of pro-inflammatory cytokines is inhibited (Elmore, 2007; Szondy et al., 2017). Apoptosis occurs via two main activation pathways. The first is the intrinsic pathway, initiated by intracellular signals as a response to cellular stress and activated by proteins released from the mitochondrial intermembrane space. The extrinsic pathway, on the other hand, is activated by the binding of ligands released from other cells to death receptors on the cell's surface, initiating the death-inducing signalling complex (Elmore, 2007). The exact number of genes underlying apoptosis is difficult to determine given the various pathways and cellular contexts apoptotic cell death occurs in.

Little evidence is to be found of an overlap of ferroptotic and apoptotic cell death. One available study published by Zheng et al. (2016) claims the MON-p53 nanomedicine to induce cell death via a ferroptosis/apoptosis hybrid pathway. The nanomedicine was created by combining ferric ions with tannic acid (a food additive that can be extracted from green tea) onto the surface of a polyethyleneimine/p53 plasmid complex. MON-p53 is said to have induced apoptosis in HT-1080 cells following the identification of upregulated levels of cleaved "executioner" caspase-3, but the authors report further evidence of apoptotic cell death to be limited (cell death following MON-p53 treatment was only mildly prevented by an apoptosis inhibitor, for example) and the authors conclude ferroptosis to be the dominant cell death pathway under these experimental conditions.

A more promising study was published by Hong et al. (2017). The group determined combination treatment of human pancreatic cancer PANC-1 and BxPC-3 cells, and human colorectal cancer HCT116 cells with ferroptotic agents (erastin or artesunate) and the apoptotic agent TRAIL (tumour necrosis

factor-related apoptosis-inducing ligand) to result in a significantly more cytotoxic effect than any single treatment. This was confirmed by a multitude of tests, including cell death assay, caspase activation, PARP-1 cleavage, flow cytometry and lipid peroxidation assay. Erastin and artesunate induced endoplasmic reticulum (ER) stress, as determined by the upregulated expression of TRB3 (tribbles homologue 3) and CHOP (c/EBP-homologous protein) – expression of these proteins is dependent on ATF4 (activating transcription factor 4), a marker of ER stress. This was confirmed by detection of the unfolded protein response, utilising the anti-ubiquitinylated protein antibody FK2 antibody. Upregulated CHOP expression was found to further promote the expression of p53 upregulated modulator of apoptosis (PUMA). Moreover, HCT116 cells lacking PUMA or CHOP-deficient mouse embryonic fibroblasts displayed no erastin/artesunate and TRAIL synergy, whereas synergistic toxicity was maintained in p53-deficient HCT116 cells. This suggests an involvement of the p53-independent CHOP/PUMA axis following ferroptotic inducer treatment, which may play a role in the sensitisation of cells to TRAIL-induced apoptosis under these conditions. When tested *in vivo*, artesunate was found to significantly reduce the volume of luciferase-expressing HCT116 xenograft tumours grown on the right hind leg of mice. Combined artesunate and TRAIL, however, was found to be significantly more affective compared to single treatment. TRAIL alone had no significant effect on tumour volume.

Autophagy

Autophagy is a regulated intracellular degradation pathway whereby unwanted cytoplasmic constituents and damaged or superfluous organelles are sequestered and delivered to lysosomes for degradation (Gatica et al., 2018; Mizushima, 2007; Mizushima et al., 2008). Regulated by over 30 autophagy-related genes (ATGs), this pathway is essential for cellular differentiation, development and homeostasis by preserving organelle function and preventing the toxic build-up of cellular waste. Additionally, the products of lysosomal degradation are recycled and can provide substrates to sustain metabolism under cellular starvation conditions (nutrient depletion or hypoxia, for example) whereby autophagy acts as a stress-response (Gao et al., 2016; Levine & Kroemer, 2008; White, 2015). Currently, three forms of autophagy are widely recognised: chaperone-mediated autophagy (CMA), microautophagy and macroautophagy. Physiological functions, mode of cargo delivery to the lysosome and cargo transported vary between forms (Levine & Kroemer, 2008). Moreover, mitophagy (autophagy of mitochondria) and lipophagy (degradation of lipids) are emerging as increasingly recognised forms (Vives-Bauza et al., 2010; Schroeder et al., 2015). Controversially, the self-cannibalistic or, paradoxically, the pro-survival functions of autophagy have been found deleterious in certain experimental disease settings, possibly through the extensive degradation of intracellular

components induced by oxidative stress as a result of ROS accumulation (Levine & Kroemer, 2008; Azad et al., 2009; Ma et al., 2017). Under these conditions, autophagy has been linked to diseases including various cancers (lung, breast, and pancreatic cancers, for example) (Guo et al., 2013; Wei et al., 2014; Yang et al., 2014).

Wu et al. (2018) determined erastin-induced ferroptosis to increase levels of lysosome-associated membrane protein 2a, to promote degradation of GPX4 via CMA. Inhibition of CMA stabilised GPX4 and reduced ferroptosis, suggesting CMA activation to be involved in ferroptosis but not overall sufficient to cause cell death. Basit and colleagues (2017) determined BAY 87-2243-induced inhibition of complex 1 of the mitochondrial respiratory chain resulted in depolarisation of the mitochondrial membrane potential, increased cellular ROS levels, lipid peroxidation and reduced GSH levels, effects paralleled by the opening of the mitochondrial permeability transition pore and stimulation of autophagosome formation, leading to mitophagy. BAY-induced cell death was inhibited by pharmacological means (α-tocopherol treatment, for example) and the genetic knockdown of *ATG5* due to inhibited autophagosome formation.

A more critical study is provided by Gao et al. (2016), who determined 11 ATGs as potentially regulating ferroptosis, in addition to other genetic targets not previously described as ferroptosis-associated. *In vitro*, treatment of MEFs and HT-1080 cells with erastin resulted in the conversion of LC3-I (cytosolic microtubule-associated protein 1A/1B-light chain 3) to LC3-II (LC3-phosphatidylethanolamine conjugate), and formation of GFP-LC3 puncta, both of which are hallmarks of an autophagic response (LC3-II is recruited to autophagosomal membranes and degraded in autolysosomes (Tanida et al., 2008)). At low erastin concentrations and in a relatively short-lived manner, Gao and colleagues (2016) found BafA1 (bafilomycin A1, an inhibitor of autophagosome-lysosome fusion) significantly blocked ferroptosis in both cell lines, preventing the accumulation of L-ROS and total ROS. The authors suggest this may be why Dixon et al. (2012) reported ferroptosis to be independent of autophagy. Knockout of ATG13 and ATG3, which function at different stages of autophagy, reduced the sensitivity of MEFs to ferroptosis, and was restored by reconstitution of these genes. Acknowledging the importance of iron, Gao determined erastin to increase the liable iron pool (LIP) in a time-dependent manner, which could also be blocked by autophagy inhibition. NCOA4 (nuclear receptor coactivator 4) is a protein mediating ferritinophagy which, using NCOA4 as the cargo receptor, delivers ferritin to the lysosome for degradation to release free iron, increasing the LIP. RNAi knockdown of NCOA4 significantly prevented erastin-induced ferroptosis and L-ROS generation. Endogenous levels of ferritin heavy chain 1 (FTH1; one half of ferritin's protein complex) were

determined to increase during ferroptosis, suggesting LIP accumulation caused compensatory upregulated transcription of this protein, confirmed by q-PCR as NCOA4-dependent. Lastly, erastin was found to induce the degradation of FTH1, which could be prevented by BafA1. Taken together, these findings suggest that upon ferroptosis induction, NCOA4-mediated ferritinophagy and degradation of excess FTH1 are activated which increases the LIP. This in turn ensures the rapid accumulation of ROS and allows ferroptosis to continue.

The underlying role of ferritinophagy in ferroptosis has been studied by a number of groups. Hou et al. (2016) determined knockout of *ATG5* and *ATG7* (critical to autophagosome formation) to inhibit erastin-induced cell death in MEFs, two human pancreatic cancer cell lines and HT-1080 cells. Moreover, intracellular Fe^{2+} and MDA levels were significantly reduced in *ATG5*- and *ATG7*-deficient MEFs and HT-1080 cells following erastin treatment, but not treatment with CQ (chloroquine; a lysosomal inhibitor). Furthermore, levels of FTH1 were found to be significantly increased in ATG5-deficient MEFs with or without erastin treatment, suggesting ATG5 to be involved in ferritinophagy. Previous evidence has shown ATG5-mediated lipidation of LC3 to be necessary for the conversion of LC3-I to LC3-II; Hou and colleagues determined knockdown of ATG5 to inhibit erastin-induced LC3-II and GFP-LC3 puncta formation. Evidence of ferritinophagy *in vivo* is provided Zhang et al. (2018) following a longitudinal study of HCC patients receiving sorafenib monotherapy; sorafenib treatment resulted in a marked upregulation of *NCOA4* expression, suggesting an increase of ferritinophagy to release iron from FTH1, leading to ferroptotic events including *PTGS2* upregulation, redox-active iron accumulation, ROS generation and lipid peroxidation. More recently, Du et al. (2019) reported the ω-3 PUFA DHA to induce ferritinophagy occurring in three acute myeloid leukaemia cell lines by regulating the AMPK/mTOR/p70S6k signalling pathway. The free iron released in this degradation process then initiated ferroptosis. Consistently, pharmacological and genetic inhibition of autophagy significantly inhibited DHA-induced ferroptosis, whereas the overexpression of ISCU (iron-sulphur cluster assembly enzyme) rescues cells from ferroptotic cell death by regulating iron metabolism and mitochondria function.

In contrast, Buccarelli et al. (2018) determined impairment of autophagic processes through treatment of quinacrine (QN) to increase the susceptibility of glioblastoma-like stem cells (GSC; cancer stem cells hypothesised to be involved in the recurrence and poor prognosis of glioblastoma-affected patients) to cell death induced by temozolomide (TMZ), an oral chemotherapy drug. Accumulation of lipid radicals, MDA and cell death following combined QN/TMZ treatment was significantly attenuated by treatment of DFOM and Fer-1 as quantified by BODIPY-C11-associated flow cytometry, but no other

compounds tested. Moreover, GPX4 activity was reduced following QN/TMZ treatment and was again fully reversed by DFOM or Fer-1. In terms of autophagic processes, immunofluorescence intensity analysis showed a significant increase in LC3 expression in GSC xenograft tumours using the combined treatment approach. Taken together, this suggests that in contrast to those studies outlined above, overcoming a pro-survival autophagic response via inhibition instead allows for ferroptotic cell death to occur.

This is somewhat supported by Ma et al. (2017), who determined cotreatment of siramesine (a lysosomal disruptor) and lapatinib, a dual tyrosine kinase inhibitor, to induce ferroptosis in MDA MB 231, SKBR3 and MCF-7 breast cancer cells 4 hours after treatment in that Fer-1 pre-treatment significantly decreased cell death. 24 hours after treatment, however, Fer-1 had little effect. Interestingly, inhibition of autophagy with 3-methuladenine (3-MA) and spautin-1 significantly increased cell death in siramesine and lapatinib co-treated MDA MB 231 and SKBR3 cells at 4 hours, but significantly reduced cell death at 24 hours. Knockdown of *ATG5* or *BENC1*, a gene involved in the conversion of LC3-II and autophagosome generation (Kang et al., 2011), instead resulted in increased cell death at 4 hours and reduced cell death at 24 hours post-treatment. Measuring of autophagy via western blotting LC3-II levels determined autophagic flux to increase over a 24-hour period. Moreover, western blotting of lysed cells that received cotreatment revealed levels of transferrin, the cellular iron importer, to be significantly increased at 24 hours and FTH1 to be significantly decreased at 24 hours. In cells pre-treated with 3-MA, FTH1 was instead significantly increased. Similar results occurred following knockdown of *ATG5*, suggesting ferritinophagy to occur. Additionally, iron level and ROS generation were found to increase following cotreatment in a time-dependent manner. Taken together, this evidence suggests ferroptosis to occur in the initial hours following treatment, during which the autophagic response is pro-survival. The role of ferroptosis in cell death then diminishes, and autophagy switches to favour cell death. Recently, Li and colleagues (2019) constructed a carrier-free nanodrug called NFER, or nanoparticle ferritin-bound erastin and rapamycin. *In vitro* studies confirmed the combined ferroptosis- and autophagy-inducing abilities of NFER and showed improved control of tumour recurrence in a 4T1 breast cancer cell tumour resection model. High stability of the nanodrug was reported in water and PBS for days.

Necrosis

In comparison to apoptosis and autophagy, necrosis is considered an unprogrammed cell death pathway and is almost always associated with detrimental pathological processes. To date, six morphologically distinctive forms of necrosis have been identified; coagulative and liquefactive are

the most well-documented, in addition to gangrenous, caseous, fat and fibrinoid necrosis. Coagulative necrosis is associated with ischemic or hypoxic injury in every organ except the brain and is characterised by firm tissue in which the architecture is maintained for several days following cell death, and preserved cell outlines without nuclei are visible microscopically. Liquefactive necrosis is instead associated with infection or ischemic injury to the brain, and is characterised by the release of autolysis-causing digestive enzymes from the dying cell's lysosomes and constituents of neutrophils. In cases of infection, the release of heterolysis-causing enzymes and inflammatory cells originating from the invading organism are additionally characteristic. Autolysis (and heterolysis) results in liquified tissue that may be creamy in colour. Necrosis is associated with the death of cells following irreversible injury as a result of mechanical cell damage and pathogen insult. Reports suggests that necrosis does not occur during development (Adigun et al., 2019; Kumar et al., 2010).

As briefly outlined in the introduction of this paper, metabolised or oxidised haemoglobin (heme or hemin, respectively) released from lysed erythrocytes following ICH (intracerebral haemorrhage) causes ROS-associated tissue damage and cell death in brain regions surrounding the site of rupture. ICH can additionally be induced by collagenase treatment; Li et al. (2017) determined ferroptosis inhibitor Fer-1 to protect against haemoglobin-induced cell death in OHSCs (organotypic hippocampal slice cultures) and collagenase-induced cell death in mice. TEM examination of cellular ultrastructure at 3- and 6-days post-collagenase ICH induction showed shrunken mitochondria in soma and axons, as is characteristic of ferroptosis, but the authors also observed cytoplasmic and organelle swelling and plasma membrane rupture, indicative of necrotic cell death, suggesting these two cell death pathways occur simultaneously in collagenase-induced murine models of ICH. The authors highlight that combinatorial Fer-1 and Nec-1 treatment decreased cell death more than either inhibitor individually, as determined by propidium iodide staining. Similar observations were determined by the group in 2018 with the report of varying degrees of necrotic cell death occurring in brain regions within 1 mm of the hematoma margin during the subacute ICH phase, again at 3- and 6-days post-ICH induction. Li and colleagues report that the majority of cells were necrotic, although morphological ferroptosis characteristics including shrunken mitochondria were also visible (Li et al., 2018). More relative to this project, Ito et al. (2017) concluded MPP^+ to induce Nec-1- and Fer-1-sensitive necrotic cell death in SH-SY5Y cells.

Necroptosis

The cytokine TNFα (tumour necrosis factor α) was central in the distinction of necroptosis as a regulated cell death pathway distinct from the unregulated necrotic counterpart, following the

observation that this protein can induce regulated cell death with apoptotic or necrotic features in a manner that is dependent upon cell type, context and additional cell death sensitizers (Laster et al., 1988). Not dissimilar to necrosis, necroptotic cell death is morphologically characterised by cytoplasmic granulation and organelle and/or cellular swelling that results in the leakage of intracellular contents from the cell, but is associated with inflammatory cell death, acting as a consequence in certain circumstances and a trigger of necroptotic cell death in others (Vandenabeele et al., 2010; Wallach et al., 2016). One crucial difference is the tightly regulated increase in cell membrane permeability during necroptosis; the binding of TNFα to the TNF receptor (TNFR1) signals the recruitment of TNF receptor-associated death domain (TRADD) and TRAF2 (TNF receptor-associated factor 2) which further recruits RIPK1 (receptor interacting serine/threonine kinase 1). RIPK1 then recruits RIPK3 (Conrad et al., 2016). The inhibition or absence of caspase 8 and Fas-associated protein with death domain (FADD) allows for the auto- or transphosphorylation of RIPK1 and RIPK3, causing the formation of the necrosome complex. RIPK3 of the necrosome activates the pseudokinase MLKL (mixed lineage kinase domain-like protein) via phosphorylation of MLKL's activation loop, triggering a molecular switch in which MLKL unleashed its N-terminal for-helix domain and forms a membrane localised complex. This increases the permeability of the membrane and causes a loss of membrane potential (leading to bioenergetics failure by preventing the generation of ATP) before the contents of the cell are expelled into the extracellular space (Hildebrand et al., 2014; Conrad et al., 2016).

As with ferroptosis and necrosis, some suggest ferroptosis and necroptosis may occur in unison. Zille et al. (2017) determined ferroptosis inhibitors (Fer-1, DFO, N-Acetylcysteine, trolox and U0126) and Nec-1, an inhibitor of necroptosis that targets RIPK1 (Degterev et al., 2005; Degterev et al., 2008), to protect cultured primary neurones from haemoglobin- and hemin-induced toxicity by >80%. Inhibitors of caspase-dependent apoptosis, protein or mRNA synthesis (CHX and actinomycin D) or autophagy were unable to offer protection. Molecular markers of ferroptosis and necroptosis were increased following ICH *in vivo* and *in vitro*, and electron microscopy determined hemin to induce a necroptotic phenotype of cell death. These findings suggest that ICH studied under experimental conditions displays features of both ferroptotic and necroptotic cell death. The authors theorise that inhibition of either pathway would prevent a threshold of death being reached and instead allow for cell survival. In support of this, Yu et al. (2015) found low dose erastin treatment to significantly enhance the sensitivity of non-APL AML (non-acute promyelocytic leukaemia acute myeloid leukaemia) HL-60 cells to chemotherapeutic agents, including cytarabine and doxorubicin, in a RAS-independent manner as

determined by growth inhibition. This was accompanied by the combined induction of ferroptosis and necroptosis in a selective MAPK- (mitogen-activated protein kinase-) dependent manner.

Other lines of evidence suggest an involvement of GPX4 and GSH in combined ferroptotic and necroptotic cell death. Lorincz et al. (2015) report the ability of both Fer-1 and Nec-1 to maintain cell viability levels to almost that of the control following the treatment of primary mouse hepatocytes with acetaminophen (APAP; also known as paracetamol), suggesting the involvement of ferroptosis and necroptosis in APAP-induced cell death. APAP is an analgesic and antipyretic drug that induces cell death displaying characteristic overlap with ferroptosis (GPX4 inhibition, GSH depletion and caspase independency). In addition, Chen and colleagues (2017) report the rescuing of triple negative breast cancer (TNBC) cells from cystine starvation-induced cell death by Nec-1, Fer-1, necrosulfonamide (an MLKL inhibitor) and RIPK1 knockdown, suggesting an involvement of ferroptosis and necroptosis under these conditions. This was determined to occur via the activation of the GCN2-eIF2α-ATF4 pathway following the degradation of GSH by *CHAC1* (ChaC GSH-specific γ-glutamylcyclotransferase 1), a target gene of ATF4 (suggested as downstream of the RIPK1/RIPK3-MLKL pathway), in that knockdown of CHAC1 prevented the reduction of GSH under cystine starvation conditions. Interestingly, Canli et al. (2016) report *GPX4* deletion results in RIPK3-dependent necroptosis in erythroid precursor cells, independently of TNFα, that is characterised by ROS accumulation and high levels of lipid peroxidation. The authors conclude ROS and lipid hyperoxide generation to function as not-yet-recognised upstream signalling activators of RIPK3-dependent necroptosis, but it may instead be further evidence of ferroptosis and necroptosis occurring in unison.

Alternatively, Muller et al. (2017) report that resistance to ferroptosis results in increased sensitivity of cells to necroptosis and vice versa. The group determined knockout of *ASCL4* (acyl-CoA synthetase long-chain family member 4) conferred cells' protection against erastin- and RSL3-induced ferroptosis and that deletion of *MLKL* conferred protection against necroptosis. The group speculate MLKL may drive resistance to ferroptosis by depleting PUFAs, and ASCL4 allows resistance to necroptosis by reducing the ability of MLKL to permeate the cell membrane. The reliability of *ASCL4* as a biomarker of ferroptotic cell death is supported by Doll et al. (2017) who determined the enzyme to increase the density of long polyunsaturated ω6 fatty acids in cell membranes.

Summary

The determination of ferroptotic cell death as occurring is mostly concluded by pharmacological or genetic inhibition of systems or genes reportedly involved in this cell death pathway. However, as

highlighted above, the evaluation of ferroptotic cell death under experimentally manipulated conditions has led to the reporting of different conclusions by various groups. Taken together, evidence suggests that the declaration of ferroptosis as a cell death pathway unique from apoptosis, autophagy and necrosis by Stockwell's laboratory in 2012 may have been pre-emptive. Although it is almost universally accepted that ferroptosis is non-apoptotic in nature, there is debate, as outlined from the evidence presented here, as to whether ferroptosis is a necrotic/necroptotic cell death pathway or one that occurs alongside autophagy or necrosis/necroptosis. Yu et al. (2016), for example, report expression level of ACSF2 mRNA (a mitochondrial gene reported by Dixon et al. (2012) to be a key regulator of the ferroptotic genetic network that displays no overlap with apoptosis, autophagy or necrosis) to display a significant positive correlation with caspase-3 mRNA levels *in vivo*, suggesting the involvement of *ACSF2* in apoptosis-induction signalling. This study highlights that, at present, our understanding of ferroptosis (and other cell death pathways) is too immature and underdeveloped to conclusively define ferroptosis as distinct. Moreover, caution should be taken in that a relatively large number of ferroptosis-related papers currently available have been authored by those in Stockwell's laboratory or by researchers and groups with which Stockwell is closely associated. However, these researchers are similarly unable to reach a consensus regarding the novelty of ferroptosis; whilst many experimental and review papers published since the pioneering 2012 paper refer to ferroptosis as non-apoptotic rather than unique (Lewerenz et al., 2018; Shimada et al., 2016; Friedmann et al., 2014), others refer to ferroptosis as a form of regulated necrosis (Lachaier et al., 2014; Vanden Berghe et al., 2014; Linkermann et al., 2014). This is further highlighted by the inhibition of ferroptosis by necroptosis-associated inhibitor Nec-1 (Friedmann et al., 2014).

Furthermore, in comparison to apoptotic, autophagic and necrotic/necroptotic morphological features, those of cells undergoing ferroptosis – rounding up of the cell and maintenance of normal cell size – are arguably more difficult to identify. The presence of shrunken mitochondria as the gold standard in the identification of cells undergoing ferroptosis, observed utilising TEM, has been reported by groups including Li et al. (2017 & 2018) as hindering the distinction of cell death mechanisms in cells. The authors note that it is impossible to define shrunken mitochondria without quantifying a large number of cells *in vivo*, leading the group to assume ferroptotic and necrotic cells, for example, were present in the same brain regions. Similarly, the differences between necrosis and necroptosis is unclear and not universally understood – some papers reporting of necrosis or necroptosis identified the cell death pathway with little justification of the distinction between the programmed and unprogrammed cell death phenotype, which may cause confusion in the relaying of information.

Conclusions and further work

The tests conducted in this project were limited by funding, amongst other factors. Analysis of data derived from MTT cell viability assay showed initial promise, suggesting IC_{50} concentrations of erastin treatment to be 6 μM for the 24-hour condition and 4 μM for the 48-hour condition in the SH-SY5Y immortal cell line, as an *in vitro* model of PD. Co-treatment of cells with erastin and DHA (an ω-3 PUFA), $AACOCF_3$ (an inhibitor of calcium-dependent cytosolic phospholipase A_2 enzymes), Fer-1 (the first identified inhibitor of ferroptosis) and BEL, an irreversible inhibitor of calcium-independent $PLA_2\beta$ ($iPLA_2\beta$) also generated interesting output. Despite significant differences having been determined in both the time and concentration conditions in the erastin-only data sets, a lack of significant difference in either condition when cells were co-treated with erastin and Fer-1 indicates that whilst cells may be undergoing cell death, the pathway utilised may not be ferroptosis. Haemocytometer-associated trypan blue assay instead determined there to be no significant difference in either the time or concentration condition of erastin alone (when using the IC_{50} concentrations calculated from MTT output analysis) or co-treatment of erastin and DHA, AACOCF3, BEL or Fer-1 ($p > 0.05$ for all), suggesting a lack of ferroptosis and cell death in general. This was further supported by images obtained from TEM; use of the IC_{50} concentration of erastin (again calculated from the MTT data), to have a negligible effect on cell viability - 96% of cells were alive at the point of fixation, having been treated with this concentration (6 μM) for a 24-hour period. Moreover, mitochondrial size was not significantly different between the treated and untreated cell groups. Taken together, no conclusion can adequately be drawn from the data established from this project.

Given our limited understanding of ferroptosis at this point in time, particularly outside the field of oncology, it would seem logical for any further work into the potential role of ferroptosis in PD to first confirm the process of ferroptosis as occurring, based on previously outlined indicators. To do this, a two-pronged approach would be best; given the proclamation of LUHMES as sensitive to erastin-induced ferroptosis, it would be interesting to study the effect of erastin treatment in this cell line, although the more DAergic phenotype of this cell line may introduce difficulties in comparison. Additionally, the investigation of erastin in the PC12 cell line, also utilised in the study of PD, may have offered additional avenues through which to investigate ferroptosis in catecholaminergic cell lines and PD *in vitro* models, and provided more lines of evidence. The second prong would be to assess lines of ferroptotic evidence at various stages of the cell death pathway, utilising procedures and protocols

with a proven efficacy in the study of ferroptosis. For example, assessing the integrity of system x_c^- in SH-SY5Y cells and other immortal cell lines of choice, by inhibition of SLC7A11 using class I FINs other than erastin, including SAS, sorafenib or RSL5, or siRNA-mediated inhibition. If cell death were to occur, inhibition by CHX would provide an additional line of evidence as to ferroptosis occurring at this stage of the pathway. The employment of a GSH/GSSG ratio assay and BODIPY-C11 flow cytometry, as means of detecting total glutathione levels and L-ROS generation respectively, could be utilised following class I or class II FIN (and inhibitor) treatment, to provide confirmation of ferroptotic cellular activity. Confirmation of cell death could be done via MTT and calcein AM, as a verified cell viability assay for quantifying ferroptotic cell death. It would also be of interest to conduct these experiments using the original erastin and Fer-1 compounds, as well as the modified PE and IKE, and SRS11-92 and SRS16-86.

If ferroptotic cell death could be induced and confirmed successfully, investigating this process in rodent-derived primary neurones would be advantageous in terms of providing greater neuronal similarity to that of humans than immortal cell lines and would highlight any potential role played by supporting glial cells.

Interestingly, despite the proclamation of six mitochondrial genes as controlling ferroptotic cell death, no in-depth investigation of the role played by each gene in ferroptosis was performed in the original paper and little evidence has since been provided. Moreover, there seems to be little evidence to the role of each gene regardless of a ferroptotic setting; a study (possibly utilising shRNA) would be beneficial in terms of providing further evidence not only to the role of each gene but as to whether ferroptosis is a unique cell death pathway or a process that falls under an existing cell death pathway. Additionally, an in-depth investigation of molecular and morphological characteristics resulting from erastin treatment, from the point of view of determining which cell death pathway is being utilised rather than from the view of determining ferroptotic characteristics, would allow for greater awareness.

The next question would be: what is the best biomarker or signal in predicting sensitivity to ferroptosis? Whilst oncogenic RAS was determined to regulate sensitivity in the original engineered tumorigenic cell lines, it is unknown what genetically regulates sensitivity of subsequently investigated cell lines to FINs. Determination of a biomarker or signal would allow for investigation into utilising FINs as targeted therapeutic agents against diseases not only including various cancers, but potentially neurodegenerative diseases including PD.

One suggestion as to the sensitivity of SH-SY5Y cells, for example, to ferroptosis pertains to the DA content of this cell line, with some suggesting the intracellular DA content to have played a neuroprotective role. The investigation of ferroptosis in DAergic cells in relation to the role of DA and, on the other side, whether mimetic neurotoxins (for example MPP^+ and 6-OHDA) can induce ferroptotic cell death, would be of great interest in terms of ferroptosis specifically in PD or other related diseases, as would the effect of aSyn by upregulated transcription and translation of the SNCA gene and, at the very forefront of the investigation, the role of iron.

Having been highlighted as the essential link between ferroptosis and PD in this project, it was unfortunate that time-constraints meant investigating this was not possible. For future research, it would be beneficial to first quantify levels of iron in SH-SY5Y cells and other cell lines utilised, before increasing this basal level with exogenous iron to levels representing the percentage increase believed to be present in remaining DAergic PD neurones. Whilst this increase in iron would be predicted to induce increased C-ROS generation as has been found in a previous study investigating the role of ferritin following erastin treatment of SH-SY5Y cells, it would be interesting to see whether a compensatory upregulation of ferroportin transcription and translation would occur, or whether this would lead to increased efficiency in cell death.

Other imperative questions remaining include: what is the structural basis of GPX4 inhibition by RSL3 and other class II FINs? What effector molecules located downstream of lipid peroxidation are activated (or deactivated) to cause ferroptosis? How does the RAS/RAF/MEK pathway fit into ferroptotic signalling? As demonstrated by this experimental project and the questions highlighted above, our knowledge of ferroptosis (and PD pathology in general) remains in infancy, offering a plethora of exciting avenues for future research.

Acknowledgements

I would like to thank Professor David Furness and Karen Walker for their guidance in teaching me transmission electron microscopy techniques. I would also like to express my gratitude towards Doctor Michael Evans for his assistance (and patience) whilst editing my thesis.

References

Adigun, R., Basit, H., & Murray, J. (2019). *Necrosis, Cell (Liquefactive, Coagulative, Caseous, Fat, Fibrinoid, and Gangrenous)*. Treasure Island, Florida: StatPearls Publishing.

Agil, A., Duran, R., Barrero, F., Morales, B., Arauzo, M., Alba, F., Miranda, M. T., Prieto, I., Ramirez, M., & Vives F. (2006). Plasma lipid peroxidation in sporadic Parkinson's disease. Role of the L-dopa. *Journal of the Neurological Sciences, 240*(1-2), 31-36. doi: 10.1016/j.jns.2005.08.016.

Agmon, E., & Stockwell, B. R. (2017). Lipid homeostasis and regulated cell death. *Current Opinion in Chemical Biology*, *39*, 83–89. doi: 10.1016/j.cbpa.2017.06.002.

Ahuja, D., Sáenz-Robles, M. T., & Pipas, J. M. (2005). SV40 large T antigen targets multiple cellular pathways to elicit cellular transformation. *Oncogene*, *24*, 7729–7745. doi: 10.1038/sj.onc.1209046.

Albrecht, P., Lewerenz, J., Dittmer, S., Noack, R., Maher, P., & Methner, A. (2010). Mechanisms of Oxidative Glutamate Toxicity: The Glutamate/Cystine Antiporter System x_c^- as a Neuroprotective Drug Target. *CNS & Neurological Disorders - Drug Targets*, *9*(3), 373–382. doi: 10.2174/187152710791292567.

Alexander, G. E. (2004). Biology of Parkinson's disease: pathogenesis and pathophysiology of a multisystem neurodegenerative disorder. *Dialogues in Clinical Neuroscience*, *6*(3), 259–280.

Allderdice, P. W., Gardner, H. A. R., Galutira, D., Lockridge, O., Ladu, B. N., & McAlpine, P. J. (1991). The cloned butyrylcholinesterase (BCHE) gene maps to a single chromosome site, 3q26. Genomics, 11(2), 452-54. doi: 10.1016/0888-7543(91)90154-7.

Amini, R-M., Berglund, M., Rosenquist, R., von Heideman, A., Lagercrantz, S., Thunberg, U., Bergh, J., Sundstrom, C., Glimelius, B., & Enblad, G. (2002). A Novel B-cell Line (U-2932) Established from a Patient with Diffuse Large B-cell Lymphoma Following Hodgkin Lymphoma. *Leukemia & Lymphoma, 43*(11), 2179–2189. doi: 10.1080/1042819021000032917.

Akerman, K. E. O., Scott, I. G., & Andersson, L.C. (1984). Functional differentiation of a human ganglion cell derived neuroblastoma cell line SH-SY5Y induced by a phorbol ester (TPA). *Neurochemistry International, 6*(1), 77-80. doi: 10.1016/0197-0186(84)90029-9.

Aquino, C. C., & Fox, S. H. (2015). Clinical Spectrum of Levodopa-Induced Complications. *Movement Disorders, 30*(1), 80–9. doi: 10.1002/mds.26125.

Ashraf, A., Jeandriens, J., Parkes, H. G., & So, P-W. (2020). Iron dyshomeostasis, lipid peroxidation and perturbed expression of cystine/glutamate antiporter in Alzheimer's disease: evidence of ferroptosis. *Redox Biology, 32*, 101494. doi: 10.1016/j.redox.2020.101494.

American Type Culture Collection. (2016). *SH-SY5Y ATCC ® CRL-2266™ Homo sapiens bone marrow neuroblast*. [online] Available at: https://www.lgcstandards-atcc.org/products/all/CRL-2266.aspx#culturemethod [Accessed 5 Jul. 2019].

Ayala, A., Munoz, M. F., & Arguelles, S. (2014). Lipid peroxidation: production, metabolism, and signalling mechanisms of malondialdehyde and 4-hydroxy-2-nonenal. *Oxidative Medicine and Cellular Longevity, 2014*, 360-438. doi: 10.1155/2014/360438.

Azad, M. B., Chen, Y., & Gibson, S. B. (2009). Regulation of autophagy by reactive oxygen species (ROS): implications for cancer progression and treatment. *Antioxidants and Redox Signalling, 11*(4), 777-90. doi: 10.1089/ARS.2008.2270.

Baba, Y., Higa, J. K., Shimada, B. K., Horiuchi, K. M., Suhara, T., Kobayashi, M., Woo, J. D., Aoyagi, H., Marh, K. S., Kitaoka, H., & Matsui, T. (2018). Protective effects of the mechanistic target of rapamycin against excessive iron and ferroptosis in cardiomyocytes. *Heart and Circulatory Physiology*, *314*(3), 659-68. doi: 10.1152/ajpheart.00452.2017.

Badgley, M. A., Kremer, D. M., Maurer, H. C., DelGiorno, K. E., Lee, H-J., Purohit, V., Sagalovskiy, I. R., Ma, A., Kapilian, J., Firl, C. E. M., Decker, A. R., Sastra, S. A., Palermo, C. F., Andrade, L. R., Sajjakulnukit, P., Zhang, L., Tolstyka, Z. P., Hirschhorn, T., Lamb, C., Liu, T., Gu, W., Seeley,E. S., Stone, E., Georgiou, G., Manor, U., Iuga, Al., Wahl, G. M., Stockwell, B. R., Lyssiotis, C. A., & Olive, K. P. (2020). Cysteine depletion induces pancreatic tumor ferroptosis in mice. *Science. 368*(6486), 85-9. doi: 10.1126/science.aaw9872.

Băjenaru, O., Ene, A., Popescu, B. O., Szasz, J. A., Sabau, M., Muresan, D. F., Perju-Dumbrava, L., Popescu, C. D., Constantinescu, A., Buraga, I., & Simu, M. (2016). The effect of levodopa-carbidopa intestinal gen infusion long-term therapy on motor complications in advanced Parkinson's disease: a multicentre Romanian experience. *Journal of Neural Transmission, 123*(4), 407-14. doi: 10.1007/s00702-015-1496-z.

Bao, W-D., Pang, P., Zhou, X-T., Hu, F., Xiong, W., Chen, K., Wang, J., Wang, F., Xie, D., Hu, X-Z., Han, Z-T., Z, H-H., Wang, W-X., Nelson, P. T., Chen, J-G., Lu, Y., Man, H-Y., Liu, D., & Zhu, L-Q. (2021). Loss of ferroportin induces memory impairment by promoting ferroptosis in Alzheimer's disease. *Cell Death & Disfferentiation, 28*, 1548-62. doi: 10.1038/s41418-020-00685-9.

Barlie, M. F., Hopps, H. E., Grabowski, M. W., Riggs, D. B., & DelGiudice, R. A. (1973). The identification and sources of mycoplasmas isolated from contaminated cell cultures. *The New York Academy of Sciences, 225*, 251-64. doi: 10.1111/j.1749-6632.1973.tb45654.x.

Basit, F., van Oppen, L. M., Schockel, L., Bossenbroek, H. M., van Emst-de Vries, S. E., Hermeling, J. S., Grefte, S., Kopitz, C., Heroult, M., Hgm Willems, P., & Kppoman, W. J. (2017). Mitochondrial complex I inhibition triggers a mitophagy-depedent ROS increase leading to necroptosis and ferroptosis in melanoma cells. *Cell Death and Disease, 8*(3), e2716. doi: 10.1038/cddis.2017.133.

Bassi, M., Gasol, E., Manzoni, M., Pineda, M., Riboni, M., Martín, R., Zorzano, A., Borsani, G., & Palacín, M. (2001). Identification and characterisation of human xCT that co-expresses, with 4F2 heavy

chain, the amino acid transport activity system x c -. *Pflugers Archiv European Journal of Physiology*, *442*(2), 286–296. doi: 10.1007/s004240100537.

Bastide, M. F., Meissner, W. G., Picconi, B., Fasano, S., Fernagut, P. O., Feyder, M., Francardo, V., Alcacer, C., Ding, Y., Brambilla, R., Fisone, G., Jon Stoessl, A., Bourdenx, M., Engeln, M., Navailles, S., De Deurwaedere, P., Ko, W. K., Simola, N., Morelli, M., Groc, L., Rodriguez, M. C., Gurevich, E. V., Quik, M., Morari, M., Mellone, M., Gardoni, F., Tronci, E., Guehl, D., Tison, F., Crossman, A. R., Kang, U. J., Steece-Collier, K., Fox, S., Carta, M., Angela Cenci, M., & Bezard, E. (2015). Pathophysiology of L-dopa-induced motor and non-motor complications in Parkinson's disease. *Progress in Neurobiology, 132*, 96-168. doi: 10.1016/j.pneurobio.2015.07.002.

Bebber, C., Thomas, E. S., Chen, Z., Stroh, J., Androulidaki, A., Schmitt, A., Hohne, M. N., Stuker, L., de Padua Alves, C., Khonsari, A., Dammert, M. A., Parmaksiz, F., Beleggia, F., Sos, M. L., Riemer, J., George, J., Brodesser, S., Thomas, R. K., Reinhardt, H. C., & von Karstedt, S. (2020). Ferroptosis response segragates small cell lung cancer (SCLC) neuroendocrine subtypes. doi: 10.1101/2020.07.11.198408.

Belavgeni, A., Bornstein, S. R., von Massenhausen, A., Tonnus, W., Stumpf, J., Meyer, C., Othmar, E., Latk, M., Kanczkowski, W., Kroiss, M., Hantel, C., Hugo, C., Fassnacht, M., Ziegler, C. G., Schally, A. V., Krone, N. P., & Linkermann, A. (2019). Exquisite sensitivity of adrenocortical carcinomas to induction of ferroptosis. *Proceedings of the National Academy of Sciences of the United States of America, 116*(44), 22269-74. doi: 10.1073/pnas.1912700116.

Bell, M., & Zempel, H. (2020). SH-SY5Y-derived neurones: a human neuronal model system for investigating TAU sorting and neuronal subtype-specific TAU vulnerability. *Reviews in the Neurosciences*. doi: 10.1515/revneuro-2020-0152.

Bellinger, F. P., Bellinger, M. T., Seale, L. A., Takemoto, A. S., Raman, A. V., Miki, T., Manning-Bog, A. B., BerBellinger, F. P., Bellinger, M. T., Seale, L. A., Takemoto, A. S., Raman, A. V., Miki, T., Manning-Bog, A. B., Berry, M. J., White, L. R., & Ross, G. W. (2011). Glutathione peroxidase 4 is associated with neuromelanin in substantia nigra and dystrophic axons in putamen of Parkinson's brain. *Molecular Neurodegeneration, 6*(1), 8. doi: 10.1186/1750-1326-6-8.

Bellucci, A., Collo, G., Sarnico, I., Battistin, L., Missale, C., & Spano, P. F. (2008). Alpha-synuclein aggregation and cell death triggered by energy deprivation and dopamine overload are counteracted by D_2/D_3 receptor activation. *Journal of Neurochemistry, 106*(2), 560-77. doi: 10.1111/j.1471-4159.2008.05406.x.

Bensaad, K., & Vousden, K. H. (2007). p53: new roles in metabolism. *Trends in Cell Biology*, *17*(6), 286–291. doi: 10.1016/j.tcb.2007.04.004.

Bernards, A. (2006). Ras superfamily and interacting proteins database. Methods in Enzymology. 407, 1–9. doi: 10.1016/S0076-6879(05)07001-1.

Bertram, L., & Tanzi, R.E. (2005). The genetic epidemiology of neurodegenerative disease. *Journal of Clinical Investigation*, *115*(6), 1449–1457. doi: 10.1172/jci24761.

Biedler, J. L., Helson, L., & Spengler, B. A. (1973). Morphology and growth, tumorigenicity, and cytogenetics of human neuroblastoma cells in continuous culture. *Cancer Research, 33*(11), 2643-52.

Biedler, J. L., Roffler-Tarlov, S., Schachner, M., & Freedman, L. S. (1978). Multiple neurotransmitter synthesis by human neuroblastoma cell lines and clones. *Cancer research, 38*(11), 3751-57.

Birben, E., Sahiner, U. M., Sackesen, C., Erzurum, S., & Kalayci, O. (2012). Oxidative Stress and Antioxidant Defense. *World Allergy Organization Journal*, *5*(1), 9–19. doi: 10.1097/wox.0b013e3182439613.

Bjugstad, K. B., Teng, Y. D., Redmond, D. E. Jr., Elsworth, J. D., Roth, R. H., Cornelius, S. K., Snyder, E. Y., & Sladek, J. R. Jr. (2008). Human neural stem cells migrate along the nigrostriatal pathway in a primate model of Parkinson's disease. *Experimental Neurology, 211*(2), 326–369. doi: 10.1016/j.expneurol.2008.01.025.

Blanchard, H., Taha, A. Y., Cheon, Y., K, H-W., Turk, J., & Rapoport, S. I. (2014). iPLA$_2$β knockout mouse, a genetic model for progressive human motor disorders, develops age-related neuropathy. Neurochemical Research, 39(8), 1522-32. doi: 10.1007/s11064-014-1342-y.

Blandini, F., Cova, L., Armentero, M-T., Zennaro, E., Levandis, G., Bossolasco, P., Calzarossa, C., Mellone, M., Giuseppe, B., Deliliers, G. L., Polli, E., Nappi, G., & Silani, V. (2010). Transplantation of Undifferentiated Human Mesenchymal Stem Cells Protects against 6-Hydroxydopamine Neurotoxicity in the Rat. *Cell Transplantation, 19*(2), 203-17. doi: 10.3727/096368909X479839.

Bonventre, J.V. (1999). The 85-kD cytosolic phospholipase A2 knockout mouse: a new tool for physiology and cell biology. *Journal of the American Society of Nephrology, 10*(2), 404–12.

Bosch, X., Poch, E., & Grau, J. M. (2009). Rhabdomyolysis and Acute Kidney Injury. *The New England Journal of Medicine*, *361*(1), 62–72. doi: 10.1056/nejmra0801327.

Bouchaoui, H., Mahoney-Sanchez, L., Jonneaux, A., Gouel, F., Dutheli, M., Devedijan, J. C., Garcon, G., & Devos, D. (2019). Ferroptosis, a recently identified cell death, as a therapeutic target for Parkinson's disease. *Movement Disorders, 34*(Supplement 2).

Bousquet, M., Saint-Pierre, M., Julien, C., Salem, N., Cicchetti, F., & Calon, F. (2007). Beneficial effects of dietary omega-3 polyunsaturated fatty acid on toxin-induced neuronal degeneration in an animal model of Parkinson's disease. *Federation of American Societies for Experimental Biology, 22*(4), 1213-25. doi: 10.1096/fj.07-9677com.

Braak, H., Tredici, K. D., Rüb, U., de Vos, R. A. I., Jansen Steur, E.N.H. & Braak, E. (2003). Staging of brain pathology related to sporadic Parkinson's disease. *Neurobiology of Aging*, *24*(2), 197–211. doi: 10.1016/s0197-4580(02)00065-9.

Bridges, R. J., Natale, N. R., & Patel, S. A. (2012). System x_c^- cystine/glutamate antiporter: an update on molecular pharmacology and roles within the CNS. *British Journal of Pharmacology*, *165*(1), 20–34. DOI: 10.1111/j.1476-5381.2011.01480.x.

Bruck, D., Wenning, G. K., Stefanova, N., & Fellner, L. (2016). Glia and Alpha-Synuclein in Neurodegeneration: A Complex Interaction. *Neurobiology of Disease, 85*(1), 262-274. doi: 10.1016/j.nbd.2015.03.003.

Buccarelli, M., Marconi, M., Pacioni, S., De Pascalis, I., D'Alessandris, Q. G., Martini, M., Ascione, B., Malorni, W., Larocca, L. M., Pallini, R., Ricci-Vitiani, L., & Matarrese, P. (2018). Inhibition of autophagy increases susceptibility of glioblastoma stem cells to temozolomide by igniting ferroptosis. *Cell Death and Disease, 9*. doi: 10.1038/s41419-018-0864-7.

Cai, Q., Zhao, M., Liu, X., Wang, X., Nie, Y., Li, P., Liu, T., Ge, R., & Han, F. (2017). Reduced expression of citrate synthase leads to excessive superoxide formation. *Biochemical and Biophysical Research Communications, 485*(2), 388-94. doi: 10.1016/j.bbrc.2017.02.067.

Calderon, L. E., Liu, S, Arnold, N., Breakall, B., Rollins, J., & Ndinguri, M. (2015). Bromoenol lactone attenuates nicotine-induced breast cancer cell proliferation and migration. *PloS One, 10*(11), e0143277. doi: 10.1371/journal.pone.0143277.

Canil, O., Alankus, Y. B., Grootjans, S., Vegi, N., Hultner, L., Hoppe, P. S., Schroeder, T., Vandenabeele, P., Bornkamm, G. W., & Greten, F. R. (2016). Glutathione peroxidase 4 prevents necroptosis in mouse erythroid precursors. *Blood, 127*(1), 139-48. doi: 10.1182/blood-2015-06-654194.

Cantuti-Castelvetri, I., Klucken, J., Ingelsson, M., Ramasamy, K., McLean, P. J., Frosch, M. P., Hyman, B. T., & Standaert, D. G. (2005). Alpha-synuclein and chaperones in dementia with Lewy bodies. *Journal of Neuropathology & Experimental Neurology*, *64*(12), 1058–1066. doi: 10.1097/01.jnen.0000190063.90440.69.

Cao, Y., Li, Y., He, C., Yan, F., Li, J-R., Xu, H-Z., Zhuang, J-F., Zhou, H., Peng, Y-C., Fu, X-J., Lu, X-Y., Yao, Y., Wei, Y-Y., Tong, Y., Zhou, Y-F., & Wang, L. (2021). Selective ferroptosis inhibitor liproxstatin-1 attenuates neurological deficits and neuroinflammation after subarachnoid hemorrhage. *Neuroscience Bulletin, 37*(4), 535-49. doi: 10.1007/s12264-020-00620-5.

Carroll, J., He, J., Ding, S., Fearnley, I. M., & Walker, J. E. (2019). Persistence of the permeability transition pore in human mitochondria devoid of an assempled ATP synthase. *Proceedings of the National Academy of Sciences of the United States of America, 116*(26), 12816-21. doi: 10.1073/pnas.1904005116.

Casanas-Sanchez, V., Perez, J. A., Fabelo, N., Herrera-Herrera, A. V., Fernandez, C., Marin, R., Gonzalez-Montelongo, M. C., & Diaz, M. (2014). Addition of docosahexaenoic acid, but not arachidonic acid, activates glutathione and tioredoxin antioxidant systems in murine hippocampal HT22 cells: potential implications for neuroprotection. Journal of Neurochemistry, 131(4), 470-83. doi: 10.1111/jnc.12833.

Catala, A., & Diaz, M. (2016). Impact of lipid peroxidation on the physiology and pathophysiology of cell membranes. *Frontiers in Physiology, 423*(7). doi: 10.3389/fphys.2016.00423.

Chalimoniuk, M., Stolecka, A., Zieminska, E., Stepien, A., Langfort, J., & Strosznajder, J. B. (2009). Involvement of multiple protein kinases in $cPLA_2$ phosphorylation, arachidonic acid release, and cell death in in vivo and in vitro models of 1-methyl-4-phenylpyridinium-induced parkinsonism - the possible key role of PKG. *Journal of Neurochemistry, 110*(1), 307-17. doi: 10.1111/j.1471-4159.2009.06147.x.

Chartier-Harlin, M.-C., Kachergus, J., Roumier, C., Mouroux, V., Douay, X., Lincoln, S., Levecque, C., Larvor, L., Andrieux, J., Hulihan, M., Waucquier, N., Defebvre, L., Amouyel, P., Ferrer, M., & Destée, A. (2004). α-synuclein locus duplication as a cause of familial Parkinson's disease. *The Lancet*, *364*(9440), 1167–1169. doi: 10.1016/s0140-6736(04)17103-1.

Chen, C. T., Green, J. T., Orr, S. K., & Bazinet, R. P. (2008). Regulation of brain polyunsaturated fatty acid uptake and turnover. *Prostaglandins, Leukotrienes, and Essential Fatty Acids, 79*(3-5), 85-91. doi: 10.1016/j.plefa.2008.09.003.

Chen, D., Kanthasamy, A. G., & Reddy, M. B. (2015). EGCG protects against 6-OHDA-induced neurotoxicity in a cell culture model. *Parkinson's Disease, 2015*, doi: 10.1155/2015/843906.

Chen, L., Hambright, W. S., Na, R., & Ran, Q. (2015). Ablation of the Ferroptosis Inhibitor Glutathione Peroxidase 4 in Neurons Results in Rapid Motor Neuron Degeneration and Paralysis. *Journal of Biological Chemistry*, *290*(47), 28097–28106. doi: 10.1074/jbc.m115.680090.

Chen, M., Wang, S., Hsu, C., Yin, P., Yeh, T., Lee, H., Tseng, L. (2017). CHAC1 degradation of glutathione enhances cystine-starvation-induced necroptosis and ferroptosis in human triple negative breast cancer cells via the GCN2-eIF2α-ATF4 pathway. *Oncotarget, 8*, 114588-602. doi: 10.18632/oncotarget.23055.

Chen, L-D., Wu, R-H., Huang, Y-Z., Chen, M-X., Zeng, A-M., Zhuo, G-F., Xu, F-S., Liao, R., & Lin, Q-C. (2020). The role of ferroptosis in chronic intermittent hypoxia-induced liver injury in rats. *Sleep and Breathing, 24*, 1767-73. doi: 10.1007/s11325-020-02091-4.

Cheng, L., Liang, R., Li, Z., Ren, J., Yang, S., Bai, J., Niu, Q., Yu, H., Zhang, H., Xia, N., & Liu, H. (2021). Aluminum maltolate triggers ferroptosis in neurons: mechanism of action. *Toxicology Mechanisms and Methods, 31*(1), 33-42. doi: 10.1080/15376516.2020.1821268.

Chinta, S. J., Kumar, M. J., Hsu, M., Rajagopalan, S., Kaur, D., Rane, A., Nicholls, D. G., Choi, J., & Andersen, J. K. (2007). Inducible alterations of glutathione levels in adult dopaminergic midbrain neurons result in nigrostriatal degeneration. *The Journal of Neuroscience, 27*(51), 13997-4006. doi: 10.1523/JNEUROSCI.3885-07.2007.

Chinta, S. J., Woods, G., Demaria, M., Rane, A., Zou, Y., McQuade, A., Rajagopalan, S., Limbad, C., Madden, D. T., Campisi, J., & Andersen, J. K. (2018). Cellular senescence is induced by the environmental neurotoxin paraquat and contributes to neuropathology linked to Parkinson's disease. *Cell Reports, 22*(4), 930-40. doi: 10.1016/j.celrep.2017.12.092.

Choi, B-K., Choi, M-G., Kim, J-Y., Yang, Y., Lai, Y., Kweon, D-H., Lee, N.K. & Shin, Y-K. (2013). Large alpha-synuclein oligomers inhibit neuronal SNARE-mediated vesicle docking. *Proceedings of the National Academy of Sciences*, *110*(10), 4087–4092. doi: 10.1073/pnas.1218424110.

Chung, D. M., Kim, J. H., & Kim, J. K. (2015). Evaluation of MTT and trpan blue assays for radiation-induced cell viability test in Hepg2 cells. *International Journal of Radiation Research*, *13*(4), 331-5. doi: 10.7508/ijrr.2015.04.006.

Colle, D., Santos, D. B., Naime, A. A., Goncalves, C. L., Ghizoni, H., Hort, M. A. & Farina, M. (2019). Early postnatal exposure to paraquat and maneb in mice increases nigrostriatal dopaminergic susceptibility to a re-challenge with the same pesticides at adulthood: implications for Parkinson's disease. *Neurotoxicity Research, 2019*. doi: 10.1007/s12640-019-00097-9.

Colicelli, J. (2004). Human RAS Superfamily Proteins and Related GTPases. *Science Signaling*, *2004*(250), re13. doi: 10.1126/stke.2502004re13.

Cong, L., Dong, X., Wang, Y., Deng, Y., Li, B., & Dai, R. (2019). On the role of synthesised hydroxylated chalsones as dual functional amyloid-β aggregation and ferroptosis inhibitors for potential treatment of Alzheimer's disease. *European Journal of Medicinal Chemistry, 166*, 11-21. doi: 10.1016/j.ejmech.2019.01.039.

Conrad, M., & Sato, H. (2012). The oxidative stress-inducible cystine/glutamate antiporter, system x_c^-: cystine supplier and beyond. *Amino Acids, 42*(1), 231-46. doi: 10.1007/s00726-011-0867-5.

Conrad, M., & Friedmann, A. J. P. (2015). Glutathione peroxidase 4 (Gpx4) and ferroptosis: what's so special about it? *Molecular & Cellular Oncology*, *2*(3), e995047. doi: 10.4161/23723556.2014.995047.

Conrad, M., Friedmann, A. J. P., Vandenabeele, P., & Stockwell, B. R. (2016). Regulated necrosis: disease relevance and therapeutic opportunities. *Drug Discovery, 15*(5), 348-66. doi: 10.1038/nrd.2015.6.

Conway, K. A., Lee, S-J., Rochet, J-C., Ding, T. T., Williamson, R. E., & Lansbury, P. T. Jr. (2000). Acceleration of oligomerization, not fibrillization, is a shared property of both alpha -synuclein

mutations linked to early-onset Parkinson's disease: Implications for pathogenesis and therapy. *Proceedings of the National Academy of Sciences*, *97*(2), 571–576. doi: 10.1073/pnas.97.2.571.

Cotticelli, M. G., Xia, S., Lin, D., Lee., T., Terrab, L., Wipf, P., Huryn, D. M., & Wilson, R. B. (2019). Ferroptosis as a Novel Therapeutic Target for Friedreich's Ataxia. *The Journal of Pharmacology and Experimental Therapeutics, 369*(1), 47-54. doi: 10.1124/jpet.118.252759.

Covell, D. J., Robinson, J. L., Akhtar, R. S., Grossman, M., Weintraub, D., Bucklin, H. M., Pitkin, R. M., Riddle, D., Yousef, A., Trojanowski, J. Q., & Lee, V. M. (2017). Novel conformation-selective alpha-synuclein antibodies raised against different in vitro fibril forms show distinct patterns of Lewy pathology in Parkinson's disease. *Neuropathology and Applied Neurobiology*, *43*(7), 604–20. doi: 10.1111/nan.12402.

Cozzi, A., Orellana, D. I., Santambrogio, P., Rubio, A., Cancellieri, C., Giannelli, S., Ripamonti, M., Taverna, S., Di Lullo, G., Rovida, E., Ferrari, M., Forni, G. L., Fiorillo, C., Broccoli, V., & Levi, S. (2019). Stem cell modelling of neuroferritinopathy reveals iron as a determinant of senescence and ferroptosis during aging. *Stem Cell Reports, 13*(5), 832-46. doi: 10.1016/j.stemcr.2019.09.002.

Crawford, R. R., Prescott, E. T., Sylvester, C. F., Higdon, A. N., Shan, J., Kilberg, M. S., & Mungrue, I. N. (2015). Human CHAC1 protein degrades glutathione and mRNA induction is regulated by the transcription factors ATF4 and ATF3 and a Bipartite ATF/CRE element. *Journal of Biological Chemistry, 290*(25), 15878-91. doi: 10.1074/jbc.M114.635144.

Cronin, K. D., Ge, D., Manninger, P., Linnertz, C., Rossoshek, A., Orrison, B. D., Bernard, D. J., El-Agnaf, O. M., Schlossmacher, M. G., Nussbaum, R. L., & Chiba-Falek, O. (2009). Expansion of the Parkinson's disease-associated SNC-REP1 allele upregulated human alpha-synuclein in transgenic mouse brain. *Human Molecular Genetics, 18*(17), 3274-85. doi: 10.1093/hmg/ddp265.

Dahlmanns, M., Yakubov, E., Chen, D., Sehm, T., Rauh, M., Savaskan, N., & Wrosch, J. W. (2017). Chemotherapeutic xCT inhibitors sorafenib and erastin unraveled with the synaptic optogenic function analysis tool. *Cell Death Discovery, 3*. doi: 10.1038/cddiscovery.2017.30.

Dalleau, S., Baradat, M., Gueraud, F., & Huc, L. (2013). Cell death and diseases related to oxidative stress: 4-hydroxynoneal (HNE) in the balance. *Cell Death and Differentiation, 20*(12), 1615-30. doi: 10.1038/cdd.2013.138.

Danzer, K.M., Haasen, D., Karow, A.R., Moussaud, S., Habeck, M., Giese, A., Kretzschmar, H., Hengerer, B. & Kostka, M. (2007). Different species of -Synuclein Oligomers induce calcium influx and Seeding. *Journal of Neuroscience*, *27*(34), 9220–32. doi: 10.1523/jneurosci.2617-07.2007.

da Silva, T. M., Munhoz, R. P., Alvarez, C., Naliwaiko, K., Kiss, A., Andreatini, R., & Ferraz, A. C. (2008). Depression in Parkinson's disease: a double-bline, randomized, placebo-controlled pilot study of

omega-3 fatty-acid supplementation. *Journal of Affective Disorders, 111*(2-3), 351-9. doi: 10.1016/j.jad.2008.03.008.

Degterev, A., Huang, Z., Boyce, M. Li, Y., Mizushima, N., Cuny, G. D., Mitchison, T. J., Moskowitz, M. A., & Yuan, J. (2005). Chemical inhibitor of nonapoptotic cell death with therapeutic potential for ischemic brain injury. *Chemical Biology, 1*(2), 112-9. doi: 10.1038/nchembio711.

Degterev, A., Hitomi, J., Germscheid, M., Ch'en, I. L., Korkina, O., Teng, X., Abbot, D., Cuny, G. D., Yuan, C., Wagner, G., Hedrick, S. M., Gerber, S. A., Lugovsky, A., & Yuan, J. (2008). Identification of RIP1 kinase as a specific cellular target of necrostatins. *Chemical Biology, 4*, 313-21. doi: 10.1038/nchembio.83.

Denizot, F., & Lang, R. (1986) Rapid colorimetric assay for cell growth and survival. Modifications to the tetrazolium dye procedure giving improved sensitivity and reliability. *Journal of Immunological Methods, 89*(2), 271–77. doi: 10.1016/0022-1759(86)90368-6.

Deumens, R., Blokland, A. & Prickaerts, J. (2002). Modeling Parkinson's disease in rats: An evaluation of 6-OHDA lesions of the Nigrostriatal pathway. *Experimental Neurology*, *175*(2), 303–17. doi: 10.1006/exnr.2002.7891.

Deusser, J., Schmidt, S., Ettle, B., Plötz, S., Huber, S., Müller, C. P., Masliah, E., Winkler, J., & Kohl, Z. (2015). Serotonergic dysfunction in the A53T alpha-synuclein mouse model of Parkinson's disease. *Journal of Neurochemistry*, *135*(3), 589–97. doi: 10.1111/jnc.13253.

Dexter, D. T., Carter, C. J., Wells, F. R., Javoy-Agid, F., Avid, Y., Lees, A., Jenner, P., & Marsden, C. D. (1989). Basal lipid peroxidation in substantia nigra is increased in Parkinson's disease. *Journal of Neurochemistry, 52*(2), 381-89. doi: 10.1111/j.1471-4159.1989.tb09133.x.

Diogenes, M.J., Dias, R.B., Rombo, D.M., Miranda, H. V., Maiolino, F., Guerreiro, P., Nasstrom, T., Franquelim, H.G., Oliveira, L.M.A., Castanho, M.A.R.B., Lannfelt, L., Bergstrom, J., Ingelsson, M., Quintas, A., Sebastiao, A.M., Lopes, L.V. & Outeiro, T.F. (2012). Extracellular Alpha-Synuclein Oligomers modulate Synaptic transmission and impair LTP via NMDA-Receptor activation. *Journal of Neuroscience*, *32*(34), 11750–11762. doi: 10.1523/jneurosci.0234-12.2012.

Dixon, S. J., Lemberg, K. M., Lamprecht, M. R., Skouta, R., Zaitsev, E. M., Gleason, C. E., Patel, D. N., Bauer, A. J., Cantley, A. M., Yang, W. S., Morrison, B 3rd., & Stockwell, B. R. (2012). Ferroptosis: An Iron-Dependent Form of Nonapoptotic Cell Death. *Cell*, *149*(5), 1060–1072. doi: 10.1016/j.cell.2012.03.042.

Dixon, S. J., Patel, D. N., Welsch, M., Skouta, R., Lee, E. D., Hayano, M., Thomas, A. G., Gleason, C. E., Tatonetti, N. P., Slusher, B. S., & Stockwell, B. R. (2014). Pharmacological inhibition of cystine–glutamate exchange induces endoplasmic reticulum stress and ferroptosis. *eLife*, *3*, e02523. doi: 10.7554/elife.02523.

Doll, S., Proneth, B., Tyurina, Y., Panzilius, E., Kobayashi, S., Ingold, I., Irmler, M., Beckers, J., Aichler, M., Walch, A., Prokisch, H., Trumbach, D., Mao, G., Qu, F., Bayir, H., Fullekrug, J., Scheel, C. H., Wurst, W., Schick, J. A., Kagan, V. E., Friedmann, A. J. P., & Conrad, M. (2017). ACSL4 dictates ferroptosis sensitivity by shaping cellular lipid composition. *Chemical Biology, 13*(1), 91-8. doi: 10.1038/nchembio.2239.

Dolma, S., Lessnick, S. L., Hahn, W. C., & Stockwell, B. R. (2003). Identification of genotype-selective antitumor agents using synthetic lethal chemical screening in engineered human tumor cells. *Cancer Cell*, *3*(3), 285–96. doi: 10.1016/s1535-6108(03)00050-3.

Dorsey, E. R., Constantinescu, R., Thompson, J. P., Biglan, K. M., Holloway, R. G., Kieburtz, K., Marshall, F. J., Ravina, B. M., Schiftto, G., Siderowf, A., & Tanner, C. M. (2006). Projected number of people with Parkinson's disease in the most populous nations, 2005 through 2030. *Neurology*, *68*(5), 384–86. doi: 10.1212/01.wnl.0000247740.47667.03.

Do Van, B., Gouel, F., Jonneaux, A., Timmerman, K., Gelé, P., Pétrault, M., Bastide, M., Laloux, C., Moreau, C., Bordet, R., Devos, D., & Devedjian, J. C. (2016). Ferroptosis, a newly characterized form of cell death in Parkinson's disease that is regulated by PKC. *Neurobiology of Disease*, *94*, 169–78. doi: 10.1016/j.nbd.2016.05.011.

Drexler, H. G., & Uphoff, C. C. Mycoplasma contamination of cell cultures: incidence, sources, effects, detection, elimination, prevention. *Cytotechnology, 39*(2), 75-90. doi: 10.1023/A:1022913015916.

Drukarch, B., Jongenelen, C. A. M., Schepens, E., Langeveld, C., & Stoof, J. C. (1996). Glutathione is involved in the granular storage of dopamine in rat PC12 pheochromocytoma cells: implications for the pathogenesis of Parkinson's disease. *The Journal of Neuroscience, 16*(19), 6038-45. doi: 10.1523/JNEUROSCI.16-19-06038.1996.

Du, J., Wang, T., Li, Y., Zhou, Y., Wang, X., Ren, X., An, Y., Wu, Y., Sun, W., Fan, W., Zhu, Q., Wang, Y., & Tong, X. (2019). DHA inhibits proliferation and induces ferroptosis of leukemia cells through autophagy dependent degradation of ferritin. *Free Radical Biology and Medicine, 2019*. doi: 10.1016/j.freeradbiomed.2018.12.011.

ECACC. (undated). *ECACC General Cell Collection: 94030304 SH-SY5Y*. [online] Available at: https://www.phe-culturecollections.org.uk/products/celllines/generalcell/detail.jsp?refId=94030304&collection=ecacc_gc [Accessed 5 Jul. 2019].

Edsjo, A., Lavenius, E., Nilsson, H., Hoehner, J. C., Simonsson, P., Culp, L. A., Martinsson, T., Larsson, C., & Pahlman, S. (2003). Expression of *trkB* in human neuroblastoma in relation to *MYCN* expression and retinoic acid treatment. *Laboratory Investigation, 83*, 813-23. doi: 10.1097/01.LAB.0000074895.48776.D8.

Edwards, T. G., & Bloom, D. C. Lund human mesencephalic (LUHMES) neuronal cell line supports herpes simplex virus 1 latency in vitro. *Journal of Virology, 93*(6), e02210-18. doi: 10.1128/JVI.02210-18.

Electron Microscopy Sciences. (undated). *Low Viscosity Embedding Media Spurr's Kit Technical Data Sheet*. Available at: https://www.emsdiasum.com/microscopy/technical/datasheet/14300.aspx [Accessed 9th August 2019].

Eling, N., Reuter, L., Hazin, J., Hamacher-Brady, A., & Brady, N. R. (2015). Identification of artesunate as a specific activator of ferroptosis in pancreatic cancer cells. *Oncoscience, 2*(5), 517-32. doi: 10.18632/oncoscience.160.

Elkind, E., Vaisid, T., Kornspan, J. D., Barnoy, S., Rottem, S., & Kosower, N. S. (2011). Neuroprotective effects of Mycoplasma hyorhinis against amyloid-β-peptide toxicity in SH-SY5Y human neuroblastoma cells are mediated by calpastatin upregulation in the mycoplasma-infected cells. *Neurochemistry International, 58*(4), 497-503. doi: 10.1016/j.neuint.2011.01.005.

Elmore, S. (2007). Apoptosis: a review of programmed cell death. *Toxicologic Pathology, 35*(4), 495-516. doi: 10.1080/01926230701320337.

Encinas, M., Iglesias, M., Liu, Y., Wang, H., Muhaisen, A., Cena, V., Gallego, C., & Comella, J. X. (2000). Sequential treatment of SH-SY5Y cells with retinoic acid and brain-derived neurotrophic factor gives rise to fully differentiated, neurotrophic factor-dependent, human neuron-like cells. *Journal of Neurochemistry, 75*(3), 991-1003. doi: 10.1046/j.1471-4159.2000.0750991.x.

Esterbauer, H., & Cheeseman, K. H. (1990). Determination of aldehydic lipid peroxidation products: malonaldehyde and 4-hydroxynenal. *Methods in Enzymology, 186*, 407-21. doi: 10.1016/0076-6879(90)86134-H.

Fabelo, N., Martin, V., Santpere, G., Marin, R., Torrent, L., Ferrer, I., & Diaz, M. (2011). Severe alterations in lipid composition of frontal cortex lipid rafts from Parkinson's disease and incidental Parkinson's disease. *Molecular Medicine, 17*(9-10), 1107-18. doi: 10.2119/molmed.2011.00119.

Falkenburger, B. H., Saridaki, T., & Dinter, E. (2016). Cellular models for Parkinson's disease. *Journal of Neurochemistry, 139*(Supplement 1), 121-30. doi: 10.1111/jnc.13618.

Fang, X., Wang, H., Han, D., Xie, E., Yang, X., Wei, J., Gu, S., Gao, F., Zhu, N., Yin, X., Cheng, Q., Zhang, P., Dai, W., Chen, J., Yang, F., Y, H-T., Linkermann, A., Gu, W., Min, J., & Wang, F. (2019). Ferroptosis as a target for protection against cardiomyopathy. *Proceedings of the National Academy of Sciences of the United States of America, 116*(7), 2672-80. doi: 10.1073/pnas.1821022116.

Fang, X., Cai, Z., Wang, H., Han, D., Cheng, Q., Zhang, P., Gao, F., Yu, Y., Song, Z., Wu, Q., An, P., Huang, S., Pan, J., Chen, H-Z., Chen, J., Linkermann, A., Min, J., & Wang, F. (2020). Loss of cardiac ferritin H

fascilitates cardiomyopathy via Slc7a11-mediated ferroptosis. *Circulation Research, 127*, 486-501. doi: 10.1161/CIRCRESAHA.120.316509.

Ferese, R., Modugno, N., Campopiano, R., Santilli, M., Zampatti, S., Giardina, E., Nardone, A., Postorivo, A., Fornai, F., Novelli, G., Romoli, E., Ruggieri, S., & Gambardella, S. (2015). Four Copies of SNCA Responsible for Autosomal Dominant Parkinson's Disease in Two Italian Siblings. *Parkinson's Disease*, *2015*, 1–6. doi: 10.1155/2015/546462.

Filograna, R., Civiero, L., Ferrari, V., Codolo, G., Greggio, E., Bubacco, L., Beltramini, M., & Bisaglia, M. (2015). Analysis of catecholaminergic phenotype in human SH-SY5Y and BE(2)-M17 neuroblastoma cell lines upon differentiation. *PLoS One, 10*(8), e0136769. doi: 10.1371/journal.pone.0136769.

Fineberg, N.A., Haddad, P.M., Carpenter, L., Gannon, B., Sharpe, R., Young, A.H., Joyce, E., Rowe, J., Wellsted, D., Nutt, D.J. & Sahakian, B.J. (2013). The size, burden and cost of disorders of the brain in the UK. *Journal of Psychopharmacology*, *27*(9), 761–770. doi: 10.1177/0269881113495118.

Fotakis, G., & Timbrell, J. A. (2006). In vitro cytotoxicity assays: comparison of LDH, neutral red, MTT and protein assay in hepatoma cell lines following exposure to cadmium chloride. *Toxicology Letters, 160*(2), 171-7. doi: 10.1016/j.toxlet.2005.07.001.

Friedmann, A. J. P., Schneider, M., Proneth, B., Tyurina, Y. Y., Tyurin, V. A., Hammond, V. J., Herbach, N., Aichler, M., Walch, A., Eggenhofer, E., Basavarajappa, D., Radmark, O., Kobayashi, S., Seibt, T., Beck, H., Neff, F., Esposito, I., Wanke, R., Forster, H., Yefremova, O., Heinrichmeyer, M., Bornkamm, G. W., Geissler, E. K., Thomas, S. B., Stockwell, B. R., O'Donnell, V. B., Kagan, V. E., Schick, J. A., & Conrad, M. (2014). Inactivation of the ferroptosis regulator Gpx4 triggers acute renal failure in mice. *Nature Cell Biology*, *16*(12), 1180–1191. doi: 10.1038/ncb3064.

Gai, C., Yu, M., Li, Z., Wang, Y., Ding, D., Zheng, J., Lv, S., Zhang, W., & Li, W. (2019). Acetaminophen sensitising erastin-induced ferroptosis via modulation of Nrf2/heme oxygenase-1 signalling pathway in non-small-cell lung cancer. *Journal of Cellular Physiology, 235*(4), 3329-39. doi: 10.1002/jcp.29221.

Galy, B., Ferring-Appel, D., Kaden, S., Grone, H. J., & Hentze, M. W. (2008). Iron regulatory proteins are essential for intestinal function and control key iron absorption molecules in the duodenum. *Cell Metabolism, 7*(1), 79-85. doi: 10.1016/j.cmet.2007.10.006.

Gao, M., Monian, P., Pan, Q., Zhang, W., Xiang, J., Jiang, X. (2016). Ferroptosis is an autophagic cell death process. *Cell Research, 26*(9), 1021-32. doi: 10.1038/cr.2016.95.

Goa, Z., Deng, G., Li, Y., Huang, H., Sun, X., Shi, H., Yao, X., Gao, L., Ju, Y., & Luo, M. (2020). *Actinidia chinensis* Planch prevents proliferation and migration of gastric cancer associated with apoptosis, ferroptosis activation and mesenchymal phenotype suppression. *Biomedicine & Pharmacotherapy, 126*, 110092. doi: 10.1016/j.biopha.2020.110092.

Gaschler, M. M., & Stockwell, B. R. (2017). Lipid peroxidation in cell death. *Biochemical and Biophysical Research Communications, 482*(3), 419-25. doi: 10.1016/j.bbrc.2016.10.086.

Gatica, D., Lahiri, V., & Klionsky, D. J. (2018). Cargo recognition and degradation by selective autophagy. *Cell Biology, 20*(3), 233-42. doi: 10.1038/s41556-018-0037-z.

Gaugler, M. N., Genc, O., Bobela, W., Mohanna, S., Ardah, M. T., El-Agnaf, O. M., Cantoni, M., Bensadoun, J-C., Schneggenburger, R., Knott, G. W., Aebischer, P., & Schneider, B. L. (2012). Nigrostriatal overabundance of α-synuclein leads to decreased vesicle density and deficits in dopamine release that correlate with reduced motor activity. *Acta Neuropathologica, 123*(5), 653-69. doi: 10.1007/s00401-012-0963-y.

Gaven, F., Marin, P., & Claeysen, S. (2014). Primary culture of mouse dopaminergic neurones. *Journal of Visualised Experiments, 8*(91), e51751. doi: 10.3791/51751.

Geng, N., Shi, B. J., Li, S. L., Zhong, Z. Y., Li, Y. C., Xua, W. L., Zhou, H., Cai, J. H. (2018). Knockdown of ferroportin accelerates erastin-induced ferroptosis in neuroblastoma cells. *European Review for Medical and Pharmacological Sciences, 22*(12), 3826-36. doi: 10.26355/eurrev_201806_15267.

Ghorbani-Anarkooli, M., Dabirian, S., Moladoust, H., Zendedel, A., & Bahadori, M. H. (2019). Comparison of MTT, trypan blue, and clonogenic assay, to determine the viability in human anaplastic thyroid cancer cell line. *Tehran University Medical Journal, 77*(1), 26-32.

Giacinti, C., & Giordano, A. (2006). RB and cell cycle progression. *Oncogene, 25*(38), 5220-27. doi: 10.1038/sj.onc.1209615.

Giguere, N., Burke Nanni, S., & Trudeau, L. E. (2018). On cell loss and selective vulnerability of neuronal populations in Parkinson's disease. *Frontiers in Neurology, 9*, 455. doi: 10.3389/fneur.2018.00455.

Gille, G., Rausch, W. D., Hung, S-T., Moldzio, R., Ngyuen, A., Janetzky, B., Engfer, A., & Reichmann, H. (2002). Protection of dopaminergic neurons in primary culture by lisuride. *Journal of Neural Transmission, 109*(2), 157-69. doi: 10.1007/s007020200011.

Goetz, C. G. (2011). The History of Parkinson's Disease: Early Clinical Descriptions and Neurological Therapies. *Cold Spring Harbor Perspectives in Medicine*, *1*(1), a008862. doi: 10.1101/cshperspect.a008862.

Gökçal, E., Gur, V. E., Selvitop, R., Babacan Yildiz, G., & Asil, T. (2017). Motor and Non-Motor Symptoms in Parkinson's Disease: Effects on Quality of Life. *Archives of Neuropsychiatry, 54*, 143-48. doi: 10.5152/npa.2016.12758.

Goldie, B. J., Barnett, M. M., & Cairns, M. J. (2014). BDNF and the maturation of posttranscriptional regulatoru networks in human SH-SY5Y neuroblast differentiation. *Frontiers in Cellular Neuroscience, 8,* 325. doi: 10.3389/fncel.2014.00325.

GOV.UK. (2019). *Animal testing and research*. [online] Available at: https://www.gov.uk/guidance/research-and-testing-using-animals#applying-for-licences [Accessed 11 Nov. 2019].

Greenamyre, J. T., Sherer, T. B., Betarbet, R., & Panov, A. V. (2001). Complex I and Parkinson's disease. *IUBMB Life, 52*(3-5), 135-41. doi: 10.1080/15216540152845939.

Greenberg, R. A. (2005). Telomeres, crisis and cancer. *Current Molecular Medicine, 5*, 213-18.

Greene, L. A., & Tischler, A. S. (1976). Establishment of a noradrenergic clonal line of rat adrenal pheochromocytoma cells which respond to nerve growth factor. *Proceedings of the National Academy of Sciences of the United States of America, 73*(7), 2424-28. doi: 10.1073/pnas.73.7.2424.

Gui, Y, Xu, Z., Liu, H., Zhao, J., & Hu, X. (2013). Four novel rare mutations of PLA_2G6 in Chinese population with Parkinson's disease. *Parkinsonism and Related Disorders, 19*(1), 21-6. doi: 10.1016/j.parkreldis.2012.07.016.

Guo, J. Y., Xia, B., & White, E. (2013). Autophagy-mediated tumor promotion. *Cell, 155*(6), 1216-9. doi: 10.1016/j.cell.2013.11.019.

Guo, L., Zhang, T., Wang, F., Chen, X., Xu, H., Zhou, C., Chen, M., Yu, F., Wang, S., Yang, D., & Wu, B. (2020). Targeted inhibition of Rev-erb-α/β limits ferroptosis to ameliorate folic acid-induced acute kidney injury. *British Journal of Pharmacology, 178*(2), 328-45. doi: 10.1111/bph.15283.

Haacke, E. M., Liu, S., Buch, S., Zheng, W., Wu, D., & Ye, Y. (2015). Quantitative susceptibility mapping: current status and future directions. *Magnetic Resonance Imaging*, *33*(1), 1–25. doi: 10.1016/j.mri.2014.09.004.

Hahn, W. C., Counter, C. M., Lundberg, A. S., Beijersbergen, R. L., Brooks, M. W., & Weinberg, R. A. (1999). Creation of human tumour cells with defined genetic elements. *Nature, 400*(6743), 464-68. doi: 10.1038/22780.

Hahn, W. C., Dessain, S. K., Brooks, M. W., King, J. E., Elenbaas, B., Sabatini, D. M., DeCaprio, J. A., & Weinberg, R. A. (2002). Enumeration of the Simian Virus 40 Early Region Elements Necessary for Human Cell Transformation. *Molecular and Cellular Biology, 22*, 2111-23. doi: 10.1128/MCB.22.7.2111–2123.2002

Hambright, W. S., Fonseca, R. S., Chen, L., Na, R., & Ran, Q. (2017). Ablation of ferroptosis regulator glutathione peroxidase 4 in forebrain neurons promotes cognitive impairment and neurodegeneration. *Redox Biology*, *12*, 8–17. doi: 10.1016/j.redox.2017.01.021.

Hao, S., Yu, J., He, W., Huang, Q., Zhao, Y., Liang, B., Zhang, S., Wen, Z., Dong, S., Rao, J., Liao, W., & Shi, M. (2017). Cysteine dioxygenase 1 mediates erastin-induced ferroptosis in human gastric cancer cells. *Neoplasia, 19*(12), 1022-32. doi: 10.1016/j.neo.2017.10.005.

Harding, H. P., Zhang, Y., Zeng, H., Novoa, I., Li, P. D., Calfon, M., Sadri, N., Yun, C., Popko, B., Paules, R., Stojdl, D. F., Cell, J. C., Hettmann, T., Leiden, J. M., & Ron, D. (2003). An integrated stress response regulates amino acid metabolism and resistance to oxidative stress. *Molecular Cell, 11*(3), 619-33. doi: 10.1016/S1097-2765(03)00105-9.

Harris, G., Hogberg, H., Hartung, T., & Smirnova, L. (2018). 3D differentiation of LUHMES cell line to study recovery and delayed neurotoxic effects. *Current Protocols in Toxicology, 73*(1). doi: 10.1002/cptx.29.

Hauser, D. N., Dukes, A. A., Mortimer, A. D., & Hastings, T. G. (2013). Dopamine quinone modifies and decreases the abundance of the mitochondrial selenoprotein glutathione peroxidase 4. *Free Radical Biology and Medicine, 65,* 419-27. doi: 10.1016/j.freeradbiomed.2013.06.030

Hay, R. J. (1991). Operator-induced contamination in cell culture systems. *Developments in Biological Standardization, 75*, 193-204.

Hayano, M., Yang, W. S., Corn, C. K., Pagano, N. C., & Stockwell, B. R. (2016). Loss of cysteinyl-tRNA synthetase (CARS) induces the transsulfuration pathway and inhibits ferroptosis induced by cysteine deprivation. *Cell Death and Differentiation, 23*(2), 270-78. doi: 10.1038/cdd.2015.93.

He, N., Ling, H., Ding, B., Huang, J., Zhang, Y., Zhang, Z., Liu, C., Chen, K., & Yan, F. (2015). Region-specific disturbed iron distribution in early idiopathic Parkinson's disease measured by quantitative susceptibility mapping. *Human Brain Mapping*, *36*(11), 4407–20. doi: 10.1002/hbm.22928.

Hely, M. A., Reid, W. G., Adena, M. A., Halliday, G. M., & Morris, J. G. (2008). The Sydney multicenter study of Parkinson's disease: The inevitability of dementia at 20 years. *Movement Disorders*, *23*(6), 837–44. doi: 10.1002/mds.21956.

Hildebrand, J. M., Tanzer, M. C., Lucet, I. S., Young, S. N., Spall, S. K., Sharma, P., Pierotti, C., Garnier, J-M., Dobson, R. C. J., Webb, A. I., Tripaydonis, A., Babon, J. J., Mulcair, M. D., Scanlon, M. J., Alexander, W. S., Wilks, A. F., Czabotar, P. E., Lessene, G., Murphy, J. M., & Silke, J. (2014). Activation of the pseudokinase MLKL unleashes the four-helix bundle domain to induce membrane localization and necroptotic cell death. *Proceedings of the National Academy of Sciences of the United States of America, 111*(42), 15072-77. doi: 10.1073/pnas.1408987111.

Hoehn, M. M., & Yahr, M. D. (1967). Parkinsonism: onset, progression and mortality. *Neurology*, *17*(5), 427–42. doi: 10.1212/wnl.17.5.427.

Hou, W., Xie, Y., Song, X., Sun, X., Lotze, M. T., Zeh, H. J., Kang, R., & Tang, D. (2016). Autophagy promotes ferroptosis by degradation of ferritin. *Autophagy, 12*(8), 1425-8. doi: 10.1080/15548627.2016.1187366.

Hou, L., Huang, R., Sun, F., Zhang, L., & Wang, Q. (2019). NADPH oxidase regulates paraquat and maneb-induced dopaminergic neurodegeneration through ferroptosis. *Toxicology, 417*, 64-73. doi: 10.1016/j.tox.2019.02.011.

Hu, Z., Zhang, H., Yi, B., Yang, S., Liu, J., Hu, J., Wang, J., Cao, K., & Zhang, W. (2020). VDR activation attenuate cisplatin induced AKI by inhibiting ferroptosis. *Cell Death & Disease, 11*(73). doi: 10.1038/s41419-020-2256-z.

Huang, W., Bhavsar, A., Ward, R. E., Hall, J. C., Priestley, J. V., & Michael-Titus, A. T. (2009). Arachidonyl trifluoromethyl ketone is neuroprotective after spinal cord injury. *Journal of Neurotrauma, 26*(8), 1429-34. doi: 10.1089/neu.2008-0835.

Huang, Z., Shao, W., Gu, J., Hu, X., Shi, Y., Xu, W., Huang, C., & Lin, D. (2015). Effects of culture media on metabolic profiling of the human gastric cancer cell line SGC7901. *Molecular Biosystems, 7*(2015). doi: 10.1039/c5mb00019j.

Huang, L-I., Liao, X-H., Sun, H., Jiang, ,X., Liu, Q., & Zhang, L. (2019). Augmenter of liver regeneration protects the kidney from ischaemia-reperfusion injury in ferroptosis. *Journal of Cellular and Molecular Medicine, 23*(6), 4153-64. doi: 10.1111/jcmm.14302.

Huo, H., Zhou, Z., Qin, J., Liu, W., Wang, B., & Gu, Y. (2016). Erastin disrupts mitochondrial permeability transition pore (mPTP) and induces apoptotic death of colorectal cancer cells. *PLoS One, 11*(5), e0154605. doi: 10.1371/journal.pone.0154605.

Iida, Y., Okamoto-Katsuyama, M., Maruoka, S., Mizumura, K., Shimizu, T., Shikano, S., Hikishi, M., Takahashi, M., Tsuya, K., Okamoto, S., Inoue, T., Nakanishi, Y., Takahashi, N., Masuda, S., Hashimoto, S., & Gon, Y. (2021). Effective ferroptotic small-cell lung cancer cell death from SLC7A11 inhibition by sulforaphane. *Oncology Letters, 1*(7). doi: 10.3892/ol.2020.12332.

InvivoGen. (undated a). *Plasmocin | Elimination of Mycoplasma Contamination | InvivoGen*. [online] Available at: https://www.invivogen.com/Plasmocin [Accessed 11 Nov. 2019].

InvivoGen. (undated b). *Plasmocure | Elimination of Resistant Mycoplasma*. [online] Available at: https://www.invivogen.com/plasmocure [Accessed 11 Nov. 2019].

Ito, K., Eguchi, Y., Imagawa, Y., Akai, S., Mochizuki, H., & Tsujimoto, Y. (2017). MPP^+ induces necrostatin-1- and ferrostatin-1-sensitive necrotic death of neuronal SH-SY5Y cells. *Cell Death Discovery, 27*(3), 17013. doi: 10.1038/cddiscovery.2017.13.

Jeong, S., Kim, D. Y., Kang, S. H., Yun, H. K., Kim, J. L., Kim, B. R., Park, S. H., Na. Y. J., Jo, M. J., Jeong, Y. A., Kim, B. G., Lee, D. H., & Oh, S. C. (2019). Docosahexaenoic acid enhances oxaliplatin-induced autophagic cell death via the ER stress/Sesn2 pathway in colorectal cancer. *Cancers, 11*(7), E982. doi: 10.3390/cancers11070982.

Jha, N., Jurma, O., Lalli, G., Liu, Y., Pettus, E. H., Greenamyre, J. T., Liu R-M., Forman, H. J., & Andersen, J. K. (2000). Glutathione Depletion in PC12 Results in Selective Inhibition of Mitochondrial Complex I Activity. *Journal of Biological Chemistry*, *275*(34), 26096–26101. doi: 10.1074/jbc.m000120200.

Jing, K., Song, K. S., Shin, S., Kim, N., Jeong, S., Oh, H. R., Park, J. H., Seo, K. S., Heo, J. Y., Han, J., Park, J. I., Han, C., Wu, T., Kweon, G. R., Park, S. K., Yoon, W. H., Hwang, B. D., & Lim, K. (2011). Docosahexaenoic acid induces autophagy through p53/AMPK/mTOR signalling and promotes apoptosis in human cancer cells harbouring wild-type p53. *Autophagy, 7*(11), 1348-58. doi: 10.4161/auto.7.11.16658.

Jing, X., Shi, Q., Bi, W., Zeng, Z., Liang, Y., Wu, X., Xiao, S., Liu, J., Yang, L., & Tao, E. (2014). Rifampicin protects PC12 cells from rotenone-induced cytotoxicity by activating GRP78 via PERK-eIF2α-ATF4 pathway. *PLoS One, 9*(3), e92110. doi: 10.1371/journal.pone.0092110.

Johnson, J., Hague, S. M., Hanson, M., Gibson, A., Wilson, K. E., Evans, E. W., Singleton, A. A., McInerney-Leo, A., Nussbaum, R. L., Hernandez, D. G., Gallardo, M., McKeith, I. G., Burn, D. J., Ryu, M., Hellstrom, O., Ravina, B., Eerole, J., Perry, R. H., Jaros, E., Tienari, P., Weiser, R., Gwinn-Hard, K., Morris, C. M., & Singleton, A. B. (2004). SNCA multiplication is not a common cause of Parkinson's disease or dementia with Lewy bodies. *Neurology, 63*(3), 554-56. doi: 10.1212/01.wnl.0000133401.09043.44.

Junge, W., & Nelson, N. (2015). ATP synthase. *Annual Review of Biochemistry, 84*, 631-57. doi: 10.1146/annurev-biochem-060614-034124.

Kagan, V. E., Mao, G., Qu, F., Friedmann, A. J. P., Doll, S., Croix, C. S., Dar, H. H., Liu, B., Tyurin, V. A., Ritov, V. B., Kapralov, A. A., Amoscato, A. A., Jiang, J., Anthonymuthu, T., Mohammadyani, D., Yang, Q., Proneth, B., Klein-Seetharaman, J., Watkins, S., Bahar, I., Greenberger, J., Mallampalli, R. K., Stockwell, B. R., Tyurina, Y. Y., Conrad, M., & Bayir, H. (2017). Oxidized arachidonic and adrenic PEs navigate cells to ferroptosis. *Chemical Biology, 13*(1), 81-90. doi: 10.1038/nchembio.2238.

Kang, R., Zeh, H. J., Lotze, M. T., & Tang, D. (2011). The Beclin 1 network regulated autophagy and apoptosis. *Cell Death and Differentiation, 18*(4), 571-80. doi: 10.1038/cdd.2010.191.

Kasten, M., & Klein, C. (2013). The many faces of alpha-synuclein mutations. *Movement Disorders, 28*(6), 697-701. doi: 10.1002/mds.25499.

Kaur, G., & DDufour, J. M. (2012). Cell lines – valuable tools or useful artifacts. *Spermatogenesis, 2*(1), 1-5. doi: 10.4161/spmg.19885.

Kazemiha, V. M., Azari, S., Amanzadeh, A., Bonakdar, S., Moghadam, M. S., Anbouhi, M. H., Maleki, S., Ahmadi, N., Mousavi, T., & Shokrgozar, M. A. (2011). Efficiency of Plasmocin™ on various mammalian cell lines infected by mollicutes in comparison with commonly used antibiotics in cell culture: a local experience. *Cytotechnology, 63*(6), 609-20. doi: 10.1007/s10616-011-9378-1.

Kenny, E. M., Fidan, E., Yang, Q., Anthonymuthu, T. S., New, L. A., Meyer, E. A., Wang, H., Kochanek, P. M., Dixon, C., E., Kagan, V. E., & Bayir, H. (2019). Ferroptosis contributes to neuronal death and functional outcome after traumatic brain injury. *Critical Care Medicine, 47*(3), 410-18. doi: 10.1097/CCM.0000000000003555.

Kim, J. S., Choi, I. S., & Lee, M. C. (1995). Reversible parkinsonism and dystonia following probable mycoplasma pneumoniae infection. *Movement Disorders, 10*(4), 510-2. doi: 10.1002/mds.870100419.

Kim, S. W., Jang, Y. J., Chang, J. W., & Hwang, O. (2003). Degeneration of the nigrostriatal pathway and induction of motor deficit by tetrahydrobiopterin: an in vivo model relevant to Parkinson's disease. *Neurobiology of Disease*, *13*(2), 167–76. doi: 10.1016/s0969-9961(03)00037-8.

Kim, W. S., Kågedal, K., & Halliday, G. M. (2014). Alpha-synuclein biology in Lewy body diseases. *Alzheimer's Research and Therapy*, *6*(5), 73. doi: 10.1186/s13195-014-0073-2.

Kim, N., Jeong, S., Jing, K., Shin, S., Kim, S., Heo, J. Y., Kweon, G. R., Park, S. K., Wu, T., Park, J. I., & Lim, K. (2015). Docosahexaenoic acid induces cell death in human non-small cell lung cancer cells by repressing mTOR via AMPK activation and PI3K/Akt inhibition. *BioMed Research International, 2015*, 239764. doi: 10.1155/2015/239764.

Kim, S. E., Zhang, L., Ma, K., Riegman, M., Chen, F., Ingold, I., Conrad, M., Ziya, M., Gao, M., Jiang, X., Monette, S., Pauliah, M., Gonen, M., Zanzonico, P., Quinn, T., Wiesner, U., Bradbury, M. S., & Overholtzer, M. (2016). Ultrasmall nanoparticles induce ferroptosis in nutrient-deprived cancer cells and suppress tumour growth. *Nature Nanotechnology, 11*, 977-85. doi: 10.1038/NNANO.2016.164.

Kingsbury, A. E., Bandopadhyay, E., Silveira-Moriyama, L., Ayling, H., Kallis, C., Sterlacci, W., Maeir, H., Poewe, W., & Lees, A. J. (2010). Brain stem pathology in Parkinson's disease: An evaluation of the Braak staging model. *Movement Disorders, 25*(15), 2508-15. doi: 10.1002/mds.23305.

Klein, C., & Westenberger, A. (2012). Genetics of Parkinson's Disease. *Cold Spring Harbor Perspectives in Medicine*, *2*(1), a008888. doi: 10.1101/cshperspect.a008888.

Klivenyi, P., Beal, M. F., Ferrante, R. J., Andreassen, O. A., Wermer, M., Chin, M. R., & Bonventre, J. V. (1998). Mice deficient in group IV cytosolic phospholipase A2 are resistant to MPTP neurotoxicity. *Journal of Neurochemistry, 71*(6), 2634-7. doi: 10.1046/j.1471-4159.1998.71062634.x.

Knaryan, V. H., Samantaray, S., Park, S., Azuma, M., Inoue, J., & Banik, N. L. (2013). SNJ-1945, a calpain inhibitor, protects SH-SY5Y cells against MPP^+ and rotenone. *Journal of Neurochemistry, 130*(2), 280-90. doi: 10.1111/jnc.12629.

Kong, Z., Liu, R., & Cheng, Y. (2019). Artesunate alleviates liver fibrosis by regulating ferroptosis signalling pathway. *Biomedicine & Pharmacotherapy, 109*, 2043-53. doi: 10.1016/j.biopha.2018.11.030.

Korecka, J., van Kesteren, R. E., Blaas, E., Spitzer, S. O., Kamstra, J. H., Smit, A. B., Swaab, D. F., Verhaagen, J., & Bossers, K. (2013). Phenotypic characterisation of retinoic acid differentiated SH-SY5Y cells by transcriptional profiling. *PLoS One, 8*(5), e63862. doi: 10.1371/journal.pone.0063862.

Kovalevich, J., & Langford, D. (2013). Considerations for the use of SH-SY5Y neuroblastoma cells in neurobiology. *Neuronal Cell Culture, 28*(1), 101-110. doi: 10.1007/978-1-62703-640-5_2.

Kostrzewa, R. M., & Jacobowitz, D. M. (1974). Pharmacological Actions of 6-Hydroxydopamine. *Pharmacological Reviews, 26*(3), 199-288.

Krainz, T., Gaschler, M. M., Lim, C., Sacher, J. R., Stockwell, B. R., & Wipf, P. (2016). A Mitochondrial-Targeted Nitroxide Is a Potent Inhibitor of Ferroptosis. *ACS Central Science*, *2*(9), 653–659. doi: 10.1021/acscentsci.6b00199.

Kranz, L. M., Diken, M., Haas, H., Kreiter, S., Loquai, C., Reuter, K. C., Meng, M., Fritz, D., Vascotto, F., Hefesha, H., Grunwitz, C., Vormehr, M., Husemann, Y., Selmi, A., Kuhn, A. N., Buck, J., Derhovanessian, E., Rae, R., Attig, S., Diekmann, J., Jabulowsky, R. A., Heesch, S., Hassel, J., Langguth, P., Grabbe, S., Huber, C., Tureci, O., & Sahin, U. (2016). Systemic RNA delivery to dendritic cells exploits antiviral defence for cancer immunotherapy. *Nature*, *534*(7607), 396-401. doi: 10.1038/nature18300.

Krishna, A., Biryukov, M., Trefois, C., Antony, P. M., Hussong, R., Lin, J., Heinaniemi, M., Glusman, G., Koglsberger, S., Boyd, O., van den Berg, B. H., Linke, D., Huang, D., Wang, K., Hood, L., Tholey, A., Schneider, R., Galas, D. J., Balling, R., & May, P. (2014). Systems genomics evaluation of the SH-SY5Y neuroblastoma cell line as a model for Parkinson's disease. *BioMed Central Genomics, 15,* 1154. doi: 10.1186/1471-2164-15-1154.

Kroemer, G., Galluzzi, L., Vandenabeele, P., Abrams, J., Alnemri, E. S., Baehrecke, E. H., Blagosklonny, M. V., El-Deiry, W. S., Golstein, P., Green, D. R., Hengartner, M., Knight, R. A., Kumar, S., Lipton, S. A., Malorni, W., Nunez, G., Peter, M. E., Tschopp, J., Yuan, J., Piacentini, M., Zhivotovsky, B., & Melino, G. (2009). Classification of cell death: recommendations of the Nomenclature Committee on Cell Death 2009. *Cell Death and Differentiation, 16*(1), 3-11. doi: 10.1038/cdd.2008.150.

Kuete, V., Karaosmanoglu, O., & Sivas, H. (2017). Anticancer activities of African medicinal spices and vegetables. *Medicinal Spices and Vegetables from Africa*, Elsevier, 271-97. doi: 10.1016/B978-0-12-809286-6.00010-8.

Kuilman, T., Michaloglou, C., Mooi, W. J., Peeper, D. S. (2010). The essence of senescence. *Genes and Development, 24*(22), 2463-79. doi: 10.1101/gad.1971610.

Kumar, V., Abbas, A., Aster, J. and Fausto, N. (2010). *Robbins and Cotran Pathologic Basis of Disease*. 8th ed. Philadelphia: Saunders Elsevier, pp.12-41.

Kumar, A., Tikoo, S., Maity, S., Sengupta, S., Sengupta, S., Kaur, A., Bachhawat, A. K. (2012). Mammalian proapoptotic factor Chac1 and its homologouues function as γ-glutamyl cyclotransferases acting specifically on glutathione. *EMBO Reports, 13*(12), 1095-101. doi: 10.1038/embor.2012.156.

Kumar, A., Leinisch, F., Kadiiska, M. B., Corbett, J., & Mason, R. P. (2016). Formation and implications of alpha-synuclein radical in maneb- and paraquat-induced models of Parkinson's disease. *Molecular Neurobiology, 53*(5), 2983-94. doi: 10.1007/s12035-015-9179-1.

Kumari, A. (2017). *Sweet Biochemistry: Remembering Structures, Cycles, and Pathways by Mnemonics*. 1st ed. Academic Press.

Kume, T., Kawato, Y., Osakada, F., Izumi, Y., Katsuki, H., Nakagawa, T., Kaneko, S., Niidome, T., Takada-Takatori, Y., & Akaike, A. (2008). Dibutyryl cyclic AMP induces differentiation of human neuroblastoma SH-SY5Y cells into noradrenergic phenotype. *Neuroscience Letters, 443*(3), 199-203. doi: 10.1016/j.neulet.2008.07.079.

Kwizera, R., Akampurira, A., Kandole, T. K., Nielsen, K., Kambugu, A., Meya, D. B., Boulware, D. R., & Rhein, J. (2017). Evaluation of trypan blue stain in a haemocytometer for rapid detection of cerebrospinal fluid sterility in HIV patients with cryptococcal meningitis. *BioMed Central Microbiology, 17*(1), 182. doi: 10.1186/s12866-017-1093-4.

Lachaier, E., Louandre, C., Godin, C., Saidak, Z., Baert, M., Diouf, M., Chauffert, B., Galmiche, A. (2014). Sorafenid Induces Ferroptosis in Human Cancer Cell Lines Originating from Different Solid Tumors. *Anticancer Research*, *34*(11), 6417–6422.

Larraufie, M-H., Yang, W. S., Jiang, E., Thomas, A. G., Slusher, B. S., & Stockwell, B. R. (2015). Incorporation of metabolically stable ketones into a small molecule probe to increase potency and water solubility. *Bioorganic and Medicinal Chemistry Letters, 25*(21), 4787-92. doi: 10.1016/j.bmcl.2015.07.018.

Laster, S. M., Wood, J. G., & Gooding, L. R. (1988). Tumor necrosis factor can induce both apoptotic and necrotic forms of cell lysis. *Journal of Immunology, 141*(8), 2629-34.

Lautenschlager, J., Mosharov, E. V., Kanter, E., Sulzer, D., & Schierle, G. S. K. (2018). An easy-to-implement protocol for preparing postnatal ventral mesencephalic cultures. *Frontiers in Cellular Neuroscience, 12*, 44. doi: 10.3389/fncel.2018.00044.

Lee, J., Song, K., Oh, M. S., & Kim, Y. S. (2018). Neuroprotection against 6-OHDA toxicity in PC12 cells and mice through the Nrf2 pathway by a sesquiterpenoid from Tussilago farfara. *Redox Biology, 18*, 6-15. doi: 10.1016/j.redox.2018.05.015.

Lee, J-Y., Nam, M., Son, H. Y., Hyun, K., Jang, S. Y., Kim, J. W., Kim, M. W., Jung, Y., Jang, E., Yoon, S-J., Kim, J., Kim, J., Seo, J., Min, J-K., Oh, K-J., Han, B-S., Kim, W. K., Bae, K-H., Song, J., Kim, J., Huh, Y-M., Hwang, G-S., Lee, E-W., & Lee, S. C. (2020). Polyunsaturated fatty acid biosynthesis pathway determines ferroptosis sensitivity in gastric cancer. *Proceedings of the National Academy of Sciences of the United States of America, 117*(51), 32433-42. doi: 10.1073/pnas.2006828117.

Levine, B., & Kroemer, G. (2008). Autophagy in the pathogenesis of disease. *Cell, 132*(1), 27-42. doi: 10.1016/j.cell.2007.12.018.

Lewerenz, J., Hewett, S. J., Huang, Y., Lambros, M., Gout, P. W., Kalivas, P. W., Massie, A., Smolders, I., Methner, A., Pergande, M., Smith, S. B., Ganapathy, V., & Maher, P. (2013). The Cystine/Glutamate Antiporter System x_c^- in Health and Disease: From Molecular Mechanisms to Novel Therapeutic Opportunities. *Antioxidants & Redox Signaling*, *18*(5), 522–55. doi: 10.1089/ars.2011.4391.

Lewerenz, J., Ates, G., Methner, A., Conrad, M., & Maher, P. (2018). Oxytosis/ferroptosis-(Re)-emerging roles for oxidative stress-dependent non-apoptotic cell death in diseases of the central nervous system. *Frontiers in Neuroscience, 12*, 214. doi: 10.3389/fnins.2018.00214.

Li, Y., Huang, W., Huang, S., Du, J., & Huang, C., (2012). Screening of anti-cancer agent using zebrafish: comparison with the MTT assay. *Biochemical and Biphysical Research Communications, 422*(1), 85-90. doi: 10.1016/j.bbrc.2012.04.110.

Li, Q., Han, X., Lan, X., Gao, Y., Wan, J., Durham, F., Cheng, T., Yang, J., Wang, Z., Jiang, C., Ying, M., Koehler, R. C., Stockwell, B. R., & Wang, J. (2017). Inhibition of neuronal ferroptosis protects hemorrhagic brain. *JCI Insight,* 2(7), e90777. doi: 10.1172/jci.insight.90777.

Li, Q., Weiland, A., Chen, X., Lan, X., Han, X., Durham, F., Liu, X., Wan, J., Ziai, W. C., Hanley, D. F., & Wang, J. (2018). Ultrastructural characteristics of neuronal death and white matter injury in mouse brain tissues after intracerebral haemorrhage: coexistence of ferroptosis, autophagy, and necrosis. *Frontiers in Neurology, 9*, 581. doi: 10.3389/fneur.2018.00581.

Li, W., Feng, G., Gauthier, J. M., Lokshina, I., Higashikubo, R., Evans, S., Liu, X., Hassan, A., Tanaka, S., Cicka, M., Hsiao, H-M., Ruiz-Perez, D., Bredemeyer, A., Gross, R. W., Mann, D. L., Tyurina, Y., Gelman, A. E., Kagan, V. E., Linkermann, A., Lavine, K. J., & Kreisel, D. (2019b). Ferroptotic cell death and TLR4/Trif signalling initiate neutrophil recruitment after heart transplantation. *Journal of Clinical Investigation, 129*(6), 2293-304. doi: 10.1172/JCI126428.

Li, Y., Wang, X., Yan, J., Liu, Y., Yang, R., Pan, D., Wang, L., Xu, Y., Li, X., & Yang, M. (2019b). Nanoparticle ferritin-bound erastin and rapamycin: a nanodrug combining autophagy and ferroptosis for anticancer therapy. *Biomaterials Science, 7*(9), 3779-87. doi: 10.1039/C9BM00653B.

Li, Y., Feng, D., Wang, Z., Zhao, Y., Sun, B., Tian, D., Liu, D., Zhang, F., Ning, S., Yao, J., & Tian, X. (2019c). Ischemia-induced ACSL4 activation contributes to ferroptosis-mediated tissue injury in intestinal

ischaemia/reperfusion. *Cell Death & Differentiation, 26*, 2284-99. doi: 10.1038/s41418-019-0299-4.

Li, W., Li, W., Leng, Y., Xiong, Y., & Xia, Z. (2020a). Ferroptosis is involved in diabetes myocardial ischemia/reperfusion injury through endoplasmic reticulum stress. *DNA and Cell Biology, 39*(2), 210-25. doi: 10.1089/dna.2019.5097.

Li, N., Wang, W., Zhou, H., Wu, Q., Duan, M., Liu, C., Wu, H., Deng, W., Shen, D., & Tang, Q. (2020b). Ferritinophagy-mediated ferroptosis is involved in sepsis-induced cardiac injury. *Free Radical Biology and Medicine, 160*, 303-18. doi: 10.1016/j.freeradbiomed.2020.08.009.

Li, Z-J., Dai, H-Q., Huang, X-W., Feng, J., Deng, J-H., Wang, Z-X., Yang, X-M., Liu, Y-J., Wu, Y., Chen, P-H., Shi, H., Wang, J-G., Zhou, J., & Lu, G-D. (2020c). Artesunate synergises with sorafenib to induce ferroptosis in hepatocellular carcinoma. *Acta Pharmacologica Sinica, 42*, 301-10. doi: 10.1038/s41401-020-0478-3.

Li, Y., Yan, H., Xu, X., Liu, H., Wu, C., & Zhao, L. (2020d). Erastin/sorafenib induces cisplatin-resistant non-small cell lung cancer cell ferroptosis through inhibition of the Nrf2/xCT pathway. *Oncology Letters, 19*(1), 323-33. doi: 10.3892/ol.2019.11066.

Lin, M. M., & Laureno, R. (2019). Less Pulsatile Levodopa Therapy (6 Daily Doses) is Associated with a Reduced Incidence of Dyskinesia. *Journal of Movement Disorders, 12*(1), 37-42. doi: 10.14802/jmd.18046.

Liang, J-Y., Wang, D-S., Lin, H-C., Chen, X-X., Yang, H., Zheng, Y., & Li, Y-H. (2020). A novel ferroptosis-related gene signature for overall survival prediction in patients with hepatocellular carcinoma. *International Journal of Biological Sciences, 16*(3), 2430-41. doi: 10.7150/ijbs.45050.

Linkermann, A., Skouta, R., Himmerkus, N., Mulay, S. R., Dewitz, C., Zen, F. D., Prokai, A., Zuchtriegal, G., Krombach, F., Welz, P-S., Weinlich, R., Vanden Berghe, T., Vandenabeele, P., Pasparakis, M., Bleich, M., Weinberg, J. M., Reichel, C. A., Brasen, J. H., Kunzendorf, U., Anders, H-J., Stockwell, B. R., Green, D. R., & Krautwald, S. (2014). Synchronized renal tubular cell death involves ferroptosis. *Proceedings of the National Academy of Sciences*, *111*(47), 16836–41. doi: 10.1073/pnas.1415518111.

Linkous, A., & Yazlovitskaya, E. (2010). Cytosolic phospholipase A2 as a mediator of disease pathogenesis. *Cellular Microbiology, 12*(10), 1369-77. doi: 10.1111/j.1462-5822.2010.01505.x.

Lippmann, J., Petri, K., Fulda, S., & Liese, J. (2020). Redox modulation and induction of ferroptosis as a new therapeutic strategy in hepatocellular carcinoma. *TranslationalOncology, 13*(8), 100785. doi: 10.1016/j.tranon.2020.100785.

Liu, Y., Wang, W., Li, Y., Xiao, Y., Cheng, J., & Jia, J. (2015). The 5-Lipoxygenase Inhibitor Zileuton Confers Neuroprotection against Glutamate Oxidative Damage by Inhibiting Ferroptosis. *Biological & Pharmaceutical Bulletin*, *38*(8), 1234–39. doi: 10.1248/bpb.b15-00048.

Lobner, D. (2002). Comparison of the LDH and MTT assays for quantifying cell death: validity for neuronal apoptosis? *Journal of Neuroscience Methods, 96*(2), 147-52. doi: 10.1016/S0165-0270(99)00193-4.

Lőrincz, T., Jemnitz, K., Kardon, T., Mandl, J., & Szarka, A. (2015). Ferroptosis is Involved in Acetaminophen Induced Cell Death. *Pathology & Oncology Research*, *21*(4), 1115–21. doi: 10.1007/s12253-015-9946-3.

Lotharius, J., Barg, S., Wiekop, P., Lundberg, C., Raymon, H. K., & Brundin, P. (2002). Effect of mutant alpha-synuclein on dopamine homeostasis in a new human mesencephalic cell line. *Journal of Biological Chemistry,* 277(41), 38884-94. doi: 10.1074/jbc.M205518200.

Louandre. C., Ezzoukhry, Z., Godin, C., Barbare, J-C., Maziere, J-C., Chauffert, B., & Galmiche, A. (2013). Iron-dependent cell death of hepatocellular carcinoma cells exposed to sorafenib. *International Journal of Cancer, 133*(7), 1732-42. doi: 10.1002/ijc.28159.

Louandre, C., Marcq, I., Bouhlal, H., Lachaier, E., Godin, C., Saidak, Z., Francois, C., Chatelain, D., Debuysscher, V., Barbare, J-C., Chauffert, B., & Galmiche, A. (2015). The retinoblastoma (Rb) protein regulated ferroptosis induced by sorafenib in human hepatocellular carcinoma cells. *Cancer Letters, 356*(2b), 971-7. doi: 10.1016/j.canlet.2014.11.014.

Lu, L., Zhang, L., Wai, M. S., Yew, D. T., & Xu, J. (2012). Exocytosis of MTT formazan could exacerbate cell injury. *Toxicology In Vitro*, *26*(4), 636-44. doi: 10.1016/j.tiv.2012.02.006.

Ma, D., Li, C., Jiang, P., Jiang, Y., Wang, J., & Zhang, D. (2021). Inhibition of ferroptosis attenuates acute kidney injury in rats with severe acute pancreatitis. *Digestive Diseases and Sciences, 66*(2), 483-92. doi: 10.1007/s10620-020-06225-2.

Ma, S. Y., Roytta, M., Rinne, J. O., Collan, Y., & Rinne, U. K. (1997). Correlation between neuromorphometry in the substantia nigra and clinical features in Parkinson's disease using dissector counts. *Journal of the Neurological Sciences, 151*(1), 83-7. doi: 10.1016/s0022-510x(97)00100-7.

Ma, S., Dielschneider, R. F., Henson, E. S., Xiao, W., Choquette, T. R., Blankstein, A. R., Chen, Y., & Gibson, S. B. (2017). Ferroptosis and autophagy induced cell death occur independently after siramesine and lapatinib treatment in breast cancer cells. *PLoS One, 12*(8), e0182921. doi: 10.1371/journal.pone.0182921.

Ma, D., Li, C., Jiang, P., Jiang, Y., Wang, J., & Zhang, D. (2020). Inhibition of ferroptosis attenuates acute kidney injury in rats with severe acute pancreatitis. *Digestive Diseases and Sciences, 66*, 483-92. doi: 10.1007/s10620-020-06225-2.

Magalingam, K. B., Radhakrishnan, A. K., Somanath, S. D., Md, S., & Haleagrahara, N. (2020). Influence of serum concentration in retinoic acid and phorbol ester induced differentiation of SH-SY5Y human neuroblastoma cell line. *Molecular Biology Reports, 47*, 8775-88. doi: 10.1007/s11033-020-05925-2.

Malla, B., Cotton, S., Ulshoefer, R., Paul, F., Hauser, A. E., Niesner, R., Bros, H., & Infante-Duarte, C. (2020). Teriflunomide preserves peripheral nerve mitochondria from oxidative stress-mediated alterations. *Therapeutic Advances in Chronic Disease, 11*(11). doi: 10.1177/2040622320944773.

Manfredi, J. J., & Prives, C. (1994). The transforming activity of simian virus 40 large tumor antigen. *Biochimica et Biophysica Acta, 1198*(1), 65-83. doi: 10.1016/0304-419x(94)90006-x.

Maqsood, M. I., Matin, M. M., Bahrami, A. R., & Ghasroldasht, M. M. (2013). Immortality of cell lines: challenges and advantages of establishment. *Cell Biology International, 37*(10), 1038-45. doi: 10.1002/cbin.10137.

Maratos, E. C., Jackson, M. J., Pearce, R. K. B., Cannizzaro, C., & Jenner, P. (2002). Both Short- and Long-Acting D-1/D-2 Dopamine Agonists Induce Less Dyskinesia than L-DOPA in the MPTP-Lesioned Common Marmoset (*Callithrix jacchus). Experimental Neurology, 179*(1), 90-102. doi: 10.1006/exnr.2002.8055.

Marques, O. & Outeiro, T.F. (2012). Alpha-synuclein: From secretion to dysfunction and death. *Cell Death and Disease*, *3*(7), e350. doi: 10.1038/cddis.2012.94.

Martinez-Ramirez, D., Hu, W., Bona, A.R., Okun, M.S. & Shukla, A.W. (2015). Update on deep brain stimulation in Parkinson's disease. *Translational Neurodegeneration*, *4*(12). doi: 10.1186/s40035-015-0034-0.

Martinez-Martin, P., Rodriguez-Blazquez, C., Kurtis, M. M., & Chaudhuri, K. R. 2011. The impact of non-motor symptoms on health-related quality of life of patients with Parkinson's disease. *Movement Disorders, 26*(3), 399-406. doi: 10.1002/mds.23462.

Massie, A., Schallier, A., Kim, S. W., Fernando, R., Kobayashi, S., Beck, H., De Bundel, D., Vermoesen, K., Bannai, S., Smolders, I., Conrad, M., Plesnila, N., Sato, H., & Michotte, Y. (2011). Dopaminergic neurones of system x_c^--deficient mice are highly protected against 6-hydroxydopamine-induced toxicity. *Federation for American Societies for Experimental Biology Journal, 25*(4), 1359-69. doi: 10.1096/fj.10-177212.

Masutomi, K., Yu, E. Y., Khurts, S., Ben-Porath, I., Currier, J. L., Metz, G. B., Brooks, M. W., Kaneko, S., Murakami, S., DeCaprio, J. A., Weinberg, R. A., Stewart, S. A., & Hahn, W. C. (2003). Telomerase

Maintains Telomere Structure in Normal Human Cells. *Cell, 114*(2), 241-53. doi: 10.1016/S0092-8674(03)00550-6.

Mathieu, G., Denis, S., Langelier, B., Denis, I., Labialle, M., & Vancassel, S. (2010). DHA enhances the noradrenaline release by SH-SY5Y cells. Neurochemistry International, 56(1), 94-100. doi: 10.1016/j.neuint.2009.09.006.

Mayashita, N., Kawai, Y., Kato, T., Tanaka, T., Akaike, H., Teranishi, H., Nakano, T., Ouchi, K., & Okimoto, N. (2016). Rapid diagnostic method for the identification of Mycoplasma pneumoniae respiratory tract infection. *Journal of Infection and Chemotherapy, 22*(5), 327-30. doi: 10.1016/j.jiac.2016.02.005.

Mazzulli, J. R., Mishizen, A. J., Giasson, B. I., Lynch, D. R., Thomas, S. A., Nakashima, A., Nagatsu, T., Ota, A., & Ischiropoulos, H. (2006). Cytosolic Catechols Inhibit Alpha-Synuclein Aggregation and Facilitate the Formation of Intracellular Soluble Oligomeric Intermediates. *Journal of Neuroscience*, *26*(39), 10068–78. doi: 10.1523/jneurosci.0896-06.2006.

McGarrity, G. J. (1976). Spread and control of mycoplasmal infection of cell cultures. *In Vitro, 12*(9), 643-8. doi: 10.1007/bf02797464.

Melamed, E., Hefti, D., & Wurtman, E. J. (1980). Nonaminergic striatal neurons convert exogenous l-dopa to dopamine in parkinsonism. *Annals of Neurology, 8*(6), 558-63. doi: 10.1002/ana.410080603.

Menon, A., V., Tsai, H. P., & Kim, J. (2020). Cardiac iron overload promotes ferroptosis and cardiac dysfunction in mice with sickle cell disease. *The FASEB Journal, 34*(S1). doi: 10.1096/fasebj.2020.34.s1.02704.

Metman, L. V. (2002). Recognition and treatment of response fluctuations in Parkinson's disease: review article. *Amino Acids, 23*(1-3), 141-45. doi: 10.1007/s00726-001-0119-1.

Michell, A. W., Baker, R. A., Raha-Chowdhury, R., & Raha, S. K. (2005). A case of late onset sporadic Parkinson's disease with an A53T mutation in alpha-synuclein. *Journal of Neurology, Neurosurgery and Psychiatry, 76*(4), 596-97. doi: 10.1136/jnnp.2004.046425.

Miess, H., Dankworth, B., Gouw, A. M., Rosenfeldt, M., Schmitz, W., Jiang, M., Saunders, B., Howell, M., Downward, J., Felsher, D. W., Peck, B., & Schulze, A. (2018). The glutathione redox system is essential to prevent ferroptosis caused by impaired lipid metabolism in clear cell renal cell carcinoma. *Oncogene, 37*, 5435-50. doi: 10.1038/s41388-018-0315-z.

Mizushima, N. (2007). Autophagy: process and function. *Genes and Development, 21*(22), 2861-73. doi: 10.1101/gad.1599207.

Mizushima, N., Levine, B., Cuervo, A. M., & Klionsky, D. J. (2008). Autophagy dights disease through cellular self-digestion. *Nature, 451*(7182), 1069-75. doi: 10.1038/nature06639.

Mossmann, T. (1983). Rapid colorimetric assay for cellular growth and survival: application to proliferation and cytotoxicity assays. *Journal of Immunological Methods, 65*(1-2), 55-63. doi: 10.1016/0022-1759(83)90303-4.

Muenter, M. D., Forno, L. S., Hornykiewics, O., Kish, S. J., Maraganore, D. M., Caselli, R. J., Okazaki, H., Howard, F. M. Jr., Snow, B. J., & Calne, D. B. (1998). Hereditary form of parkinsonism-dementia. *Annals of Neurology, 43*(6), 768-81. doi: 10.1002/ana.410430612.

Mullen, A. R., Wheaton, W. W., Jin, E. S., Chen, P. H., Sullivan, L. B., Cheng, T., Yang, Y., Linehan, W. M., Chandel, N. S., and Deberardinis, R. J. (2011). Reductive carboxylation supports growth in tumour cells with defective mitochondria. *Nature, 481*(7381), 385–88. doi: 10.1038/nature10642.

Muller, T., Dewitz, C., Schmitz, J., Schroder, A. S., Brasen, J. H., Stockwell, B. R., Murphy, J. M., Kunzendorf, U., & Krautwald, S. (2017). Necroptosis and ferroptosis are alternative cell death pathways that operate in acute kidney failure. *Cellular and Molecular Life Sciences, 74*(19), 3631-45. doi: 10.1007/s00018-017-2547-4.

Mungrue, I. N., Pagnon, J., Kohannim, O., Gargalovic, P. S., & Lusis, A. J. (2010). CHAC1/MGC4504 is a novel proapoptotic component of the unfolded protein response, downstream of the ATF4-ATF3-CHOP cascade. *The Journal of Immunology, 182*(1), 466-76. doi: 10.4049/jimmunol.182.1.466.

Murman, D. L. (2012). Early treatment of Parkinson's disease: opportunities for managed care. *The American Journal of Managed Care*, *18*(7), S183–188.

Nagatsu, T., Levitt, M., & Udenfriend, S. (1964). Tyrosine hydroxylase. The initial step in norepinephrine biosynthesis. *Journal of Biological Chemistry, 239*, 2910-7.

National Health Service (2016a). *Parkinson's disease - Diagnosis*. [online] Available at: https://www.nhs.uk/conditions/parkinsons-disease/diagnosis/ [Accessed 26 Feb. 2019].

National Health Service. (2016b). *Parkinson's disease - Treatment*. [online] Available at: https://www.nhs.uk/conditions/parkinsons-disease/treatment/ [Accessed 28 Feb. 2019].

National Institute of Health, USA. (2018). *Parkinson's Disease: Hope Through Research | National Institute of Neurological Disorders and Stroke*. [online] Available at: https://www.ninds.nih.gov/Disorders/Patient-Caregiver-Education/Hope-Through-Research/Parkinsons-Disease-Hope-Through-Research#symptoms [Accessed 28 Feb. 2019].

National Institute of Health and Care Excellence. (2003). *Overview | Deep brain stimulation for Parkinson's disease | Guidance | NICE*. [online] Available at: https://www.nice.org.uk/guidance/ipg19 [Accessed 3 Mar. 2019].

Nebie, O., Devos, D., Vingtdeux, V., Barro, L., Devedjian, J. C., Jonneaux, A., Chou, M. L., Bordet, R., Buree, L., Knutson, F., Blum, D., & Burnouf, T. (2019). The neuroprotective activity of heat-treated human plateley lysate biomaterials manufactured from outdated pathogen-reduced

(amotosalen/UVA) platelet concentrates. *Journal of Biomedical Science, 26*(1), 89. doi: 10.1186/s12929-019-0579-9.

Neuhaus, J. F. G., Baris, O. R., Hess, S., Moser, N., Schroder, H., Chinta, S. J., Anderson, J. K., Kloppenburg, P., & Wiesner, R. J. (2014). Catecholamine metabolism drives generation of mitochondrial DNA deletions in dopaminergic neurones. *Brain, 137*(2), 354-65. doi: 10.1093/brain/awt291.

Nijman, S. M. (2011). Synthetic lethality: general principles, utility and detection using genetic screens in human cells. *FEBS Letters, 585*(1), 1-6. doi: 10.1016/j.febslet.2010.11.024.

Nikfarjam, L., & Farzaneh, P. (2012). Prevention and detection of Mycoplasma contamination in cell culture. *Cell Journal, 13*(4), 203-12.

Nyholm, D., Ashmark, H., Gomes-Trolin, C., Knutson, T., Lennernas, H., Nystrom, C., & Aquilonius, S. M. (2003). Optimizing levodopa pharmacokinetics: intestinal infusion versus oral sustained-release tablets. *Clinical Neuropharmacology, 26*(3), 156-63. doi: 10.1097/00002826-200305000-00010.

Oda, Y. (1999). Choline acetyltransferase: the structure, distribution and pathologic changes in the central nervous system. *Pathology International, 49*(11), 921-37. doi: 10.1046/j.1440-1827.1999.00977.x.

Oertel, W., & Schulz, J. B. (2016). Current and experimental treatments of Parkinson's disease: A guide for neuroscientists. *Journal of Neurochemistry, 139*(Supplement 1), 325-37. doi: 10.1111/jnc.13750.

Oertel, W., Eggert, K., Pahwa, R., Tanner, C. M., Hauser, R. A., Trenkwalder, C., Ehret, R., Azuly, J. P., Isaacson, S., Felt, L., & Stempien, M. J. (2017). Randomized, placebo-controlled trial of ADS-5102 (amantadine_ extended-release capsules for levodopa-induced dyskinesia in Parkinson's disease. *Movement Disorders*, *32*(12). doi: 10.1002/mds.27131.

Olivares, D., Huang, X., Branden, L., Greig, N.H. & Rogers, J.T. (2009). Physiological and pathological role of Alpha-synuclein in Parkinson's disease through iron mediated Oxidative stress; the role of a putative iron-responsive element. *International Journal of Molecular Sciences*, *10*(3), 1226–60. doi: 10.3390/ijms10031226.

Ou, W., Mulik, R. S., Anwar, A., McDonald, J. G., He, X., & Corbin, I. R. (2017). Low-density lipoprotein docosahexaenoic acid nanoparticles induce ferroptotic cell death in hepatocellular carcinoma. *Free Radical Biology and Medicine, 112*, 597-607. doi: 10.1016/j.freeradbiomed.2017.09.002.

Ozsoy, O., Seval-Celik, Y., Hacioglu, G., Yargicoglu, P., Demir, R., Agar, A., & Aslan, M. (2011). The influence and the mechanism of docosahexaenoic acid on a mouse model of Parkinson's disease. *Neurochemistry International, 59*(5), 664-70. doi: 10.1016/j.neuint.2011.06.012.

Pahlman, S., Ruusala, A. I., Abrahamsson, L., Mattsson, M. E., & Esscher, T. (1984). Retinoic acid-induced differentiation of cultured human neuroblastoma cells: a comparison with phorbolester-induced differentiation. *Cell Differentiation, 14*(2), 135-44. doi: 10.1016/0045-6039(84)90038-1.

Pahwa, R., Tanner, C. M., Hauser, R. A., Sethi, K., Isaacson, S. H, Truong, D. D., Struck, L., Ruby, A. E., McClure, N. L., Went, G. T., & Stempien, M. J. (2015). Amantadine extended release for levodopa-induced dyskinesia in Parkinson's disease. *Movement Disorders, 30*(6), 788-95. doi: 10.1002/mds.26159.

Pahwa, R., Tanner, C. M., Hauser, R. A., Isaacson, S. H., Nausieda, P. A., Truong, D. D., Agarwal, P., Hull, K. L., Lyons, K. E., Johnson, R., & Stempien, M. J. (2017). ADS-5102 (Amantadine) extended release capsuled for levodopa-induced dyskinesia in Parkinson's disease: a randomized clinical trial. *JAMA Neurology, 74*(8), 941-49. doi: 10.1001/jamaneurol.2017.0943.

Pakkenberg, B., Moller, A., Gundersen, H. J., Mouritzen Dam, A., & Pakkenberg, H. (1991). The absolute number of nerve cells in substantia nigra in normal subjects and in patients with Parkinson's disease estimated with an unbiased stereological method. *Journal of Neurology, Neurosurgery and Psychiatry, 54*(1), 30-3. doi: 10.1136/jnnp.54.1.30.

Pan, X., Lin, Z., Jiang, D., Yu, Y., Yang, D., Zhou, H., Zhan, D., Liu, S., Peng, G., Chen, Z., & Yu, Z. (2019). Erastin decreases radioresistance of NSCLC cells partially by inducing GPX4-mediated ferroptosis. *Oncology Letters, 17*(3), 3001-8. doi: 10.3892/ol.2019.9888.

Park, S., Oh, J., Kim, M., & Jin, E-J. (2018). Bremelain effectively suppresses Kras-mutant colorectal cancer by stimulating ferroptosis. *Animal Cells and Systems, 22*(5), 334-40. doi: 10.1080/19768354.2018.1512521.

Park, T-J., Park, J. H., Lee, G. S., Lee, J-Y., Shin, J. H., Kim, M. W., Kim, Y. S., Kim, J-Y., Oh, K-J., Han, B-S., Kim, W-K., Ahn, Y., Moon, J. H., Song, J., Bae, K-H., Kim, D. H., Lee, E-W., & Lee, S. C. (2019). Quantitative proteomic analyses reveal that GPX4 downregulation during myocardial infarction contributes to ferroptosis in cardiomyocytes. *Cell Death & Disease, 10*(11), 835. doi: 10.1038/s41419-019-2061-8.

Parkinson, J. (2002). An Essay on the Shaking Palsy. *The Journal of Neuropsychiatry and Clinical Neurosciences*, *14*(2), 223–36. doi: 10.1176/jnp.14.2.223.

Paumier, K. L., Luk, K. C., Manfredsson, F. P., Kanaan, N. M., Lipton, J. W., Collier, T. J., Steece-Sollier, K., Kemp, C. J., Celano, S., Schulz, E., Sandoval, I. M., Fleming, S., Dirr, E., Polinski, N. K., Trojanowski, J. Q., Lee, V. M., & Sortwell, C. E. (2015). Intrastriatal injection of pre-formed mouse α-synuclein fibrils into rats triggers α-synuclein pathology and bilateral nigrostriatal degeneration. *Neurobiology of Disease, 82*, 185-99. doi: 10.1016/j.nbd.2015.06.003.

Petrucci, S., Ginevrino, M., & Valente, E. M. (2016). Phenotypic spectrum of alpha-synuclein mutations: New insights from patients and cellular models. *Parkinsonism and Related Disorders, 22*(Supplement 1), S16-20. doi: 10.1016/j.parkreldis.2015.08.015.

Pizato, N., Luzete, B. C., Kiffer, L. F. M. V., Correa, L. H., de Oliviera Santos, I., Assumpcao, J. A. F., Kiyomi, M., & Magalhaes, K. G. (2018). Omega-3 docosahexaenoic acid induces pyroptosis cell death in triple-negative breast cancer cells. *Scientific Reports, 8*. doi: 10.1038/s41598-018-27850-y.

Poewe, W. (2008). Non-motor smptoms in Parkinson's disease. *European Journal of Neurology, 15*(Supplement 1), 14-20. doi: 10.1111/j.1468-1331.2008.02056.x.

Polymeropoulos, M. H., Lavedan, C., Leroy, E., Ide. S. E., Dehejia, A., Dutra, A., Pike, B., Root, H., Rubenstein, J., Boyer, R., Stenroos, E. S., Chandrasekharappa, S., Athanssiadou, A., Papapetropoulos, T., Johnson, W. G., Lazzarini, A. M., Duvoisin, R. C., Di Iorio, G., Golbe, L. I., & Nussbaum, R. L. (1997). Mutations in the α-Synuclein Gene Identifies in Families with Parkinson's Disease. *Science, 276*(5321), 2045-47. doi: 10.1126/science.276.5321.2045.

Poulin, D. L., Kung, A. L., & DeCaprio, J. A. (2004). p53 Targets Simian Virus 40 Large T Antigen for Acetylation by CBP. *Journal of Virology, 93*(1), e01330-18. doi: 10.1128/JVI.01330-18.

Presgraves, S. P., Ahmed, T., Borwege, S., & Joyce, J. N. (2004a). Terminally differentiated SH-SY5Y cells provide a model system for studying neuroprotective effects of dopamine agonists. *Neurotoxicity Research, 5*(8), 579-98. doi: 10.1007/BF03033178.

Presgraves, S. P., Borwege, S., Millan, M. J., & Joyce, J. N. (2004b). Involvement of dopamine D_2/D_3 receptors and BDNF in the neuroprotective effects of S32504 and pramipexole against 1-methyl-4-phenylpyridinium in terminally differentiated SH-SY5Y cells. *Experimental Neurology, 190*(1), 157-70. doi: 10.1016/j.expneurol.2004.06.021.

Redmond, D. E. Jr., Bjugstad, K. B., Teng, Y. D., Ourednik, V., Ourednik, J., Wakeman, D. R., Parsons, X. H., Gonzalez, R., Blanchard, B. C., Kim, S. U., Gu, Z., Lipton, S. A., Markakis, E. A., Roth, R. H., Elsworth, J. D., Sladek, J. R. Jr., Sidman, R. L., & Snyder, E. Y. (2007). Behaviorsl improvement in a primate Parkinson's model is associated with multiple homeostatic effects of human neural stem cells. *Proceedings of the National Academy of Sciences of the United States of America, 104*(29), 12175-180. doi: 10.1073/pnas.0704091104.

Riahi, Y., Cohen, G., Shamni, O., & Sasson, S. (2010). Signalling and cytotoxic functions of 4-hydroxyalkenals. *American Journal of Physiology, Endocrinology and Metabolism, 299*(6), 879-86. doi: 10.1152/ajpendo.00508.2010.

Rice, M. E., & Cragg, S. J. (2008). Dopamine spillover after quantal release: Rethinking dopamine transmission in the nigrostriatal pathway. *Brain Research Reviews*, *58*(2), 303–13. doi: 10.1016/j.brainresrev.2008.02.004.

Rodenhuis, S. (1992). Rats and human tumors. *Seminars in Cancer Biology, 3*(4), 241-47.

Rosenberry, T. L. (1975). Acetylcholinesterase. *Advances in Enzymology and Related Areas of Molecular Biology, 43*. doi: 10.1002/9780470122884.ch3.

Ross, R. A., Biedler, J. L., Spengler, B. A., & Reis, D. J. (1981). Neurotransmitter-synthesising enzymes in 14 human neuroblastoma cell lines. *Cellular and Molecular Neurobiology, 1*(3), 301-12. doi: 10.1007/BF00710685.

Ross, R. A., & Biedler, J. L. (1985). Presence and regulation of tyrosine activity in human neuroblastoma cell variants *in vitro*. *Cancer Research, 45*(4), 1628-32.

Ross, O. A., Braithwaite, A. T., Skipper, L. M., Kachergus, J., Hulihan, M. M., Middletone, F. A., Nishioka, K., Fuchs, J., Gasser, T., Maraganore, D. M., Adler, C. H., Larvor, L., Chartier-Harlin, M. C., Nilsson, C., Langston, J. W., Gwinn, K., Hattori, N., & Farrer, M. J. (2008). Genomic investigation of alpha-synuclein multiplication and parkinsonism. *Annals of Neurology, 63*(6), 743-50. doi: 10.1002/ana.21380.

Salazar, J., Mena, N., Hunot, S., Prigent, A., Alvarez-Fischer, D., Arredondo, M., Duyckaerts, C., Sazdovitch, V., Zhao, L., Garrick, L. M., Nunez, M. T., Garrick, M. D., Raisman-Vozari, R., & Hirsch, E. C. (2008). Divalent metal transporter 1 (DMT1) contributes to neurodegeneration in animal models of Parkinson's disease. *Proceedings of the National Academy of Sciences of the United States of America*, *105*(47), 18578–83. doi: 10.1073/pnas.0804373105.

Samadi, P., Gregoire, L., Rouillard, C., Bedard, P. J., Di Paolo, T., & Levesque, D. (2006). Docosahexaenoic acid reduces levodopa-induced dyskinesias in 1-methyl-4-phenyl-1,2,3,6-tetrahydropyridine monkeys. *Annals of Neurology, 59*(2), 282-8. doi: 10.1002/ana.20738.

Sato, H., Nomura, S., Maebara, K., Sato, K., Tamba, M., & Bannai, S. (2004). Transcriptional control of cystine/glutamate transporter gene by amino acid deprivation. *Biochemical and Biophysical Research Communications*, *325*(1), 109–16. doi: 10.1016/j.bbrc.2004.10.009.

Sato, M., Kusumi, R., Hamashima, S., Kobayashi, S., Sasaki, S., Komiyama, Y., Izumikawa, T., Conrad, M., Bannai, S., & Sato, H. (2018). The ferroptosis inducer erastin irreversibly inhibits system x_c^- and synergizes with cisplatin to increase cisplatin's cytotoxicity in cancer cells. *Scientific Reports, 8*(1), 968. doi: 10.1038/s41598-018-19213-4.

Savica, R., Grossardt, B.R., Bower, J.H., Ahlskog, J.E. & Rocca, W.A. (2016). Time trends in the incidence of Parkinson's disease. *JAMA Neurology*, *73*(8), 981–89. doi: 10.1001/jamaneurol.2016.0947.

Schneider, C., Tallman, K. A., Porter, N. A., & Brash, A. R. (2001). Two distinct pathways of formation of 4-hydroxynonenal. *Journal of Biological Chemistry, 276*, 20831-38. doi: 10.1074/jbc.M101821200.

Scholz, D., Poltl, D., Genewsky, A., Weng, M., Waldmann, T., Schildknecht, S., & Leist, M. (2011). Rapid, complete and large-scale generation of post-mitotic neurons from the human LUHMES cell line. *Journal of Neurochemistry, 119*(5), 957-71. doi: 10.1111/j.1471-4159.2011.07255.x.

Schroeder, B., Schulze, R. J., Weller, S. G., Sletten, A. C., Casey, C. A., & McNiven, M. A. (2015). The small GTPase Rab7 as a central regulator of hepatocellular lipophagy. *Hepatology, 61*(6), 1896-907. doi: 10.1002/hep.27667.

Seshacharyulu, P., Pandey, P., Datta, K., & Batra, S. K. (2013). Phosphatase: PP2A structural importance, regulation and its aberrant expression in cancer. *Cancer Letters, 335*(1), 9-18. doi: 10.1016/j.canlet.2013.02.036.

Shamoto-Nagai, M., Maruyama, W., Hashizune, Y., Yoshida, M., Osawa, T., Riederer, P., & Naoi, M. (2007). In parkinsonian substantia nigra, α-synuclein is modified by acrolein, a lipid-peroxidation product, and accumulates in the dopamine neurons with inhibition of proteasome activity. *Journal of Neural Transmission, 114*(12), 1559-67. doi: 10.1007/s00702-007-0789-2.

Shang, Y., Luo, M., Yao, F., Wang, S., Yuan, Z., & Yang, Y. (2020). Ceruloplasmin suppresses ferroptosis by regulating iron homeostasis in hepatocellular carcinoma cells. *Cellular Signalling, 72*, 109633. doi: 10.1016/j.cellsig.2020.109633.

Sharma, P., Shimura, T., Banwait, J. K., & Goel, A. (2020). Andrographis-mediated chemosensitisation through activation of ferroptosis and suppression of β-catenin/Wnt-signalling pathways in colorectal cancer. *Carcinogenesis, 41*(10), 1385-94. doi: 10.1093/carcin/bgaa090.

Shay, J.W. & Bacchetti, S. A survey of telomerase activity in human cancer. *European Journal of Cancer, 33*(5), 787-91. doi: 10.1016/S0959-8049(97)00062-2.

Sheng, X-H., Cui, C-C., Shan, C., Li, Y-Z., Sheng, D-H., Sun, B., & Chen, D-Z. (2018). *O*-Phenylenediamine: a privileged pharmacophore of ferrostatins for radical-traping reactivity in blocking ferroptosis. *Organic and Biomolecular Chemistry, 16*(21), 3952-60. doi: 10.1039/C8OB00546J.

Shi, Z. H., Nie, G., Duan, X. L., Rouault, T., Wu, W. S., Ning, B., Zhang, N., Chang, Y. Z., Zhao, B. L. (2010). Neuroprotective mechanism of mitochondrial ferritin on 6-hydroxydopamine-induced dopaminergic cell damage: implication for neuroprotection in Parkinson's disease. *Antioxidants and Redox Signalling, 13*(6), 783-96. doi: 10.1089/ars.2009.3018.

Shimada, K., Skouta, R., Kaplan, A., Yang, W. S., Hayano, M., Dixon, S. J., Brown, L. M., Valenzuela, C. A., Wolpaw, A. J., & Stockwell, B. R. (2016). Global survey of cell death mechanisms reveals metabolic regulation of ferroptosis. *Chemical Biology, 12*(7), 497-503. doi: 10.1038/nchembio.2079.

Shokrgozar, M. A., Zali, H., Rezaei Tavirani, M., & Amanzadeh, A. (2007). Comparison of two staining assays; trypan blue and MTT in vitro evaluation of human calprotectin proliferation inhibition on human gastric cancer cells. *Kowsar Medical Journal, 12*(2), 127-37.

Shurtleff, M. J., Itzhak, D. N., Hussmann, J. A., Schirle Oakdale, N. T., Costa, E. A., Jonikas, M., Weibezahn, J., Popova, K. D., Jan, C. H., Sinitcyn, P., Vembar, S. S., Hernandez, H., Cox, J., Burlinhame, A. L., Brodsky, J. L., Frost, A., Borner, G. H. H., & Weissman, J. S. (2018). The ER membrane protein complex interacts cotranslationally to enable biogenesis of multipass membrane proteins. *eLife, 7*, e37018. doi: 10.7554/eLife.37018.

Siddiqui, I. J., Pervaiz, N., & Abbasi, A. A. (2016). The Parkinson's Disease gene SNCA: Evolutionary and structural insights with pathological implication. *Scientific Reports*, *6*, 24475. doi: 10.1038/srep24475.

Siddique, Y. H., Ara, G., Jyoti, S., & Afzal, M. (2012). Protective effects of curcumin in transgenic *Drosophila melanogaster* model of Parkinson's disease. *Alternative Medicine Studies, 2*(1), e3. doi: 10.4081/ams.2012.e3.

Skaper, S. D., Mercanti, G., & Facci, L. (2012). Culture and characterisation of rat mesencephalic dopaminergic neurons. *Methods in Molecular Biology, 846*, 91-101. doi: 10.1007/978-1-61779-536-7_9.

Skouta, R., Dixon, S. J., Wang, J., Dunn, D. E., Orman, M., Shimada, K., Rosenberg, P. A., Lo, D. C., Weinberg, J. M., Linkermann, A., & Stockwell, B. R. (2014). Ferrostatins Inhibit Oxidative Lipid Damage and Cell Death in Diverse Disease Models. *Journal of the American Chemical Society*, *136*(12), 4551–56. doi: 10.1021/ja411006a.

Sliwka, L., Wiktorska, K., Suchocki, P., Milczarek, M., Mielczarek, S., Lubelska, K., Cierpial, T., Lyzwa, P., Kielbasinski, P., Jaromin, A., Flis, A., & Chilmonczyk, Z. (2016). The comparison of MTT and CVS assays for the assessment of anticancer agent interactions. *PLoS One, 11*(5), e0155772. doi: 10.1371/journal.pone.0155772.

Smirnova, L., Harris, G., Delp, J., Valadares, M., Pamies, D., Hogberg, T., Waldmann, T., Leist, M., & Hartung, T. (2016). A LUHMES 3D dopaminergic neuronal model for neurotoxicity testing allowing long-term exposure and cellular resilience analysis. *Archives of Toxicology, 90*(11), 2725-43. doi: 10.1007/s00204-015-1637-z.

Song, W., Bossy, B., Martin, O. J., Hicks, A., Lubitz, S., Knott, A. B., & Bossy-Wetzel, E. (2008). Assessing mitochondrial morphology and dynamics using fluorescence wide-field microscopy and 3D image processing. *Methods, 46*(6), 295-303. doi: 10.1016/j.ymeth.2008.10.003.

Song, Z., Xiang, X., Li, J., Deng, J., Fang, Z., Zhang, L., & Xiong, J. (2020). Ruscogenin induces ferroptosis in pancreatic cancer cells. *Oncology Reports, 43*(2), 516-24. doi: 10.3892/or.2019.7425.

Spinelli, K.J., Taylor, J.K., Osterberg, V.R., Churchill, M.J., Pollock, E., Moore, C., Meshul, C.K. & Unni, V.K. (2014). Presynaptic Alpha-Synuclein aggregation in a mouse model of Parkinson's disease. *The Journal of Neuroscience*, *34*(6), 2037–50. doi: 10.1523/jneurosci.2581-13.2014.

Stacey, G. (2006). Primary cell cultures and immortal cell lines. *Encyclopedia of Life Sciences*. doi: 10.1038/npg.els.0003960.

Stillwell, W., & Wassall, S. R. (2003). Docosahexaenoic acid: membrane properties of a unique fatty acid. *Chemistry and Physics of Lipids, 126*(1), 1-27. doi: .1016/S0009-3084(03)00101-4.

Stockert, J. C., Blazquez-Castro, A., Canete, M., Horobin, R. W., & Villanueva, A. (2012). MTT assay for cell viability: intracellular localisation of the formazan product is in lipid droplets. *Acta Histochemica, 114*(8), 785-96. doi: 10.1016/j.acthis.2012.01.006.

Stockwell, B. R., Friedmann, A. J. P., Bayir, H., Bush, A. I., Conrad, M., Dixon, S. J., Fulda, S., Gascon, S., Hatzios, S. K., Kagan, V. E., Noel, K., Jiang, X., Linkermann, A., Murphy, M. E., Overholtzer, M., Oyagi, A., Pagnussat, G. C., Park, J., Ran, Q., Rosenfeld, C. S., Salnikow, K., Tang, D., Torti, F. M., Torti, S. V., Toyokuni, S., Woerpel, K. A., & Zhang, D. D. (2017). Ferroptosis: a regulated cell death nexus linking metabolism, redox biology, and disease. *Cell, 171*(2), 273-85. doi: 10.1016/j.cell.2017.09.021.

Street, I. P., Lin, H. K., Laliberte, F., Ghomashchi, F., Wang, Z., Perrier, H., Tremblay, N. M., Huang, Z., Weech, P. K., & Gelb, M. H. (1993). Slow- and tight-binding inhibitors of the 85-kDa human phospholipase A2. *Biochemistry, 32*(23), 5935-40. doi: 10.1021/bi00074a003.

Su, L., Jinag, X., Yang, C., Zhang, J., Chen, B., Li, Y., Yao, S., Xie, Q., Gomez, H., Murugan, R., & Peng, Z. (2019). Pannexin 1 mediates ferroptosis that contributes to renal ischemia/reperfusion injury. *Cell Biology, 294*(50), 19395-404. doi: 10.1074/jbc.RA119.010949.

Sui, M., Jiang, X., Chen, J., Yang, H., & Zhu, Y. (2018). Magnesium osoglycyrrhizinate ameliorates liver fibrosis and hepatic stellate cell activation by regulating ferroptosis signalling pathway. *Biomedicine & Pharmacotherapy, 106*, 125-33. doi: 10.1016/j.biopha.2018.06.060.

Sui, X., Zhang, R., Liu, S., Duan, T., Zhai, L., Zhang, M., Han, X., Xiang, Y., Huang, X., Lin, H., & Xie, T. (2018). RSL3 drives ferroptosis through GPX4 inactivation and ROS production in colorectal cancer. *Frontiers in Pharmacology, 9*, 1371. doi: 10.3389/fphar.2018.01371.

Suissa, M., Suda, K., & Schatz, G. (1984). Isolation of the nuclear yeast genes for citrate synthase and fifteen other mitochondrial proteins by a new screening method. *The EMBO Journalm 3*(8), 1773-81. doi: 10.1002/j.1460-2075.1984.tb02045.x.

Sun, L., Li, J., & Yan, B. (2015). Gene expression profiling analysis of osteosarcoma cell lines. *Molecular Medicine Reports, 12*(3), 4266-72. doi: 10.3892/mmr.2015.3958.

Sun, X., Ou, Z., Chen, R., Niu, X., Chen, D., Kang, R., & Tang, D. (2015). Activation of the p62-Keap1-NRF2 pathway protects against ferroptosis in hepatocellular carcinoma cells. *Hepatology, 63*(1), 173-84. doi: 10.1002/hep.28251.

Sylvester, P. W. (2011). Optimization of the tetrazolium dye (MTT) colorimetric assay for cellular growth and viability. *Methods in Molecular Biology, 716*, 157-68. doi: *10.1007/978-1-61779-012-6_9.*

Szondy, Z., Sarang, Z., Kiss, B., Garabuczi, E., & Koroskenyi, K. (2017). Anti-inflammatory mechanisms triggered by apoptotic cells during their clearance. *Frontiers in Immunology, 8*, 909. doi: 10.3389/fimmu.2017.00909.

Tadokoro, T., Ikeda, M., Ide, T., Deguchi, H., Ikeda, S., Okabe, K., Ishikita, A., Matsushima, S., Koumura, T., Yamada, K-I., Imai, H., & Tsutsui, H. (2020). Mitochondria-dependent ferroptosis plays a pivotal role in doxorubicin cardiotoxicity. *JCI Insight, 5*(9), e132747. doi: 10.1172/jci.insight.132747.

Takahashi, J. (2019). Preparing for first human trial of induced pluripotent stem cell-derived cells for Parkinson's disease: an interview with Jun Takahashi. *Regenerative Medicine, 14*(2), 93-95. doi: 10.2217/rme-2018-0158.

Takahashi, J., & Yamanaka, S. (2006). Induction of pluripotent stem cells from mouse embryonic and adult fibroblast cultures by defined factors. *Cell, 126*(4), 663-76. doi: 10.1016/j.cell.2006.07.024.

Tang, H. M., & Tang, H. L. (2019). Cell recovery by reversal of ferroptosis. *Biology Open, 2019*(8). doi: 10.1242/bio.043182.

Tang, H., Chen, D., Li, C., Zheng, C., Wu, X., Zhang, Y., Song, Q., & Fei, W. (2019). Dual GSH-exhausting sorafenib loaded manganese-silica nanodrugs for inducing the ferroptosis of hepatocellular carcinoma cells. *International Journal of Phaemaceutics, 572*, 118782. doi: 10.1016/j.ijpharm.2019.118782.

Tanida, I., Ueno, T., & Kominami, E. (2008). LC3 and autophagy. *Methods in Molecular Biology, 445*, 77-88. doi: 10.1007/978-1-59745-157-4_4.

Tattoli, I., Sorbara, M. T., Vuckovic, D., Ling, A., Soares, F., Carneiro, L. A., Yang, C., Emili, A., Philpott, D. J., & Girardin, S. E. (2012). Amino acid starvation induced by invasive bacterial pathogens triggers an innate host defense program. *Cell Host and Microbe, 11*(6), 563-75. doi: 10.1016/j.chom.2012.04.012.

Tay, C. G., Fong, C. Y., & Ong, L. C. (2014). Transient parkinsonism following mycoplasma pneumoniae infection with normal brain magnetic resonance imaging (MRI). *Journal of Child Neurology, 29*(12), 193-5. doi: 10.1177/0883073813510741.

Taylor-Robinson, D., & Bebear, C. (1997). Antibiotic susceptibilities of mycoplasmas and treatment of mycoplasmal infections. *Journal of Antimicrobial Chemotherapy, 40*(5), 622-30. doi: 10.1093/jac/40.5.622.

Thanvi, B., & Lo, T. (2004). Long term motor complications of levodopa: clinical features, mechanisms and management strategies. *Postgraduate Medical Journal, 80*(946), 452-58. doi: 10.1136/pgmj.2003.013912.

Thomas, C., Mackey, M. M., Diaz, A. A., & Cox, D. P. (2009). Hydroxyl radical is produced via the Fenton reaction in submitochondrial particles under oxidative stress: implications for diseases associated with iron accumulation. *Redox Report*, *14*(3), 102–08. doi: 10.1179/135100009x392566.

Toffa, S., Kunikowska, G. M., Zeng, B. Y., Jenner, P., & Marsden, C. D. (1997). Glutathione depletion in rat brain does not cause nigrostriatal pathway degeneration. *Journal of Neural Transmission, 104*(1), 67-75. doi: 10.1007/BF01271295.

Tong, Z-B., Hogberg, H., Kuo, D., Sakamuru, S., Xia, M., Smirnova, L., Hartung, T., & Gerhold, D. (2018). Characterisation of three human cell line models for high-throughput neuronal cytotoxicity screening. *Journal of Applied Toxicology, 37*(2), 167-80. doi: 10.1002/jat.3334.

Toroser, D., & Sohal, R. S. (2007). Age-associated perturbations in glutathione synthesis in mouse liver. *Biochemical Journal*, *405*(3), 583–89. doi: 10.1042/bj20061868.

Traber, M. G., & Atkinson, J. (2007). Vitamin E, antioxidant and nothing more. *Free Radical Biology and Medicine*, *43*(1), 4–15. doi 10.1016/j.freeradbiomed.2007.03.024.

Tuo, Q-Z., Lei, P., Jackman, K. A., Li, X-I., Xiong, H., Li, X-I., Liuyang, Z-Y., Roisman, L., Zhang, S-T., Ayton, S., Wang, Q., Crouch, P. J., Ganio, K., Wang, X-C, Pei, L., Lu, Y-M., Cappai, R., Wang, J-Z., Liu, R., & Bush, A. I. (2017). Tau-mediated iron export prevents ferroptotic damage after ischemic stroke. *Molecular Psychiatry, 22*, 1520-30. doi: 10.1038/mp.2017.171.

Uphoff, C. C., Denkmann, S-A., & Drexler, H. G. (2012). Treatment of Mycoplasma contamination in cell cultures with Plasmocin. *Journal of Biomedicine and Biotechnology, 2012*. doi: 10.1155/2012/267678.

Vandenabeele, P., Galluzzi, L., Vanden Berghe, T. & Kroemer, G. Molecular mechanisms of necroptosis: an ordered cellular explosion. *Nature Reviews Molecular Cell Biology*. *11*, 700–714.

Vanden Berghe, T., Linkermann, A., Jouan-Lanhouet, S., Walczak, H., & Vandenabeele, P. (2014). Regulated necrosis: the expanding network of non-apoptotic cell death pathways. *Nature Reviews Molecular Cell Biology, 15*(2), 135-47. doi: 10.1038/nrm3737.

van Kampen, J. M., & Eckman, C. B. (2006). Dopamine D_3 Receptor Agonist Delivery to a Model of Parkinson's Disease Restores the Nigrostriatal Pathway and Improves Locomotor Behaviour. *The Journal of Neuroscience, 26*(27), 7272-80. doi: 10.1523/JNEUROSCI.0837-06.2006.

van Meerloo, J., Kaspers, G. J., & Cloos, J. (2011). Cell sensitivity assays: the MTT assay. *Methods in Molecular Biology*, *731*, 237-45. doi: 10.1007/978-1-61779-080-5_20.

van Rensburg, C. E., Anderson, R., Joone, G., Myer, M. S., & O'Sullivan, J. F. (1997). Novel tetramethylpiperidine-substituted phenazines are potent inhibitors of P-glycoprotein activity in a multidrug resistant cancer cell line. *Anticancer Drugs, 8*(7), 708-13. doi: 10.1097/00001813-199708000-00010.

van Tonder, A., Joubery, A. M., & Duncan Cromarty, A. (2015). Limitations of the 3-(4,5-dimethylthiazol-2-yl)-2,5-diphenyl-2H-tetrazolium bromide (MTT) assay when compared to three commonly used cell enumeration assays. *BioMed Central Research Notes, 8*. doi: 10.1186/s13104-015-1000-8.

Vigil, D., Cherfils, J., Rossman, K. L., & Der, C. J. (2010). Ras superfamily GEFs and GAPs: validated and tractable targets for cancer therapy? *Nature Reviews Cancer, 10*(12), 842-57. doi: 10.1038/nrc2960.

Vives-Bauza, C., Zhou, C., Huang, Y., Cui, M., de Vries, R. L., Kim, J., May, J., Tocilescu, M. A., Liu, W., Ko, H. S., Magrane, J., Moore, D. J., Dawson, V. L., Grailhe, R., Dawson, T. M., Li, C., Tieu, K., & Przedbroski, S. (2010). PINK1-dependent recruitment of Parkin to mitochondria in mitophagy. *Proceedings of the National Academy of Sciences of the United States of America, 107*(1), 378-83. doi: 10.1073/pnas.0911187107.

Wallach, D., Kang, T. B., Dillon, C. P., & Green, D. R. (2016). Programmed necrosis in inflammation: toward identification of the effector molecules. *Science, 352*(6281), aaf2154. doi: 10.1126/science.aaf2154.

Wallis, M. A., & Griffin, R. L. (1973). A routine method for embedding animal tissues in Spurr resin for electron microscopy. *Journal of Clinical Pathology, 26*(1), 77-78. doi: 10.1136/jcp.26.1.77.

Wang, S., Yu, H., & Wickliffe, J. K. (2011). Limitation of the MTT and XTT assays for measuring cell viability due to superoxide formation induced by nano-scale TiO_2. *Toxicology in Vitro, 25*(8), 2147-51. doi: 10.1016/j.tiv.2011.07.007.

Wang, D., Peng, Y., Xie, Y., Zhou, B., Sun, X., Kang, R., Tang, D. (2016). Antiferroptotic activity of non-oxidative dopamine. *Biochemical and Biophysical Research Communications, 480*(4), 602-07. doi: 10.1016/j.bbrc.2016.10.099.

Wang, Y. Q., Chang, S. Y., Wu, Q., Gou, Y. J., Jia, L., Cui, Y. M., Yu, P., Shi, Z. H., Wu, W. S., Gao, G., & Chang, Y. Z. (2016). The protective role of mitochondrial ferritin on erastin-induced ferroptosis. *Frontiers in Aging Neuroscience, 8*, 308. doi: 10.3389/fnagi.2016.00308.

Wang, K., Zhang, Z., Wang, M., Cao, X., Wang, D., Gong, A., & Zhu, H. (2018). Role of GRP78 inhibiting artesunate-induced ferroptosis in *KRAS* mutant pancreatic cancer cells. *Drug Design, Development and Therapy, 13*, 2135-44. doi: 10.2147/DDDT.S199459.

Wang, L., Zhang, Z., Li, M., Wang, F., Jia, Y., Zhang, F., Shao, J., Chen, A., & Zheng, S. (2018). P53-dependent induction of ferroptosis is required for artemether to alleviate carbon tetrachloride-induced liver fibrosis and hepatic stellate cell activation. *IUBMB Life, 71*(1), 45-56. doi: Citations: 30.

Wang, L., Liu, Y., Du, T., Yang, H., Lei, L., Guo, M., Ding, H-F., Zhang, J., Wang, H., Chen, X., & Yan, C. (2019). ATF3 promotes erastin-induced ferroptosis by suppressing system x_c^-. *Cell Death & Differentiation, 27*, 662-75. doi: 10.1038/s41418-019-0380-z.

Wang, Y., Quan, F., Cao, Q., Lin, Y., Yue, C., Bi, R., Ciu, X., Yang, H., Yang, Y., Birnbaumer, L., Li, X., & Gao, X. (2021). Quercetin alleviates acute kidney injury by inhibiting ferroptosis. *Journal of Advanced Research, 28*, 231-43. doi: 10.1016/j.jare.2020.07.007.

Watkins, P. A., Maiguel, D., Jia, Z., & Pevsner, J. (2007). Evidence for 26 distinct acyl-coenzyme A synthetase genes in the human genome. *Journal of Lipid Research, 48*(12), 2736-50. doi: 10.1194/jlr.M700378-JLR200.

Wei, H., Wang, C., Croce, C. M., & Guan, J-L. (2014). p62/SQSTM1 synergizes with autophagy for tumor growth in vivo. *Genes Development, 28*(11), 1204-16. doi: 10.1101/gad.237354.113.

Weigand, I., Schreiner, J., Rohrig, F., Sun, N., Landwehr, L-S.., Urlaub, H., Kendl, S., Kiseljak-Vassiliades, K., Weirman, M. E., Angeli, J. P. F., Walch, A., Sbiera, S., Fassnacht, M., & Kroiss, M. (2020). Active steroid hormone synthesis renders adrenocortical cells highly susceptible to type II ferroptosis induction. *Cell Death & Disease, 11*(192). doi: 10.1038/s41419-020-2385-4.

White, E. A., Kramer, R. E., Hwang, J. H., Fernando, A. T. P., Naetar, N., Hahn, W. C., Roberts, T. M., Schaffhausen, B. S., Livingston, D. M., & Howley, P. M. (2014). Papillomavirus E7 Oncoproteins Share Functions with Polyomavirus Small T Antigens. *Journal of Virology*, *89*(5), 2857–65. doi: 10.1128/jvi.03282-14.

White, E. (2015). The role for autophagy in cancer. *The Journal of Clinical Investigation, 125*(1), 42-6. doi: 10.1172/JCI73941.

Wilhelm, S., Carter, C., Lynch, M., Lowinger, T., Dumas, J., Smith, R. A., Schwartz, B., Simantov, R., & Kelley, S. (2006). Discovery and development of sorafenib: a multikinase inhibitor for treating cancer. *Nature Reviews Drug Discovery, 5*(10), 835-44. doi: 10.1038/nrd2130.

Wise, D. R., DeBerardinis, R. J., Mancuso, A., Sayed, N., Zhang, X. Y., Pfeiffer, H. K., Nissim, I., Daikhin, E., Yudkoff, M., McMahon, S. B., and Thompson, C. B. (2008). Myc regulates a transcriptional program that stimulates mitochondrial glutaminolysis and leads to glutamine addiction. *Proceedings of the National Academy of Sciences of the United States of America, 105*(48), 18782-87. doi: 10.1073/pnas.0810199105.

Woo, J. H., Shimoni, Y., Yang, W. S., Subramaniam, P., Iyer, A., Nicoletti, P., Rodriguez-Martinez, M., Lopez, G., Mattioli, M., Realubit, R., Karan, C., Stockwell, B. R., Bansal, M., & Califano, A. (2015). Elucidating Compound Mechanism of Action by Network Perturbation Analysis. *Cell, 162*(2), 441-51. doi: 10.1016/j.cell.2015.05.056.

Wu, X., Lin, M., Li, Y., Zhao, X., & Yan, F. (2009). Effects of DMEM and RPMI-1640 on the biological behaviour of dog periosteum-derived cells. *Cytotechnology, 59*(2), 103-11. doi: 10.1007/s10616-009-9200-5.

Wu, C., Zhao, W., Yu, J., Lin, L., & Chen, X. (2018). Induction of ferroptosis and mitochondrial dysfunction by oxidative stress in PC12 cells. *Science Reports, 8*(1), 574. doi: 10.1038/s41598-017-18935-1.

Wu, Z., Geng, Y., Lu, X., Shi, Y., Wu, G., Zhang, M., Shan, B., Pan, H., & Yuan, J. (2018). Chaperone-mediated autophagy is involved in the execution of ferroptosis. *Proceedings of the National Academy of Sciences of the United States of America, 116*(8), 2996-3005. doi: 10.1073/pnas.1819728116.

Wu, G., Wang, Q., Xu, Y., Li, Q., & Cheng, L. (2020). A new survival model based on ferroptosis-related genes for prognostic prediction in clear cell renal cell carcinoma. *Aging, 12*(14), 14933-48. doi: 10.18632/aging.103553.

Wu, J., Liu, Q., Zhang, X., Wu, X., Zhao, Y., & Ren, J. (2021). STING-dependent induction of lipid peroxidation mediates intestinal ischemia-reperfusion injury. *Free Radical Biology and Medicine, 163*, 135-40. doi: 10.1016/j.freeradbiomed.2020.12.010.

Wullner, U., Loschmann, P. A., Schulz, J. B., Schmid, A., Dringen, R., Eblen, F., Turski, L., & Klockgether, T. (1996). Glutathione depletion potentiates MPTP and MPP^+ toxicity in nigral dopaminergic neurones. *Neuroreport, 7*(4), 921-23. doi: 10.1097/00001756-199603220-00018.

Xia, Y., Liu, S., Li, C., Ai, Z., Shen, W., Ren, W., & Yang, X. (2020). Discovery of a novel ferroptosis inducer-talaroconvolutin A – killing colorectal cancer cells in vitro and in vivo. *Cell Death & Disease, 11*(988). doi: 10.1038/s41419-020-03194-2.

Xiao, B., Ng, H. H., Takahashi, R., & Tan, E. K. (2016). Induced pluripotent stem cells in Parkinson's disease: scientific and clinical challenges. *Journal of Neurology, Neurosurgery and Psychiatry, 87*(7), 697-702. doi: 10.1136/jnnp-2015-312036.

Xicoy, H., Wieringa, B., & Martens, G.J.M. (2017). The SH-SY5Y cell line in Parkinson's disease research: a systematic review. *Molecular Neurodegeneration*, *12*(10). doi: 10.1186/s13024-017-0149-0.

Xie, Y., Hou, E., Song, X., Yu, Y., Huang, J., Sun, X., Kang, R., & Tang, D. (2016a). Ferroptosis: process and function. *Cell Death and Differentiation, 23*(3), 369-79. doi: 10.1038/cdd.2015.158.

Xie, Y., Song, X., Sun, X., Huang, J., Zhong, M., Lotze, M. T., Zeh, H. J., Kang, R., & Tang, D. (2016b). Identification of baicalein as a ferroptosis inhibitor by natural product library screening. *Biochemical and Biophysical Research Communications*, *473*(4), 775–80. doi: 10.1016/j.bbrc.2016.03.052.

Xie, B-S., Wang, Y-Q., Lin, Y., Mao, Q., Feng, J-F., Gao, G-Y., & Jiang, J-Y. (2018). Inhibition of ferroptosis attenuates tissue damage and improves long-term outcomes after traumatic brain injury in mice. *CNS Neuroscience & Therapeutics, 25*(4), 465-75. doi: 10.1111/cns.13069.

Xu, X., Zhang, X., Wei, C., Zheng, D., Lu, X., Yang, Y., Luo, A., Zhang, K., Duan, X., & Wang, Y. (2020). Targeting SLC7A11 specifically suppresses the progression of colorectal cancer stem cells via inducing ferroptosis. *European Journal of Pharmaceutical Sciences, 152*, 105450. doi: 10.1016/j.ejps.2020.105450.

Xue, M., Ge, Y., Yu, C., Zheng, Z., He, X., & Zhao, J. (2017). Apoptosis is induced by docosahexaenoic acid in breast cancer cells via death receptor and mitochondria-mediated pathways. *Molecular Medicine Reports, 16*(1), 978-82. doi: 10.3892/mmr.2017.6678.

Xun, Z., Lee, D-Y., Lim, J., Canaria, C. A., Barnebey, A., Yanonne, S. M., & McMurray, C. T. (2012). Retinoic acid-induced differentiation increases the rate of oxygen consumption and enhances the spare respiratory capacity of mitochondria in SH-SY5Y cells. *Mechanisms of Ageing and Development, 133*(4), 176-85. doi: 10.1016/j.mad.2012.01.008.

Xun, Z., Rivera-Sánchez, S., Ayala-Peña, S., Lim, J., Budworth, H., Skoda, E. M., Robbins, P. D., Niedernhofer, L. J., Wipf, P., & Mcmurray, C. T. (2012). Targeting of XJB-5-131 to Mitochondria Suppresses Oxidative DNA Damage and Motor Decline in a Mouse Model of Huntington's Disease. *Cell Reports*, *2*(5), 1137–42. doi: 10.1016/j.celrep.2012.10.001.

Yagoda, N., von Rechenberg, M., Zaganjor, E., Bauer, A. J., Yang, W. S., Fridman, D. J., Wolpow, A. J., Smukste, I., Peltier, J. M., Boniface, J. J., Smith, R., Lessnick, S. L., Sahasrabudhe, S., & Stockwell, B. R. (2007). RAS-RAF-MEK-dependent oxidative cell death involving voltage-dependent anion channels. *Nature, 447*, 865-9. doi: 10.1038/nature05859.

Yamada, N., Karasawa, T., Wakiya, T., Sadatomo, A., Ito, H., Kamata, R., Watanabe, S., Komada, T., Kimura, H., Sanada, Y., Sakuma, Y., Mizuta, K., Ohno, N., Sata, N., & Takahashi, M. (2020). Iron overload as a risk factor for hepatic ischemia-reperfusion injury in liver transplantation: potential role of ferroptosis. *American Journal of Transplantation, 20*(6), 1606-18. doi: 10.1111/ajt.15773.

Yamaguchi, K., Cochran., E. J., Murrell, J. R., Polymeropoulos, M. H., Shannon, K. M., Crowther, R. A., Goedert, M., & Ghetti, B. (2005). Abundant neuritic inclusions and microvacuolar changes in a case of diffuse Lewy body disease with the A53T mutation in the α-synuclein gene. *Acta Neuropathologica, 110*(3), 298-305. doi: 10.1007/s00401-005-1042-4.

Yamaguchi, Y., Kasukabe, T., & Kumakura, S. (2018). Piperlongumine rapidly induces the death of human pancreatic cancer cells mainly through the induction of ferroptosis. *International Journal of Oncology, 52*(3), 1011-22. doi: 10.3892/ijo.2018.4259.

Yamagami, T., Porada, C. D., Pardini, R. S., Zanjani, E. D., & Almeida-Porada, G. (2014). Docosahexaenoic acid induces dose dependent cell death in an early undifferentiated subtype of acute myeloid leukemia cell line. *Cancer Biology and Therapy, 8*(4), 331-7. doi: 10.4161/cbt.8.4.7334.

Yang, H. C., Mosior, M., Ni, B., & Dennis, E. A. (1999). Regional distribution, otogeny, purification, and characterization of the Ca^{2+}-independent phospholipase A2 from rat brain. *Journal of Neurochemistry, 73*(3), 1278-87. doi: 10.1046/j.1471-4159.1999.0731278.x

Yang, W. S., & Stockwell, B. R. (2008). Synthetic Lethal Screening Identifies Compounds Activating Iron-Dependent, Nonapoptotic Cell Death in Oncogenic-RAS-Harboring Cancer Cells. *Chemistry & Biology*, *15*(3), 234–45. doi: 10.1016/j.chembiol.2008.02.010.

Yang, W. S., Sriramaratnam, R., Welsch, M. E., Shimada, K., Skouta, R., Viswanathan, V. S., Cheah, J. H., Clemons, P. A., Shamji, A. F., Clish, C. B., Brown, L. M., Girotti, A. W., Cornish, V. W., Schreiber, S. L., & Stockwell, B. R. (2014). Regulation of Ferroptotic Cancer Cell Death by GPX4. *Cell*, *156*(1-2), 317–31. doi: 10.1016/j.cell.2013.12.010.

Yang, A., Rajeshkumar, N. V., Wang, X., Tabuuchi, S., Alexander, B. M., Chu, G. C. Van Hoff, D. D., Maitra, A., & Kimmelman, A. C. (2014). Autophagy is critical for pancreatic tumor growth and progression in tumors with p53 alterations. *Cancer Discovery, 4*(8), 905-13. doi: 10.1158/2159-8290.CD-14-0362.

Yang, W. S., Kim, K. J., Gaschler, M. M., Ptel, M., Shchepinov, M. S., & Stockwell, B. R. (2016). Peroxidaton of polyunsaturated fatty acids by lipoxygenases drives ferroptosis. *Proceedings of the National Academy of Sciences of the United States of America, 113*(34), e4966-75. doi: 10.1073/pnas.1603244113.

Yang, W. S., & Stockwell, B. R., (2016). Ferroptosis: death by lipid peroxidation. *Trends in Cell Biology, 26*(3), 165-76. doi: 10.1016/j.tcb.2015.10.014.

Yang, W-H., Ding, C-K. C., Sun, T., Rupprecht, G., Lin, C-C., Hsu, D., & Chi, J-T. (2019). The hippo pathway effector TAZ regulates ferroptosis in renal cell carcinoma. *Cell Reports, 28*(10), 2501-08. doi: 10.1016/j.celrep.2019.07.107.

Yano, M., Kishida, E., Iwasaki, M., Kojo, S., & Masuzawa, Y. (2000). Docosahexaenoic acid and vitamin E can reduce human monocytic U937 cell apoptosis induced by tumor necrosis factor. *The Journal of Nutrition, 130*(5), 1095-101. doi: 10.1093/jn/130.5.1095.

Yasuhara, T., Matsukawa, N., Hara, K., Yu, G., Xu, L., Maki, M., Kim, S. U., & Borlongan, C. (1006). Transplantation of human neural stem cells exerts neuroprotection in a rat model of Parkinson's disease. *The Journal of Neuroscience, 26*(48), 12497-511. doi: 10.1523/JNEUROSCI.3719-06.2006.

Ye, Z., Hu, Q., Zhuo, Q., Zhu, Y., Fan, G., Liu, M., Sun, Q., Zhang, Z., Liu, W., Xu, W., Ji, S., Yu, X., Xu, X., & Qin, Y. (2020). Abrogation of ARF6 promotes RSL3-induced ferroptosis and mitigates gemcitabine resistance in pancreatic cancer cells. *American Journal of Cancer Research, 10*(4), 1182-93.

Yoshinaga, N., Yasuda, Y., Murayama, T., & Nomura, Y. (2000). Possible involvement of cytosolic phospholipase A2 in cell death induced by 1-methyl-4-phenylpyridium ion, a dopaminergic neurotoxin, in GH3 cells. *Brain Research, 855*(2), 244-51. doi: 10.1016/s0006-8993(99)02340-9.

Yu, Y., Xie, Y., Cao, L., Tang, L., Yang, M., Lotze, M. T., Zeh, H. J., Kang, R., & Tang, D. (2015). The ferroptosis inducer erastin enhances sensitivity of acute myeloid leukemia cells to chemotherapeutic agents. *Molecular and Cellular Oncology, 2*(4), e1054549. doi: 10.1080/23723556.2015.1054549.

Yu, S., Wei, W., Xia, M., Jiang, Z., He, D., Li, Z., Han, H., Chu, W., Liu, H., & Chen, J. (2016). Molecular characterisation, alternative splicing and expression analysis of *ACSF2* and its correlation with egg-laying performance in geese. *Animal Genetics, 47*(4). doi: 10.1111/age.12435.

Yu, H., Yang, C., Jian, L., Guo, S., Chen, R., Li, K., Qu, F., Tao, K., Fu, Y., Luo, F., & Liu, S. (2019). Sulfasalazine-induced ferroptosis in breast cancer cells is reduced by the inhibitory effect of estrogen receptor on the transferrin receptor. *Oncology Reports, 42*(2), 826-38. doi: 10.3892/or.2019.7189.

Zakeri, Z., & Lockshin, R. A. (2008). Cell death: history and future. *Advancements in Experimental Medicine and Biology, 615*, 1-11. doi: 10.1007/978-1-4020-6554-5_1.

Zhang, X. M., Yin, M., & Zhang, M. H. (2014). Cell-based assays for Parkinson's disease using differentiated human LUHMES cells. *Acta Pharmacologica Sinica, 35*(7), 945-56. doi: 10.1038/aps.2014.36.

Zhang, Z., Yao, Z., Wang, L., Ding, H., Shao, J., Chen, A., Zhang, F., & Zheng, S. (2018). Activation of ferritinophagy is required for the RNA-binding protein ELAVL1/HuR to regulate ferroptosis in hepatic stellate cells. *Autophagy, 14*(12), 2083-103. doi: 10.1080/15548627.2018.1503146.

Zhang. Y., Tan, H., Daniels, J. D., Zandkarimi, F., Liu, H., Brown, L. M., Uchida, K., O'Connor, O. A., & Stockwell, B. R. (2019). Imidazole ketone erastin induces ferroptosis and slows tumor growth in a mouse lymphoma model. *Cell Chemical Biology, 26*(5), 623-33. doi: 10.1016/j.chembiol.2019.01.008.

Zhang, Y., Sun, C., Zhao, C., Hao, J., Zhang, Y., Fan, B., Li, B., Duan, H., Liu, C., Kong, X., Wu, P., Yao, X., & Feng, S. (2019). Ferroptosis inhibitor SRS 16-86 attenuates ferroptosis and promotes functional

recovery in contusion spinal cord injury. *Brain Research, 1706*, 48-57. doi: 10.1016/j.brainres.2018.10.023.

Zhang, L., Liu, W., Liu, F., Wang, Q., Song, M., Yu, Q., Tang, K., Teng, T., Wu, D., Wang, X., Han, W., & Li, Y. (2020). IMCA induces ferroptosis mediated by SLC7A11 through the AMPK/mTOR pathway in colorectal cancer. *Oxidative Medicine and Cellular Longevity.* doi: 10.1155/2020/1675613.

Zhang, H., Deng, T., Liu, R., Ning, T., Yang, H., Liu, D., Zhang, Q., Lin, D., Ge, S., Bai, M., Wang, X., Zhang, L., Li, H., Yang, Y., Ji, Z., Wang, H., Ying, G., & Ba, Y. (2020). CAF secreted miR-522 suppresses ferroptosis and promotes acquired chemo-resistance in gastric cancer. *Molecular Cancer, 19*(43). doi: 10.1186/s12943-020-01168-8.

Zhao, Z., Wu, J., Xu, H., Zhou, C., Han, B., Zhu, H., Hu, Z., Ma, Z., Ming, Z., Yao, Y., Zeng, R., & Xu, G. (2020). XJB-5-131 inhibited ferroptosis in tubular epithelial cells after ischemia-reperfusion injury. *Cell Death & Disease, 11*(629). doi: 10.1038/s41419-020-02871-6.

Zhao, L., Peng, Y., He, S., Li, R., Wang, Z., Huang, J., Lei, X., Li, G., & Ma, Q. (2021). Apatinib induced ferroptosis by lipid peroxidation in gastric cancer. *Gastric Cancer, 24*, 642-54. doi: 10.1007/s10120-021-01159-8.

Zheng, D. W., Lei, Q., Zhu, J. Y., Fan, J. X., Li, C. X., Xu, Z., Cheng, S. X., & Zhang, X. Z. (2017). Switching apoptosis to ferroptosis: metal-organic network for high efficiency anticancer therapy. *Nano Letters, 17*(1), 284-91. doi: 10.1021/acs.nanolett.6b04060.

Zhou, X., Hollern, D., Liao, J., Andrechek, E., & Wang, H. (2013). NMDA receptor-mediated excitotoxicity depends on the coactivation of synaptic and extrasynaptic receptors. *Cell Death & Disease*, *4*, e560. doi: 10.1038/cddis.2013.82.

Zhou, Q., Yen, A., Rymarczyk, G., Asai, H., Trengrove, C., Aziz, N., Kirber, M. T., Mostoslavsky, G., Ikezu, T., Wolozin, B., & Bolotina, V. M. (2016). Impairment of PARK14-dependent Ca^{2+} signalling is a novel determinant of Parkinson's disease. *Nature Communications, 12*(7), 10332. doi: 10.1038/ncomms10332.

Zhou, Q., Zhang, H., Wu, Q., Shi, J., & Zhou, S. (2017). Pharmacological manipulations of autophagy modulate paraquat-induced cytotoxicity in PC12 cells. *International Journal of Biochemistry and Molecular Biology, 8*(2), 13-22.

Zhou, C., Zhang, E., Chen, W., Yin, Y., Atyah, M., Liu, S., Guo, L., Shi, Y., Ye, Q., Dong, Q., & Ren, N. (2017). Integrated analysis of copy number variations and gene expression profiling in hepatocellular carcinoma. *Scientific reports, 7*. doi: 10.1038/s41598-017-11029-y.

Zhou, L., Sun, C., Ren, J., Wang, C., Ma, R., Sun, L., Yang, D., Gao, S., Ning, K., Wang, Z., Chen, X., Chen, S., Zhu, H., Gao, Z., & Xu, J. (2019). Stress-induced precocious aging in PD-patient iPSC-derived NSCs may underlie the pathophysiology of Parkinson's disease. *Cell Death and Disease, 105*(10).

Zilka, O., Shah, R., Li, B., Friedmann, A. J. P., Griesser, M., Conrad, M., & Pratt, D. A. (2017). On the mechanism of cytoprotection by ferrostatin-1 and liproxstatin-1 and the role of lipid peroxidation in ferroptotic cell death. *ACS Central Science, 3*(3), 232-43. doi: 10.1021/acscentsci.7b00028.

Zille, M., Karuppagounder, S. S., Chen, Y., Gough, P. J., Bertin, J., Finger, J., Milner, T. A., Jonas, E. A., & Ratan, R. R. (2017). Neuronal death after hemorrhagic stroke *in vitro* and *in vivo* shares features of ferroptosis and necroptosis. *Stroke, 48*(4), 1033-43. doi: 10.1161/STROKEAHA.116.015609.

Zou, Y., Wang, R., Guo, H., & Dong, M. (2015). Phytoestrogen β-ecdysterone protects PC12 cells against MPP^+-induced neurotoxicity *in vitro*: involvement of PI3K-Nrf2-regulated pathway. *Toxicological Sciences, 147*(1), 28-38. doi: 10.1093/toxsci/kfv111.